Development of Bio-inks for Bioprinting Applications

A thesis submitted to the Faculty of Science, Agriculture and Engineering for the Degree of Doctor of Philosophy

by

Ricardo Ribeiro

School of Engineering

Newcastle University

February 2019

Abstract

Bioprinting allows cells and materials to be deposited to create tissue pre-cursors. However, the quality of the bioprinted constructs depends on bio-inks, which need optimisation to enable repeatable processes, achieve physiological cell densities and tailored structures.

The primary aim of this research was to develop reliable bio-inks for printing single cells and cells in gels.

A novel bio-ink formulation has been developed to allow reliable inkjet bioprinting of small cell numbers, allowing single cell deposition. Poly-L-lysine (PLL) was investigated as temporary speckled coating, which would allow to avoid nozzle blockage during the printing process. Different PLL concentrations were evaluated, with 10 µg/mL exhibiting the highest viability and metabolic activity similar to control samples on three different cell lineages. At the optimised concentration, fast internalisation and metabolisation of PLL was observed with no subsequent effect on cell behaviour. Repeatable inkjet cell printing was achieved, whilst maintaining cell function.

High cell density cell-laden hydrogels were produced using a bioprinting technique called Reactive Jet Impingement (ReJI), developed at Newcastle University as part of a related project. A protocol for using ReJI to produce a collagen-alginate-fibrin (CAF) gel was established and used to create cell-laden gels. The fabricated hydrogels exhibited rapid solution uptake and porous structures, both essential for cell migration. When culturing mesenchymal stem cells in the CAF gel a cell density of 40 million cells/ml supported faster osteogenic differentiation than a cell density of 4 million cells/ml. Additionally, increased cell density produced more organised tissue structures and increased expression of osteogenic biomarkers, indicative of accelerated bone tissue formation.

This research has developed and characterised the performance of two bio-inks for two bioprinting techniques. It is concluded that careful consideration of the processing techniques and bio-ink formulation can allow for the creation of effective cell printing techniques for both single cells and cell-laden hydrogels.

To Sara and my family,

for always supporting me during these four years away

Acknowledgements

This PhD would not be achievable without several people that here are acknowledge for all the guidance, help and, most of all, friendship.

First of all, I would like to deeply express my gratitude to my supervisory team, Professor Kenny Dalgarno, Dr. Kenny Rankin, Dr. Ana Ferreira Duarte and Dr. Matthew Benning, for making this PhD possible. During the last four years, each one guided me through my PhD, allowing me to grow as a researcher. Each advice, each discussed idea and each meeting were essential for this work. Also, I would like to acknowledge Matthew Benning for the development of the ReJI system.

I would like to acknowledge the support of the SAgE Doctoral Training Award from Newcastle University for funding this research.

To Dr. Deepali Pal, Dr. Piergiorgio Gentile, and Zakareya Gamie, I thank you for the collaboration on interesting projects, sharing of ideas and friendship. In this thesis, I would like to acknowledge Deepali Pal for the trilineage differentiation of primary cells.

I would like to thank my colleagues at Mechanical and Medical school for sharing all this experience with me. Each of you were truly important during my journey in Newcastle.

To Jiayu, Duan and E-Lin, 我的朋友, I want to thank you for making the first year at Leazes Terrace both easier and unforgettable. 谢谢你们!

Furthermore, I would like to thank you all my friends in Portugal for constantly caring and asking for me during my absence.

To my family, my grandparents, Américo and Irene, my parents, António and Ana, and my brother, João, for all the love, help and support during these four years away. This was only possible because of you.

And finally, to my wonderful fiancée Sara, who I constantly missed during this PhD, I thank you for all the patience and for always being here/there for me. I would not be able to finish this work without all your love and support.

Table of contents

List of figures

List of tables

List of abbreviations

2-NBDG - (2-(N-(7-Nitrobenz-2-oxa-1,3-diazol-4-yl)Amino)-2-Deoxyglucose)

2D - Two-dimensional

3D - Three-dimensional

AM - Additive Manufacturing

ALP - Alkaline Phosphatase

β-ME - Beta-mercaptoethanol

bECs - Bovine aortic endothelial cells

BMSC-hTERT - Bone marrow stem cells using human telomerase reverse transcriptase

$CaCl_2$ - Calcium chloride

CAF - Collagen-fibrin-alginate

Calcein AM - Calcein acetoxymethyl

$CaSO_4$ - Calcium sulfate

dSMCs - Canine smooth muscle cells

DAPI - 4′,6-diamidino-2-phenylindole

dECM - Decellularised extracellular matrix

DNA - Deoxyribonucleic acid

DMEM - Dulbecco's Modified Eagle Medium

DPBS - Dulbecco's phosphate-buffered saline

EBB - Extrusion-based bioprinting

ECM - Extracellular matrix

EDTA - Ethylenediamine tetraacetic acid

EthD-1 - Ethdium homodimer-1

FACS - Fluorescence-activated cell sorting

FBS - Fetal bovine serum

FBR - Foreign-body reaction

FDM - Fused deposition modelling

FGF-2 - Fibroblast growth factor-2

FITC - Fluorescein isothiocyanate

GelMA - gelatin methacrylamide

hAFSCs - Human amniotic fluid-derived stem cells

HBSS - Hanks' Balanced Salt solution

hESC - Human embryonic stem cells

hiPSC - Human induced pluripotent stem cells

IR - Infra-red

LAB - Laser-assisted bioprinting

LBL - Layer-by-layer

LIFT - Laser induced forward transfer MSCs - Mesenchymal stem cells

MTT - (3-(4,5-Dimethylthiazol-2-yl)-2,5-Diphenyltetrazolium Bromide)

MW - Molecular weight

NaAlg - Sodium alginate

Neo-NHDF - Neonatal normal human dermal fibroblasts

PAH - Poly(allylamine hydrochloride)

PEG - Polyethylene glycol

PEGDA - Polyethylene glycol diacrylate

PEGMA - Poly(ethylene glycol) dimethacrylate

PEI - Polyethylenimine

PLL - Poly-L-Lysine

PnPP - P-nitrophenyl phosphate

PSS - Poly(styrene sulfonate)

PI - Propidium iodide

ReJI - Reactive Jet Impingement

RNA - Ribonucleic Acid

RT-PCR - Real-time polymerase chain reaction

SEM - Scanning electron microscopy

TE - Tissue Engineering

TEM - Transmission electron microscopy

TGF- β1 - Transforming growth factor β1

UV - Ultraviolet

VEGF - Vascular endothelial growth factor

Chapter 1. Introduction

The evolution of science and technology has increased the human life expectancy. However, living longer brings consequences – tissues and organs start failing, cells may mutate and originate cancers and the immune system becomes weak allowing a simple flu to be deathly. To try to address these problems, tissue engineering and regenerative medicine seek to revolutionise the way medicine is undertaken. The possibility to promote tissue regeneration, produce tissues for replacements or increase the efficiency of drug screening tests, is the subject of much research, directed at using new techniques to closely mimic human body characteristics, resulting in a more biomimetic approach (Vacanti and Langer, 1999; Akter, 2016).

Two-dimensional (2D) cell culture systems have been reported to not be able to simulate the human environment. Gene expression, metabolic activity, cell physiology and morphology and spatial organization are all affected by cells being 2D rather than three-dimensional (3D), which present a major drawback when evaluating medicines and other substances (Edmondson *et al.*, 2014; Duval *et al.*, 2017). Lately, 3D cell culture techniques, such as spheroids, organoids, organs-on-chip or scaffold-based cell cultures, have been developed and show the ability to emulate natural cell-cell interactions on a much smaller scale (Di Maggio *et al.*, 2011; Huh *et al.*, 2011; Thoma *et al.*, 2014; Thakuri *et al.*, 2017; de Souza, 2018; Mosaad *et al.*, 2018; Vacanti and Langer, 1999; Huh *et al.*, 2011). However, these 3D cell culture systems present problems over reliability and repeatability, but also in terms of tissue complexity, which makes them not ideal for high-throughput applications (Friedrich *et al.*, 2007; Breslin and O'Driscoll, 2013; van Duinen *et al.*, 2015; Junaid *et al.*, 2017).

Since the commercialisation of the first automatic printers in the late 70's, printing technology has developed rapidly from 2D to 3D in which is used successive layers of material to form 3D shapes (Kolesky *et al.*, 2014; Murphy and Atala, 2014). This recent technology is revolutionising both industry, and the consumer sector, in the way the products are being produced - consumers may quickly fabricate their personalized products in a range just limited by machine and material characteristics – rapid prototyping (Rengier *et al.*, 2010). Researchers have been using 3D printers to develop cheaper, personalised and biocompatible scaffolds, or even modifying the 3D printing

technology to fabricate 3D functional living human tissue and organs – bioprinting (Mironov *et al.*, 2007; Sachs, 2016). This way, bioprinting allows to address the reported limitations of manual 3D cell culture systems.

After the first report and patent, accomplished by Boland and colleagues in 2003 (Wilson and Boland, 2003), bioprinting has seen constant progress, emerging as an influential field for biomedical research. Bioprinting involves additional complexity than 3D printing, as printed materials are made of biological matter. Through combining biocompatible materials, cells and growth and differentiation factors, the so-called bio-inks, microtissue production is one significant aim (Donderwinkel *et al.*, 2017). Inkjet microvalve, extrusion-based, and laser-assisted bioprinting represent the main strategies behind the field, however, each presents its very own advantages and limitations (Tasoglu and Demirci, 2013; Seol *et al.*, 2014). Nozzle clogging due to cell aggregation and not allowing high cell densities, slow process and low cell viability due to high shear stress, or low repeatability with high maintenance costs, respectively, are the main drawbacks of the technologies above (Murphy and Atala, 2014). Additional disadvantages are represented by the limited number of bio-inks currently available due to the material compatibility with cells and bioprinting techniques (Gudapati, *et al.*, 2016; Ozbolat and Hospodiuk, 2016; Hospodiuk *et al.*, 2017). These must obey tight characteristics, such as non-toxicity, mechanical integrity or controlled biodegradability rate.

Although very recent, the bioprinting field has developed quickly. Some flaws are still observed, namely in terms of the relationship between bio-inks and the equipment itself, which reduces the reliability and repeatability of the process. However, microtissues or organ-like structures, such as ears, muscle tissue, mini-livers, kidney's structures and brains have been developed during the last few years (Homan *et al.*, 2016; Kang *et al.*, 2016; Kizawa *et al.*, 2017; Thomas and Willerth, 2017; Grix *et al.*, 2018).

1.1 Aim and objectives of the work

This research has the aim to develop bio-inks to allow 1) reliable and repeatable inkjet bioprinting and 2) emulation of tissue complexity by manufacturing high-cell density microtissues through the reactive jet impingement (ReJI) process (a process developed at Newcastle University). Two major issues have been identified to accomplish the research purposed:

1) Inkjet bioprinting is limited by nozzle blockage originated from cell aggregation. These issues cause poor reliability of the process, short experiment times and only allows the use of low cell density bio-inks, which are not ideal for printing tissue-like structures.

2) High-cell density bio-inks are desirable for controllable printing of microtissues, however, not many bioprinting techniques allows this due to technical problems. Inkjet and microvalve are limited by nozzle blockage and respective low cell density bio-inks; extrusion-based bioprinting do not allow tight control of cell numbers, plus poor cell viability is evidenced when printing high-cell density bio-inks.

These problems have been addressed by formulating a novel polycationic coating-based bio-ink, that inhibits natural cell aggregation, and, this way, avoids nozzle blockage, allowing reliable and repeatable inkjet printing for at least 60 minutes. On the other hand, to produce controllable cell dense structures, a collagen-alginate-fibrin bio-ink and an in-house developed bioprinting technique (ReJI) were optimised and used to develop high and low cell density cell-laden hydrogels. This has clearly shown the importance of cell density on microtissue formation.

To achieve what is written above, the following objectives are stated:

1. Establishment of a single cell coating system to avoid cell agglomeration in bio-inks;
2. Evaluation of the effect of the coating system on cell function before and after inkjet bioprinting;
3. To study inkjet bioprinting reliability with and without cell coating as part of the bio-ink formulation;
4. Optimisation of the methodology for the biofabrication of high cell density collagen-alginate-fibrin hydrogels through ReJI;
5. Characterisation of the mechanical and biological properties of the produced cell-laden hydrogels.

1.2 Thesis structure

To accomplish the research objectives defined above, this thesis is divided in nine chapters.

The current **Chapter 1** provides an overall introduction to the theme, defining the aim and objectives to be obtained during this work. Additionally, it also highlights how the thesis is organised.

Chapter 2 reviews the literature behind the concepts that support the work developed in this thesis. It gives a general overview about tissue engineering and regenerative medicine and a brief insight on encapsulation systems, including cellular coatings. Finally, an in-depth cover of the different main bioprinting techniques, focusing on the processes, its bio-inks, limitations and applications, is also reviewed.

Chapter 3 reports the general methodology as well as original methods developed during this research. The coating technique, inkjet and reactive jet impingement bioprinting, hydrogel development and respective characterisation of the processes in terms of biological, functional and mechanical properties are described here.

The main results obtained during the experimental work are reported in **Chapters 4** and **5**. **Chapter 4** describes the performance of the developed single cell coating process. It also focuses on the application of the process to allow reliable and viable inkjet cell printing. Finally, **Chapter 5** presents the data acquired during the development of a new cell-laden hydrogel through an in-house printing technique for microtissue development. In each of these chapters, an interin discussion is included.

An overall discussion about the main findings is found in **Chapter 6**. Here, the novelty of this investigation is also examined. Finally, **Chapter 7** outlines the global conclusions of the research, including the limitations found and potential future improvements.

Chapter 2. Literature Review

2.1 Tissue Engineering

Autografts and allografts are common treatments when diseases or injuries heavily damage the human body. Although these strategies are often life-savers, they are also expensive and painful, being associated to infection or tissue rejection due to the host's immune system. Additionally, the recovery process is slow, being able to take several months, and are limited by donor availability (Khan *et al.*, 2008; O'Brien, 2011). Xenografts have also been used, however using animals as tissue and organ donors possesses several rejection challenges (hyperacute, acute vascular, cellular and chronic) with higher rejection level than allografts (Cascalho and Platt, 2008).

Tissue Engineering (TE) is a recent field that aims to i) avoid tissue replacement by developing innovative therapies to promote regeneration and create healthy and functional tissues and organs for grafting and transplantation and ii) to establish reliable *in vitro* models of tissues and diseases to foster therapeutic advancements (Ozbolat and Gudapati, 2016; Patra and Young, 2016). This scientific area brings together tools and knowledge of different scientific fields by combining cells, scaffolds and growth and differentiation factors (Figure. 2.1).

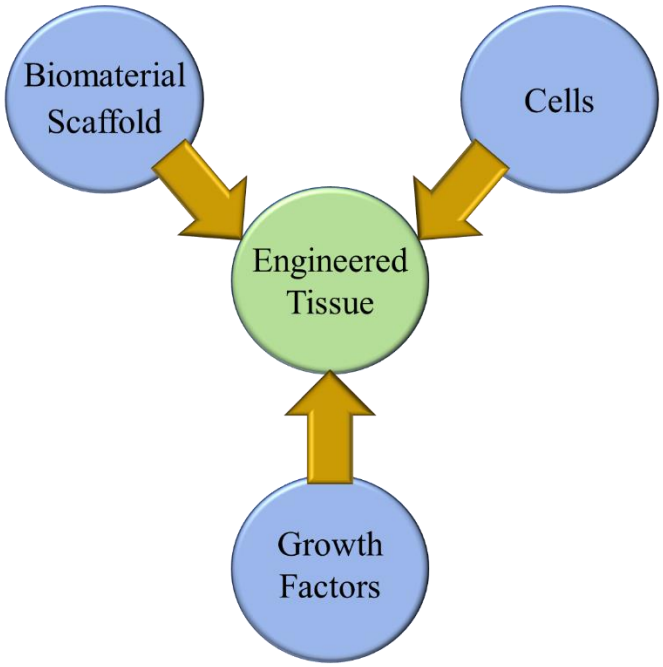

Figure 2.1 – The Tissue Engineering triad – Biomaterials, cells and growth factors.

Earlier, TE used different physical and chemical approaches (such as, salt-leaching or phase separation) to produce biomimetic three-dimensional structures, followed by cell entrapment inside the fabricated scaffold. . These constructs could be used and designed in three different ways: as support systems, i.e. solely offering topographical cues to the cells; fostering cell and tissue growth through the addition of biological cues, such as growth factors; or as a carrier for cell delivery behaving as a protective shell to avoid host immune reaction (Howard *et al.*, 2008; Garg *et al.*, 2012). However, although these solutions were able to produce simple engineered structures, these presented several limitations (Ikada, 2006; Place, Evans and Stevens, 2009; Cui, Boland, *et al.*, 2012; Nerem and Schutte, 2014; Vacanti and Vacanti, 2014):

i) Tissues with complex structures, such as organs, are constituted by different cell types with precise locations and organisation. Cell seeding by pipetting does not allow to accurate placement of cells into scaffolds.
ii) Scaffold production techniques offer little control over porosity, size or architecture, producing scaffolds with different properties in the same batch.
iii) Cell seeding into scaffolds does not allow homogenous cell distribution due to deficient seeding techniques and/or to poor scaffold designs.
iv) Uneven distribution of growth factors along scaffolds.
v) Lack of vascularisation, necessary for thick tissue survival.

These issues are responsible for the lack of complexity observed , but also for the reduced reliability and repeatability observed in these engineered systems.

Although the limitations pointed above slowed down the initial improvements observed in early TE, additive manufacturing (AM) was able to offer new strategies to the Tissue Engineering field (Morouço, Lattanzi and Alves, 2017). Three-dimensional biological structures were able to be produced by AM, via layered fabrication of 3D structures using biological inks – 3D Bioprinting. As it will be possible to observe during this literature review, 3D Bioprinting is able to overcome most of the constraints stated above by efficiently producing cell-laden constructs with architectural complexity and custom designs (Bishop *et al.*, 2017).

2.2 Bioprinting

Bioprinting is a computer-assisted technology that aims to precisely fabricate biological three-dimensional structures in an organised and optimised manner on a layer-by-layer basis, by depositing small droplets or filaments into specific substrates (Malda, 2011; Lee and Yeong, 2016). This technique has lately gained large importance due to its accuracy, efficiency and possibility for scaling-up, posing as a revolutionary technique to current healthcare problems (Dababneh and Ozbolat, 2014). Since first reported, bioprinting field has been gaining more attention year by year, with a constant increase on the number of publications in this field (Figure 2.2)

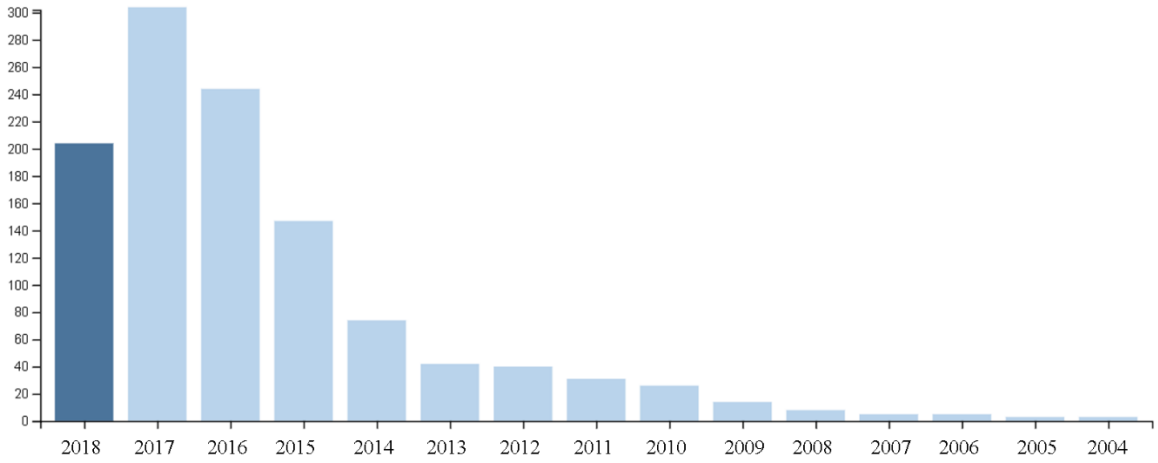

Figure 2.2 – Number of peer reviewed papers with the keyword “Bioprinting” listed at the ISI Web of Science.

Bioprinting aims to create mature tissues and organs for human replacement in the future (Mironov *et al.*, 2009). However, a myriad of challenges mean that it cannot achieve this yet. Organs present an accurately organised multi-cellular pattern, complex architecture and highly branched vascularisation networks that no technology is able to mimic nowadays (Miller, 2014; Murphy and Atala, 2014). Additionally, organs are constituted by cell densities not yet reproducible (Miller, 2014). Despite these limitations, bioprinting has been successfully applied to different areas: cancer research, drug screening, cardiovascular structures, cartilage, mini-organ assembly, and organ-on-chip, among others (Li *et al.*, 2016; Peng *et al.*, 2017; Yang, Lian and Xu, 2017; B. Zhang *et al.*, 2018). The possibility to reliably produce 3D models or tissues is already changing the

pharmaceutical industry by replacing the two-dimensional disease models, which are constantly reported by its poor capability on mimicking the human environment (Peng *et al.*, 2017; Combellack, Jessop and Whitaker, 2018).

Tissue engineering comprises three main strategies: 1) cell therapy; 2) scaffold-based approach; 3) cell-laden constructs. In the first, cells are delivered to the patient; in the scaffold-based approach, AM processes are used to produce 3D biocompatible and biodegradable porous scaffolds that will be seeded with cells; finally, AM processes are used to print bioinks – bioprinting – to produce cell-laden constructs (Pereira and Bartolo, 2015). Four main bioprinting technologies are used: microvalve bioprinting, inkjet bioprinting, extrusion-based bioprinting and laser-assisted bioprinting (Figure 2.4) (Chua and Yeong, 2014; Murphy and Atala, 2014; Seol *et al.*, 2014). Each technique presents unique characteristics that make them more suitable for certain applications than others (Table 2.1).

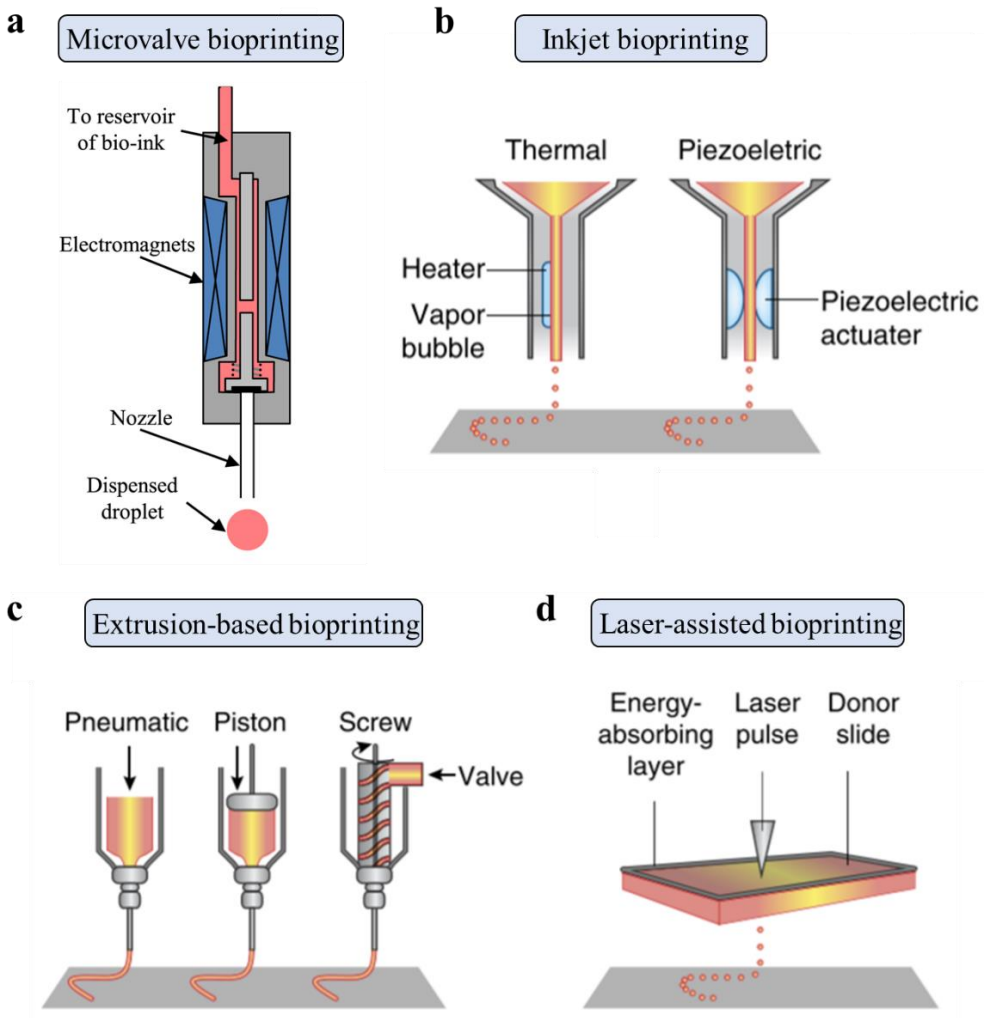

Figure 2.3 – **a** Microvalve bioprinting; **b** Inkjet bioprinting; **c** Extrusion-based bioprinting; **d** Laser-assisted bioprinting. Adapted from (Shu, 2013; Murphy and Atala, 2014).

Bioprinting highly relies on biomaterial(s) and cell(s) selection that will be dependent on the tissue engineering application. Once selected, these are normally mixed into one single solution, forming a bio-ink. Bio-inks must be tailored-specific to each bioprinting technique, as the working principles differ from each other, and must fulfil rigorous specifications to be used in bioprinting: rheology, gelling speed, printability, degradation kinetics and bi-products, among others (Dai *et al.*, 2017; Ji and Guvendiren, 2017; Gungor-Ozkerim *et al.*, 2018). This way, the number of materials possible to be used in bioprinting is highly limited. For example, viscosity significantly controls the shear stress suffered by cells when leaving the printing nozzle, which is determinant on cell viability (Ovsianikov, 2016). Printing cells impose strict requirements to minimise cell death,

therefore, all the non-necessary stimulus, mechanical forces and crosslinking processes must be discarded. If extra manipulation is necessary, this must be carefully studied not only in terms of cell viability, but also cell behaviour may be affected, leading to unexpected outcomes.

Table 2.1 – Comparison between advantages and disadvantages of different bioprinting technologies.

Bioprinting technique	Advantages	Disadvantages
Inkjet Bioprinting	Allow concentration gradients; Accuracy; Versatility; Easy to modify; Low cost; Resolution; High drop deposition rate; Ejection of single cells; Non-contact printing; Substrate independent; Reported to produced high cell viability.	Reported to produce low cell viability; Limited number of materials; May only use low viscosity bio-inks; Low cell concentration (<$5x10^6$ cells/mL); Unreliable due to frequent nozzle blockage; Needs crosslinking; Fast droplet drying due to reduced size.
Microvalve Bioprinting	Accuracy; Viability; High drop deposition rate; Non-contact printing; Substrate independent; Low cost.	Limited number of materials; May only use low viscosity solutions and hydrogels; May be unreliable due to nozzle blockage; Needs crosslinking.
Extrusion-based Bioprinting	Most versatile bioprinting technique; High range of materials; High volume deposition rate; High cell densities.	Low viability; Nozzle blockage due to ink solidification; Bio-inks must grant fast gelation kinetics; Hardware issues; Slow process.
Laser-assisted Bioprinting	Allow concentration gradients; Accuracy; Resolution Ejection of single cells; No nozzle blockage or shear stress; High cell densities; High range of viscosities.	Expensive; Very slow; Bio-inks must grant fast gelation kinetics; Laser irradition may affect cells.

The following pages of this literature review aim to present the technologies, bio-inks and biomaterials used in the bioprinting field.

2.2.1 *Inkjet bioprinting*

Inkjet bioprinting is a bioprinting method that allows accurate deposition of cells and materials. This technique was originally developed by improvements on the widely used

2D inkjet printing, which is normally associated to a computer-based text printing method (Saunders and Derby, 2014). The 2D inkjet ink is substituted by a mixture of biomaterials, cells and cell factors (called bio-ink) and the paper by a computer-controlled moving stage that allows precise *xyz* movement. Inkjet bioprinters have been widely used to impinge different biological materials, such as cells, enzymes, DNA or proteins (Campbell and Weiss, 2007).

Inkjet bioprinting is sub-divided in three methods: electro-hydrodynamic jet bioprinting, continuous inkjet bioprinting and drop-on-demand inkjet bioprinting (Gudapati, Dey and Ozbolat, 2016). Only drop-on-demand will be reviewed as the latter category is the most used technology among research groups. Drop-on-demand inkjet bioprinting includes thermal or piezoelectric inkjet bioprinting (Figure 2.5).

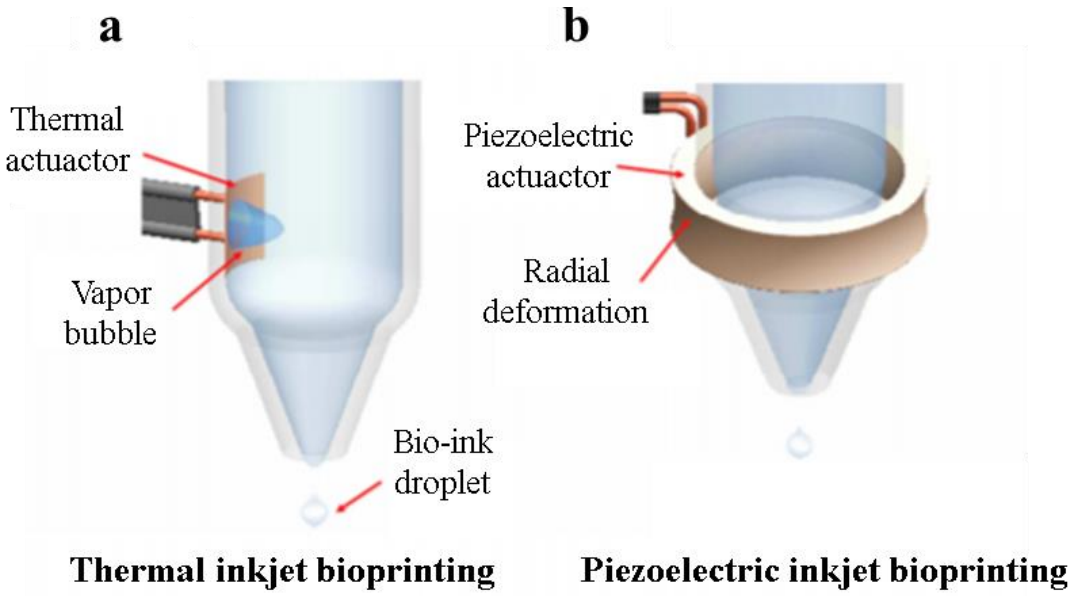

Figure 2.4 – Drop-on-demand inkjet bioprinting: **a** thermal, **b** piezoelectric inkjet bioprinting. Adapted from (Gudapati, *et al.*, 2016).

The first comprises an electrical thermal actuator located in the printhead that once generating heat will form small air bubbles that produce pulses of pressure by collapsing. The bio-ink is then ejected from the fluid chamber through the nozzle by overcoming the surface tension at the orifice (Cui *et al.*, 2012; Seol *et al.*, 2014; Ozbolat and Hospodiuk, 2016). The volume dispensed ranges from 10 to 150 pL (Cui *et al.*, 2012; Saunders and Derby, 2014; Iwanaga *et al.*, 2015). The thermal printheads heat during short periods, around 2 µs, ranging high temperatures from 200°C to 300°C (Cui *et al.*, 2012;

Ovsianikov, 2016; Bishop *et al.*, 2017). Although reaching extremely high temperatures the impact is normally described to be low as cells only feel an increase of 4°C−10°C, with cells retaining their functionality, phenotype or proliferation capacities, with high cell viability (Cui *et al.*, 2012; Cui *et al.*, 2012; Jose *et al.*, 2016; Bishop *et al.*, 2017). However, several research groups report that the thermal stress induced by the short heating is enough to negatively affect the cells, by originating damage or cell death (Xu *et al.*, 2006, 2013). This way a careful study on apoptosis, cell membrane pore size or heat-shock proteins expression is suggested to evaluate the potential damage (Derby, 2008; Cui *et al.*, 2012; Saunders and Derby, 2014). Droplet size may vary not only due to the nozzle diameter, but also due to the pulse frequency, cell concentration, ink viscosity and temperature gradient (Cui *et al.*, 2012; Derakhshanfar *et al.*, 2018).

In piezoelectric inkjet bioprinting, a piezoelectric actuator mediates the droplet formation. The electrical impulse generates a contraction and expansion of the actuator, causing a deformation in the fluid chamber and resulting in a pressure wave. This pressure change leads to uniform droplet ejection by overcoming the surface tension at the nozzle (Singh *et al.*, 2009; Li *et al.*, 2015). Contrary to the thermal technology, due to the lack of heating and by supplying alternating voltage at a chosen frequency, the piezoelectric system produces directional and equal size droplets (Nakamura *et al.*, 2005; Saunders *et al.*, 2008; Lee and Dai, 2015). Additionally, controlled cell numbers are able to be deposited in the substrate (Ribeiro *et al.*, 2017). These allow to create accurate concentration gradients, representing an advantage on the use of this technology in *in vitro* studies, as well as, drug discovery and diagnostics (Miller *et al.*, 2009; Jose *et al.*, 2016; Hong *et al.*, 2017). Parameters of the piezoelectric inkjet bioprinting include the voltage pulse characteristics (amplitude, rise and fall times, dwell time, echo time, and frequency), nozzle diameter and bio-ink viscosity (Fauzia *et al.*, 2010; Christensen *et al.*, 2014; Murphy and Atala, 2014; Ribeiro *et al.*, 2017). Some studies report that the movement and vibration frequencies may cause cell membrane damage, leading to lysis (Borthwick *et al.*, 2005). However, other teams show that viability is barely affected by inkjet process (Saunders *et al*., 2008; Martin, 2014; Smith, 2016). Additionally, lower voltage pulses with bigger dwell and rise/fall times are recommended in detriment of using high pulse amplitude and short dwell and rise/fall times, as the second increases the shear stress that cells suffer (Saunders and Derby, 2014).

Regarding the advantages, inkjet bioprinting present high versatility, being able to be easily modified, and are low cost, when comparing to the other bioprinting techniques. They are fast and present high resolution due to the high drop deposition rate (1-10000 droplets per second) and to the low-volume droplet generation, ranging from 1 to 300 pL (Miller *et al.*, 2009; Nair *et al.*, 2009; Jones, 2012; Jana and Lerman, 2015; Li *et al.*, 2016). The possibility to tightly control the droplet position allows to create gradients, precise patterns and ejection of single cells (Roth *et al.*, 2004; Liberski *et al.*, 2011; Park *et al.*, 2017). *In situ* bioprinting poses as an interesting application for inkjet bioprinting as there is no need for immovable substrate and this does not need to be flat, being able to present any conformation (Binder *et al.*, 2010; Skardal *et al.*, 2012). Cells are reported to be printed with high viability, however, some studies identify thermal and mechanical stress as two inkjet bioprinting properties that may increase cell death (Cui *et al.*, 2012; Blaeser *et al.*, 2015; Jose *et al.*, 2016).

However, inkjet bioprinting is limited by the reduced number of compatible biomaterials for bio-ink composition. Inkjet printing bio-inks must be presented in the form of a liquid solution, with low viscosity, otherwise viscous solution will block the nozzle and cause high shear stress to cells (Dababneh and Ozbolat, 2014; Murphy and Atala, 2014; Wu *et al.*, 2016; Bishop *et al.*, 2017). Consequently, the printed droplets lack structure, rigidity or mechanical properties. Crosslinking techniques are commonly used after printing to confer the desired properties (Ovsianikov, 2016; Hong *et al.*, 2017). Crosslinking can be chemical, photo, thermal and pH crosslinking (Saunders and Derby, 2014; Iwanaga *et al.*, 2015; Jose *et al.*, 2016). The first is characterised by the combination of two or more substances that once mixed form a solid (Arora *et al.*, 2017). Photocrosslinking uses a light source (UV, IR or visible) instead (Cui *et al.*, 2012). Materials that change their properties with temperature use thermal crosslinking (Ji and Shi, 2013). Finally, pH crosslinking is used when changing the material pH (Yoon *et al.*, 2016). However, the need for crosslinking constitutes an extra step, slowing down the bioprinting and due to the nature of the process, being able to modify natural extracellular matrix (ECM), changing their chemical and physical properties (X. Wang *et al.*, 2017a). The crosslinking technique must be carefully chosen as some required conditions and materials are often toxic to cells, limiting their functionality and viability (Hennink and van Nostrum, 2002; Delgado *et al.*, 2015). Crosslinking may occur before or after the printing process (Ovsianikov, 2016; Pereira *et al.*, 2018).

Another drawback of inkjet bioprinting is cell sedimentation. This limits the cell density able to be used within this technology, as cell sedimentations leads to nozzle blockage (Dababneh and Ozbolat, 2014; Murphy and Atala, 2014; Mandrycky *et al.*, 2016). Hence, physiological cell densities, which are desirable for tissue printing, are not possible to be processed. Nozzle blockage results in an unreliable process that causes deficient droplet formation and high shear stress, damaging cells. To overcome this issue, some groups have added surfactants and other materials to neutralise the bio-ink buoyancy (Cheung, 2010; Chahal *et al*. 2012; Ferris *et al.*, 2013). However, this addition may cause negative effects in cells due to the potential toxicity of these compounds (Jose *et al.*, 2016). Disadvantages also include the fast droplet drying due to the low volume (Iwanaga *et al*., 2015). This way, fast crosslinking after printing or droplet deposit in aqueous media are required to avoid cell damage. However, using aqueous solutions, all the resolution will be lost as drops will get mixed with the watery medium (Nishiyama, 2010).

In terms of applications, Xui and colleagues modified an office thermal inkjet printer to fabricate cartilage tissue *in situ*. Using a poly(ethylene glycol) dimethacrylate (PEGDMA) with human chondrocytes solution, defects in osteochondral plugs were successfully repaired. High glycosaminoglycan production and conserved cell phenotype were observed after printing and respective crosslinking. Printed cells originated cartilaginous tissue with high host tissue integration. This group also observed the importance of growth factors on bioprinted constructs. The treatment with fibroblast growth factor-2/transforming growth factor β1 (FGF-2/TGF-β1) promoted cell proliferation and ECM production increasing the regeneration speed (Cui *et al*., 2012). Boland and his team fabricated a small vascular network using thermal inkjet printing. Here, the researchers modified a commercial inkjet printer and using a fibrin hydrogel, cells were deposited successively. 3 weeks later, cells had fused to each other, creating small vessel-like structures (Cui and Boland, 2009). Using a modified thermal inkjet printer, Xu and colleagues developed a drug screening array. Different antibiotics were tested in bioprinted bacteria entrapped inside alginate hydrogels and compared to common micropipetting technique. Bioprinting produced similar results to the micropipetted bacteria, however it has shown to be a high-throughput technique being able to print 213 assays per second (Xu, 2012). Kim and researchers verified that importance of piezoelectric inkjet printing on accurate *in vitro* studies for cell-cell communication. Colony size, spacing distance, printing timing and patterns were

observed to be the most important governing factors on cell-cell communication (Choi *et al.*, 2011). Atala et al used a commercial inkjet printer to fabricate a multi-cell construct encapsulated in a collagen-alginate hydrogel. Cells from different species were used - human amniotic fluid-derived stem cells (hAFSCs), canine smooth muscle cells (dSMCs), and bovine aortic endothelial cells (bECs). Cells were viable, proliferative and conserved phenotype. Normal electrophysiological behaviour was observed in dSMCs and vasodilation was noted on bECs. hAFSCs were able to osteogenic differentiate and vasculature was obtained after *in vivo* implantation (Figure 2.6**a**) (Xu *et al.*, 2013). Akashi and colleagues developed a high-throughput array of 3D human tissues for screening. Using a layer-by-layer (LbL) approach, layers of cells were separated by fibronectin-gelatin films to recreate native ECM. High viability and hepatocellular functions were observed, as well as cell-cell interaction (Figure 2.6**b**) (Matsusaki *et al.*, 2012). Markwald and colleagues used a piezoelectric inkjet printer to produce zigzag tubes through an overhanging strategy. Using a sodium alginate (NaAlg) cell-loaded bio-ink, droplets were printed into a calcium chloride ($CaCl_2$) bath for instant crosslinking forming a tube with a complex shape. This group concluded that cells survived to this process and the developed strategy may constitute an advancement for complex microvasculature printing (Figure 2.6**c**) (Xu *et al.*, 2012). Similarly, Huang and colleagues, have developed branched and hollow vascular-like structures using inkjet bioprinting. High cell viability was confirmed after printing the complex structures (Christensen *et al.*, 2014).

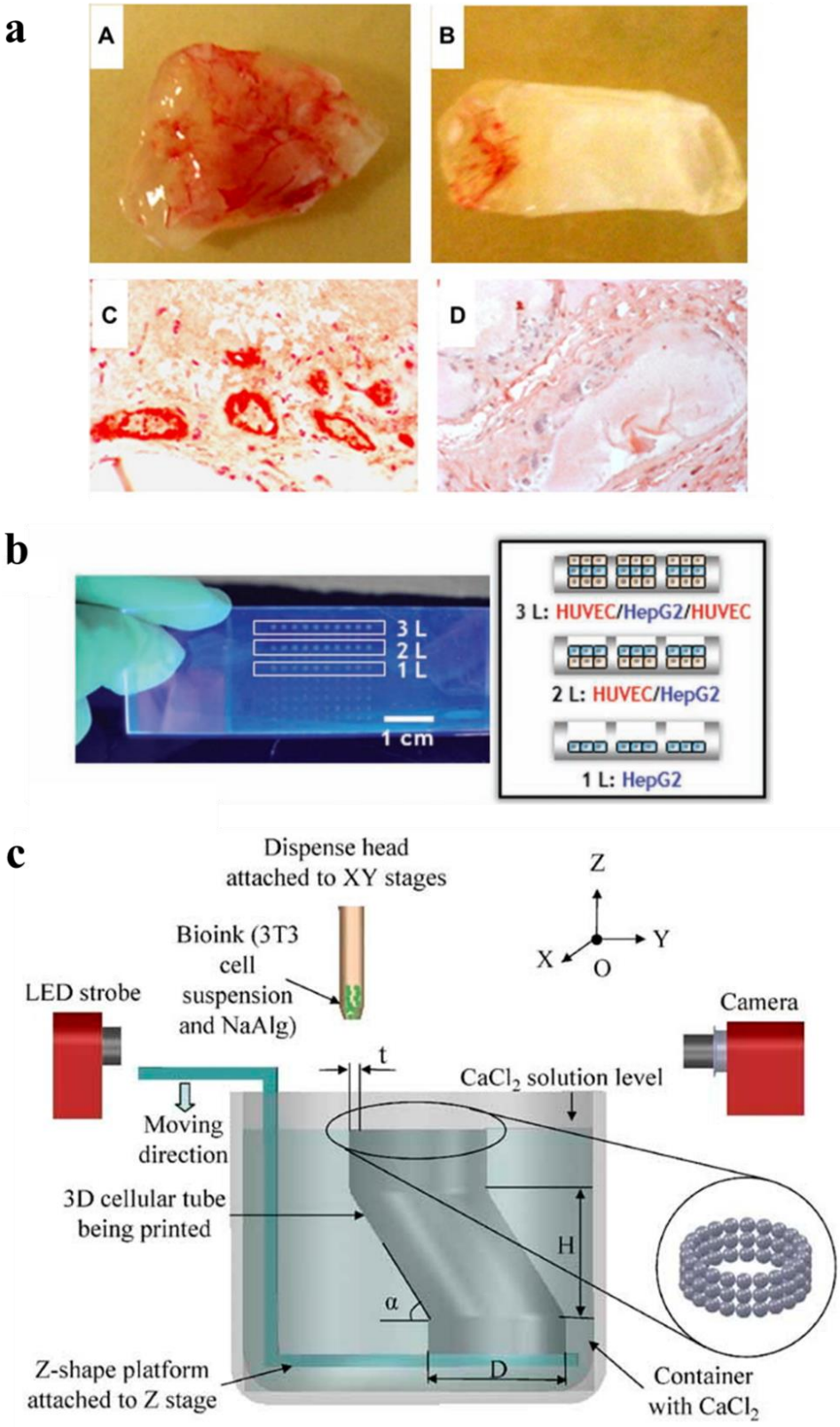

Figure 2.5 – **a** Vascularisation of the printed cell construct; **b** 3D bioprinted human tissue array; **c** methodology used to obtain zigzag hollow vasculature tubes. Adapted from (Matsusaki *et al.*, 2012; Xu *et al.*, 2012, 2013).

2.2.2 *Microvalve bioprinting*

Microvalve bioprinters are composed by a computer-controlled stage and a certain number of microvalve printheads (Lee *et al.*, 2009). Each microvalve is individually connected to a (positive) pneumatic pressure system and to a power supply, both responsible for droplet ejection (Ng *et al.*, 2017). Once voltage is applied (Figure 2.7), a magnetic field is induced in the solenoid coil, pulling the plunger up and opening the nozzle orifice, controlling the time the orifice is opened and closed (Figure 2.8) (Gudapati *et al*., 2016; Ng *et al*., 2016; Ng *et al.*, 2017). A reservoir contains the bio-ink that flows to the microvalve when the pneumatic pressure is able to overcome the fluid surface tension. By carefully controlling the valve opening time and the pneumatic system, microvalve bioprinting can generate droplets by two modes: continuous jetting or droplet-on-demand (Gudapati *et al*., 2016; Suntornnond *et al*., 2016).

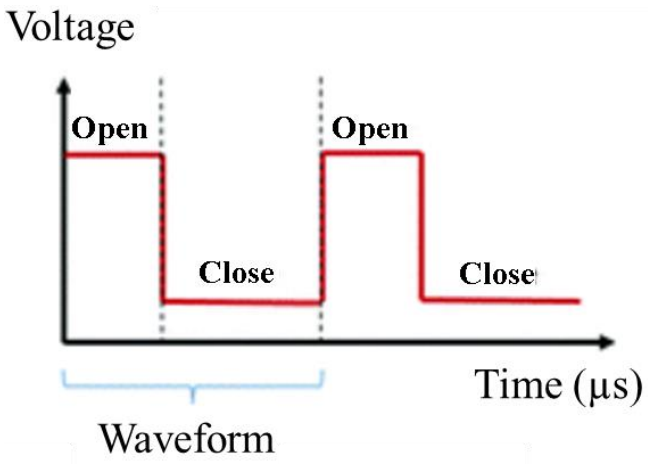

Figure 2.6 – Microvalve typical electrical waveform. Adapted from (Ng *et al.*, 2017).

The bio-ink deposition is dependent on the rheological properties of the fluid, the nozzle size, the pneumatic pressure, cell concentration and the applied voltage pulse (Shu, 2013). These parameters must be optimised for each specific bio-ink. The deposition of viscous solutions is possible by increasing the valve opening and closing time and increasing pneumatic pressure (Sun *et al.*, 2009). However, droplet generation will stop when the printability range is exceeded. Additionally, increased valve opening and closing periods will induce satellite droplet formation (Sun *et al.*, 2009). On the other hand, if pressure is below the minimum necessary for droplet ejection, a considerable droplet will be formed

on the nozzle orifice. This happens when the pneumatic pressure is not able to overcome the fluid surface tension (Ng *et al.*, 2017).

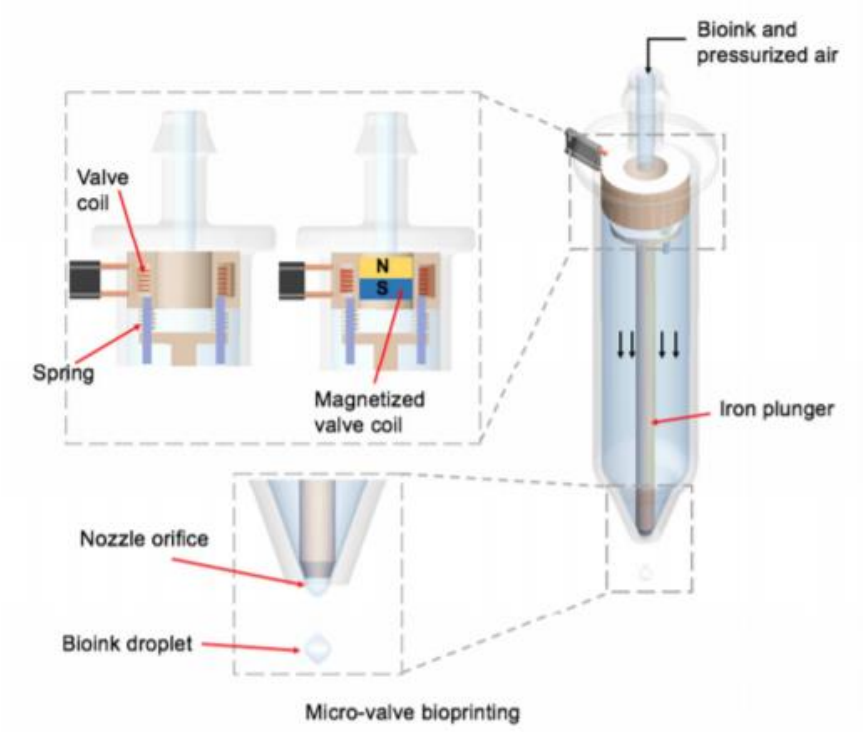

Figure 2.7 – Microvalve composition and working principle. From (Gudapati, Dey and Ozbolat, 2016).

Although producing droplets with higher diameters (50–300 µm) when compared to other bioprinting techniques, such as inkjet or laser-assisted bioprinting, accuracy and high-throughput are evidenced when using microvalves (Gudapati *et al.*, 2016; Ng *et al.*, 2017). The concept behind this technique and the increased nozzle diameter allows materials with higher viscosities (~1 to 200 mPa/s) and reduced nozzle blockage when compared to inkjet printing. However, despite reduced, cell sedimentation is still a problem noted when using microvalves (Lee *et al.*, 2009, 2013). Nozzle size is an easy way to control the droplet diameter, however prior studies have noted that smaller diameters have narrower opening and closing times, which will have an implication on the number of materials able to be jetted using small diameter nozzles (Ng *et al.*, 2017). Microvalve bioprinting grants high cell viability due to the gentle fluid releasing system (Shu, 2013; Horváth *et al.*, 2015). Also, prior studies evidenced that microvalve bioprinting did not affect cell functionality, genotype or phenotype, as well as

differentiation capacity (Shu, 2013). Moreover, the lack of complexity makes this technology user-friendly.

Microvalve bioprinting has been widely applied in tissue engineering. In 2015, Shu and colleagues reported the first microvalve bioprinting using human induced pluripotent cells cells (hiPSC), showing that this technology did not affect these cells not only in terms of viability, but also regarding their pluripotency capability. The latter was observed by comparing control hiPSC with bioprinted iPSC for different biomarkers. Additionally, human embryonic stem cells (hESC) and hiPSc were differentiated into hepatocytes and the fabricated cell-laden alginate hydrogels showed to allow cells to retain their hepatic function (Shu, 2015). Skardal and his group demonstrated growth of skin tissue from a culture made using an in-situ microvalve bioprinter (Figure 2.9**a**). A cell-laden collagen and fibrinogen solution were deposited alternately with thrombin solution to form a hydrogel to cover the wound in the back of murines. Two different cell types were studied in order to compare its regenerative properties – amniotic fluid-derived stem cells (AFSCs) and mesenchymal stem cells (MSCs). Both cell types were comparable and accelerated the healing process, resulting in wound contraction, re-epithelisation and neovascularisation. Ng's team also worked in skin by fabricating 3D human pigmented skin constructs from keratinocytes, melanocytes and fibroblasts. High similarity between the obtained constructs and native skin was observed by the different characterisation techniques. This highlights how useful this kind of system can be for drug testing and other *in vitro* assays (Skardal *et al.*, 2012).

The reliability and consistency of microvalve printing has been shown by Okubo and colleagues. When comparing with manual pipetting, bioprinting with an agitator showed highly reduced coefficient of variance, from 23.9 – 34.7 to 8.3 – 9. Additionally, viability was observed to remain high. This study clearly shows the importance of microvalve bioprinting for *in vitro* assays (Okubo *et al.*, 2016). Cartilage has been fabricated by Gurkan's team by printing hMSCs in a gelatin methacrylamide (GelMA) and growth factors solution. To improve the mechanical strength and give structure, ultraviolet (UV) crosslinking was carried after printing. Cell organisation showed to mimic native fibrocartilage with hMSCs showing simultaneous upregulation of osteogenic and chondrogenic genes (Gurkan *et al.*, 2014). Rothen-Rutishauser and colleagues have engineered 3D air-blood tissue barrier to mimic lung tissue (Figure 2.9**b**). By adapting a layer-by-layer approach using three distinct layers, two cell layers using alveolar

epithelial type II cells and endothelial cells and a middle one composed by matrigel. The group observed that the microvalve bioprinted model resembled the structure and functionality of the native tissue. Additionally, manual co-cultures were compared to the bioprinting ones, showing poor structure and, therefore, deficient cell-cell interaction. Microvalve bioprinting was also used to produce neural tissue models (Horváth *et al.*, 2015). Yoo (2010) and his colleagues produced a layered construct made of collagen, fibrin and murine neural stem cells to study neuronal migration (Figure 2.9**c**). After printing each gel-precursor (collagen precursor and fibrinogen) was crosslinked. The neural stem cells were stimulated by the addition of vascular endothelial growth factor (VEGF) in the fibrin hydrogel promoting cell migration and proliferation successfully (Lee *et al.*, 2010).

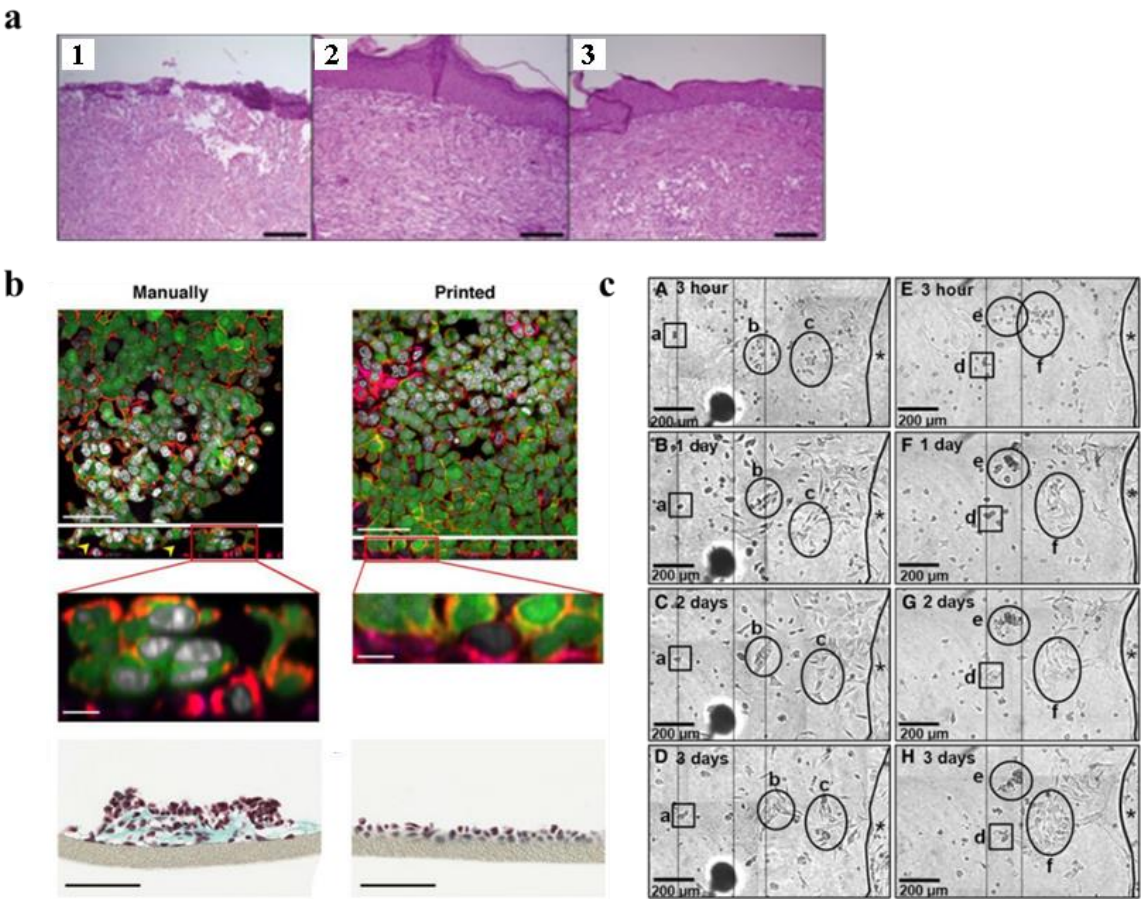

Figure 2.8 – **a** Deficient re-epithelialization without bioprinting (1) and well-defined epithelium after using cell printing (2 and 3); **b** Bioprinted structures presented a microenvironment similar to the native one, while manually seeded cells resulted in thick layers of cells; **c** VEGF supported cells migration towards fibrin gels when encapsulated

in a collagen construct. Adapted from (Lee *et al.*, 2010; Skardal *et al.*, 2012; Horváth *et al.*, 2015).

2.2.3 *Extrusion-based bioprinting*

Extrusion-based bioprinting (EBB) was originally developed as an AM technique for industrial applications, such as shape-specific fabrication of plastic (Ozbolat and Hospodiuk, 2016). The introduction of this AM technology into the TE field allowed to fabricate tailor-made scaffolds to study cell behaviour in specific 3D constructs (Hutmacher *et al.*, 2001; Zein *et al.*, 2002; Hollister, 2005). The use of this AM technique combined with hydrogels and cells (bio-inks) brought promising results, contributing to the fast dissemination of the extrusion technology and attracting research groups that lead to advances in the bioprinting field.

This bioprinting technology is the most widely used bioprinting technique. Here, a computer-controlled dispensing system allows precise cell-laden filaments to be deposited in 3D custom-shaped constructs onto a mobile or immobile stage (Murphy and Atala, 2014; Seol *et al.*, 2014; Ozbolat and Hospodiuk, 2016). Furthermore, apart the components mentioned above, some systems also include a photoinitiator, such as an UV source, to aid on the material gelation (Murphy and Atala, 2014). To form 3D structures, a layer-by-layer approach is followed, i.e. after the solidification of the first layer, a new one is deposited on the top of it (Li *et al.*, 2016; Ning and Chen, 2017).

Extrusion-based technology uses pneumatic or mechanical (piston or screw-based) systems to extrude the material filaments (Figure 2.10) (Chang *et al.*, 2011; Malda, 2013; Bertassoni *et al.*, 2014; Skardal *et al.*, 2015; Liu *et al.*, 2017). Each technique uses a different driving force: pneumatic systems use air pressure, while vertical and rotation mechanical forces are responsible for pulling the material through the nozzle on piston and screw-based bioprinting, respectively (Derakhshanfar *et al.*, 2018). Comparing the systems, it is reported that pneumatic-based bioprinting provides tighter control over the material extrusion by defining the pulse frequency, i.e. the valve opening time, and the air pressure provided by the pneumatic system (Ozbolat and Hospodiuk, 2016). Additionally, the delay of the compressed air volume demonstrates to better control the material flow (Murphy and Atala, 2014; Ovsianikov, 2016; Hong *et al.*, 2017). Regarding the mechanical-based extrusion bioprinters, the piston and screw-based extrusion provides

more spatial control, since their parts can be managed electronically, and higher deposition forces allow highly viscous solutions to be easily printed (Malda *et al.*, 2013; Murphy and Atala, 2014; Hong *et al.*, 2017). However, the latter may produce pressure drops along the nozzle or needle that results in a shear stress increase and potential harm to the cells and is more susceptible to malfunctions due to its complex parts (Dababneh and Ozbolat, 2014). The printing process is controlled by several parameters, such as the bio-ink viscosity and flow rate, the applied pressure and the nozzle shape and size (Ozbolat and Hospodiuk, 2016; Jungst, 2017; Webb and Doyle, 2017). By carefully optimising these specifications it is possible to control the amount of deposited bio-ink.

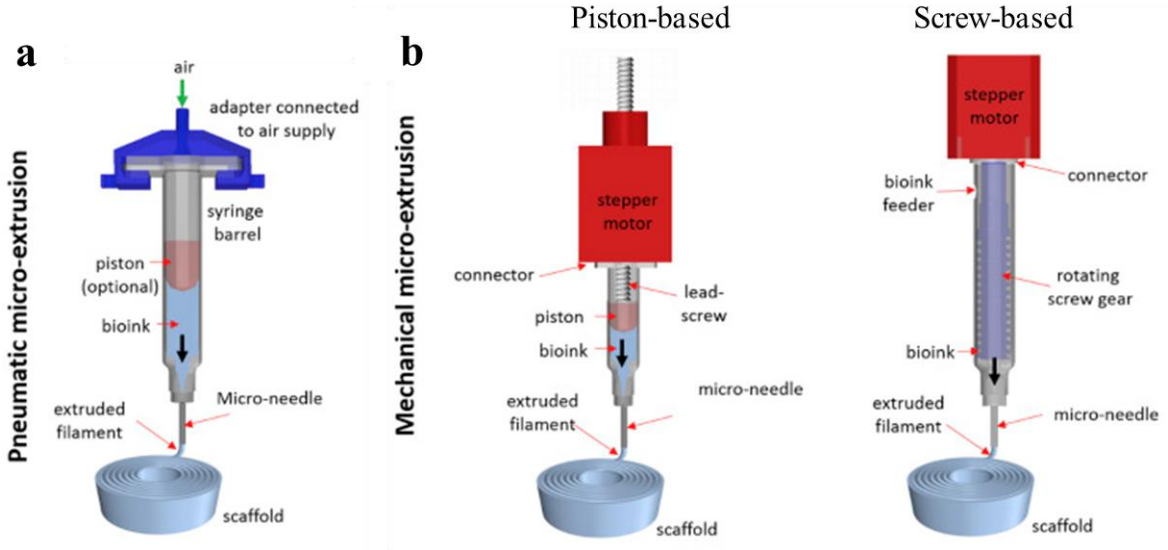

Figure 2.9 – Extrusion-based bioprinting. **a** Pneumatic and **b** mechanical extrusion-based bioprinting. Adapted from (Ozbolat and Hospodiuk, 2016).

Different printing strategies are possible to be adopted when using this bioprinting technology. The first is based on the extrusion of a highly viscous cell-laden solutions that manage to directly form 3D constructs due to the rheological properties (Seol *et al.*, 2014; Thayer *et al.*, 2018). However, this procedure is responsible for low cell survival as high shear and extensional stress is produced during the extrusion of the bio-ink (Chang *et al.*, 2008; Nair *et al.*, 2009). To reduce the cell damage, less viscous cell-laden solutions are used and combined with gelation methods to provide shape fidelity and mechanical integrity to the 3D construct (Ahn *et al.*, 2015; Skardal and Atala, 2015; Derakhshanfar *et al.*, 2018). Different gelation mechanisms are normally used, such as physical (e.g., temperature), chemical (e.g. ionic) or photo-crosslinking (e.g. UV source)

(Axpe and Oyen, 2016; Liu *et al.*, 2017; Suntornnond *et al.*, 2017; X. Wang *et al.*, 2017b; Li *et al.*, 2018). Extrusion-based bioprinting also allows cell agglomerates to be printed successively in a certain pattern. These are able to fuse over time and form complex structures (Norotte *et al.*, 2009; Yurie *et al.*, 2017; Q. Zhang *et al.*, 2018).

Extrusion-based bioprinting is the most versatile bioprinting technique allowing to print a high range of viscosities (30 mPa/s to 6×10^7 mPa/s) and, this way, different types of materials can be used, from hydrogels to copolymers, micro-carriers or cell spheroids (Khalil and Sun, 2009; Mironov *et al.*, 2009; Mateos-Timoneda, 2014). High cell densities are also managed to be printed, contributing to a faster formation of neotissues (Murphy and Atala, 2014; Suntornnond *et al.*, 2016). The emergence of a number of companies, such as CELLINK or Allevi, turned screw and piston-based systems portable, affordable and user-friendly, without needing an air compressor unit or other accessories (Choudhury *et al.*, 2018). On the other hand, pneumatic-based technologies allow to achieve higher accuracy and precision than the latter, despite increasing the equipment cost (Ozbolat and Hospodiuk, 2016).

However, the number of different challenges and limitations are a downside on extrusion-based bioprinting. The most challenging parameter is related to the bio-ink viscosity as it not only affects the process itself as it has capital importance on cell survival (Murphy and Atala, 2014; Ozbolat and Hospodiuk, 2016). The bio-ink must have sufficient viscosity in a way that overcomes the surface-tension-driven droplet formation. Otherwise, straight filament printing will not be possible. High viscosity is also related to nozzle blockage (Ozbolat and Hospodiuk, 2016). Bio-ink solidification inside the nozzle, as well as cell agglomerate formation are responsible for not allowing the cell-laden material to correctly flow through the nozzle. Viscosity is also bounded to the stress that cells are subjected during printing (shear stress and extensional stress) that affect not only their viability, but also their functions (Gupta *et al.*, 2006; Yourek *et al.*, 2010; Wolfe and Ahsan, 2013). During the printing process, the cell-laden bio-ink is forced to flow through the nozzle or needle. This movement deforms the cells until a limit that membrane disruption may happen and cause cell death. Even if the latter does not happen, cells may not be able to recover from the deformation suffered, causing non-expected behaviours (Fletcher and Mullins, 2010). More viscous solutions demand higher driving forces that increase the stress that, consequently, will cause more damage to the cells (Chang *et al.*, 2008; Murphy and Atala, 2014). Billiet and colleagues have observed that cell damage is

increased when subjecting to lower stress during increased amounts of time, when compared to when exposed to considerable stresses during short periods of time (Billiet *et al.*, 2014). Extensional stress is also an issue on extrusion bioprinting. This happens when there is a sudden change in the nozzle geometry as the bio-ink is flowing through it (Ning and Chen, 2017). Studies have shown that extensional stress causes higher cell death than shear stress. To reduce the impact of stress in cells, the nozzle shape must be carefully designed to minimize the extensional stress. The nozzle material must also be precisely selected due to the friction coefficient, which regulates the shear stress caused by the bio-ink flow (Ozbolat and Hospodiuk, 2016). Moreover, low viscosity and shear thinning bio-inks should be used instead of viscous materials as they allow to lower the dispensing pressure, reducing the stress caused to cells (Guvendiren *et al.*, 2012; Ovsianikov, 2016). Increasing the nozzle orifice diameter is also a measure to attenuate the issues reported.

For the reasons above, different studies report low cell survival using this technology, ranging from 40% to 80%, with viability decreasing with increasing pressure (Chang *et al.*, 2008; Atala, 2015). However, others refer that extrusion-based bioprinting causes little cell harm, when compared to other techniques (Gao *et al.*, 2018). Additionally, extrusion-based bioprinting has generally low resolution, with a minimum reported to be over 100 µm (Murphy and Atala, 2014). Despite extrusion-based bioprinting allow more materials than the other bioprinting techniques, still the number of materials that can be applied is also a concern as fast gelation kinetics are required for cell encapsulation and stack successive layers (Derakhshanfar *et al.*, 2018).

Other disadvantages are related to hardware issues (Ozbolat and Hospodiuk, 2016). The air used in the pneumatic microextrusion bioprinting must be sterile to prevent contaminations. To minimise this issue, filters are normally used. On mechanical-based technologies, it is possible to autoclave several nozzle component parts, keeping the printing environment sterile. Mechanically driven extrusion bioprinters must have their extrusion parts carefully checked before printing, otherwise malfunctions may cause additional friction forces or leakage of bio-ink, for example.

Extrusion-based bioprinting has been widely used in different scientific works. Kang and colleagues developed a dual bioprinter that combined the fused deposition modelling and extrusion bioprinting in one machine (Figure 2.11**a**). The first technique offers a support structure to the construct, working like a skeleton, being then filled by the hydrogels and

sacrificial inks extruded from the second technique. By developing sophisticated nozzles, using fast-crosslinking materials and using sacrificial materials to create microchannels for nutrient and oxygen diffusion, human-scale mandible bone, ear-shaped cartilage and organized skeletal muscle were obtained. Additionally, a calvarial bone defect was reconstructed. Clinical image data was used to obtain relevant human structures. The different engineered tissues presented high cell viability, as well as the desired functionality. These authors developed an equipment that is able to fabricate human complex structures with mechanical integrity. The in vivo application of the designed structures showed to mimic the native functionality of the tissues, as it is represented by the tissue maturation observed in the application to the calvarial defect filling and by the formation of highly orientated myofiber bundles on the muscle tissue application (Kang *et al.*, 2016). Similarly to Kang and colleagues, Pati et al developed a decellularised extracellular matrix cell-laden constructs supported by a PCL framework (Figure 2.11**b**). By decellularizing cartilage and adipocyte tissue, the three-dimensional structures revealed high cell viability and functionality, as well as ECM production. The decellularized tissue used in the bio-ink was reported to commit cell differentiation into adipogenic and chondrogenic lineage, if adipogenic or chondrogenic decellularized ECM (dECM) bio-ink was used respectively. This technique is particularly interesting in terms of recapitulating native tissue microenvironment (Pati *et al.*, 2014). Similarly, Cho's group printed a multi-cellular ear shape structure using an in-house developed system that allowed to deposit six different biomaterials independently, at the same time structural support was given by a printed polycaprolactone (PCL) framework. Adipogenic tissue formation was shown on the earlobe, at the same time the auricular cartilage was regenerated. It was observed that the structure had mechanical properties similar to native ear (Cho, 2014). Woodfield and colleagues fabricated complex hierarchical chondrogenic structures that granted high cell viability and deposition of cartilage-specific ECM, at the same allowed to microtissue to fuse to each other in order to form highly complex structures. The developed system has potential to be applied to *in vitro* microtissue applications, such as drug screening or cancer research (Woodfield, 2018).

Differently, Tan and co-workers developed a cell-laden microsphere bio-ink for extrusion-based bioprinting. This strategy allowed to print increased cell numbers with high viability, at the same time the cells were protected from the stress and strain produced during extrusion. The authors advance that this technique would be highly

suitable for freeform fabrication (Tan *et al.*, 2016). Yue's group have developed a portable extrusion-based "bio-pen" for osteochondral defects. The aim of this technology is to be used at the theatre to aid on healing the wounds developed by late osteoarthritis stages. The pen was able to extrude a gelMA/hyaluronic acid–methacrylate hydrogel that was crosslinked after printing by an UV source. Similarly to other extrusion processes, the pressure demonstrated to affect the resolution achieve by the device. The viability of adipose stem cells was exhibited to be similar to control samples.

Nowadays, some systems allow multiple reservoirs to deposit multi-material filaments in a continuous manner being able to keep printing without stopping in-between reservoir switching (Figure 2.11**c**). Gradient structures were developed with cells retaining cell viability and function. This technique may open new avenues in the bioprinting area by being able print highly complex and multi-cellular structures (W. Liu *et al.*, 2016). Apart from human application, extrusion bioprinting is also being applied to plants by Lode's group. Here, a callus-derived bio-ink was used to encapsulate basil cells that showed the expected viability and functionality after printing. This group advances the importance of this application to study cell responses to environment changes (Lode, 2017).

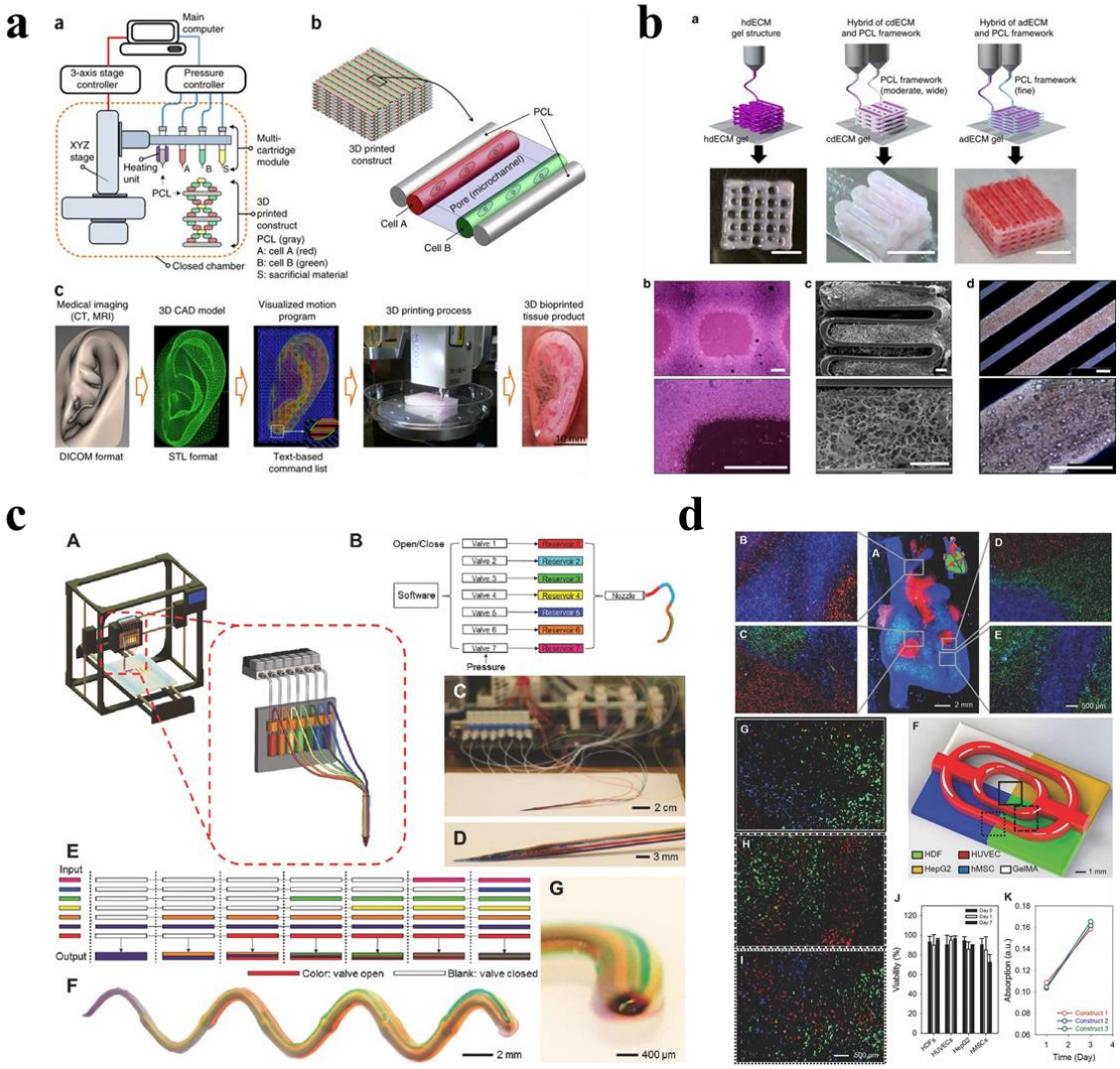

Figure 2.10 – Dual extrusion bioprinting has been used to fabricate different structures such as **a** ears or **b** dECM cell-laden hydrogels. These combine a PCL framework to give structure, a cell-laden hydrogel and, sometimes, sacrificial inks. **c** Printing of different cell lineages using a continuous extrusion printing technique. Cell viability remains high and proliferation is verified. Adapted from (Pati *et al.*, 2014; Kang *et al.*, 2016; W. Liu *et al.*, 2016).

2.2.4 *Laser-assisted bioprinting*

Laser-Assisted Bioprinting (LAB) most popular technique is Laser Induced Forward Transfer (LIFT) (Dababneh and Ozbolat, 2014). The latter was initially used to pattern metals in industries (e.g. chip fabrication), however, Odde and colleagues introduced laser patterning of biological scaffolds after equipment modifications (Odde and Renn, 1999). Afterwards, printing of biological materials, such as DNA, enzymes or cells,

became possible (Li *et al.*, 2016; Sorkio *et al.*, 2018). Five main components can be identified in common LAB equipment: a pulsed laser source, a focusing system, a ribbon, a biomaterial layer (such as cells and/or hydrogels) and a receiving substrate (Figure 2.12) (Hong *et al.*, 2017; Keriquel *et al.*, 2017). The ribbon is composed by a support material (e.g. glass) that is covered with a thin absorbing layer of metal (titanium or gold, for example) and a bio-ink layer below. The absorbing layer can transfer the energy to the ribbon and then to the material layer.

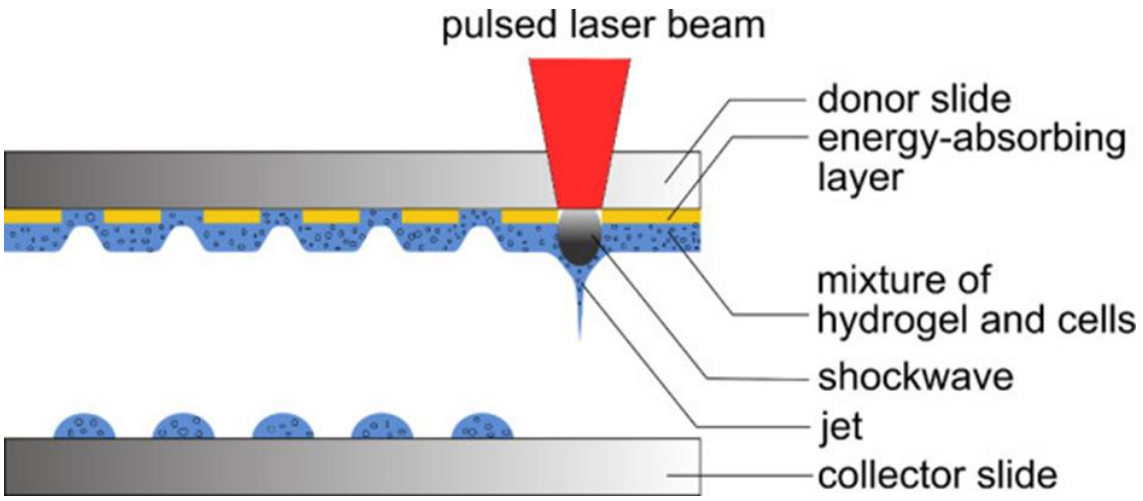

Figure 2.11 – Laser-assisted bioprinting main components. From (Gruene, Unger, *et al.*, 2011).

The LAB working principle relies on high-pressure bubbles induced by the energetic laser pulse (Guillotin *et al.*, 2010; Skardal and Atala, 2015; Pati, *et al.*, 2016). Short duration laser pulses (in the order of nanoseconds) with UV or near-UV wavelengths are used. The laser beam causes evaporation of the material, originating pressurised bubbles that create shock waves when collapsing. This way material-containing droplets are propelled towards the substrate. By moving the substrate or the laser focus in the ribbon, different patterns are acquired. Similarly to inkjet and microvalve bioprinting, substrates may be chosen accordingly to the user's desire as any configuration may be adopted (Catros *et al.*, 2015; Keriquel *et al.*, 2017).

Precise and small bio-ink volumes are dispensed using LAB with high accuracy and resolution (10-100 µm), with single cell printing being achievable (Guillotin *et al.*, 2010).

However, the sensitivity to its control parameters makes LAB difficult to apply. Laser energy and frequency, material's rheological properties, thickness of the absorbing and bio-ink layers, distance between the ribbon and the substrate or printing speed are some of the parameters that have impact on the resolution of the printed material (Guillotin *et al.*, 2010; Murphy and Atala, 2014; Gudapati *et al*., 2016). LAB is a nozzle free technique; therefore, cell agglomeration and nozzle blockage are avoided, contrary to what happens in other bioprinting techniques. This specification avoids shear stress caused when cells and materials pass through nozzles and needles. Additionally, the bio-ink layer may include materials with high viscosities (1–300 mPa/s) and high cell densities (up to 10^8 cells/mL) (Murphy and Atala, 2014). Multiple cell types can be printed due to the laser accuracy with frequencies as high a 5 kHz and speeds up to 1,600 mm/s (Guillotin *et al.*, 2010).

However, the disadvantages of LAB outweigh the advantages. The small printing volume and high resolution demand the use of materials with fast gelation kinetics, as well as, fast moving stage (Skardal and Atala, 2015). This is essential to achieve not only shape fidelity, but also cell viability preservation, as demonstrated by Gudapati and colleagues (Chrisey, 2014). Also, the lack of photocurable materials is an issue. LAB is not indicated for high-throughput applications as the preparation of the ribbon, especially when it includes biological materials, is time-consuming (Skardal and Atala, 2015). Additionally, to fabricate structures with considerable size, preparation of multiple ribbons may be needed and, therefore, reloading is indispensable. On the other hand, the printing process itself is fast. Also, metallic residues were found to contaminate the bioprinted constructs because of the vaporization of the metallic laser-absorbing layer during printing (Murphy and Atala, 2014). However, non-metallic absorbing layers may be adopted. Although LAB may use materials with a considerable range of viscosities, accurate targeting and precise cell deposition may be difficult when using bio-inks with lower viscosities (Murphy and Atala, 2014). The biological effect of LAB is the most discussed disadvantage. Some groups state that little or no cell damage is caused by the printing process, however, others note that the heat and UV exposure may affect cells. Additionally, Hopp (2012) and colleagues verified that femtosecond pulse laser caused less thermal damage when compared to nanosecond laser irradiation. However, this group found that cell viability was below 85% (Hopp *et al.*, 2012). Finally, the high cost of LAB is also a disadvantage, which limits the number of studies available.

In terms of applications, Koch (2017) and colleagues used LAB to print fibroblasts and keratinocytes (skin cell lines) and hMSCs. Here this group observed the impact of the printing technology on cell viability, proliferation or phenotype. It was demonstrated that cells kept the ability to proliferate with viability. No cell exhibited increased apoptosis and phenotypes were conserved (Koch *et al.*, 2017). Guillotin (2010) and his team showed that LAB can accurately deposit cells with high resolution, fabricating miniaturized tissues. Using a thrombin and $CaCl_2$ cell-laden solution, cells were printed onto a fibrinogen "biopaper". Cells showed high viability, even when using high cell densities ($6x10^7$ cells/mL) and speeds up to 200 mm/s. The best resolution was acquired for printing at 5 kHz. LAB has been also used for cardiac regeneration (Guillotin *et al.*, 2010). Gaebel (2011) and his team seeded human umbilical vein endothelial cells and hMSCs into polyester urethane cardiac patches both manually and using LAB. These were evaluated by *in vivo* implantation after infarction. It was noted that LAB cell seeding influenced the cell behaviour generating increased vessel formation. Additionally, infarcted hearts were more functional with LAB cardiac patches than with the manually seeded ones (Gaebel *et al.*, 2011). Skin substitutes were engineered by Michael (2013) and colleagues (Figure 2.13**a**). Keratinocytes and fibroblasts were precisely placed onto a Matriderm layer. After maturation, these constructs were tested *in vivo* by covering a skin wound in nude mice. The engineered skin showed to completely attach to the skin surrounds after 11 days. Cells proliferated the skin stratum corneum and basal layer and were able to form multi-layered epidermis. Blood vessel formation was also demonstrated in the wound area (Michael *et al.*, 2013). Catros (2010) and colleagues used LAB to print nano-hydroxyapatite into *in vivo* mouse calvaria defect (Figure 2.13**b**). Three month later, mature bone tissue was observed (Catros, 2010).

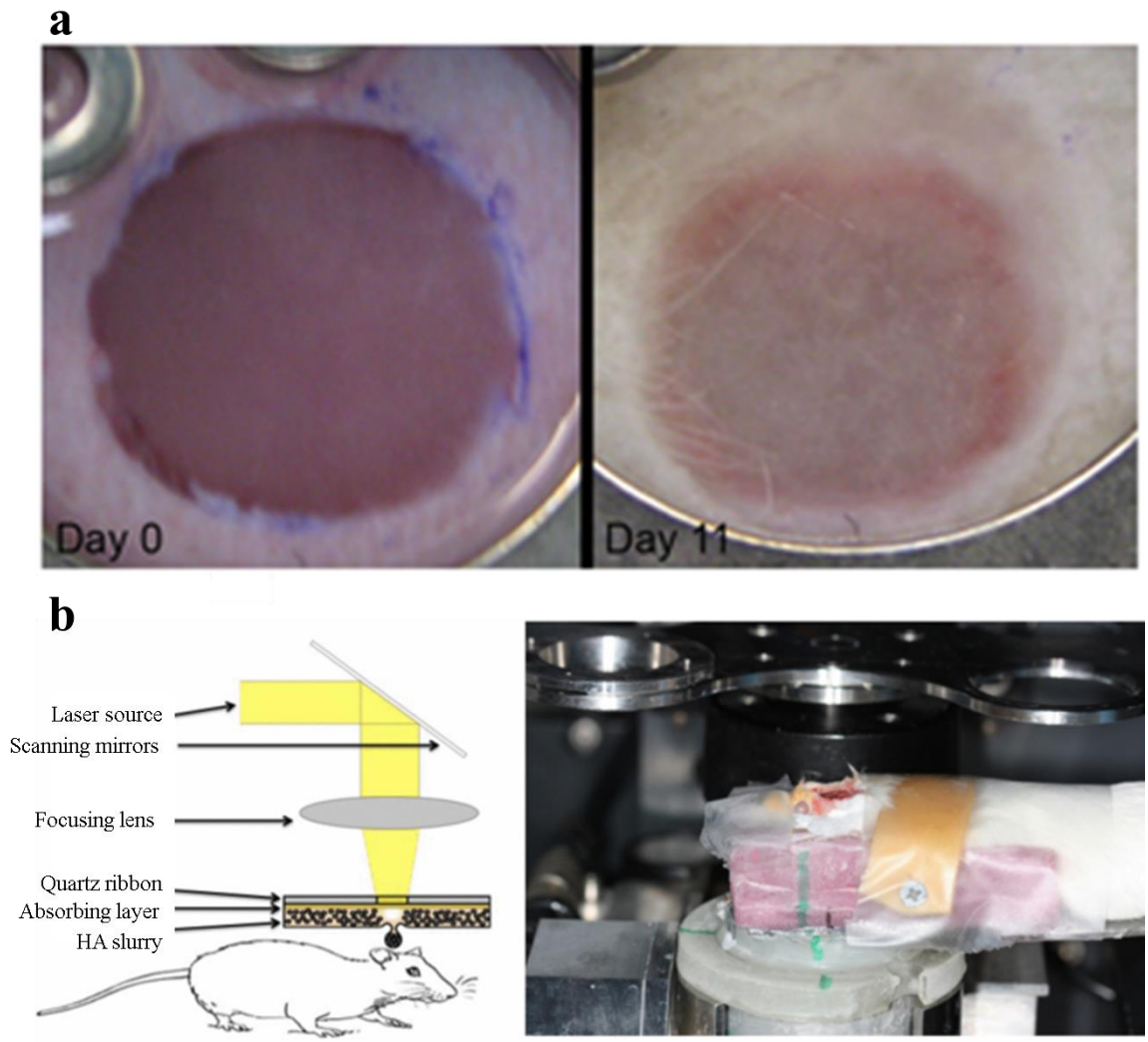

Figure 2.12 – **a** Skin regeneration 11days after implantation of LAB engineered skin tissue; **b** *In situ* strategy used by Keriquel and co-workers to print nano-hydroxyapatite to a calvaria defect. Adapted from (Catros, 2010; Michael *et al.*, 2013).

2.3 Bio-inks

Bio-inks are the most important component on bioprinting. These are constituted by soft materials, cells and growth factors that, once processed by a bioprinting technique may originate 3D cell-laden structures (Stanton, et al, 2015; Hospodiuk *et al.*, 2017). As observed before, depending on the bioprinting modality, i.e. extrusion-based, microvalve, inkjet or laser-assisted bioprinting, bio-inks must consider different properties in order to release not only the full potential of the process, but also allowing cells and materials to behave has expected (Guillotin *et al.*, 2010; Pati *et al.*, 2014; Ribeiro *et al.*, 2017). Material ejection or extrusion is obtained by manipulating external pressure, electrical

inputs, nozzle sizes and designs, as well as, shear stress and the material nature (Murphy and Atala, 2014; Gudapati, et al, 2016; Ozbolat and Hospodiuk, 2016).

The number of complex requirements makes bio-ink design extremely challenging (Table 2.3). Bio-inks must: i) be bioprintable (Dababneh and Ozbolat, 2014; Murphy and Atala, 2014; Jose *et al.*, 2016; Bishop *et al.*, 2017; Hospodiuk *et al.*, 2017); ii) allow the production of 3D structures with mechanical integrity, stability and shape fidelity (Murphy and Atala, 2014; Jose *et al.*, 2016; Bishop *et al.*, 2017; Hospodiuk *et al.*, 2017); iii) work as a biomimetic microenvironment to support not only cell maintenance during all bioprinting stages, but also cell attachment, proliferation or differentiation (Murphy and Atala, 2014; Jose *et al.*, 2016; Bishop *et al.*, 2017; Hospodiuk *et al.*, 2017); iv) be biocompatible, not causing any inflammatory reaction (Murphy and Atala, 2014; Jose *et al.*, 2016; Bishop *et al.*, 2017; Hospodiuk *et al.*, 2017); and v) be biodegradable, not producing toxic by-products and with controllable degradation kinetics (Murphy and Atala, 2014; Jose *et al.*, 2016; Bishop *et al.*, 2017; Hospodiuk *et al.*, 2017). Additionally, to build complex biological systems, cell-cell and cell-ECM interactions must naturally occur and angiogenesis must be promoted (Murphy and Atala, 2014; Jose *et al.*, 2016; Hospodiuk *et al.*, 2017). However, the lack of materials that can be processed via bioprinting modalities and, at the same time, conserve the properties mentioned above, is very low (Murphy and Atala, 2014; Hospodiuk *et al.*, 2017).

Currently, bio-inks are composed by individual cells or cell aggregates suspended in liquid solutions, such as cellular medium or other cell-friendly solutions, or more frequently by cells mixed with hydrogel precursors or hydrogels (Mironov *et al.*, 2009; Malda, 2013; Mateos-Timoneda, 2014; Lee and Yeong, 2016; Ribeiro *et al.*, 2017; X. Wang *et al.*, 2017a). Hydrogels are normally made of natural or synthetic components (Nicodemus and Bryant, 2008; Zhu and Marchant, 2011). Natural components, such as gelatin, collagen, alginate, among others, specifically mimic natural ECM, granting biomimetic properties, which are essential on cell microenvironment (Hospodiuk *et al.*, 2017). This biomimicry is of importance as it will also potentiate cell migration, which is crucial when obtaining microtissues (Murphy and Atala, 2014; Reig *et al.*, 2014; Bishop *et al.*, 2017; Hospodiuk *et al.*, 2017). They also possess inherent bioactivity. Furthermore, natural materials are degraded by enzymatic processes and replaced by cell-produced ECM and promote cell viability and functionality (Murphy and Atala, 2014; Hospodiuk *et al.*, 2017). However, these are normally soft, which causes mechanically weak constructs

with poor shape fidelity and printing resolution (Ashby *et al.*, 1995; Murphy and Atala, 2014; Ozbolat and Hospodiuk, 2016). Synthetic materials, such as polyethylene glycol (PEG) or GelMA, can have their physical properties carefully designed to facilitate the bioprinting process and control cell characteristics (Langer and Tirrell, 2004; Lutolf and Hubbell, 2005; Saha *et al.*, 2007; Murphy and Atala, 2014; Hospodiuk *et al.*, 2017). Similarly to natural materials, synthetic materials used in bioprinting are also degradable, but via hydrolytic mechanisms. However, challenges including poor ECM mimicking and biocompatibility, as well as toxic by-products, represent drawbacks for using these materials (Murphy and Atala, 2014; Hospodiuk *et al.*, 2017). Some research groups have been studying the use of hybrid materials to gather the properties of natural materials to the synthetic ones. In this sub-chapter hydrogels and the most common bio-ink used materials are reviewed.

Table 2.2 - Bio-ink characteristics for each bioprinting methodology.

Bio-ink property	Inkjet bioprinting	Microvalve bioprinting	Extrusion-based bioprinting	Laser-based bioprinting
Printability	Low viscosity, non-fibrous characteristics and low cell density.	Low viscosity, non-fibrous characteristics and low cell density.	Shear thinning and thixotropic fluids.	Transfer thermal energy to kinetic energy; Adhesion and low surface tension properties
Biocompatibility	Should support cell maintenance during printing process, as well as promote cell survival, proliferation and differentiation. Should not cause adverse immune reaction if implanted.			
Biodegradability	Should be able to control the degradation kinetics, at the same time no toxic by-products are produced.			
Mechanical integrity	Very weak - Crosslinking needed	Usually weak - Crosslinking often needed	Good - Crosslinking often needed	Usually weak - Crosslinking needed
Materials used	Liquid solutions	Liquid solutions/soft hydrogels/cell aggregates	Hydrogels and cell aggregates	Hydrogels

2.3.1 *Hydrogels*

Hydrogels were first reported in 1960 by Wichterle and Lim in their work where poly-2-hydroxyethylmethacrylate (PHEMA) was used for contact lens applications (Wichterle

and Lim, 1960). Hydrogels are constituted by three-dimensional meshes made of hydrophilic polymers that are crosslinked after the reaction of one or more monomers with other substances, crosslinker and/or initiator, or stimulus, such as temperature or UV irradiation. (Nicodemus and Bryant, 2008; Slaughter *et al.*, 2009; Caló and Khutoryanskiy, 2015; Buwalda *et al*., 2017). These are able to swell through the absorption of water or other biological fluids up to a thousand times, but are water insoluble, may turn into any desired physical forms and possess tissue-like elasticity, behaving similarly to normal ECM (Nicodemus and Bryant, 2008; Zhu and Marchant, 2011). Furthermore, hydrogels are able to be tuned in terms of porosity and density of cross-links. However, hydrogel synthesis may pose some concerns, such as low solubility and degradability, poor mechanical properties or the use of harmful crosslinkers (Ullah *et al.*, 2015). To overcome these issues, natural and synthetic polymers are combined to maximise the properties of the desired hydrogel (Ahmed, 2015; Freudenberg *et al.*, 2016; Buwalda *et al*., 2017). Synthetic materials have been widely used due to its tunable characteristics: degradation rate, mechanical properties or water absorption capability (Zhu and Marchant, 2011; Ahmed, 2015; Trimaille *et al.*, 2016). On the other hand, natural materials add high biocompatibility and tissue-like ECM (Hinderer *et al*., 2016).

After mixing cells with the liquid precursors, crosslinking is normally needed to give the desired structure and mechanical properties to the hydrogel. Depending on the molecular arrangement of the crosslinked material, hydrogels can be defined as reversible (physical) or permanent (chemical) (Caló and Khutoryanskiy, 2015; Akhtar *et al*., 2016). They are physical if the hydrogel network is formed via hydrophobic or ionic forces or hydrogen bonds (Hennink and van Nostrum, 2002). As the classification suggests, these are reversible by dissolution through different processes, such as temperature or pH. Contrarily, chemical hydrogels are irreversible due the covalently bonded, i.e. by sharing electron pairs, network of macromolecular chains (Hennink and van Nostrum, 2002). Crosslinking processes must be carefully controlled as high crosslinking degrees will confer brittle structures and swelling limitations to the hydrogel (Place *et al.*, 2009). On the other hand, low crosslinking degrees produce materials with poor mechanical properties. Additionally, crosslinking constitutes a major challenge, as these techniques are able to affect cell viability and functionality (Nicodemus and Bryant, 2008; Gasperini, *et al*., 2014). To minimize the impact, recently, hydrogels have been developed in order to be crosslinkable using natural and non-harming processes, such as visible light (Hu *et*

al., 2012). Optimisation of the crosslink procedure is needed to obtain a hydrogel with the desired characteristics.

2.3.2 *Natural materials*

Natural materials are normally derived from animal tissues or plants. These materials are normally highly biocompatible and support cell viability, proliferation and differentiation. Additionally, these materials possess biomimetic characteristics that allow cells to behave similarly as to when in the human environment. However, natural materials normally lack structural integrity and form very soft gels. This issue affects bioprinting negatively by decreasing the shape fidelity and printing resolution. To solve this common problem, natural materials are normally combined with other natural or synthetic materials. The material hybridization not only is able to maintain the advantages, but also eliminates the concerns reported above. In the following pages, some of the most commonly bioprinted natural materials are reviewed.

2.3.2.1 *Fibrin*

Fibrin is a natural hydrogel that is produced from the enzymatically reaction between fibrinogen and thrombin (Smith, 1980; Weisel, 2005). This naturally occurs in the human body having primary importance in wound healing, hemostasis, fibrinolysis and tumour growth (Gurtner *et al.*, 2008; Lee *et al.*, 2010; Kołodziejczyk and Ponczek, 2013; Litvinov and Weisel, 2016). Fibrin is formed "via thrombin-catalysed cleavage of two pairs of fibrinopeptides that exposes binding sites in the central nodule complementary to sites constitutively available at the ends of the molecule" (Figure 2.14) (Litvinov and Weisel, 2016).

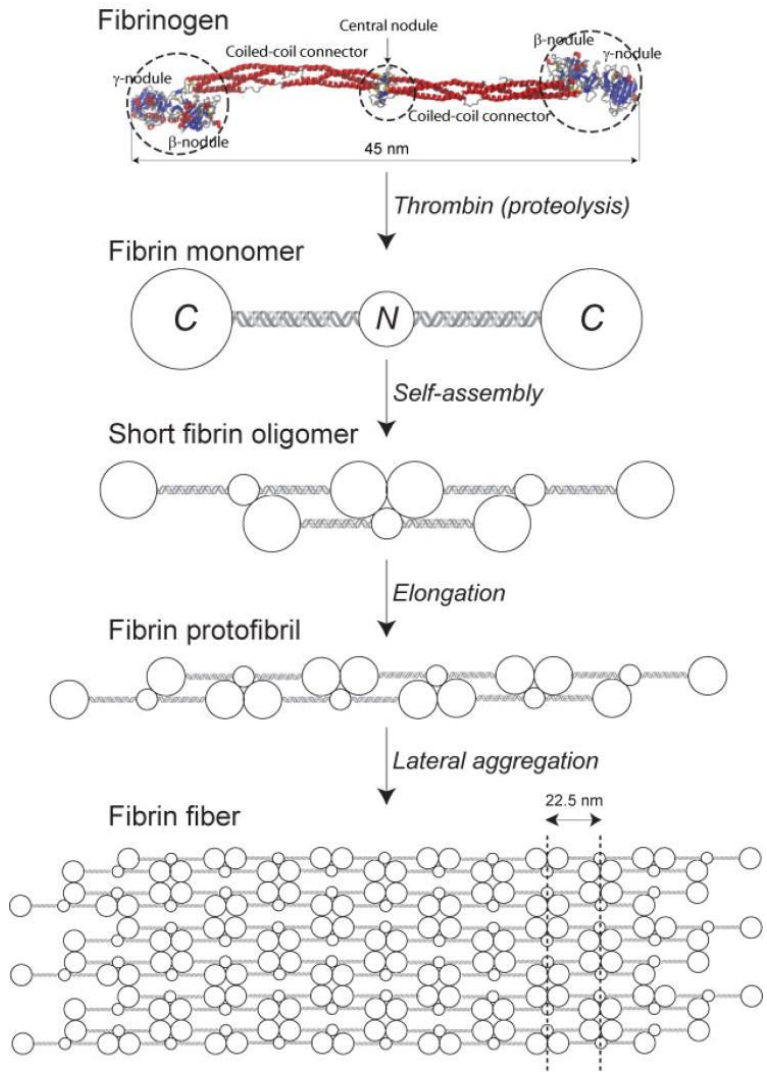

Figure 2.13 – Fibrin formation via reaction between fibrinogen and thrombin. From (Litvinov and Weisel, 2016).

Fibrin has gained a lot of attention, not only for its high biocompatibility, but also for its mechanical properties (Jung *et al.*, 2009; Litvinov and Weisel, 2016). This property prevents damage when encapsulating cells inside a fibrin hydrogel. Additionally, as an important ECM component, it mimics the human microenvironment by having an important role in cell-ECM interactions (Tibbitt and Anseth, 2009; Geckil *et al.*, 2010; Kim *et al.*, 2016). Fibrin is easily functionalised, promotes angiogenesis and supports cell viability and proliferation (Brown and Barker, 2014; Y. Li *et al.*, 2015). However, disease transmission or immune reaction is a disadvantage in the use of heterologous proteins. To avoid sample contamination, the production of fibrinogen and thrombin via recombination technology and virus and bacteria inactivation is essential (Hennis *et al.*, 1992; Chen and Jain, 2010; Hirashima *et al.*, 2016). Another limitation is how dependent

the crosslinking speed is on the thrombin concentration (Weisel, 2005). This may result in slow or poor crosslinking when using low thrombin concentrations. Consequently, shape fidelity and early mechanical properties will be low (Gruene *et al.*, 2011).

Fibrin forms fibrils that easily cause nozzle blockage. Also, it has been reported that only very low concentrations (<2 mg/mL) of fibrinogen are able to be used with inkjet bioprinting with these producing hydrogels with very weak mechanical properties (Hospodiuk *et al.*, 2017). On the other hand, thrombin solutions present low viscosity, not constituting a problem for inkjet bioprinting. Hence, the most common strategy is to print thrombin solution into a fibrinogen substrate, as reported by Cui and Boland (Cui and Boland, 2009). Within this approach, human-like microvasculature was fabricated. On the other hand, Atala and colleagues use the "alternating ink" strategy to produce fibrin-collagen hydrogels (Figure 2.15) (Atala, 2013). This group demonstrated ejecting hybrid cell-laden fibrinogen-collagen solution onto an electrospun PCL layer. The hydrogel was then crosslinked by printing a thrombin solution layer after each gel precursor layer. The fabricated 3D construct allowed the formation of *in vitro* and *in vivo* cartilage-like tissues.

The nozzle clogging limitation makes microvalve systems a preferable drop-on-demand system to be used with fibrin hydrogels. Lee and colleagues avoided the possibility of clog formation by printing fibrinogen and thrombin from two different reservoirs (Lee *et al.*, 2010). This group used microvalves to produce a cell-laden fibrin hydrogel containing VEGF to study the influence of this growth factor on neural stem cells. Hybrid fibrin-based materials can be processed in extrusion-based bioprinting, as it allows higher viscosities. However, fibrin is not regularly used due to its fast and irreversible crosslinking, which make this natural material difficult to extrude (Hospodiuk *et al.*, 2017). Despite this problem, Soker and colleagues fabricated a hybrid fibrin/collagen hydrogel for skin wounds (Skardal *et al.*, 2012). By encapsulating AFSCs to modulate the inflammatory response, *in vivo* skin wound has showed to close and angiogenesis was promoted. Laser-assisted bioprinting also presents concerns for printing fibrin as the material sensitive structures may be affected by laser pulses.

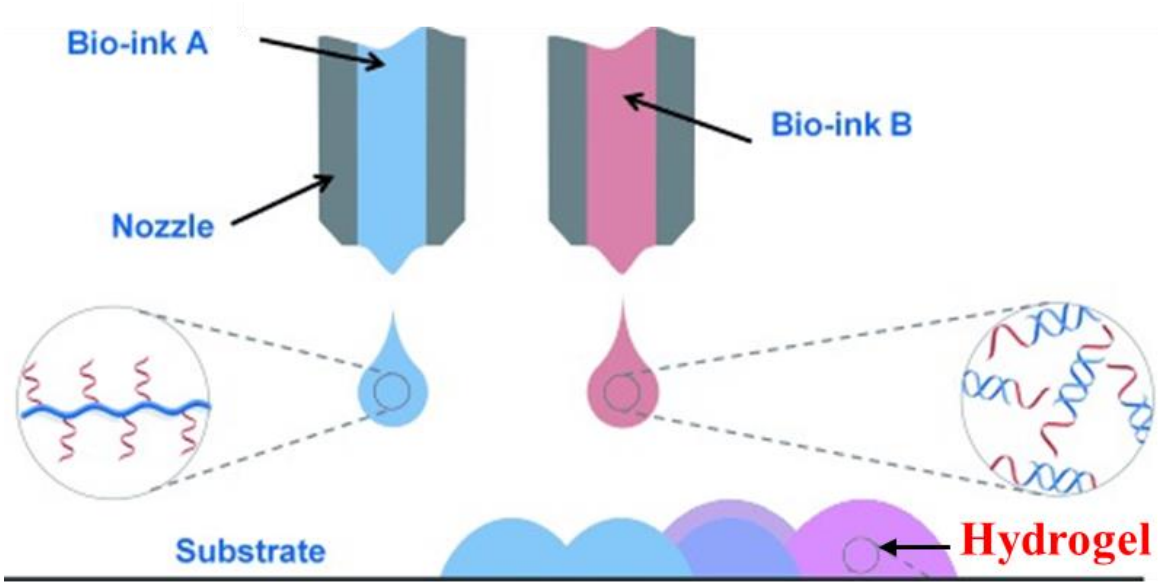

Figure 2.14 – Alternating-ink strategy to produce *in situ* hydrogels. Adapted from (C. Li *et al.*, 2015).

2.3.2.2 Agarose

Agarose is a polysaccharide molecule that is extracted from certain seaweeds (Hospodiuk *et al.*, 2017; Tarassoli *et al.*, 2018). It is widely used in electrophoresis to separate molecules, such as deoxyribonucleic acid (DNA) (Lee *et al.*, 2012). Different types of agarose solidify and melt at different temperatures, a propriety called thermal hysteresis (Indovina *et al.*, 1979). These temperatures depend on the type and agarose solution concentration, however it thermally crosslinks at low temperatures, depending on the hydroxyethylation, and presents a liquid conformation between 20 and 70°C (Ozbolat and Hospodiuk, 2016). Non-covalent hydrogen bonds connect agarose fibres to each other, forming a mesh of helical fibre bundles that hold to each other, granting a solid structure by lowering the temperature (Stellwagen, 2009). Once solidified, agarose forms brittle structures with shape fidelity. Like any other hydrogel, agarose must be hydrated, otherwise drying will quickly happen. Cell viability and functionality may be affected by lack of cell attachment to the agarose hydrogels (Livoti and Morgan, 2010). However, agarose is used in combination with other materials to provide stability and thermally induced crosslinking (Duarte Campos *et al.*, 2014). Agarose hydrogels are also adapted for cell aggregate bioprinting, working as support structures (Ozbolat, 2015). Although not highly viscous, agarose rheological properties are prohibitive for inkjet bioprinting. Although sharing the same concerns, microvalve printing allows agarose printing

(Hospodiuk *et al.*, 2017). However, a temperature controlling nozzle and reservoir are needed to avoid agarose solidification. Tan and colleagues bioprinted an agarose-collagen hybrid hydrogel as vehicle for poly(lactic-co-glycolic acid) (PLGA) encapsulated cells (Figure 2.16a) (Tan *et al.*, 2016). The hydrogel and encapsulation protected cells during extrusion, which resulted in high viability and proliferation rates. A hybrid agarose-matrigel loaded with intestinal epithelial cells was extruded by Fan *et al.*(2016). This group verified that nutrient and oxygen diffusion was diminished, which lead to low viabilities after 10 days. In laser-assisted bioprinting, agarose has been used as a coating on the substrate due to its viscoelasticity and fast crosslinking mechanism (Koch *et al.*, 2009).

2.3.2.3 *Gelatin*

Gelatin is a hydrolised form of collagen that is extracted from animal tissue: skin, bones, tendons, etc (Gómez-Guillén *et al.*, 2002; Olsen *et al.*, 2003). It is biocompatible and biodegradable, being able to be synthesised at a very low cost (Rose *et al.*, 2014). These properties make gelatin one of the most used materials in pharmaceutical and medical fields (G. Yang *et al.*, 2018). Gelatin gels at low temperatures by inducing gelatin strands self-organisation into helical conformations (Guo *et al.*, 2003; Bode *et al.*, 2013). By heating, this organisation is, once again, replaced by random coil arrangement. Liquification can be obtained at 37°C. Gelatin behaviour is related to different factors, such as pH, concentration or temperature (Osorio *et al.*, 2007). Normal cell adhesion and behaviour, as well as migration have been observed using gelatin hydrogels (Yang *et al.*, 2016). However, gelatin is highly degradable, which makes difficult for gelatin constructs to retain mechanical integrity and shape fidelity: gelatin is normally combined with other materials to avoid dissolution (Ng *et al.*, 2016; Hospodiuk *et al.*, 2017; Li *et al.*, 2018). Another strategy is use chemical or enzymatic crosslinking to increase the hybrid gelatin construct mechanical properties (Hospodiuk *et al.*, 2017).

Gelatin has been mixed with alginate and collagen to fabricate cell-laden hydrogel with controllable degradation. Wu et al showed high cell viability and proliferation rates and specific markers expression after hydrogel extrusion (Wu *et al.*, 2016). Xu and colleagues reported cell differentiation and self-organisation by extruding a hybrid cell-laden hydrogel, containing gelatin, alginate and fibrinogen (Xu *et al.*, 2010). Additionally, this

system was useful as an *in vitro* model for metabolic syndrome study. Wang *et al* (2006) printed cell-laden gelatin hydrogels via extrusion-based bioprinting. These authors demonstrated high hepatocyte viability during more than 2 months. Contrary to the increased number of works published in extrusion-based bioprinting, not many are available in either inkjet and microvalve bioprinting. However, Boland and colleagues used an alginate/gelatin blend to produce 3D constructs (Boland *et al.*, 2007). Here, $CaCl_2$ was accurately inkjet printed onto the hybrid solution bath (Figure 2.16b). Cells were culture on the top of the fabricated hydrogels showing attachment. Gelatin has been also adapted for laser-based bioprinting. Huang and colleagues tested gelatin as absorbing layer coating material and verified that post printing cell survival and DNA double-strand breaks were reduced by 10 and 50%, respectively (Huang, 2017). Additionally, droplet size and jet velocity were also reduced.

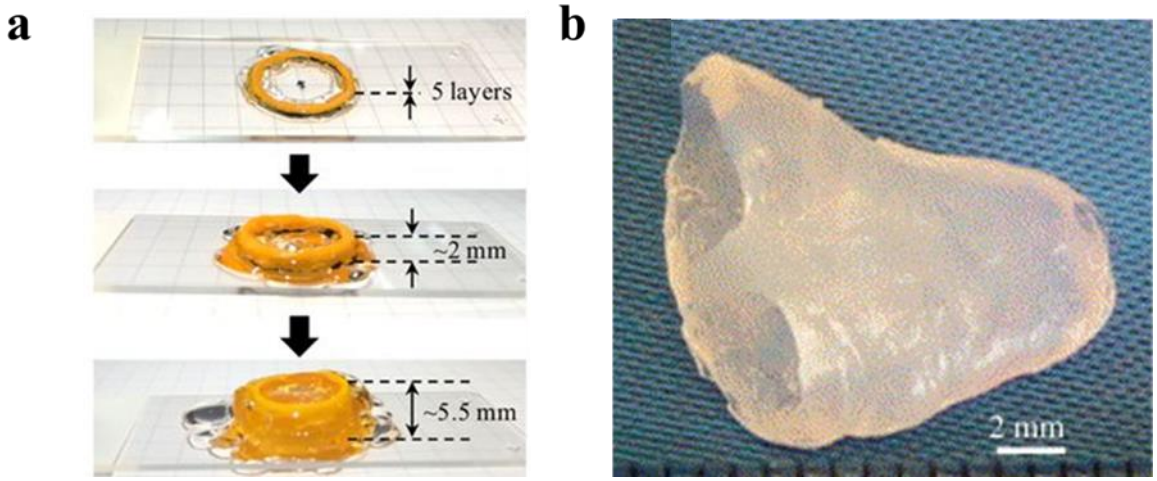

Figure 2. 15 – **a** Agarose-collagen hydrogel; **b** Alginate-gelatin hydrogel. Adapted from (Tan *et al.*, 2016; Boland *et al*., 2007).

2.3.2.4 *Collagen*

Collagen is a fundamental component of the ECM of various tissues. It is highly abundant in the human body, constituting between one quarter and one third of the total body protein tissue (Shoulders and Raines, 2009; Ferreira *et al.*, 2012). Collagen has been widely used for its abundancy, easy processing, biocompatibility or hydrophilicity (Skardal and Atala, 2015; Gudapati *et al*., 2016). Additionally, it presents low antigenicity as collagen is conserved between species, which causes minimal immune

responses (Hospodiuk *et al.*, 2017). Cell attachment and proliferation are highly supported by the collagen matrix (Murphy *et al*., 2010). However, crosslinking is difficult to control as it remains liquid at low temperatures and forms fibrils at temperatures higher than 37°C or at neutral pH. Collagen is rarely used in bioprinting on its own, otherwise, cell distribution would be controlled by gravity until effective crosslinking (Hospodiuk *et al.*, 2017). To overcome this issue and the lack of mechanical properties, collagen is widely combined with other materials, such as gelatin, fibrinogen, alginate, among others, to form hybrid materials with superior characteristics (Wu *et al.*, 2016; He *et al.*, 2018; Holder *et al.*, 2018; X. Yang *et al.*, 2018).

The fibrous micro-architecture of collagen does not allow it to be processed by inkjet bioprinting, otherwise, nozzle blockage would occur (Hospodiuk *et al.*, 2017). Yanez et al used cell-laden coated substrate and an inkjet bioprinted cell-laden fibrin layer to obtain a stratified skin tissue using collagen as dermal layer (Yanez *et al.*, 2015). In another study, Lee and colleagues used microvalve bioprinting to fabricate skin tissue (Figure 2.17a) (Lee *et al.*, 2014). Keratinocytes and fibroblasts were printed on the top of a printed collagen solution. Quick collagen gelation was obtained by nebulized sodium bicarbonate. Histology and microscopy results revealed that the model obtained was similar to the native *in vivo* tissue. Using extrusion-based bioprinting, as reported before, a fibrinogen-collagen cell-laden hydrogel was produced to form *in vitro* and *in vivo* cartilage-like tissue (Atala, 2013). Similarly, collagen has been successfully used in laser-assisted bioprinting. Michael and colleagues developed a collagen cell-laden bio-ink to produce skin constructs to implant in a *in vivo* model (Michael *et al.*, 2013). This technique allowed the formation of stratified skin with highly viable cells. This system also actively promoted angiogenesis.

2.3.2.5 *Alginate*

Alginate is a naturally derived polysaccharide that is obtained from algae or seaweed (Tønnesen and Karlsen, 2002; Gudapati, Dey and Ozbolat, 2016). It is made of alternating and covalently linked blocks of (1-4)-linked β-D-mannuronate (M) and its C-5 epimer α-L-guluronate (G) (Axpe and Oyen, 2016; Gelinsky, 2018). The most common crosslinking method involves ionic gelation with $CaCl_2$ or calcium sulfate ($CaSO_4$) – the attraction of carboxylic groups from two alginate chains forms a bridge between the

divalent calcium ions (Axpe and Oyen, 2016; Lai *et al*., 2016). Other crosslinking techniques are also used, such as physical or covalent crosslinking (Lee and Mooney, 2012). Alginate is one of the most used materials in tissue engineering research, and is widely used in bioprinting, due to the low price and ease of use and combination with other materials to fabricate 3D constructs (Hospodiuk *et al.*, 2017; Zanoletti *et al.*, 2018). Additionally, it presents high biocompatibility and supports cell differentiation (Bozza *et al.*, 2014; Laronda *et al.*, 2014; Chen *et al.*, 2015). Chemical modifications are widely used to improve alginate mechanical properties and to promote higher cell survival and desired cell functions (Hospodiuk *et al.*, 2017).

Alginate bio-inks are widely used in extrusion-based bioprinting. Due to its viscosity, alginate is able to be extruded as gel precursor solution or pre-crosslinked. Giuseppe and his team produced different cell-laden alginate/gelatin hydrogels by extrusion-based bioprinting to test several proprieties, such as printing accuracy, compressive behaviour and cell viability (Giuseppe *et al.*, 2018). Aortic valve conduits were successfully printed by Duan and colleagues through the use of a cell-laden alginate/gelatin bio-ink (Figure 2.17b) (Duan *et al.*, 2012). High viability and expression of alpha-smooth muscle actin were demonstrated. However, for drop-on-demand applications, alginate rheological characteristics are normally a concern. It has been reported that only alginate concentrations lower than 2% are able to be inkjet bioprinted (Hospodiuk *et al.*, 2017). To overcome this limitation, Atala and his team produced a cell-laden $CaCl_2$ solution that was once deposited inside a sodium-alginate/collagen bath (Xu *et al.*, 2013). The fast crosslinking allowed rapid cell attachment. Additionally, cells presented normal cell behaviour and phenotypic expression. Once implanted *in vivo* the bioprinted tissues were able to mature and angiogenesis was noted. Alginate has been successfully adapted to laser-assisted bioprinting. Guillemot and his research team used a cell-laden alginate bio-ink to fabricate tissue-like constructs that presented highly viable cells (Guillotin *et al.*, 2010).

2.3.2.6 Decellularised extracellular matrix

The demand for truly biomimetic bioprinting has led some groups to process decellularized tissues to produce custom bio-inks. The concept is generally slow, difficult and costly. Generally, tissues are subjected to chemical, physical and enzymatic processes

that actively remove all the cellular content and only preserve the extracellular matrix (Crapo *et al.*, 2011; Brancato *et al.*, 2016; Ji and Guvendiren, 2017). After DNA quantification, which must represent less than 2% from the original content, the decellularized tissue is crushed and then dissolved in buffers to form a gel-like bio-ink, the dECM bio-ink (Hospodiuk *et al.*, 2017; Ji and Guvendiren, 2017). This technique not only provides an unlimited source for bio-inks, but also closely mimics specific native cell microenvironment, positively influencing cell-cell and cell-ECM interactions (Zhang *et al.*, 2016). To improve the bio-inks characteristics such as rheology or crosslinking properties, hydrogels and other materials are normally mixed with the dECM (Pati *et al.*, 2014; Toprakhisar *et al.*, 2018). Apart from being slow and laborious, sample contaminations must be considered due to the chemical manipulation (Hospodiuk *et al.*, 2017).

dECM heart, cartilage and adipose tissue derived bio-inks were produced by Pati and colleagues (Figure 2.17c) (Pati *et al.*, 2014). This group fabricated cell-laden dECM hydrogels supported by a PCL structure for tissue formation. High levels of cell viability, ECM formation and differentiation commitment were obtained. Additionally, different tissue formation was observed to be guided by cell-cell interactions. In another work, the same Cho's group used a similar strategy to produce adipose dECM cell-laden hydrogels supported by PCL constructs (Pati *et al.*, 2015). Before *in vivo* experiments, it was observed that cells overexpress adipogenic genes without any adipogenic supplementation. This clearly shows the level of influence of specific dECMs bio-ink in cells. Once implanted, the construct showed to aid tissue remodelling and adipose tissue formation was detected. Moreover, no immune reaction was reported. Dong-Woo Cho group also used the strategy above to produce a cardiac patch for *in vivo* applications (Jang *et al.*, 2017). Tissue formation, vascularisation and enhancement of cardiac function were reported.

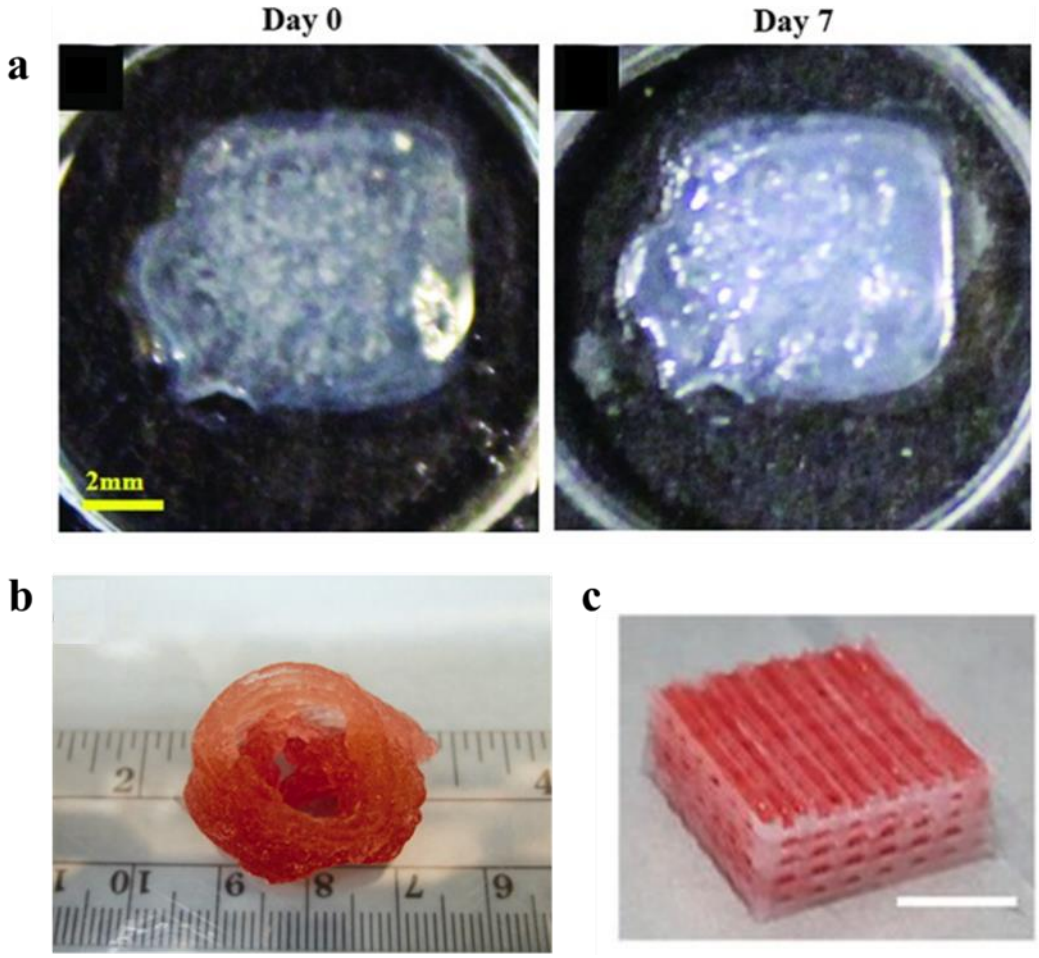

Figure 2.16 – **a** Collagen-based bioprinted skin on day 0 and 7; **b** Alginate/gelatin aortic valve conduit; **c** dECM-based tissue construct. Adapted from (Lee *et al.*, 2014; Duan *et al.*, 2012; Pati *et al.*, 2014).

2.3.2.7 Methacrylated Gelatin

Methacrylated gelatin is a denatured form of collagen that consists of methacrylate groups conjugated to its amine side groups (Gudapati *et al*., 2016). GelMA is normally synthesised by a direct reaction of gelatin with methacrylic anhydride (MA) in phosphate buffer at 50 °C (Yue *et al.*, 2015; Shirahama *et al.*, 2016). In this reaction, methacryloyl substitution groups are introduced on the reactive amine and hydroxyl groups of the amino acid residues. Due to its controllable mechanical characteristics and biocompatibility it has been widely used in tissue engineering (Wang *et al.*, 2014; Yue *et al.*, 2015; Zhao *et al.*, 2016). Additionally, GelMA is a biomimetic material that can be degraded enzymatically (Benton *et al.*, 2009; Arya *et al.*, 2016), at the same time it produces high cell survival and proliferation rates (Nichol *et al.*, 2010; Klotz *et al.*, 2016).

Photoinitiators are generally used to allow photocrosslinking by exposing the material to UV light (Benton *et al.*, 2009; Xiao *et al.*, 2011). This forms covalently crosslinked hydrogels. GelMA concentration has been reported to influence cell migration, with 10% and 15% of movement inhbition inside the gel (Hospodiuk *et al.*, 2017).

GelMA is widely used in bioprinting due to its ability to be manipulated. Bertassoni and colleagues demonstrated that mechanical properties and printability are dependent on the GelMA concentration used on the cell-laden bio-inks (Figure 2.18a) (Bertassoni *et al.*, 2014). In another work, by combining gelatin with GelMA bio-inks Yin and colleagues improved the crosslinking mechanism of GelMA (Yin *et al.*, 2018). This feature allowed to improve the bio-ink rheology and consequently increase the shape fidelity after printing. Bone marrow stem cells showed high viability on the optimised bio-ink concentration. Hoch and colleagues showed to be able to inkjet print GelMA through chemical modifications (Hoch *et al.*, 2013). A second acetylation reaction was able to modulate the physical and rheological properties of the solution and, consequently, allowing to be use in piezoelectric inkjet printers. High cell viability was obtained after printing. The fibrocartilage microenvironment was mimicked by using microvalves to print a cell-laden GelMA bio-ink that incorporated bone morphogenetic protein 2 and transforming growth factor beta 1 (Gurkan *et al.*, 2014). Gurkan and his group showed that with this tailored bio-ink hMSCs were able to differentiate into chondrocytes and osteoblasts. Also, Stratesteffen and colleagues printed a cell-laden GelMA/collagen blend using a microvalve bioprinter (Stratesteffen *et al.*, 2017). Capillary-like structures were obtained with cell viability shown to be directly linked to the UV light exposure necessary for crosslinking. GelMA was observed to increase the mechanical properties of the construct, while collagen contributed to enhance cell spreading. The benefits of combining natural to synthetic materials by mixing GelMA to polyethylene glycol diacrylate (PEGDA) were shown by Wang and colleagues (Z. Wang *et al.*, 2015). The hybrid material showed improved characteristics, such as visible light crosslinkable, high biocompatibility and printability or increased mechanical properties.

2.3.3 Synthetic materials

Contrarily to natural materials, synthetic materials can be tailored in terms of physical and chemical properties (Bishop *et al.*, 2017; Abelardo, 2018). Through careful design, a

desired material can be obtained to target a specific tissue. Mechanical properties, type of crosslinking, gelation speed or molecular weight are some of the tunable properties (Bishop *et al.*, 2017; Hospodiuk *et al.*, 2017; Gungor-Ozkerim *et al.*, 2018). However, synthetic materials lack biomimetic properties and natural cell attachment sites (Skardal and Atala, 2015). These properties may not only affect cell behaviour, but also cell survival. Polyethylene glycol (PEG) is one of the most used synthetic materials (Skardal *et al.*, 2010; Schuurman *et al.*, 2013; Gao *et al.*, 2015; Jose *et al.*, 2016; McBeth *et al.*, 2017).

2.3.3.1 Polyethylene glycol

Polyethylene glycol is a polyether-based material that has been widely used for medical and pharmaceutical applications (Thomas *et al.*, 2014; Hospodiuk *et al.*, 2017). It is a hydrophilic substance and must be combined with other materials, such as polymers, to gain adhesion capability to cells and proteins (Ji and Guvendiren, 2017). Nevertheless, some cells can survive inside PEG capsules without using any additive (Hospodiuk *et al.*, 2017). PEG gives a higher strength than natural materials, but the strength remains low. To overcome this limitation, PEG is generally functionalised with diacrylate (DA) or methacrylate (MA) (Gudapati *et al.*, 2016; Ozbolat and Hospodiuk, 2016). This functionalization process introduces C=C bonds into the polymer backbone, therefore exposure to UV is necessary to photocrosslink the materials.

Due to the water solubility of PEG, drop-on-demand printing techniques are able to use this material as bio-ink. Cui and colleagues used a modified inkjet printer for *in situ* repair of osteochondral plugs using a chondrocyte-laden PEGDMA bio-ink (Cui *et al.*, 2012). The mechanical properties matched the native articular cartilage and high viability was obtained. This group verified that simultaneous photocrosslinking increased viability, when compared with photopolymerisation after printing. Printed chondrocytes infiltrated the native tissue, producing high proteoglycan deposition at the interface between printed and native cartilage. In another work, Cui and his team used thermal inkjet printing to produce chondrocyte-laden PEGMA hydrogels (Figure 2.18b) (Cui *et al.*, 2012). Using growth factors (TGF-β1 and FGF-2), as well as an insulin-transferrin-selenium based medium, high cell proliferation and chondrogenic ECM deposition was observed. Ultimately, this lead to the formation of new cartilaginous tissue. Using extrusion-based

bioprinting side, Kaplan and his team combined PEG with silk to form a cell-laden bio-ink (Zheng *et al.*, 2018). The EBB printed structures showed high shape fidelity and resolution, at same time cells presented high survival and proliferation rates. *In vivo* implantation demonstrated that the fabricated hydrogels are able to conserve encapsulated cell survival for 6 weeks. Hockaday et al fabricated aortic valve constructs using extruded cell-laden PEGDA hydrogels (Butcher, 2012). High shape fidelity and good mechanical properties were obtained. Porcine aortic valve interstitial cells were shown to remain viable and functional during 21 days of culture. PEGDA has been also used in laser-based bioprinting, being first demonstrated by Boland and his team (Dhariwala *et al*, 2004). The authors demonstrated that cell survival was determined by photoinitiator concentration.

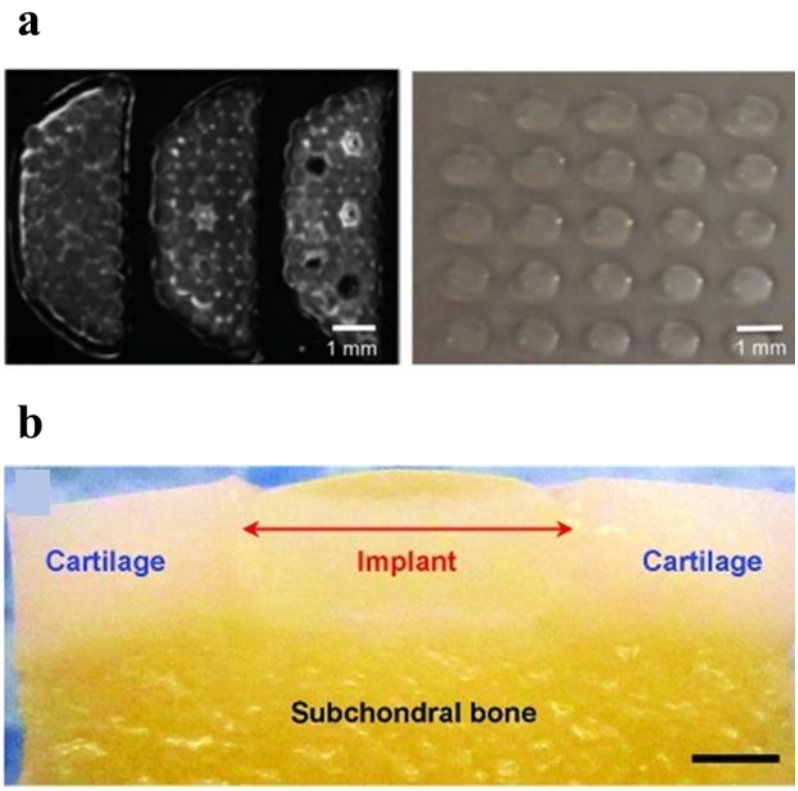

Figure 2.17 – **a** Cross-section and array of cell-laden GelMA-based hydrogels; **b** – Cell-laden PEG construct for cartilage regeneration. Adapted from (Bertassoni *et al.*, 2014; Cui, *et al.*, 2012).

2.3.4 Cell carrier techniques

In the research presented in this thesis, a polycationic cell coating is used as part of a bio-ink formulation. In this sub-chapter, cell carrier techniques are briefly reviewed to offer the reader an insight on these techniques that are widely used in cell and drug delivery.

Cells and molecules have been reported to have the ability to heal different diseases, from aggressive cancers to endocrinological chronic conditions, such as diabetes (Orive, Hernández, *et al.*, 2003; Orive *et al.*, 2015). However, long-term cell transplantation is not successful without the following of a rigorous immunosuppressive protocol, necessary to avoid graft rejection (Ryan *et al.*, 2002; Duncan and Wilkes, 2005; Zarrinpar *et al.*, 2016). As an alternative, immune-isolating cell carriers have been widely investigated in the last few decades. These avoid the high costs and low quality of life of chronic administration of immunosuppressants, responsible by the development of opportunistic infections and other worse conditions, at the same time it increases outcome of cell therapies (Su *et al.*, 2010; Krishnan *et al.*, 2014). Cell immuno-isolation can be defined as the immobilization of cells inside a perm-selective capsule, i.e. a semi-permeable membrane that allows influx of oxygen and nutrients, at same time it grants outflux of cellular waste, avoids immune-mediated reactions, and offers protection from mechanical stress (Uludag *et al*., 2000; Nafea *et al*., 2011; Orive *et al.*, 2015). The perm-selective membrane must have the desired degradation kinetics, biocompatibility, physical, chemical and mechanical properties and well-defined permeability to avoid cell escape and possible formation of teratomas (Murua *et al.*, 2008; Kirk *et al.*, 2014). This technology is highly-versatile allowing cell delivery via intravascular, oral or subcutaneous routes, among others, depending on the cell carrier design (Murua *et al.*, 2008; De Vos *et al*., 2010). Additionally, cell immobilisation may consider the transplantation of non-human cells, which would help on the shortage of donor tissue, and the immune-isolation of genetically engineered cells to express any required substance without affecting the host's genome (Lathuilière *et al.*, 2014; Wang *et al.*, 2015). The therapy performance may be increased through the addition of molecules and virus to the system (Martinez-Quintanilla *et al.*, 2015).

The concept of cell carrier is offered by different cell encapsulation strategies: macroencapsulation, microencapsulation and single cell encapsulation (Figure 2.19) (Orive, Gascón, *et al.*, 2003; Park *et al.*, 2014; Steele *et al.*, 2014).

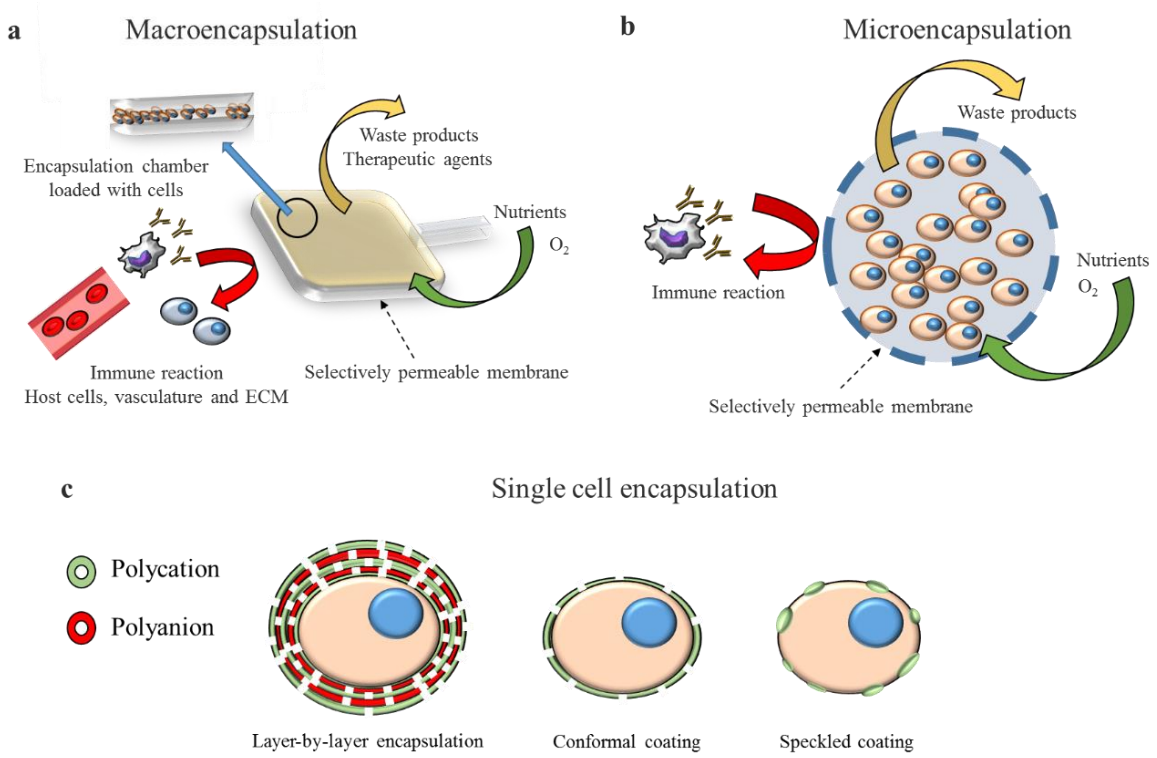

Figure 2.18 – Cell delivery techniques. a) Macroencapsulation; b) Microencapsulation; c) Single cell encapsulation.

Briefly, macroencapsulation comprises the use of implantable flat-sheet devices or hollow-fiber membranes that imprison a large number of cells (millions) that are released in a controlled-manner (Orive *et al.*, 2003). Microencapsulation involves the use of small sized capsules, in range from 100 µm to 750 µm, or conformally coated tissues, that encapsulate hundreds to thousands of cells, allowing the maximization of oxygen and nutrients influx due to a large surface/volume ratio (Murua *et al.*, 2008; Song and Roy, 2016). Finally, single cell encapsulation requires the use of thin conformal coatings that encapsulate cells at a unity level (Fakhrullin *et al.*, 2012; Song and Roy, 2016).

2.3.4.1 Macroencapsulation

Macroencapsulation systems are normally equipped with semi-permeable membranes on its boundaries to allow adequate diffusion of oxygen and nutrients and outflux of waste, necessary to maintain cell survival and renewal, at the same time it protects the encapsulated cells from the host immune response (Uludag *et al.*, 2000; Desai and Shea, 2017). Additionally, macroencapsulation systems must support neovascularization of its

surroundings in order to maximize nutrient and oxygen delivery (Wang *et al.*, 2016). Good oxygen diffusion is essential in macrodevices to avoid cell core necrosis, and respective failure of the implant (K. Wang *et al.*, 2015). Device design, size and thickness are important properties as the system geometry is able to affect the way cells are delivered, conditioning cell survival (Veiseh *et al.*, 2015; Desai and Shea, 2017). Physicochemical and mechanical properties of the macroencapsulation apparatus must be well controlled to provoke minimal innate immune response, which may originate the formation of a fibrotic capsule around the system and affecting its performance (K. Wang *et al.*, 2015; Desai and Shea, 2017).

Nowadays, macroencapsulation devices are mainly researched for cell and molecule delivery, however, when they first appeared in the middle of last century, they were used to study tumour development and tissue rejection through the maintenance of mouse homografts in extravascular diffusion chambers (Algire, 1943; Gray, 2006). During these experiments, Algire and colleagues (1943) found the importance of having the encapsulated tissue/cells apart from the host tissue, which granted cell survival. Nonetheless, xenografts were rapidly rejected due to the passage of smaller proteins and molecules, such as antibodies, which highlighted the importance of the perm-selective property of the membrane. The first macroencapsulation device was commercialized by the Millipore Corporation in the 70's applying the knowledge obtained from Algire and colleagues (Scharp and Marchetti, 2014). This was first applied to diabetes through islet entrapment for insulin delivery. Still today, diabetes affects millions in the world, which presents an incredible commercial potential that lead to the appearance of various biotechnological companies. The search for a solution to this problem has developed macroencapsulation devices in terms of reliability and performance (Scharp and Marchetti, 2014; Desai and Shea, 2017; Skrzypek *et al.*, 2017). The improvement and creation of new designs and use of coatings and new biomaterials on the device manufacture opened avenues to new clinical applications.

Macroencapsulation systems include majorly two main types: flat sheet devices and hollow fibers (Figure 2.20a,b) (Uludag *et al*., 2000; Lathuilière, *et al.*, 2014; Lathuilière *et al*., 2015; Skrzypek *et al.*, 2017). In flat sheet devices cells are immobilized inside an isolated compartment formed by two porous membranes attached to opposite sides. An outer pre-vascularised or vascularisation supporting layer holds the whole system and a cell loading port are also essential parts of this system. For hollow fibers, cells are

entrapped inside the lumen of a selective permeable membrane being the ends of the fibre closed to prevent undesired cell escape. Depending on the engraftment type, macroencapsulation apparatus can be intravascular or extravascular, if the device is engrafted to the host's vasculature or supports neovascularization on its surroundings, respectively (Vaithilingam and Tuch, 2011; Song and Roy, 2016).

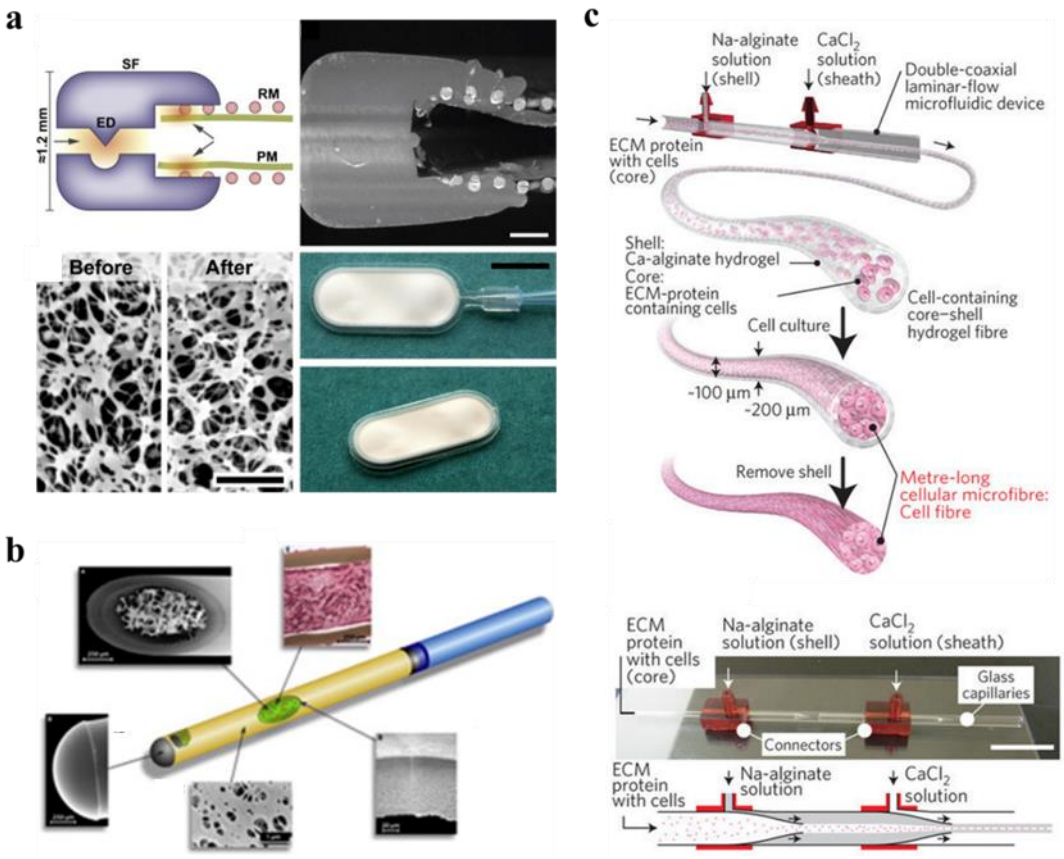

Figure 2.19 – Macroencapsulation systems. a) Flat sheet; b) hollow fibre; c) cell-laden microfibers. Adapted from (Lathuilière *et al.*, 2014; Schwenter *et al.*, 2011; Onoe *et al.*, 2013).

More recently, a new macroencapsulation system has been developed by microfluidic spinning – cell laden microfibers (Figure 2.20c) (Onoe *et al.*, 2013). Using a double-coaxial laminar flow consisting on a pre-gel solution containing cells (core), a second pre-gel solution (shell) and a crosslinking agent (sheath), cells are able to be continuously encapsulated inside a solid and porous hydrogel fibre. This technique does not limit the fibre size, the diameter and length are easily tuned up by the flow rate, being able to reach nanometres to hundreds of micrometers in diameter and meters in size, and presents high

reproducibility and does not rely on voltages or temperatures. Additionally, patterns were obtained, allowing single fibre production and insignificant damage is caused to the cells. However, this process is time-consuming and relatively slow.

2.3.4.2 Microencapsulation

The first cell microencapsulation system was reported by Chang and colleagues in 1964 (Chang, 1964), and in 1980, microcapsules were firstly applied to diabetes treatment by Lim and Sum (Lim and Sun, 1980). Due to the reduced size, 100-750 μm, microencapsulation attracted attention due to the ability to deliver and implant cells and other therapeutics via small diameter catheters, avoiding any major surgery (Rabanel *et al.*, 2009; Al Kindi *et al.*, 2011; Perán *et al.*, 2012). Microencapsulation systems are mostly constituted by polymeric or polyelectrolyte capsules, coatings or hydrogels. Simple and gentle methodologies are vital to grant normal cell behaviour after the encapsulation or coating process (Fakhrullin *et al.*, 2012; Drachuk *et al*., 2013; Song and Roy, 2016). Most of the procedures use aqueous conditions, such as cell medium, which is beneficial for cells. Slow processes and harsh reagents may compromise cell viability but develop a capsule with better mechanical properties (Uludag *et al*., 2000).

Similarly to macroencapsulation devices, microencapsulation systems are constituted by a thin and semipermeable membrane to allow influx of oxygen and nutrients and outflux of cell by-products (Orive *et al.*, 2004; De Vos *et al.*, 2012). Lack of nutrient and oxygen diffusion will lead to hypoxia and, ultimately, necrosis (Ma *et al.*, 2013). The perm-selectivity capacity of the membrane allows to exclude the entrance of high molecular weight cells and molecules, such as macrophages or antigens, which can originate foreign-body reaction (FBR) and respective fibrotic tissue deposition (Tomeit *et al.*, 2015). However, macrophages and other cells produced cytokines and low molecular weight proteins may cross the barrier and affect cell. It has been reported that 50-150 kDa represents the ideal molecular weight cut-off for microencapsulation systems (Tomeit *et al.*, 2015). Additionally, the surrounding membrane immune-isolates the encapsulated cells from the external environment, at the same time it confers the mechanical integrity and resilience necessary to avoid capsule disruption or cell stress (Orive *et al.*, 2003; Drachuk *et al.*, 2013). The capsule or coating enable a controlled release of cells and/or

therapeutic products, avoiding any toxic effect to the surrounding tissues as consequence of a potential rapid release (Orive *et al.*, 2004).

Microencapsulation systems must be designed carefully, attending to three main properties: composition, transplantation site and geometry (Figure 2.21) (Olabisi, 2015; Tomeit *et al.*, 2015). These characteristics affect the system performance, both *in vitro* and *in vivo*, and ultimately, result in inflammatory reactions and graft failure. Spherical structures are commonly adopted to better mimic the morphology and physiology of cells in living tissues and to provide an ideal surface-to-volume ratio for nutrient diffusion (Orlando *et al.*, 2014; Tomeit *et al*., 2015). These two proprieties allow cells to maintain their viability and functions when comparing to other geometries. Additionally, a spherical shape avoids sharp surfaces that worsen inflammatory responses. Nowadays, most the capsules and coatings are "conformal", where the material or materials cover the cell, right on the cell membrane, which constitutes an important step to reduce the internal mass transfer resistance (Uludag, De Vos *et al*., 2000; Drachuk *et al.*, 2013). Biocompatibility is connected to material properties, such as chemical composition and surface charge, as well as to physical properties, such as surface roughness, shape and size (Drachuk *et al*., 2013; Bhujbal *et al.*, 2014; Tomeit *et al*., 2015). Biomaterials must support normal cell behaviour, such as proliferation, migration and differentiation.

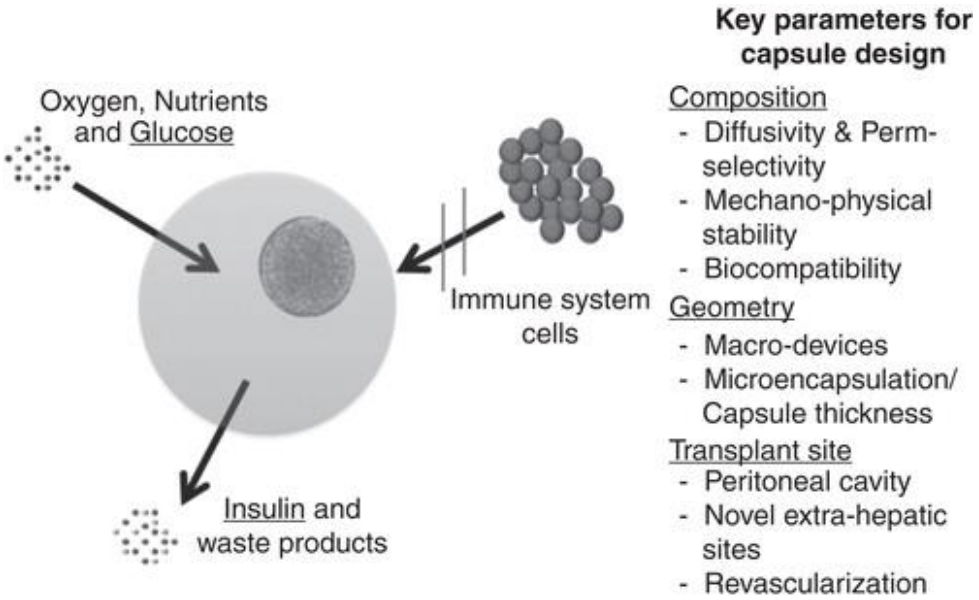

Figure 2.20 – Microencapsulation key parameters for capsule design. From Tomeit *et al*., 2015).

Cell microencapsulation has been also widely used in bioprocessing techniques. Due to the increased demand on cell therapies, scaling-up is necessary to shift from small studies in laboratories to industrialised batches. Nowadays, suspension bioreactors are the main tools used in industrial bioprocessing (Wilson *et al.*, 2013; Allazetta and Lutolf, 2015). Here, cells are held in suspension and rotated within the suspending solution, suffering hydrodynamic shear stress, which end up affecting cell viability and phenotype (Serra *et al.*, 2011; Fernandes *et al.*, 2013; Wilson and Mcdevitt, 2013; Wilson *et al.*, 2014). This technique is not recommended, especially when using stem cells, since these are extremely sensitive to external stimuli, changing its properties in adverse conditions (Fernandes *et al.*, 2013; Wilson and Mcdevitt, 2013; Wilson *et al.*, 2014). Another major issue of the use of suspension bioreactors is the low volumetric productivity obtained (Westman *et al.*, 2012). To minimise the effect of external cues and control the cell microenvironment and, at the same time, increase the productivity, cells have been immobilised recurring to different 3D suspension culture methods: self-aggregated spheroids, cell immobilization on microcarriers or cell microencapsulation (Fan *et al.*, 2015).

3D aggregate spheroids are widely used in stem cell science. These structures allow the re-establishment of cell-cell contacts, mimicking cell microenvironment and, therefore, enhancing cell behaviour and promoting stem cell differentiation (Achilli *et al.*, 2012; Xie *et al.*, 2017). 3D cell aggregates are presented as an interesting and easy strategy for translation to industrial bioprocessing, since these can be cultured in suspension and used in suspension bioreactors (Serra *et al.*, 2011).

In microcarrier-based cultures, small beads are suspended in medium and used as substrate for cell proliferation (Schop *et al.*, 2008; Dias *et al.*, 2017). The microcarrier must be chosen according to the cell characteristics and desired application, however some cells require an extra microcarrier functionalisation in order to not compromise cell characteristics (Alves *et al.*, 2012). The flexibility of this technology is represented by the ease of scaling up, since increasing the substrate area, directly increase the cell seeding area (Badenes *et al.*, 2016). This reduces the volume of any consumables needed, decreasing the total cost of cell bioprocessing.

Although 3D aggregate spheroids and microcarriers present interesting advantages for bioprocessing applications, some problems compromise their use. For both strategies cells

suffer different mechanical forces due to the stirring in bioreactors, which end up affecting cell characteristics, namely cell differentiation, morphology and metabolism (Fan *et al.*, 2015). Additionally, both systems are able to form uncontrolled aggregate sizes and microcarrier clumping, which lead to necrotic centers and/or promotion/inhibition of cell differentiation (Alves *et al.*, 2012). In terms of cryopreservation, an essential process for scaling up, cell viability is compromised after thawing, when using both systems (Serra *et al.*, 2011).

Cell microencapsulation has shown to overcome the bioprocessing problems stated above. The capsule is able to protect the cell from the hydrodynamic shear stress and avoid the clumping of aggregates and microcarriers in culture through the prevention of excessive cell agglomeration (Serra *et al.*, 2011). This matrix works as a semi-permeable membrane that allow influx of nutrients, oxygen, and growth factors, and outflux of waste products (Wilson and Mcdevitt, 2013). As reported earlier, the capsule is able to be designed in terms of materials, porosity and thickness, in order to best mimic the microenvironment, modulating the cell phenotype and controlling its differentiation. However, it must be noted that biomaterials must be carefully chosen. When in stirred bioreactors, scaffolds suffer hydrodynamic forces, which are not present in static cultures, and that may change not only the scaffold properties and structural integrity, but also the cell properties (Rathore *et al.*, 2013; Fan *et al.*, 2015). It was observed that microencapsulated cells improve cell post-thaw functions for different cell types due to the maintenance of cell-cell contacts and protection from ice crystal damage (Fernandes *et al.*, 2013). This is an important characteristic for bioprocessing in order to turn into a high-throughput process in terms of cell preservation for storage and transportation of cell products.

2.3.4.2.1 *Microcapsules*

As reported earlier, microcapsules are widely used in tissue engineering and bioprocessing research, due to the beneficial properties. In both applications, high-throughput is essential to produce the high cell number needed for implantation or therapeutic production. The most used encapsulation methods include extrusion technologies and emulsion techniques (Mazzitelli *et al.*, 2011; Selimović *et al.*, 2012; Sánchez *et al.*, 2013; Rakszewska *et al.*, 2014; Oliveira *et al.*, 2015). The latter is based

on combining a cell-laden aqueous solution with an immiscible organic phase, such as oil. When well dispersed, the capsule is formed by adding a crosslinker. On the other hand, in extrusion techniques, capsule formation is based on the extrusion of a cell-laden gel precursor, droplet formation and respective crosslinking. Different extrusion technologies have been used to fabricate microencapsulated cells (Figure 2.22): Simple dripping, electrostatic extrusion, coaxial flow, vibrating nozzle, jet cutting and spinning disk atomization (Sánchez *et al.*, 2013; J.-Z. Wang *et al.*, 2017; Némethová *et al.*, 2017). Each technology has its own pros and cons (Table 2.4), however these do not allow to produce capsules with sizes smaller than 200-300 µm.

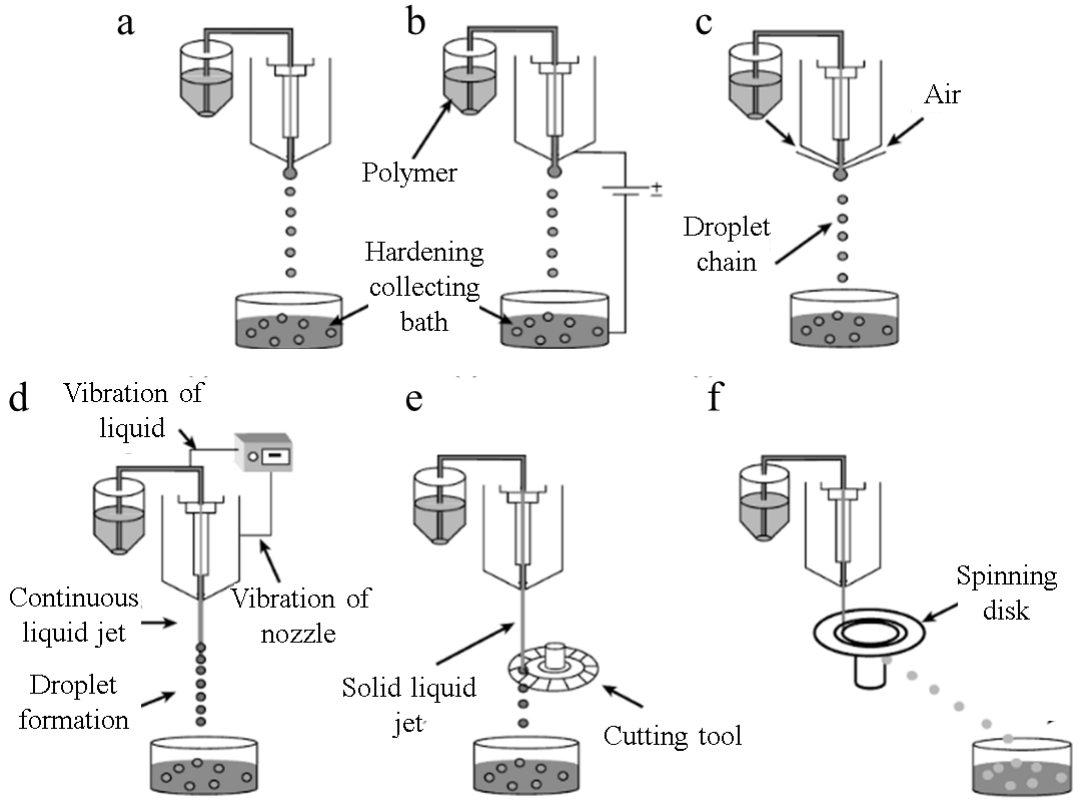

Figure 2.21 – Different microcapsule production methodologies. **a** Simple dripping, **b** electrostatic extrusion, **c** coaxial flow, **d** vibrating nozzle, **e** jet cutting, and **f** spinning disk atomization. From (Mishra, 2015).

Simple dripping or gravitational dripping is based on the extrusion of cell-laden gel precursor through a small needle (Zhang and Ma, 2016). As the constant pressure is applied, droplets will start to form until they break from the needle and fall due to the gravity into a hardening bath. This bath is filled with a crosslinker solution that will gel

the hydrogel precursor. In electrostatic extrusion, an electric potential is applied between the needle and the hardening bath (Manojlovic *et al.*, 2006; Zhang and Ma, 2016). Droplets are formed due to the electrostatic force, surface tension and gravity. Coaxial flow is a similar method to the simple dripping (Andersen *et al.*, 1980; Oliveira *et al.*, 2015; Némethová *et al.*, 2017). However, instead of recurring to the gravity force to form and break down the gel precursor droplet, this technique applies compressed gas to force the droplet breakage and consequently fall into the hardening bath. Vibrating nozzle uses vibration to break down a continuous jet of gel precursor into droplets (Zhang and Ma, 2016; Némethová *et al.*, 2017). These are then crosslinked when falling into the hardening bath. Jet Cutter technology is based on a continuous stream of cell-laden gel precursor that is cut by a rotating cutting wires (Sánchez *et al.*, 2013; Paulo *et al.*, 2017). This way, droplets are formed and fall to the hardening bath. The spinning disk extrusion method used a spinning disk to cut the continuous stream of cell-laden gel precursor (Senuma *et al.*, 2000; Teunou and Poncelet, 2005). The droplets are then formed and fall to the hardening bath to produce a resilient capsule. Detailed reviews on extrusion methodologies can be found elsewhere (Mishra, 2015; J.-Z. Wang *et al.*, 2017; Némethová *et al.*, 2017). Comparing the different extrusion techniques, vibrating nozzle shows to enable the repeatable and standardised production of homogenous microcapsules, in a sterile and operator-friendly environment (Némethová *et al.*, 2017). Additionally, this technique presents low variability between batches, at the same time it may be used for high throughput production of microcapsules.

Table 2.3 - Characterisation of the different microencapsulation extrusion methodologies. Adapted from (Némethová *et al.*, 2017).

Requirements	Droplet extrusion technologies				
	Coaxial air-flow enhanced dropping	Electrostatic enhanced dropping	Atomization by a rotating disc or rotating nozzles	Jet-cutter	Vibration
Reproducibility	✓	✓	✗	✗	✓
Standardisation	✓	✓	✓	✓	✓
Size scalibility	✓	✓	✓	✓	✓
Low size dispersity	✓	✓	✗	✗	✓
Minimal batch-to-batch variability	✓	✓	✗	✗	✓
High throughput production	✗	✗	✓	✓	✓
Sterile work conditions	✓	✓	✓	✓	✓
Operator independency	✓	✓	✓	✓	✓
User-friendliness	✓	✓	✓	✓	✓

2.3.4.2.2 *Conformal coatings*

Conformal coatings are characterised by a thin, protective and semi-permeable layer attached to the cell membrane. These can be fabricated with different materials: polyelectrolytes, biomolecules, metal nanoparticles or oxides (Fakhrullin *et al.*, 2012; Dai *et al.*, 2018). Just like microcapsules, these layers protect cells from external cells and stimulus, at the same time they grant nutrient, oxygen and waste transport to and from the coated cell. Contrarily to microcapsule fabrication, which produces capsules much larger than cells, resulting in inefficient mass transport, these coatings present reduced thickness, ability to coat single cells and tightly fit the cell membrane (Uludag *et al.*, 2000). The thickness of the protective layer can be ultrathin, reaching nanometers in size (2–100 nm). Conformal coatings are normally produced via emulsion, covalent or non-covalent techniques (Kellam *et al.*, 2003; Wilson *et al.*, 2009; Drachuk *et al.*, 2013). Covalent techniques rely on ionic and hydrophobic interactions between the cellular

membrane and the material (Kellam *et al.*, 2003). On the other hand, non-covalent methodologies comprise the introduction of new physical and chemical characteristics onto the cellular membrane through the adsorption of biomolecules and by electromagnetic interactions (Kellam *et al.*, 2003; Prescher and Bertozzi, 2005; Rabuka *et al.*, 2008). Conformal coatings via emulsion techniques use similar strategy to what is described in microcapsules sub-chapter.

Non-covalent cell surface modification offers the advantage over covalent techniques of minimal perturbation of the cell physiology, thereby preventing interference with important cellular functions governed by cell surface molecules (Kellam *et al.*, 2003; Prescher and Bertozzi, 2005; Rabuka *et al.*, 2008). Also, reversibility is possible due to weak bounds between the cell membrane and material (Thibault *et al.*, 2003; Di Crescenzo *et al.*, 2014). On the other hand, covalent techniques are generally irreversible and may interfere with cellular functions after gelation mechanisms (Nicodemus and Bryant, 2008; Khetan *et al.*, 2013). However, this procedure presents better mechanical properties than non-covalent surface modification (Wipff *et al.*, 2009). Nowadays, LbL methods are presented as the most advanced conformal coating strategy for cell delivery, allowing single cell coating with a fully controlled environment as number of layers, porosity, mechanical properties, thickness and composition are able to be tuned (Johnston *et al.*, 2006; Guzmán *et al.*, 2017). This technique is achieved through the deposition of successive layers of negatively and positively charged materials on a cell surface. LbL successfully avoids membrane disruption caused by electrostatic coating, a consequence of the lack of polysaccharides on mammal cell membrane (Menger *et al.*, 2003; Fakhrullin *et al.*, 2012; Matsusaki *et al.*, 2012; Vaidyanathan *et al.*, 2015). However, it can be a laborious and time-consuming process, as it requires multiple 10–15-min sequential depositions of oppositely charged monolayers onto the cell surface with intermediate washes, with up to a 2-h interval between layers to guarantee good viability and typically four to six bilayers (Menger *et al.*, 2003; Fakhrullin *et al.*, 2012; W. Li *et al.*, 2015). Different polyelectrolytes have been used with LbL technique – Poly-L-Lysine (PLL), poly(allylamine hydrochloride) (PAH), poly(styrene sulfonate) (PSS) or polyethylenimine (PEI). Nanoparticles and nanotubes can be also applied by using polyelectrolyte layers as templates (Fakhrullin *et al.*, 2012).

2.3.4.2.3 *Hydrogels as Cell Carriers*

The use of hydrogels in bio-inks (effectively a special case of cell carrying) has previously been described in section 2.3.1. The control over degradability and molecule release on hydrogels has also attracted interest for drug delivery applications (Van Vlierberghe *et al.*, 2011; Caló and Khutoryanskiy, 2015; Xue *et al.*, 2015). Natural and synthetic hydrogels are also widely in tissue engineering research, for cell delivery, space filling agents or as cell scaffolding, due to their beneficial properties. Decellularised meniscus ECM hydrogels were used as cell carrier for hMSCs for meniscus defects. Yuan and colleagues observed the upregulation of fibrochondrogenic marks, at the same time the hydrogels successfully delivered the cells to wound area (Yuan *et al.*, 2017). Tissue regeneration was demonstrated, and hydrogels offered protection against the development of pathologies, such as osteoarthritis. Ballios et al used a hybrid hydrogel made of hyaluronan and methylcellulose to encapsulate retinal stem-progenitor cells (Ballios *et al.*, 2010). It was exhibited that, once applied in the sub-retinal space, the hydrogel remained intact for 7 days. This technique showed to be a promising cell carrier as the cell distribution in the sub-retinal space was more homogenously than when using recurring saline solutions. In another study, hydrogels were found to be extremely useful to understand how the microenvironment influenced cells. Benoit and colleagues used distinct functionalised PEG hydrogels that showed that differentiation pathways were affected by the functionalisation type (Benoit *et al.*, 2008). Additionally, Khetan and colleagues reported that hMSC behaviour is also regulated by the mechanical properties offered by the hydrogel (Khetan *et al.*, 2013). Kerscher and her team developed a PEG-fibrinogen encapsulation system to provide a specific microenvironment to differentiation human pluripotent stem cells in to heart tissues (Kerscher *et al.*, 2016). This system allowed correct heart tissue development and maturation. To avoid the crosslinking negative effects, Foo and colleagues developed a cell encapsulation system using hydrogels that combined WW and proline-rich domains (Wong Po Foo *et al.*, 2009). This two-component hydrogel was used to encapsulate neural stem cells that retained their normal behaviour, including differentiation and self-renewal (Figure 2.23**a**). More recently, hydrogels were also used to encapsulate living organisms for long-term microscopy periods due to its high hydration that stabilised the nematode Caenorhabditis elegans (Figure 2.23**b**) (Burnett *et al.*, 2018).

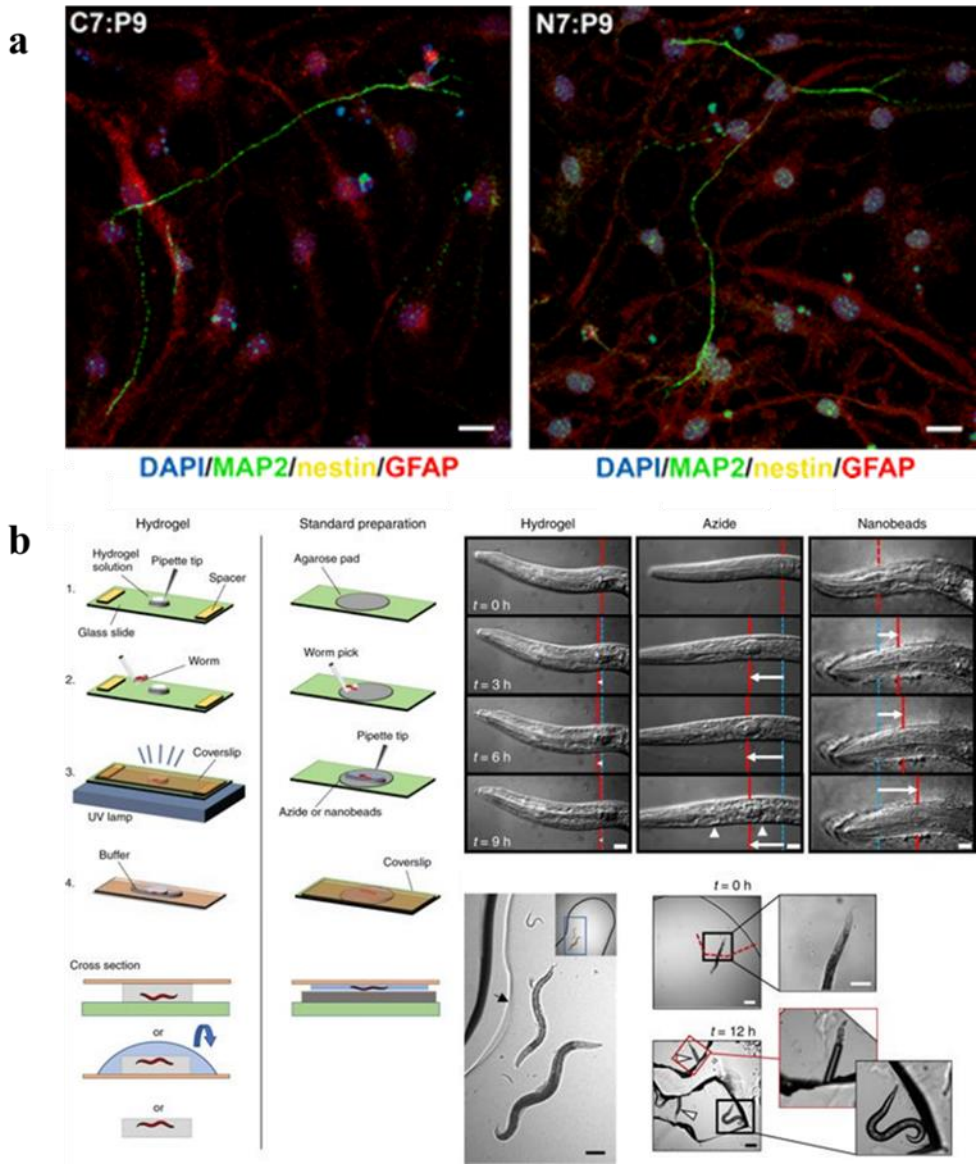

Figure 2.22 – **a** Hydrogel encapsulated differentiated neurons showing neuronal marker MAP2 (green), glial marker (red), progenitor marker nestin (yellow) and nuclei (blue); **b** Methodology used for long-term microscopy of C. Elegans. It is observed normal worm function even after 12 hours. Adapted from (Wong Po Foo *et al.*, 2009) and (Burnett *et al.*, 2018).

2.4 Summary

The literature review has showed that:

- Tissue Engineering aims i) to promote regeneration and create healthy and functional tissues and organs for grafting and transplantation and ii) to establish reliable *in vitro* models of tissues and diseases to foster therapeutic advancements.

- There are 4 main bioprinting technologies: inkjet, microvalve, extrusion-based and laser-assisted bioprinting. Each technique provides different advantages and disadvantages and its selection must be based on the desired application.

- Bio-inks are composed by biomaterials, cells and differentiation and growth factors that, once processed by a bioprinting technique may originate 3D cell-laden structures. Currently, hydrogels and hydrogel precursors are the most used type of materials on bio-inks. However, cell aggregates and single cells in suspension may be also adopted for bio-ink formulation.

- Bio-inks can be composed by natural (alginate, collagen, among others) and/or synthetic (PEG, etc). Materials must be carefully chosen depending on the desired properties and bioprinting technique.

From the literature review above, it is possible to conclude that bioprinting is allowing a more controllable and biomimetic 3D cell culture systems. Each bioprinting technique presents different specifications (Table 2.1), which make each of them ideal for certain applications. However, limitations are inherent to each technology.

In the following chapters, two novel bio-inks are developed to overcome limitations on inkjet bioprinting and production of high cell dense cell-laden hydrogels. The first bio-ink introduces positive electrical charges on the cell membrane which results on the inhibition of natural cell aggregation. This way, nozzle blockage on inkjet bioprinting is avoided, allowing printing for at least 60 minutes, at the same time it increases the technology's reliability. Secondly, a collagen-alginate-fibrin hydrogel bio-ink was formulated and used with a proprietary drop-on-demand bioprinting technology to develop high cell dense cell-laden hydrogels. Here, cell densities of 40×10^6 cells/mL were possible to be impinged, without nozzle blockage or low cell viability. The same does not happen when using other bioprinting techniques, such as inkjet, microvalve and extrusion-based bioprinting. In the first two, nozzle blockage conditions the cell density used, which normally allow bio-inks with a maximum of 5×10^6 cells/mL. On the other hand, although high cell dense bio-inks can be applied in extrusion-based bioprinting, cell viability is normally reduced due to the shear stress.

Table 2.4 – Comparison between the four main bioprinting methodologies.

	Inkjet bioprinting	Single microvalve bioprinting	Extrusion bioprinting	Laser-assisted bioprinting	Ref.
Viscosity of Material Deposited on the Substrate	3–30 mPa/s	1–70 mPa/s	30 mPa/s to >$6x10^7$ mPa/s	1–300 mPa/s	(Murphy and Atala, 2014; Donderwinkel, van Hest and Cameron, 2017; Ng *et al.*, 2017)
Printing Speed	1 – 10 000 droplets/s	6 500 droplets/s	10 µm/s – 700 mm/s.	100 – 5000 droplets/s	(Guillotin *et al.*, 2010; Murphy and Atala, 2014; Bakhshinejad and D'souza, 2015; Gudapati, Dey and Ozbolat, 2016; Lee and Yeong, 2016; Ovsianikov, 2016; Ozbolat and Hospodiuk, 2016; Donderwinkel, van Hest and Cameron, 2017; Gao *et al.*, 2017; Ozbolat, 2017)
Volume deposition rate	160 µL/s	40 µL/s	3-15 µL/s	175 - 1800 nL/s	(Guillotin *et al.*, 2010; Gudapati, Dey and Ozbolat, 2016; Graham *et al.*, 2017; Koch *et al.*, 2017; Zhang, 2018)
Resolution	pL droplets	pL to nL droplets	5 µm to mm size deposited track	<pL droplets	(Murphy and Atala, 2014; Ozbolat, 2017)
Cell viability	>85%	>90%	40-80%	>95%	(Murphy and Atala, 2014; Ozbolat, 2017)
Crosslinking Process	Post-printing	Post-printing	Pre-, post-printing	Post-printing	(Murphy and Atala, 2014; Lee and Yeong, 2016)
Cell density	Low, <$5x10^6$ cells/mL	High, 10^7/mL	High, cell spheroids	High, 10^8 cells/mL	(Murphy and Atala, 2014; Donderwinkel, van Hest and Cameron, 2017; Ozbolat, 2017)

Chapter 3. Materials and methods

3.1 General methods

In this sub-chapter, the general assays used in this research will be described. Unless otherwise stated, all the reagents were obtained from Sigma-Aldrich, USA.

3.1.1 *Cell Culture*

Tissue culture was carried out in aseptic conditions using a class II laminar flow hood, previously decontaminated using a 70% ethanol solution. Different cell types were used during this study, osteosarcoma (U2OS, ATCC® HTB-96™), Ewing's sarcoma (TC-71, kindly donated by Dr. Britta Vormoor, Newcastle University (Vormoor *et al.*, 2014), Neo-Natal Human Dermal Fibroblasts (Neo-NHDF, Lonza, Switzerland), and immortalized human bone marrow stem cells using human telomerase reverse transcriptase (BMSC-hTERT) - Y2O1 cells - (kindly donated by Professor Paul Genever, York University (James *et al.*, 2015). Primary MSCs were kindly donated by Dr. Deepali Pal. U2OS, TC-71 and Neo-NHDF were cultured using high-glucose Dulbecco's Modified Eagle Medium (DMEM, Life Technologies) supplemented with 10% Fetal Bovine Serum (FBS) and 5000 U/mL penicillin/streptomycin at 37 °C and 5% CO_2. Y2O1 cells were culture in the same previous medium but also supplemented with pyruvate at 110 mg/L. For osteogenic differentiation, the Y2O1 basal medium was supplemented with L-Ascorbic acid 2-phosphate sesquimagnesium salt, ß-Glycerophosphate, and Dexamethasone, at a final concentration of 50 µg/mL, 5 mM, and 10 nM, respectively. Trilineage differentiation was carried by Dr. Deepali Pal, where primary MSCs were firstly incubated during 16 days in low glucose DMEM supplemented with 20% FBS and 1% penicillin/streptomycin, followed by a 14-day incubation using osteogenesis differentiation kit (Thermo Fisher Scientific, USA), chondrogenesis differentiation kit (Thermo Fisher Scientific, USA) and adipogenesis differentiation kit (Thermo Fisher Scientific, USA) for osteogenic, chondrogenic and adipogenic differentiation, respectively. All cell lines used in this study were obtained from the indicated suppliers and were tested for mycoplasma contamination.

Cells were passaged when reached to 70-80% of confluency. Cells were washed with pre-warmed DPBS (Dulbecco's phosphate-buffered saline) without calcium and magnesium

and detached using trypsin/ Ethylenediamine tetraacetic acid (EDTA) or 0.5% EDTA/DPBS, following 5-10 min incubation at 37 °C and 5% CO_2. After cell detachment have been visually confirmed using a microscope, trypsin was neutralised using pre-warmed cell medium and the cell suspension centrifuged at 1200 rpm during 5 min. The supernatant medium was aspirated, and the cell pellet diluted in fresh and pre-warmed supplemented medium in an appropriate volume to subculture the cells at a ratio of 1 to 3 (one flask to three flasks).

3.1.2 *Cytotoxicity and Metabolic Assays*

Cytotoxic and metabolic assays are tools that quantify the cell response to these external factors in terms of viability or metabolism. In this research, the effect of different PLL concentrations on cell viability was measured recurring to Live/Dead and caspase-3 activity detection and membrane permeability assays and cell metabolism studied through 3-(4,5-dimethylthiazol-2-yl)-2,5-diphenyltetrazolium bromide (MTT) assay. Additionally, Live/Dead was also used to characterise the cell-loaded collagen-alginate-fibrinogen (CAF) hydrogels.

Live/Dead assay (Molecular Probes by Life Technologies, USA) was used to distinguish live from dead cells based on intracellular esterase activity and integrity of plasma membrane. Calcein acetoxymethyl (calcein AM) is a green fluorescent dye that stains live cells in presence of esterase activity. On the other hand, when plasma integrity is compromised, ethidium homodimer-1 (EthD-1) binds to nucleic acids staining dead cells with a bright red. This is a versatile assay that may be used to both quantitative and qualitatively examine cell viability, however, during this study Live/Dead assay was merely used as qualitatively assay through staining analysis using a fluorescence microscopy.

The reagent stock solutions were removed from the freezer and warmed to room temperature and were mixed using the manufacturer's recommendations to obtain a 4 μM ethidium homodimer and 2 μM calcein AM solution. For microscope slides, after a HBSS (Hanks' Balanced Salt Solution) wash, approximately 5×10^4 cells were cultured, followed by the addition of 100 μL of Live/Dead working solution and a 40-minute incubation at room temperature. For six-well plates, after a HBSS wash, approximately 2×10^5 cells were cultured, followed by the addition of 500 μL of Live/Dead working

solution, and a 40-minute incubation at room temperature. For CAF hydrogels, after a HBSS wash, Live/Dead solution was used to completely cover each hydrogel during one-hour incubation at room temperature. Slides and well plates were imaged with a fluorescence microscope (Leica DM IL LED, Leica Microsystems) using the suggested filters: fluorescein filter for calcein (live cells) and Texas red filter for ethidium homodimer (dead cells). Images were captured using SPOT Advanced software (SPOT Imaging Solutions). CAF hydrogels were imaged using a Nikon A1R (Nikon, Japan).

Caspase-3 activity detection and membrane permeability assay was used to quantify the cell viability, being able to distinguish the cell death pathway between apoptosis and necrosis. NucView™ 488 Caspase-3 Substrate (Cambridge Bioscience) was used to detect caspase-3 activity in cells and to identify apoptotic cells. The NucView 488 DNA dye is attached to a caspase-3 substrate peptide sequence DEVD, which makes the dye unable to couple to DNA and be fluorescent. Once crossing the cell membrane, in presence of caspase-3 due to cell apoptosis, the substrate is cleaved, and the probe migrates to the nucleus staining it with green fluorescence (Figure 3.1a). The cell membrane permeability was studied using propidium iodide (PI, BD Biosciences), a membrane impermeant dye that binds to DNA staining the cell in red when cell membrane is compromised, a common characteristic of necrotic cells (Figure 3.1b).

The caspase-3 activity detection and membrane permeability assay were adapted from the manufacturer instructions (Cambridge Bioscience, UK). After the coating procedure, 0.2 mL of cells at a density of 1×10^6 cells/mL in DPBS was collected, and 1 µL of 0.2 mM NucView 488 substrate stock solution and 2.5 µL of PI stock solution (BD Biosciences, USA) were added. After the solutions had been mixed, the cells were incubated at 37 °C and 5% CO_2 for 15–30 min, protected from light. Before cell analysis on an ImageStream X Mark II Imaging Flow Cytometer (Merck Millipore, Germany) - nearly 9500 events for each concentration - 200 µL of DPBS was added to each sample. Samples were analysed using IDEAS software (Merck Millipore).

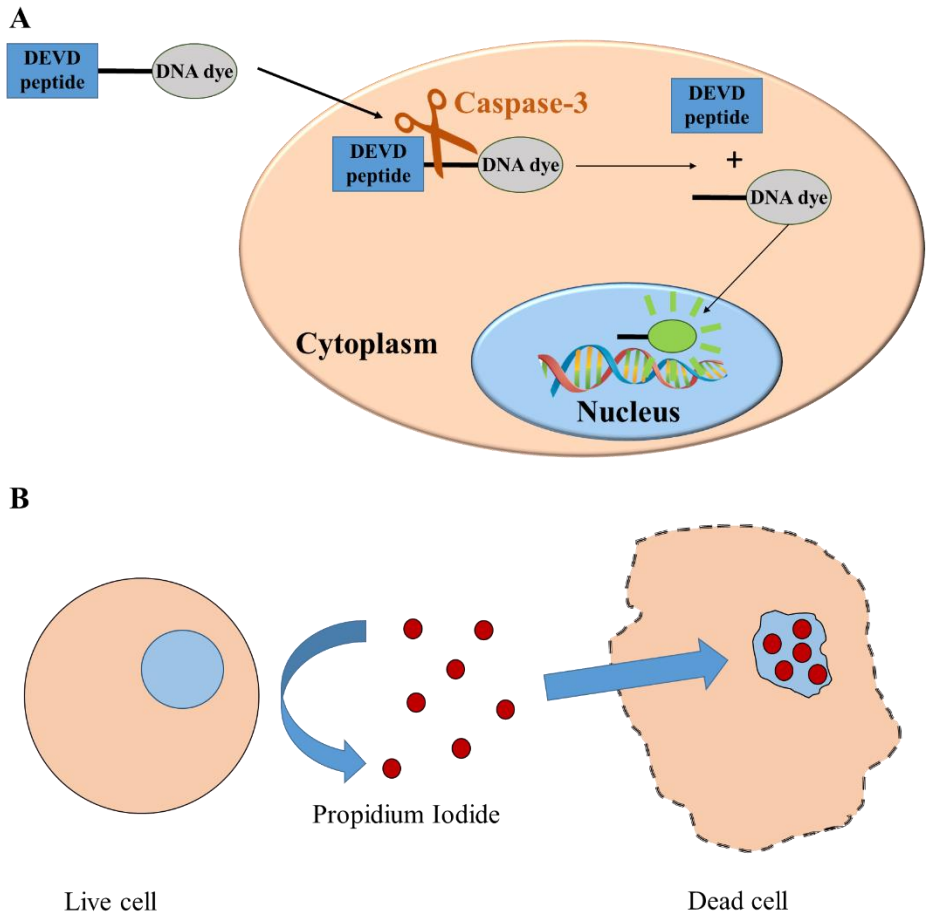

Figure 3.1 - **a** Diagram showing intracellular caspase-3 detection using NucView 488 Caspase-3 Substrate. The DNA dye is not fluorescent until cleavage by caspase-3 and DNA binding. **b** Schematic showing the principle behind the cell membrane permeability assay with PI. PI is only able to penetrate a disrupted cell membrane, staining the nucleus.

The MTT assay is a frequently used colorimetric assay for cell metabolism study. When introduced into cell culture, the yellow coloured MTT is converted into water-insoluble purple formazan by the succinate dehydrogenase enzyme produced by the active mitochondria (Figure 3.2).

Cells at a density of ~1 × 10^5/mL were seeded in 24-well plates and incubated at 37 °C and 5% CO_2 for 4, 24, 72, and 168 h. Following the incubation period, supplemented DMEM was replaced by serum-free DMEM and MTT solution (5 mg/mL in PBS), reaching a final concentration of 0.5 mg/mL. After a 4-h incubation period at 37 °C and 5% CO_2, serum-free DMEM was replaced by 200 µL of isopropanol (Fisher Scientific, USA) under gentle agitation for 20–30 min and protected from light. Afterward, 100 µL

of dissolved formazan was transferred to a 96-well plate, and the absorbance was measured with a spectrophotometer (Sunrise, Tecan, Switzerland) at 570 nm.

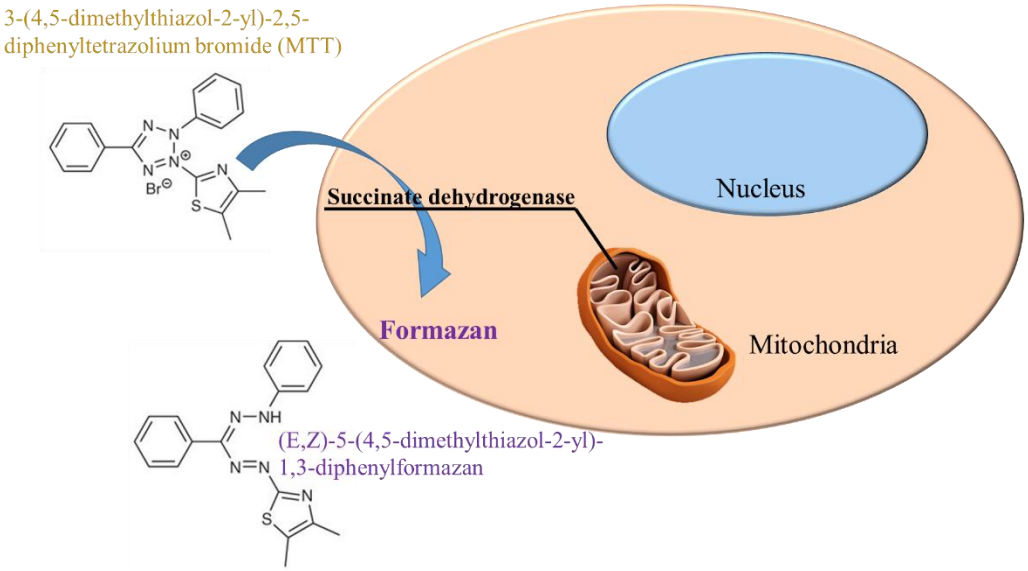

Figure 3.2 - MTT assay concept representation. The mitochondrial produced succinate dehydrogenase reduces the MTT forming formazan.

3.1.3 *Cell Fixation and Probe Staining for Confocal Microscopy*

Cellular staining is essential in microscopy to reliable detect cell constituents (from cell membrane to nucleus and organelles) allowing a precise study on cell behaviour upon the introduction of an external factor. During this work, two different cell staining have been used: Phalloidin–Tetramethylrhodamine B isothiocyanate (phalloidin) and (4',6-diamidino-2-phenylindole) (DAPI, Vector Laboratories, USA). The first uses a toxin derived from the mushroom *Amanita phalloides* that strongly binds to polymeric F actin, creating highly stabilized actin filaments and, due to rhodamine, staining the cell with a red fluorescence. DAPI is a commonly used nuclear staining that binds to the Adenine-Thymine bonds in the DNA, emitting a blue fluorescence. A green coloured fluorescein isothiocyanate labelled PLL was also used along this work.

Coated cells were fixed immediately after the coating process or 1h, 2h, 3h, 4h, or 1 day later once attached and proliferating using 4% paraformaldehyde for 15 min at room temperature. Cells were washed three times using 0.1% DPBS/Tween 20 (Sigma Life Science) and phalloidin (1 mg/mL) added during a 20-min light-protected incubation period at room temperature. After further washing, DAPI (1:2500 solution) was added,

and the solution was subjected to a 15-min light-protected incubation period at room temperature. Cells were washed and resuspended in 500 μL of 0.1% DPBS/Tween 20 solution. CAF hydrogels followed the same protocol, however, phalloidin and DAPI incubation periods were increased to 60 and 40 min, respectively. Fixed cells and hydrogels were stored protected from light at 4 °C. Cells coated with PLL-Fluorescein isothiocyanate (PLL-FITC) were visualized using a Leica TCS SP2 UV AOBS MP (Upright) point scanning confocal microscope (Leica Microsystems) at 20× magnification. Cell loaded hydrogels were studied using a Nikon A1R point scanning confocal microscope (Nikon, Japan) at 10× magnification.

3.1.4 *Polymer Uptake Detection by Transmission Electron Microscopy*

Transmission Electron Microscopy (TEM) is an ultrastructural microscopy technique that uses an electron beam to pass through an ultrathin nanometric resin covered section of a pre-treated cell or tissue sample. Once the electron beam is passing through the sample, it will be absorbed or scattered, being then collected by a detector and forming a 2D black and white image. Due to the ultra-resolution (≈20 nm) of this technique it is possible to precisely study different cell organelles, viruses or bacteria.

The polymer localization examination was performed using a Phillips CM 100 Compustage (FEI) transmission electron microscope (Philips, Netherlands), and digital images were collected using an AMT CCD camera (Deben, UK). Coated cells were fixed using a solution of 2% glutaraldehyde (TAAB Laboratory Equipment, UK) in sodium cacodylate buffer at 4 °C, followed by a secondary fixation with 1% osmium tetroxide (Agar Scientific, UK). Cells were subjected to several dehydration steps, embedded in resin, and cut in ultrathin sections (approximately 70 nm) using a diamond knife on a Leica EM UC7 ultramicrotome (Leica Microsystems). The sections were stretched with chloroform to eliminate compression and mounted on Pioloform-filmed copper grids (Agar Scientific).

3.1.5 *Polymer Metabolisation by Flow-Activated Cell Sorting*

Flow cytometry is widely used biochemical method that allows a complete cell characterisation. It works on a single cell basis and uses a number of lasers to analyse cell

size and roundness as well as the expression of fluorescent cell surface and intracellular markers. This allows the identification of different cells from a heterogenous population being able to organise the cell in sub-population depending on its physical characteristics and expressed markers. During this work, Flow-Activated Cell Sorting (FACS) was used to measure the fluorescein isothiocyanate intensity during the PLL-FITC metabolisation by coated cells.

PLL-FITC-coated cells were analysed 15 min, 24 h, and 48 h following coating. A cell density of ~2×10^6/mL in HBSS without phenol red was prepared, and data were acquired on a FACSCalibur flow cytometer (BD Biosciences). Forward-scattered and sideways-scattered data were used to gate in intact cells and exclude cell debris. The obtained data were analysed using Flowing Software v2.5.

3.1.6 *G-Band Karyotyping*

G-band karyotyping is a conventional cytogenetic analysis that allow the observation of genetic aberrations in chromosomes. Cells are arrested in the metaphase, the cell cycle phase when the chromosomes are the second most-condensed and highly coiled, following processing to obtain a characteristic banding pattern that allow chromosome identification as well as their numerical and structural aberrancies.

Cells were incubated with 0 or 10 μg/mL PLL until 50–80% confluency. On the day before the harvest, 10 μL/mL colcemid was added to each cell culture flask and incubated overnight. Cells were gently washed with DPBS, and trypsin was used to detach the cells. After a 7-min 400*g* centrifugation, 0.075 M potassium chloride was added to the pellet with vortexing to ensure mixing. Then, 5 mL of Fresh Carnoy's Fixative was added dropwise, and another 5 mL of the same fixative added without mixing. Subsequently, the mixture was centrifuged at 400*g*, the supernatant was removed, and an additional 5 mL of fixative was added. To evaluate whether the slide provided good-quality information on the harvest, the following protocol was used: cells were centrifuged at 400*g* for 5 min, and the supernatant was removed until only 300 to 500 μL remained, after which the cells were gently resuspended. Drops of the cell suspension were pipetted onto a slide, and fresh Carnoy's Fixative was added. Finally, for G-banding, the slides were aged at 60 °C overnight and immersed in 50 mL of PBS and 1 mL of 10× trypsin (0.5%), before being stained with Leishmann and Giemsa Staining Solution for 3 min. Slides were then

allowed to completely dry. DPX mountant was finally added, and the slides were observed using a light microscope at 1250× magnification.

3.1.7 *CAF hydrogel compression test*

Mechanical properties of scaffolds are of capital importance on 3D cell cultures. Cells sense shear stress, stiffness or hardness of materials, shaping their morphology, activity, and even fate [Harnessing Traction-Mediated Manipulation of the Cell-Matrix]. Therefore, it is essential to guarantee that the produced CAF hydrogels presented similar mechanical properties to natural soft tissue. Compression tests were performed using a tensile tester EZ-SX (Shimadzu, Japan) prepared with a 20 N load cell. Three samples were cut to a parallelepiped shape with a dimension average of 0.65x0.65x0.33 cm. The crosshead speed was set at 1 $mm \cdot min^{-1}$ and the test was carried at room temperature. The compressive modulus was calculated on the linear elastic regime (10-20%) following the equation below:

$$E_c = \frac{\sigma_c}{\varepsilon_c} \tag{3.1}$$

where E_c represents the compressive modulus (Pa), σ_c is stress in Pascal, and ε_c is the strain represented by the elastic portion of the stress-strain curve.

3.1.8 *Gel precursor viscosity*

The microvalves used during this work do not allow to jet materials with superior viscosities. Therefore, it was essential to understand the viscosities of the gel precursors used during this work to characterise the microvalve compatibility. The rheological measurements for viscosity were performed on a HR-2 Discovery Hybrid Rheometer (TA Instruments, USA), with a standard steel parallel plate geometry (40 mm) and 1 mm of gap. Each tested sample had a volume of 1.2 mL and all measurements were performed at 25^{o}C.

3.1.9 *Hydrogel degradation assay*

The hydrogels produced in this work aim to be used as matrix for the development of microtissues, therefore slow degradation was necessary to assure for long incubation periods. CAF hydrogel degradation was obtained through gravimetric analysis. Once printed, each sample was wiped with filter paper and weighted before immersion in high-glucose with pyruvate DMEM at 37ºC and 5% CO_2 for 1, 3, 7, and 14 days. After the test end, samples were dried with filter paper to remove the excess of medium and reweighted. The degradation was calculated using the following equation:

$$Degradation\ (\%) = 1 - \frac{W_f}{W_i} \times 100 \tag{3.2}$$

where W_i represents the sample weight after printing (day 0) in grams, and W_f is the sample weight after 1,3, 7 or 14 days of immersion in DMEM in grams.

3.1.10 *Glucose uptake*

High-cell density hydrogels were produced during this research therefore, it was important to guarantee that nutrients were able to diffuse to the most inner site of the hydrogel. For this, a glucose analogue, 2-(N-(7-Nitrobenz-2-oxa-1,3-diazol-4-yl)Amino)-2-Deoxyglucose (2-NBDG; Thermo Fisher Scientific, USA), was used to study the hydrogel capacity on solution uptake. A 0.06845 mg/mL 2-NBDG in DPBS without calcium or magnesium solution was prepared and protected from light. After washing the samples with DPBS without calcium or magnesium, 2 mL of 2-NBDG solution was added to each gel during different time-points. Once reached the time-point, gels were transferred to a new well-plate with DPBS without calcium or magnesium to release the absorbed 2-NBDG. The resultant was read at an excitation/emission of 465/540 nm using a LS-50B Luminescence Spectrometer (Perkin Elmer, USA).

3.1.11 *Scanning electron microscopy*

To assess the inner and outer morphology of CAF hydrogels, as well as to observe microtissue development and calcium deposition, a Tescan Vega LMU (Tescan, UK). scanning electron microscopy (SEM) was used. Before image acquisition, specimens

without cells were freeze-dried and then mounted on carbon discs (TAAB Laboratory Equipment) and gold-coated using a Polaron E5000 SEM Coating unit (Quorum Technologies Ltd (Polaron Division), UK). For hydrogels with cells, samples were first fixed using a pre-warmed solution of 2% glutaraldehyde (TAAB Laboratory Equipment) in Sorensons buffer. The constructs were then stored at 4 °C overnight followed by dehydration steps using 25%, 50%, 75%, and 100% ethanol. Afterwards, specimens were stored at 4 °C in 100% ethanol until critical point dried using a BAL-TEC 030 Critical Point Dryer (Leica Geosystems Ltd, UK). Finally, cell-loaded hydrogels were also mounted on carbon discs and gold-coated.

3.1.12 *Picogreen and Alkaline Phosphatase (ALP)*

Cell proliferation and DNA content was assessed at day 0, 7 and 14 using PicoGreen DNA quantitation assay (Thermo Fisher Scientific, USA). Three samples from each specimen at different time-points were immersed in 1.5 mL of molecular grade sterile water following freezing at -20 ºC for later analysis. Standards were prepared following manufacturer's recommendations. Briefly, serial dilutions (Table 3.1) using DNA working solution (DNA std stock 1:50 in 1X TE buffer) were used to obtain the DNA standard curve.

Table 3.1 – DNA standard serial dilutions.

Final [C] DNA (ng/mL)	Volume of 1X TE (µL)	Volume of working DNA (2µg/mL) (µL)	Volume of PicoGreen in 1X TE (1:200)	Final [C] DNA in PicoGreen [1:1] (ng/mL)
0 (blank)	300	0	200	0
10	298.5	1.5	200	5
50	292.5	7.5	200	25
100	285	15	200	50
250	262.5	37.5	200	125
500	225	75	200	250
750	187.5	112.5	200	375
1000	150	150	200	500
2000	0	300	200	1000

The same way serial cell dilutions were used to obtain a standard cell curve (Table 3.2). All the dilutions were prepared from a volume (1200 µL) of molecular grade sterile water with $4x10^6$ cells.

Table 3.2 – Cell serial dilutions for PicoGreen.

Volume of water with cells (µL)	Number of cells	Volume of 1X TE (µL)	Number of cells per 100 µL	Volume of PicoGreen (1:200)	Final cell concentration in PicoGreen [1:1] cells/mL
300	1 000 000	0	333 333	200	166 666
150	500 000	150	166 666	200	83 333
90	300 000	210	100 000	200	50 000
30	100 000	270	33 333	200	16 666
15	50 000	285	16 666	200	8 333
7.5	25 000	292.5	8 433	200	4 216
3	10 000	297	3 333	200	1 111
0	0	300	0	200	0

Before analysis, samples undergone three cycles of freezing and thawing, followed by 20 min of immersion in an ultrasonic bath for cell lysis. 50 µL of the cell lysate were combined with 100 µL 1xTE and 150 µL PicoGreen dye in 1x TE (1:200) before loading a 96 opaque well plate in triplicate. After a 10-min room temperature incubation protected from light, samples were read (excitation/emission 485/530 nm) using a Spectramax Gemini XPS microplate reader (Molecular Devices, USA). The same cell lysate was used to measure the alkaline phosphatase (ALP) activity by combining it with 1-Step PNPP (p-nitrophenyl phosphate) Substrate Solution (Thermo Fisher Scientific). The results were compared with the serial dilution of a p-nitrophenol standard solution. For each sample, in triplicate and in a transparent 96-well plate, 80 µL of the cell lysate was combined with 120 µL of 1-Step PNPP Substrate Solution. After a 1-hour incubation at 37°C, the absorbance was read at 405 nm using a Biotek ELX800 (Biotek, Winooski, USA).

3.1.13 *Ribonucleic acid isolation and quantification*

Ribonucleic acid (RNA) isolation was performed in low and high-cell density samples at different time-points using RNeasy Mini kit (Qiagen, Germany) and following the manufacturer's recommendations. Briefly, RLT buffer with β-mercaptoethanol (β-ME) was prepared by adding 10 µL of β-ME to 1 mL of RLT buffer. To start, 700 µL of RLT buffer with β-ME was added to each sample for cell disruption. The resulting was frozen at -20ºC until analysis. The starting solution was then homogenized by pipetting and vortexing during 1 min in a QIAshredder spin column. 1 volume of 70% of ethanol was added for further homogenization followed by pipetting. Afterwards, samples were

centrifuged for 30 s at 13 000 rpm (discarding the flow-through) and genomic DNA contamination was eliminated by using 80 µL of DNase I incubation mix (constituted by 10 µL DNase I stock solution and 70 µL of RDD buffer), preceded by the addition of 350 µL of RW1 buffer and further centrifugation for 30 s at 13 000 rpm (discarding the flow-through). A new RW1 buffer wash was carried by adding 350 µL of this buffer, followed by new centrifugation for 30 s at 13 000 rpm, with flow-through discarded. Two washes using 500 µL of RPE buffer were then performed, the first for 30 s at 13 000 rpm and the second for 2 min at 13 000 rpm to remove all the residual ethanol. The RNeasy spin column was placed in a new collection tube and a centrifugation for 1 min at 13 000 rpm was carried. Finally, 30 µL of RNase-free water was added to the spin column membrane and a final centrifugation for 1 min at 13 000 rpm was performed for RNA elution. RNA concentration was quantified by using a nanodrop (ND-1000; Thermo Fisher Scientific, USA).

3.1.14 *Complementary DNA (cDNA) synthesis*

Complementary DNA was synthetized using the RT2 First Strand Kit (Qiagen) and following the recommended protocol. Briefly, after thawing, all the reagents were centrifuged for 30 s to assure good mixing. A genomic DNA elimination mix for each RNA sample was prepared by mixing 200 ng of RNA with 2 µL of GE buffer and RNase-free water to perform a total volume of 10 µL per sample. This mixture was incubated for 5 min at 42ºC and then placed on ice for at least 1 min. For each sample, the reverse transcription mix was prepared by adding 4 µL of 5x BC3 buffer, 1 µL of control P2, 2 µL of Reverse Transcriptase mix RE3 and 3 µL of RNase-free water. The total 10 µL of the reverse transcription mix was combined by pipetting with the 10 µL of genomic DNA elimination mix. 91 µL of RNase-free water was added to each sample and mixed by pipetting. All samples were placed on ice before loading to the real-time polymerase chain reaction (RT-PCR) array plate.

3.1.15 *Gene expression using RT-PCR arrays*

Before loading the RT-PCR arrays, the PCR component mix per sample was obtained by mixing 650 µL of 2x SYBR Green Master Mix, 102 µL of cDNA synthesis reaction and

548 µL of RNase-free water. 10 µL of the PCR component mixture was loaded to each well of the RT-PCR array. Gene expression was analysed using a ViiA7384-well block (Applied Biosystems, USA).

3.1.16 *Statistical Analysis*

Data are expressed as mean ± standard deviation. Mean values and standard deviations were calculated from at least three independent experiments of triplicates per group. Comparisons were performed by one-way analysis of variance (ANOVA) in conjunction with Tukey's multiple comparison test using levels of statistical significance of $P < 0.05$ (*), $P < 0.01$ (**), $P < 0.001$ (***), and $P < 0.0001$ (****).

3.2 Methods developed for this research

During the research presented in this thesis, original methods have been developed. Here, these will be reported. Unless otherwise stated, all reagents used during this investigation were obtained from Sigma-Aldrich, USA.

3.2.1 *Single Cell Coating*

Cells were coated using a polycation – poly-l-lysine – to avoid natural cell agglomeration due to the presence of positively charged polymeric particles coupled to the cell membrane, which favours the electrical repulsion between cells.

Before the coating process, poly-l-lysine hydrobromide (Molecular Weight (MW) = 15–30 kDa) was dialyzed for 2 days and then dissolved in Dulbecco's phosphate-buffered saline without calcium and magnesium until a concentration of 1 mg/mL had been reached. A 1 mg/mL solution of PLL-FITC (MW = 15–30 kDa) was also prepared using DPBS. Both polymeric solutions were dissolved in HBSS without phenol red at four different concentrations: 100, 50, 10, and 0 µg/mL (control). Following cell detachment, a cell suspension of 2×10^6 per 200 µL was prepared for each polymer concentration, and a volume of 1 mL was made up with HBSS without phenol red. The cells were incubated within the polymer for 15 min at 37 °C and 5% CO_2 for coating. Afterward, coated cells

were washed twice with HBSS without phenol red, using centrifugation at 250g for 5 min to remove any polyelectrolyte excess. The process is illustrated in the Figure 3.3.

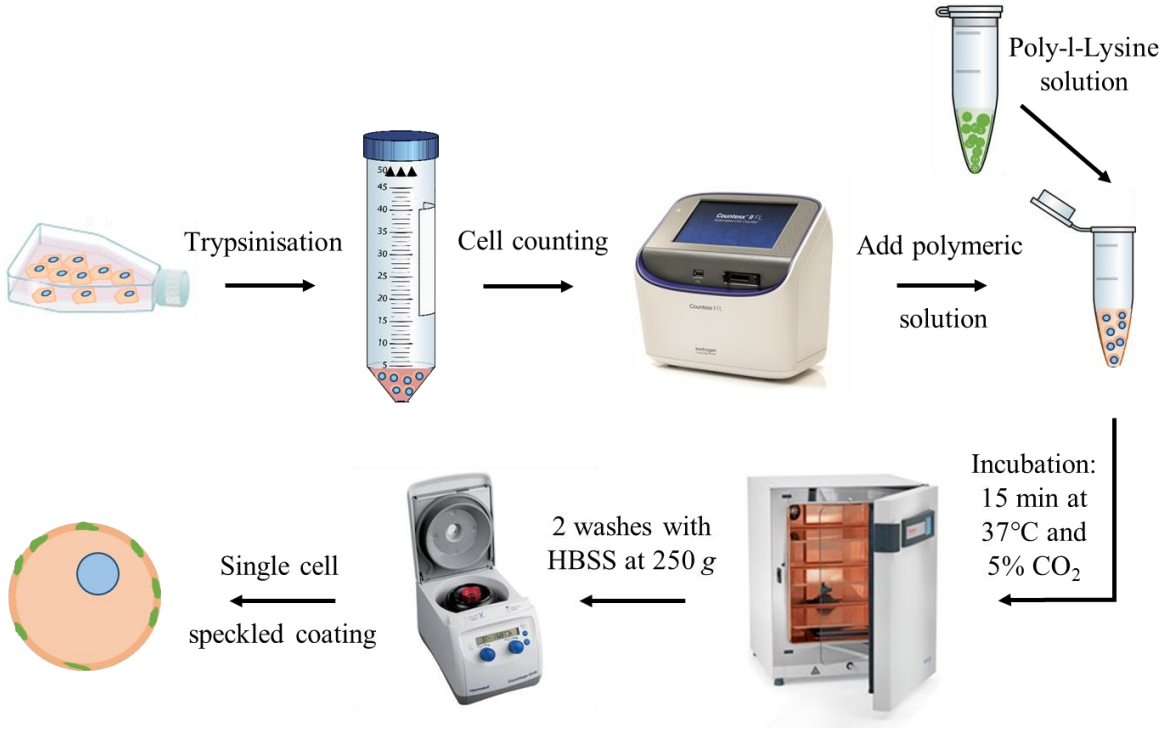

Figure 3.3 - Illustration representing the poly(l-lysine) cell speckled coating procedure.

3.2.2 *Cell Aggregation Test and Aggregate Area Quantification*

Cell aggregation is a common problem in bioprocessing. To evaluate the effect of the single cell coating, 1×10^6 coated cells were suspended in 1 mL of high-glucose (DMEM) supplemented with 10% fetal bovine serum (FBS) and 5000 U/mL penicillin/streptomycin inside a 1 mL syringe. Ten drops were dispensed through a 21-gauge needle every hour up to 3 h (Figure 3.4). The drops were observed using a fluorescence microscope (Leica DM IL LED, Leica Microsystems, Germany). Between depositions, cells were incubated at 37 °C and 5% CO_2. The images obtained were processed using ImageJ software (National Institutes of Health, USA). Each image from the triplicate biological experiment was processed using the *Threshold* function, and 20 samples were selected at random through *ROI manager* and subjected to area measurement.

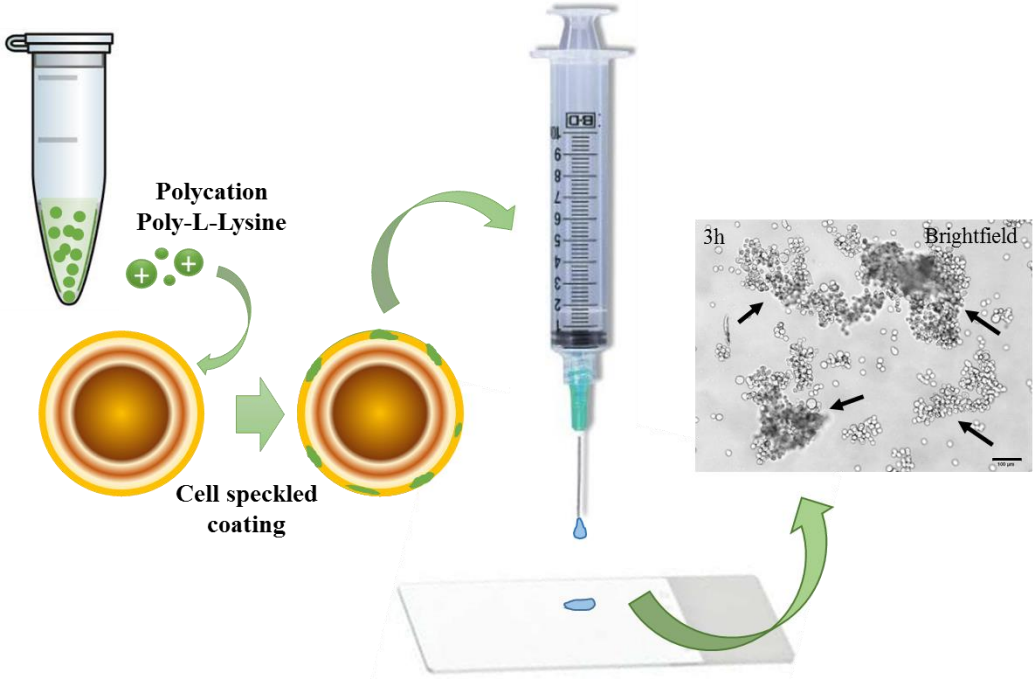

Figure 3.4 – Cell aggregation test diagram. Once coated, cells were mixed with supplemented cell medium and loaded into a syringe. Cell drops were dispensed every hour up to three hours and the size of cell clusters visualised under microscope.

3.2.3 *Cell Printing – general information*

A commercial Microfab Jetlab4 (Microfab Inc., USA) single orifice piezoelectric, droplet-on-demand, printer was used for all printing experiments in the present study (Figure 3.5a and Figure 3.5b). The printer has been customized by Dr. Matthew Benning to operate with versatility using both microvalve (Figure 3.6a) and inkjet printheads (Figure 3.6b). In the same way, an in-house reservoir coupled to an agitator was developed (Figure 3.6c and Figure 3.6d, respectively). During this work, INKX0514950A microvalves (The Lee Company, USA) and 60 µm MJ-AT-01 inkjets (Microfab Inc., USA) have been used.

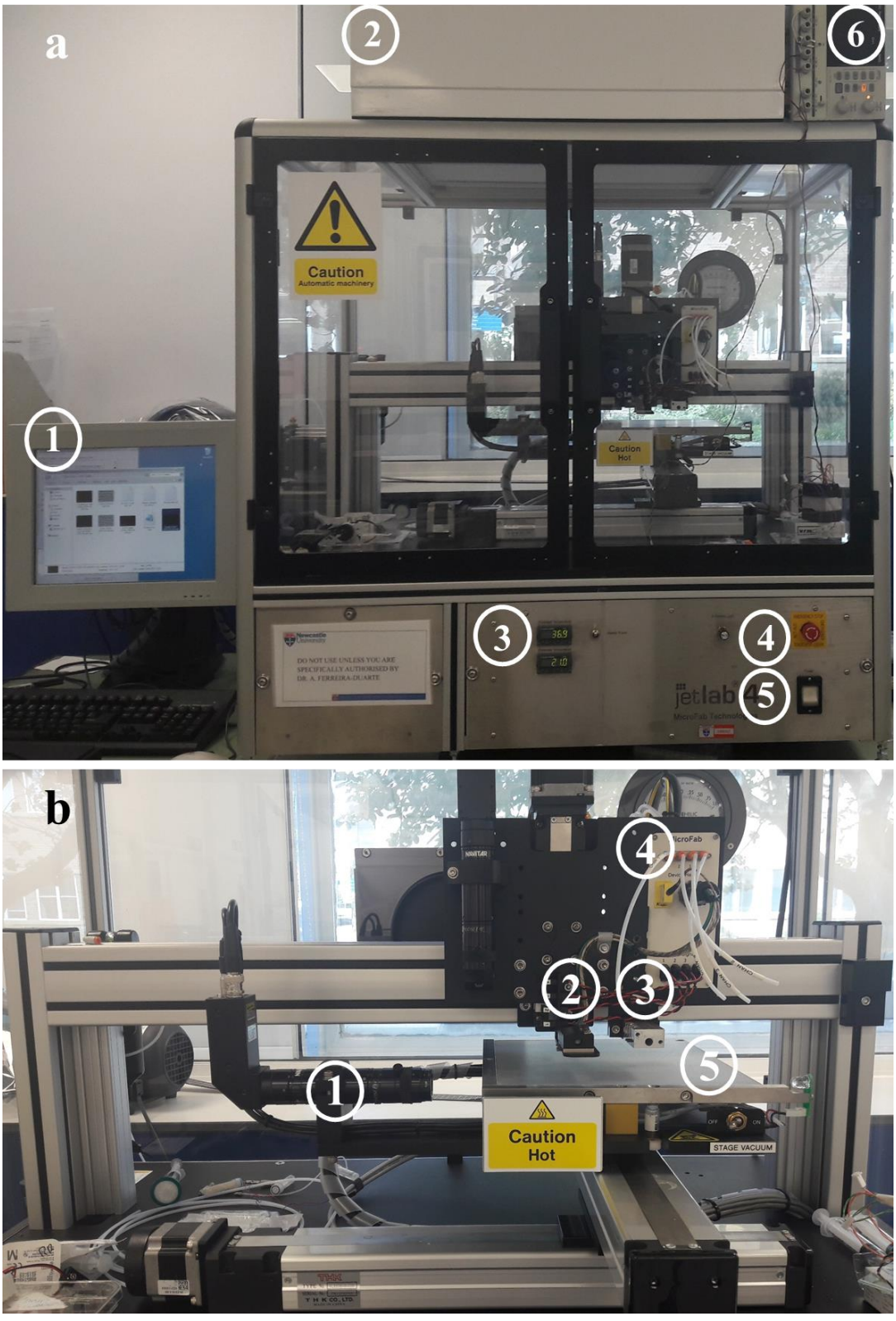

Figure 3.5 – (A) Microfab Jetlab 4 apparatus. 1 – Computer; 2 – HEPA filter; 3 – Temperature controller; 4 – STOP button; 5 – ON/OFF button; 6 – Power supply for the agitator; (B) Microfab Jetlab4 apparatus (detail). 1 – LED stroboscope; 2 – Inkjet holder; 3 – Microvalve holder; 4 – Pressure cables; 5 – xyz stage.

The Microfab Jetlab 4 printer comes with a dedicated software that is mainly organized in three distinct tabs (Figure 3.7). The first one, "*Jet Setup*" (Figure 3.7a), is responsible for the controlling of the electrical waveform that expands and contracts of the piezoelectric crystal for inkjet printheads, and that is also accountable for the opening and closing of the mechanical shutter for microvalves. The camera strobe delay and the jet trigger mode are also controllable from here. The second tab "*Motion*" (Figure 3.7b) is responsible for the *xyz* position of the printheads. Finally, an automatic air pressure controller is used to assist the printing process with a backpressure, essential to hold the solution inside the reservoir until the electrical impulse orders to do so. However, an analogic pneumatic controller CT-PT4 (Microfab Technologies, Inc.) (Figure 3.6e) has been used during this work. This way, the backpressure was set via knob rotation. The printer also allows the printing of black and white bitmap (.bmp) images and simple coded files, ideal for high-throughput, that are loaded in the "*Print Patterns*" and "*Print*" tabs.

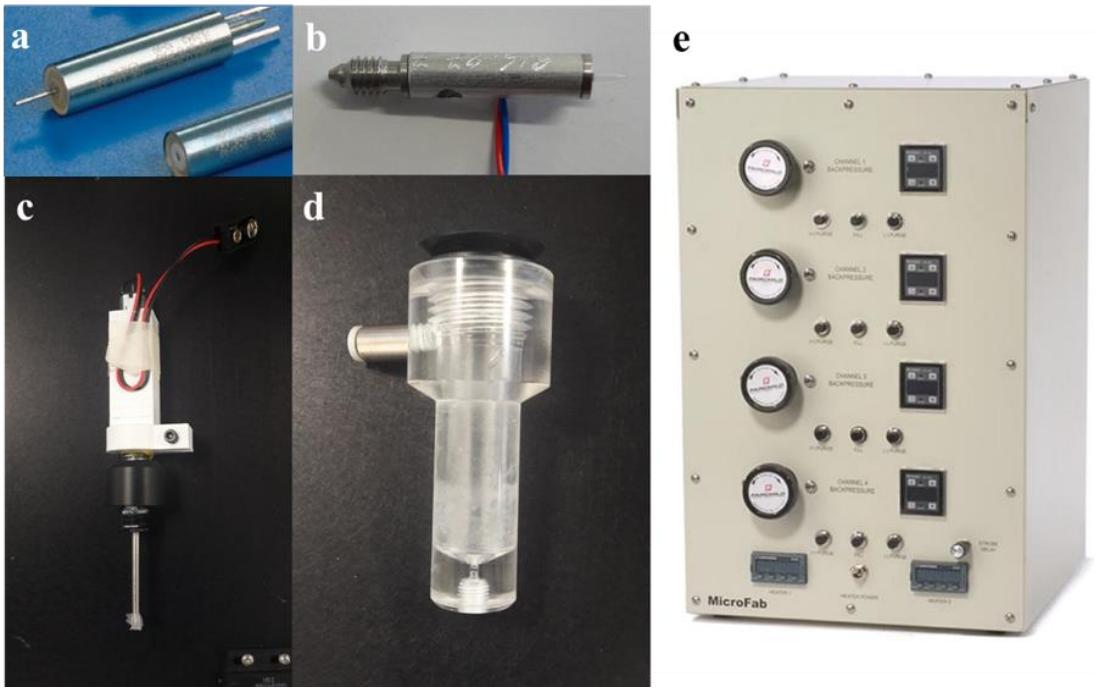

Figure 3.6 – Components using on cell printing. (A) INKX0514950A microvalve; (B) 60 µm Microfab inkjet printhead MJ-AT-01; (C) In-house developed motorised agitator; (D) In-house developed reservoir; (E) Analogic pneumatic controller CT-PT4.

3.2.4 *Cell printing – Inkjet printing*

For inkjets, droplet ejection was achieved through the actuation of the piezoelectric material within the inkjet head, affected by the application of a voltage differential. The wave impulse was applied in a simple trapezoidal form with a rise time, dwell time, fall time, dwell voltage and droplet frequency of 3 µs, 25 µs, 3 µs, 22 V and 1 kHz, respectively. Droplet formation is achieved when the electrical impulse reaches the piezoelectric material making it expand and contract. Firstly, the expansion, combined with the backpressure, is responsible for the fluid to come out from equilibrium position (Figure 3.8a). Secondly, the piezoelectric material contraction controls the emersion of the fluid (Figure 3.8b and Figure 3.8c). Finally, the arrival of a new wave form that expands the piezoelectric system pulls back the fluid (Figure 3.8d and Figure 3.8e), leading it to break off (Figure 3.8f) and leave the orifice in the form of a droplet (Figure 3.8g). Droplet formation was confirmed prior to printing using a LED stroboscope. Following single cell coating, encapsulated cells diluted in filtered fresh serum-free media (bio-ink) were placed in the printing reservoirs. The bio-inks were printed using a 60 µm diameter inkjet printhead, onto a chosen substrate, using different scripts.

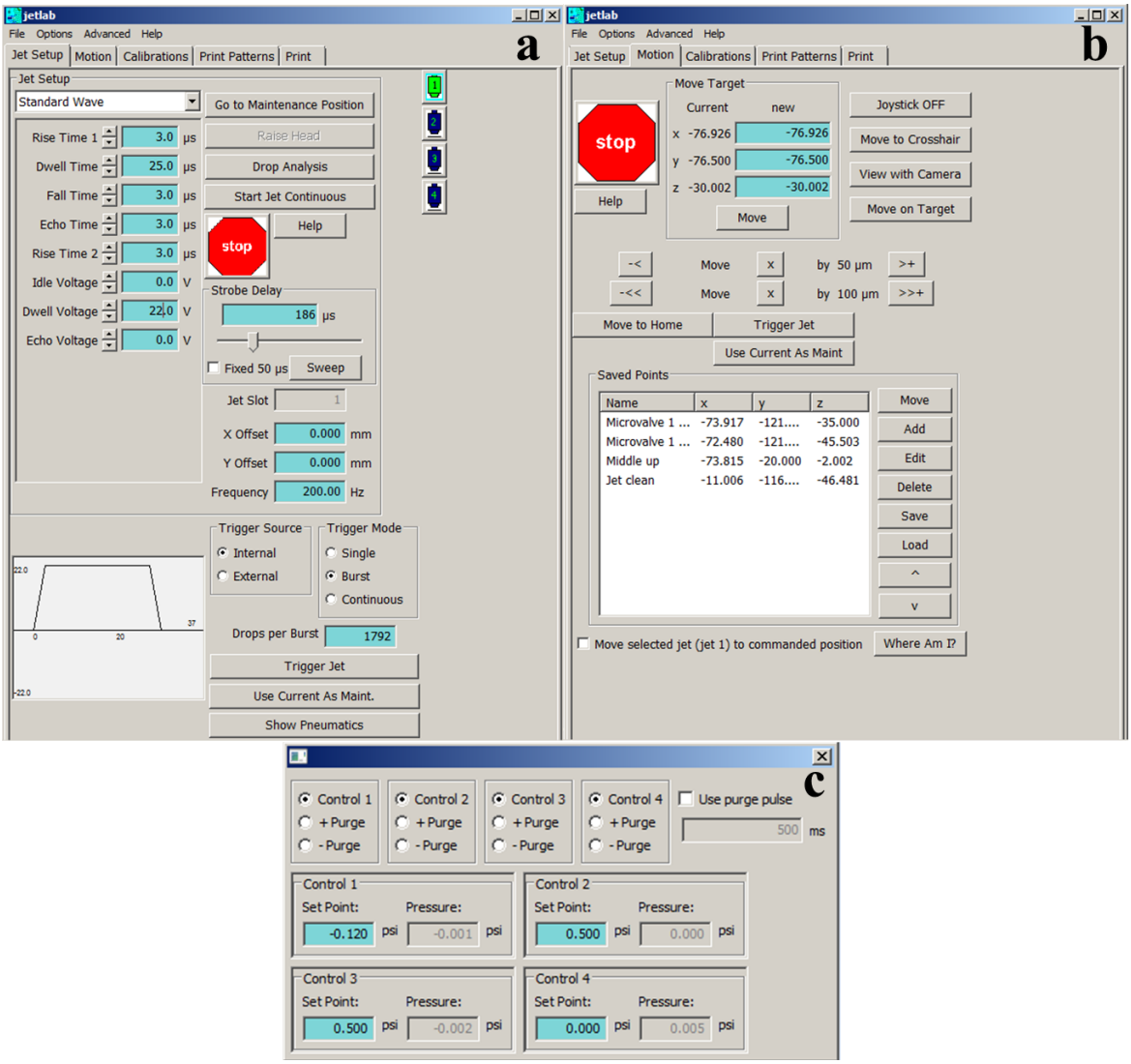

Figure 3.7 – Jetlab 4 dedicated software. (a) “Jet Setup” tab; (b) “Motion” tab; (c) Pressure control tab.

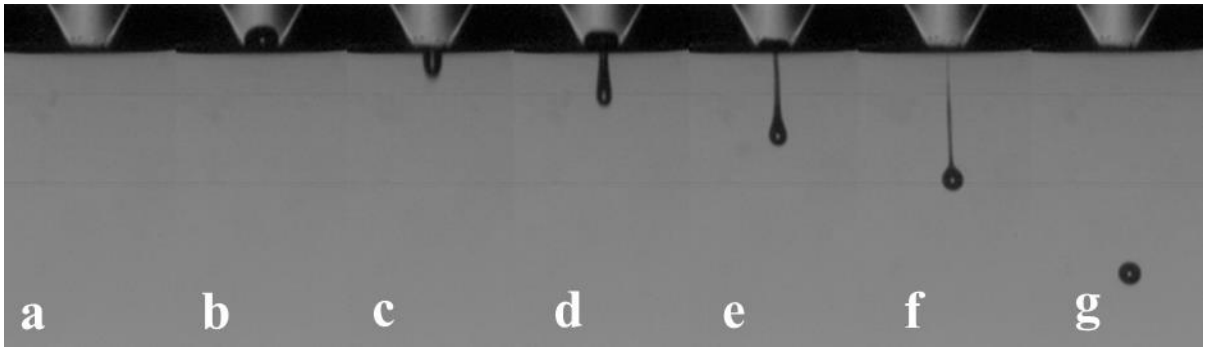

Figure 3.8 – Sequence of events representing from equilibrium (a) to droplet ejection (g). Adapted from www.microfab.com.

To obtain the reliability of the bio-ink with coated cells, two 1 x 10^6 cell/mL bio-inks containing PLL coated or non-coated cells were dispensed from a 60 μm diameter inkjet printhead using the apparatus described above, onto glass microscope slides. 10 depositions of 50 droplets were printed in a 1x10 array at 7 time-points (0 to 60 minutes) in ten-minute increment. Each sample was analysed after deposition using an inverted microscope (Leica DM IL LED, Leica Microsystems, USA) and the number of cells recorded.

3.2.5 *Reactive Jet Impingement*

The ReJI system is an in-house printhead for bioprinting developed by Dr. Matthew Benning (Figure 3.9a) (Benning and Dalgarno, 2017). It is composed by one or more pairs of solenoid valves INKX0514950A located in opposite sides at 55º of inclination, connected to two spike and hold drivers (The Lee Company, USA) per pair to control the opening and closure of the valves (Figure 3.9b). The microvalves were also connected to the ink loading reservoirs (Figure 3.9c), which are attached to the pneumatics controller CT-PT4. Droplet ejection was obtained by applying an electrical impulse in the form of a rectangular waveform with a dwell time, amplitude and frequency of 800 μs, 5 V and 400 Hz. By optimising the pressure and the waveform, simultaneous droplet printing can be achieved and allowing in-air droplet mixing, before falling onto the stage. A schematic may be observed in (Figure 3.9d). Differently to inkjets, microvalves rely on an actuating voltage (spike voltage) to open mechanical shutter and on a hold voltage to close the same shutter. The period that the shutter is open, i.e. spike duration, is regulated by a resistor and a capacitor built in the connected spike and hold driver.

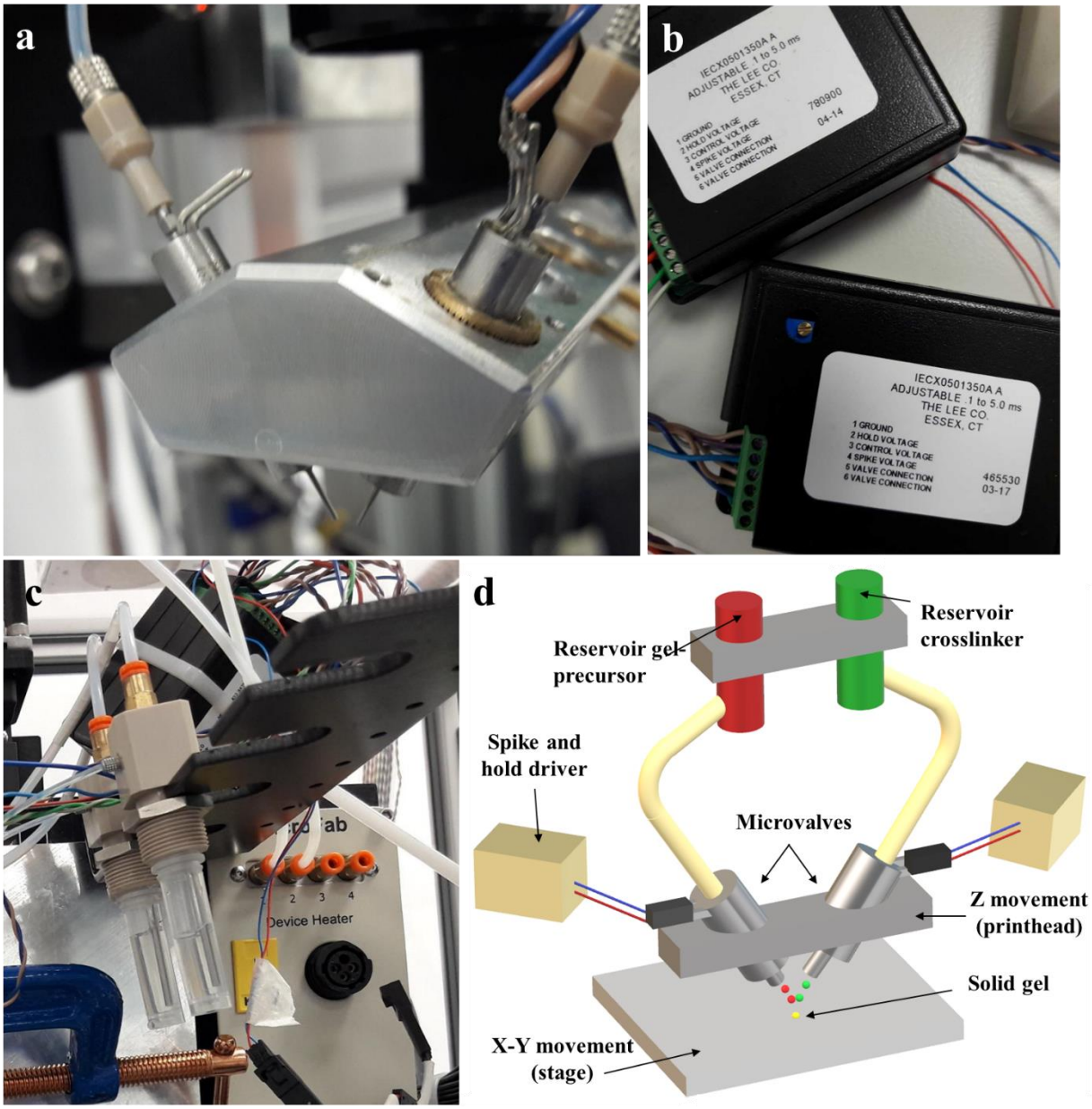

Figure 3.9 – ReJI components and schematic. (a) The ReJI printhead detail with one pair of microvalves; (b) IECX0501350A A spike and hold drivers used with ReJI; (c) Ink loading reservoirs; (d) Schematic showing the main components of the ReJI system.

3.2.6 *Collagen/Alginate/Fibrin hydrogel components formulation*

CAF hydrogels were initially developed by Dr. Ana Ferreira-Duarte (Montalbano *et al.*, 2018), however its optimisation towards a bio-ink to be used on the ReJI system has been developed on the course of this work. Before obtaining the printed CAF hydrogels, the hydrogel precursors (pre-gel and crosslinking solutions) were formulated. Prior to the pre-gel solution preparation, a 37.5 mg/mL fibrinogen solution was obtained by gently

dissolving fibrinogen in DPBS without calcium and magnesium at 37 °C. A 2.5% NaAlg in DPBS without calcium and magnesium solution was also prepared. To achieve the pre-gel solution, the two preceding mixtures were gently mixed with a 6 mg/mL collagen solution in hydrochloric acid (Collagen Solutions, UK) to a ratio of 0.25;0.5;2 of collagen, alginate and fibrinogen, respectively. As crosslinking solution, a 500 U/mL of thrombin dissolved in high-glucose with pyruvate DMEM with 0.1% of $CaCl_2$ was used.

3.2.7 *Fibrin hydrogel formulation*

As the higher percentage of CAF hydrogel is composed by fibrin, before jetting CAF hydrogel, different fibrin hydrogels were formulated in order to optimise its characteristics, namely the crosslinking time and hydrogel viscosity. Fibrin hydrogels were obtained by mixing different concentrations of fibrinogen and thrombin solutions. Firstly, fibrinogen from bovine plasma was gently dissolved in DPBS without calcium and magnesium at 37 °C to obtain the following concentrations: 100, 50 and 25 mg/mL. 10 kU of thrombin from bovine plasma was dissolved in 20 mL of supplemented DMEM with pyruvate to obtain the concentration of 500, 250 and 100 U/mL. Both fibrinogen and thrombin solutions were mixed through manual pipetting at 1:1 and 2:1 ratio to make fibrin hydrogels as observed in Figure 3.10.

Figure 3.10 – Fibrin hydrogels obtained using different fibrinogen and thrombin solutions at 1:1 and 2:1 ratio.

3.2.8 *Cell-loaded CAF gels printing*

Two specific cell concentrations were used on the course of this work – 4×10^6 and 40×10^6 cells/mL. The desired cell suspension was obtained by mixing 1 mL of 500 U/mL of thrombin solution with 0.1% of $CaCl_2$ with the cell pellet. The pre-gel and cell-containing crosslinking solution were loaded at 37ºC into two separate reservoirs and the cell-filled hydrogels were fabricated by simultaneous droplet jetting from each precursor that, when mixed in air, formed a gel before reaching the stage (Figure 3.11). To jet the pre-gel and cell-containing crosslinking solution, the pressure system was in the range of 270–310 mmHg and 450–550 mmHg, respectively. A specific pattern was achieved by coding and loading a script into the Jetlab4 software. After printing, the cell-laden constructs were incubated in osteogenic medium at 37 °C and 5% CO_2.

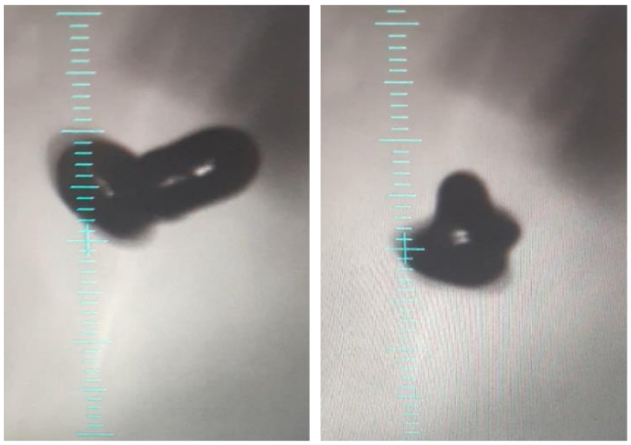

Figure 3.11 – Stroboscopic image of gel precursor and crosslinking solutions meeting in flight.

Chapter 4. Single cell coating using poly-L-lysine and reliable inkjet cell printing

4.1 Introduction

In this chapter, a simple and fast non-covalent cell surface modification using a positively charged polymer, PLL, has been applied in an attempt to reduce cell agglomerates without otherwise affecting cell behaviour. Afterwards, PLL coating was used as part of bio-ink formulation in order to increase inkjet cell bioprinting reliability. This chapter describes how different PLL concentrations affect the cells in terms of viability and metabolism, morphology and genetic information. Polymer ingestion and metabolisation, as well as PLL effect on agglomeration, are also characterised and discussed. Finally, tests on inkjet printing reliability are presented, including after-printing cell morphology and viability.

4.2 Single cell coating concept

The concept behind the PLL coating relies on the attraction between positively charged materials and the negatively charged cell membrane, similarly to other noncovalent cell surface modifications. Here, after immersing in the polycationic solution, cells get coated rather than imprisoned inside a complete capsule, as a result of the low polymeric concentrations used. Once attaching to a substrate, cells show to be able to ingest and metabolise the PLL coating depending on the polycation concentration used. The process reported is illustrated in Figure 4.1.

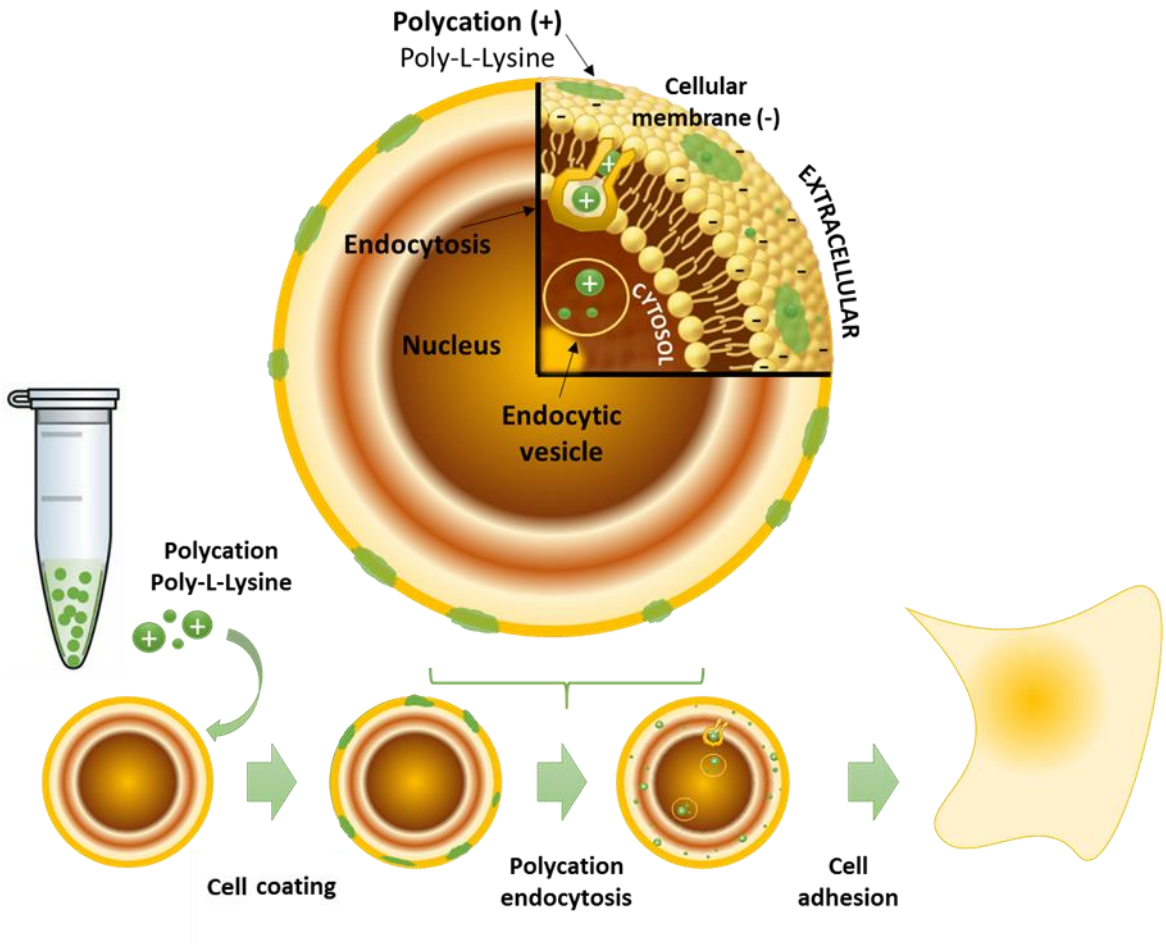

Figure 4.1 - Illustration of temporary cellular coating using poly(l-lysine) and further uptake of the biodegradable polycation.

4.3 *In Vitro* Cell Viability Studies

To evaluate the effect of the different PLL concentrations (100, 50, 10, and 0 µg/mL) on cell viability, four complementary assays were used. The first studied cell death as consequence of PLL damage on cell membrane – caspase-3 activity and cell permeability detection. Live/Dead assay reported cell viability by means of two fluorophores that attach to the cells depending on their condition, i.e. if they are alive or dead. The third relied on the cell metabolism by analysing the mitochondrial activity of the cells – MTT assay. Finally, cell karyotype was inspected to look for potential chromosomic aberrations caused by the PLL coating.

As stated above, cell death as a cause of the coating process was studied through caspase-3 activity and cell permeability detection on U2OS cells immediately after coating

(Figure 4.2). It was verified that, immediately after coating, only 62% of the 10 μg/mL coated cells were negative for both PI and NucView488, compared to 90% for untreated cells (Figure 4.2a). For the other two concentrations, 50 and 100 μg/mL, 34% and 10% of cells, respectively, were viable. Image flow cytometry reported that most of dead cells have suffered apoptosis, finding themselves at a late apoptotic stage, or necrosis, accounting over 5% for control samples, over 30% for 10 μg/mL specimens, approximately 65% for 50 μg/mL coated cells and almost 90% of the total cells for 100 μg/mL (Figure 4.2b). On the other hand, although negligible, only control and 10 μg/mL samples presented cells in an early apoptotic stage. The reported cell survival is obtained by analysing not only the dye expression, but also through morphology observation (Figure 4.2c-f). Morphologically speaking, necrosis has been seen to increase with the PLL concentration, however, double positive populations for PI and Nucview488 were observed for the different conditions. 50 and 100 μg/mL coated cells presented, respectively, 34.72% and 65.19% double positive samples, and 31.20% and 24.86%, respectively for PI-only positive cells. The same did not happen for uncoated and 10 μg/mL PLL coated cells, that presented less than 1% of double positives, but exhibiting 5.13% and 35.38% PI positive cells, respectively.

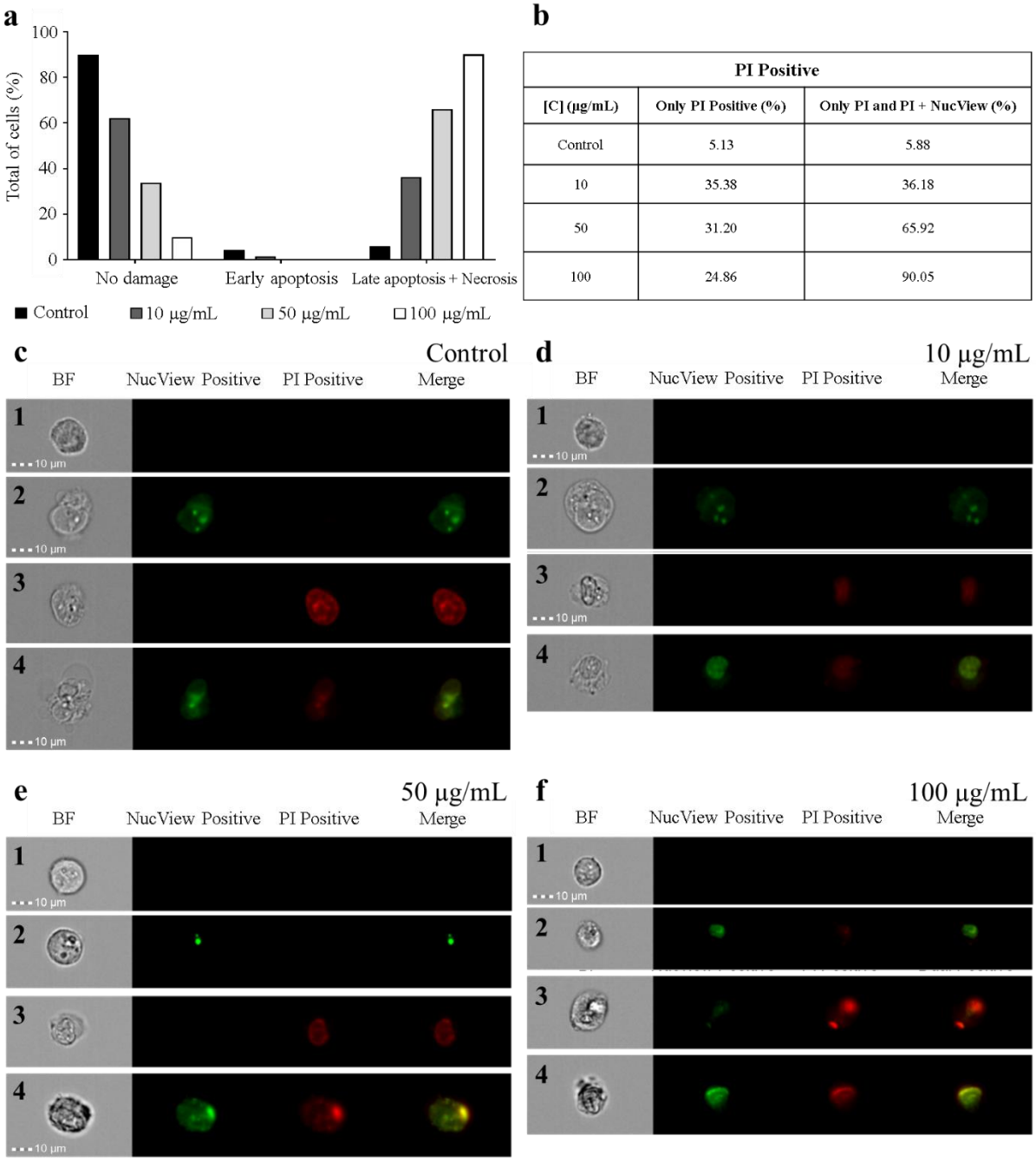

PI Positive		
[C] (µg/mL)	Only PI Positive (%)	Only PI and PI + NucView (%)
Control	5.13	5.88
10	35.38	36.18
50	31.20	65.92
100	24.86	90.05

Figure 4.2 - Caspase-3 activity and cell permeability detection for U2OS cells. (a) Cell death scores after analysis. (b) Total number of events for PI and PI and Nucview488 positive cells. (c–f) ISx analysis samples: (c) control, (d) 10 µg/mL, (e) 50 µg/mL, (f) 100 µg/mL. Scale bars, 10 µm. Double negative, apoptotic cells, necrotic cells, and double positive are represented by the numbers 1, 2, 3, and 4, respectively.

Live/Dead assay was also used to qualitatively characterise the cells in terms of viability (Figure 4.3). Here, it is observable that the number of live cells (green) decreased by

increasing the PLL concentration, at the same time a raise on the number of dead cells (red) was accounted.

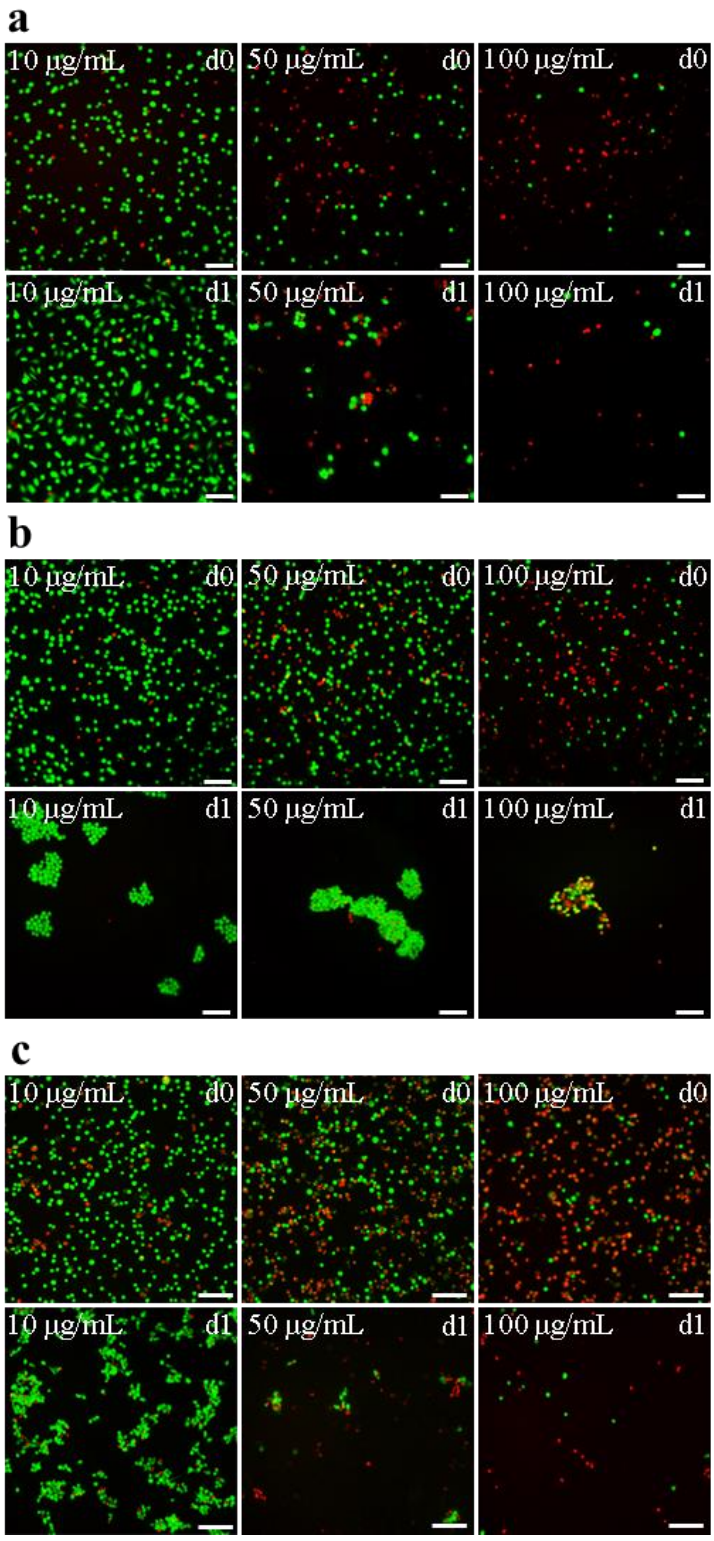

Figure 4.3 – Live/Dead assay for (a) U2OS, (b) TC-71, and (c) Neo-NHDF cells. For each cell type, top pictures represent cells 4 hours after coating and bottom pictures show cells 24 hours after coating. Scale bars are 100 µm.

Cell metabolism after coating was characterised using MTT assay (Figure 4.4). U2OS cells coated using the 10 μg/mL PLL solution (Figure 4.4a) revealed a metabolic activity similar to that of the untreated cells (control) during the course of the experiment, reaching the same metabolic levels by day 7. Cell coating with the 50 μg/mL PLL solution reduced cell metabolic activity by more than 50% at day 0 compared to the control; however, a recovery was observed at later time points accounting absorbance values not far from control. Finally, the 100 μg/mL concentration showed to completely inhibit the mitochondrial activity as it is represented by the negligible absorbance values obtained.

Ewing's sarcoma cells response to the PLL concentrations was similar to that for the U2OS cells (Figure 4.4b). Cells coated using the 10 μg/mL concentration exhibited a metabolic behaviour identical to that of the control, however, by day 7, the 10 μg/mL coated cells ended up by overcoming control's metabolic activity; the 50 μg/mL concentration initially decreased cell metabolic activity, but a sharp recovery was noted between days 3 and 7, showing cells metabolically more active when compared to the other PLL concentrations; to the 100 μg/mL concentration, a low metabolic response was observed, although a slightly slower cytotoxic response was found than for the U2OS cells at the end of the experiment.

The Neo-NHDF (Figure 4.4c) cell behaviour was slightly different. These cells presented an initial lower metabolic activity compared to control for the 10 μg/mL concentration, although the activity recovered steadily over the first 3 days post-coating. The 50 μg/mL coated cells exhibited similar behaviour in terms of metabolic activity, but from a lower starting point and with a marked recovery at days 3 and 7. The 100 μg/mL coated cells barely presented any metabolic activity at day 0, improved slowly up to day 3, and then showed a significant recovery between days 3 and 7.

Cell karyotyping was used to observe if the coating procedure could lead to any genetic mutation in the studied cells. Neo-NHDF 10 μg/mL coated cells presented unchanged karyotype after coating (Figure 4.5a,b), and TC-71 cells coated with the same PLL concentration conserved the translocation t(11;22)(q24;q12), an important hallmark of Ewing's sarcoma (Figure 4.5c,d).

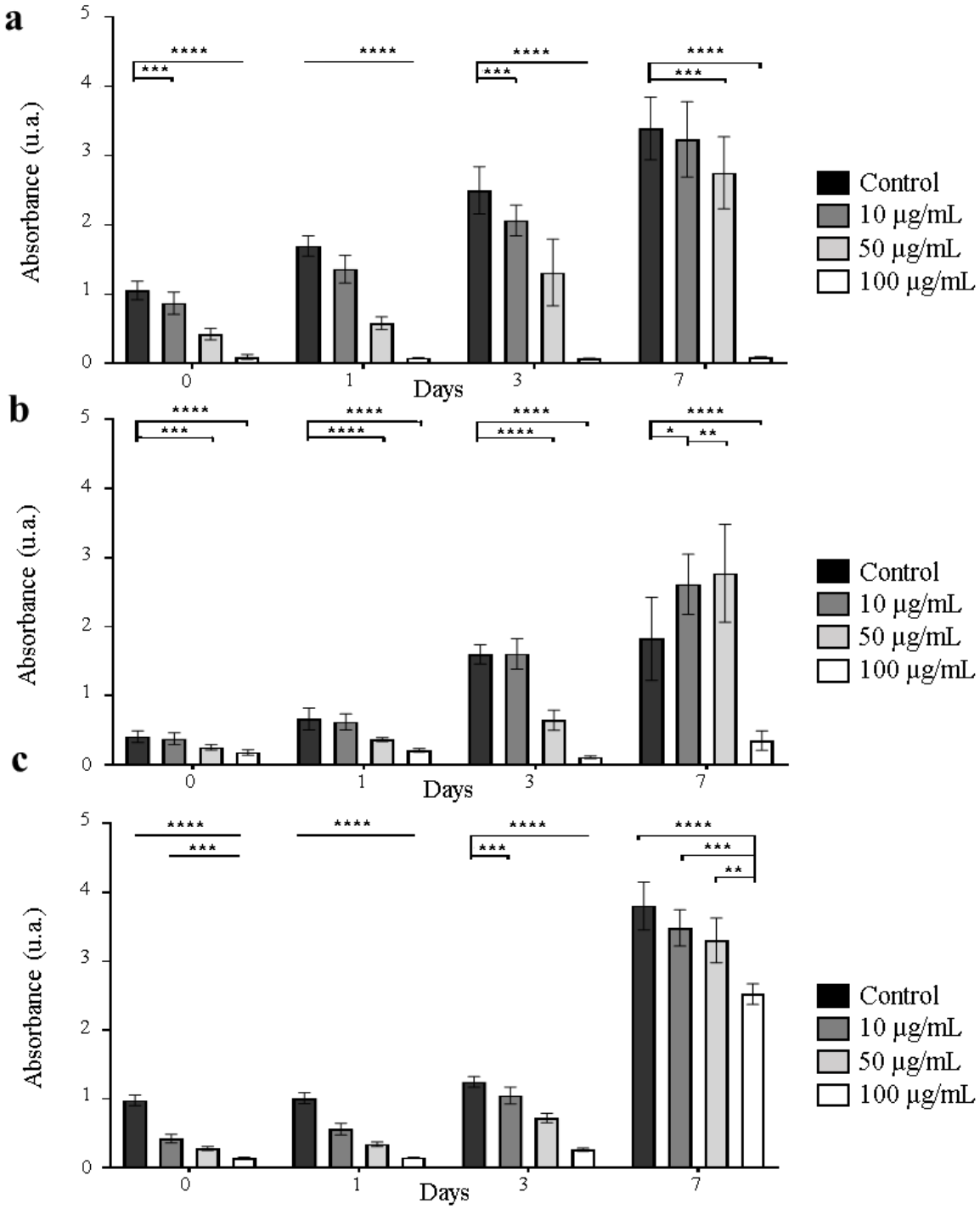

Figure 4.4 - MTT assay scores for days 0, 1, 3, and 7 for a) U2OS; b) TC-71; c) Neo-NHDF. The data are shown as mean ± SD. Results are relative to control at the same time point. *, **, ***, and **** indicate a significant difference between groups at the levels $p < 0.05$, $p < 0.01$, $p < 0.001$, and $p < 0.0001$, respectively. Error bars represent the standard deviation (n = 3).

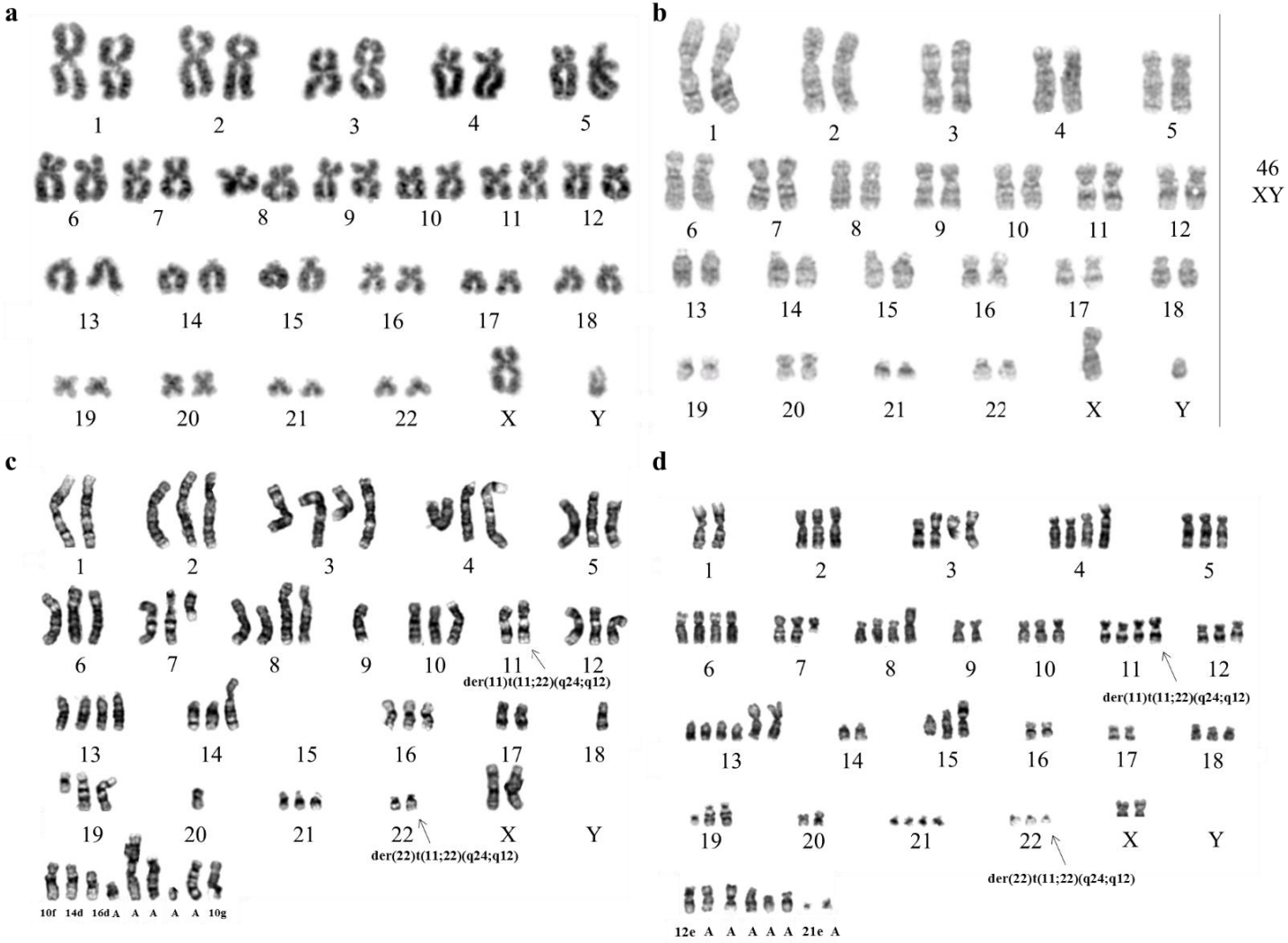

Figure 4.5 – Cell karyotype for Neo-NHDF (a – before coating; b – after coating) and TC-71 (c – before coating; d – after coating) cell lines.

4.4 Morphological analysis

Cell and coating morphologies were investigated by confocal microscopy and transmission electron microscopy (TEM). Analysis of cell and coating morphologies showed cell integrity after the coating process and indicated that the polycation was tightly bound to the membrane for all three cell types (Figures 4.6, 4.7 and 4.8, U2OS, TC-71 and Neo-NHDF, respectively).

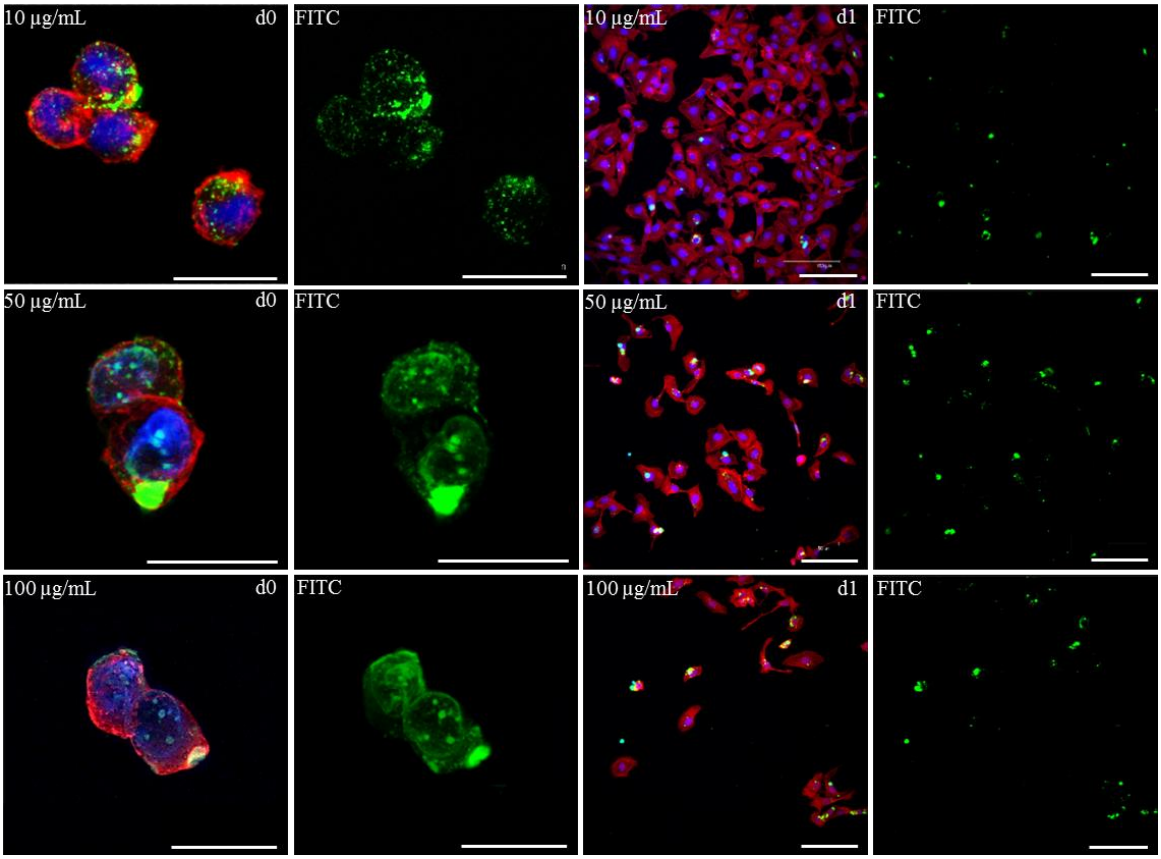

Figure 4.6 - Cell and shell morphology after PLL coating for U2OS cells. A concentration-dependent capsule tightly fitting the cellular membrane immediately after coating is observed (d0). Shell release through internalisation processes and attachment and proliferation were observed one day after coating (d1). The nucleus is represented in blue (DAPI), f-actin in red (Phalloidin), and the PLL capsule in green (FITC). Scale bars, 50 µm (day 0) and 150 µm (day 1).

The PLL concentration used to coat the cells determined similar coating morphology for the different cellular lineages. For the 10 µg/mL concentration, cell membrane presented sparse PLL particles speckled around its surface. At higher concentrations, 50 and 100

μg/mL, it was observed an increase of polycation around the cell surface, which completely encapsulated the cell inside a PLL shell when using the 100 μg/mL PLL coating. One day after coating, the 10 μg/mL coated cells had ingested the majority of PLL and exhibited normal attachment and proliferation: U2OS cells presented a heterogeneous population showing attachment and spreading, TC-71 cells grew in clumps, and fibroblasts were flattened and elongated.

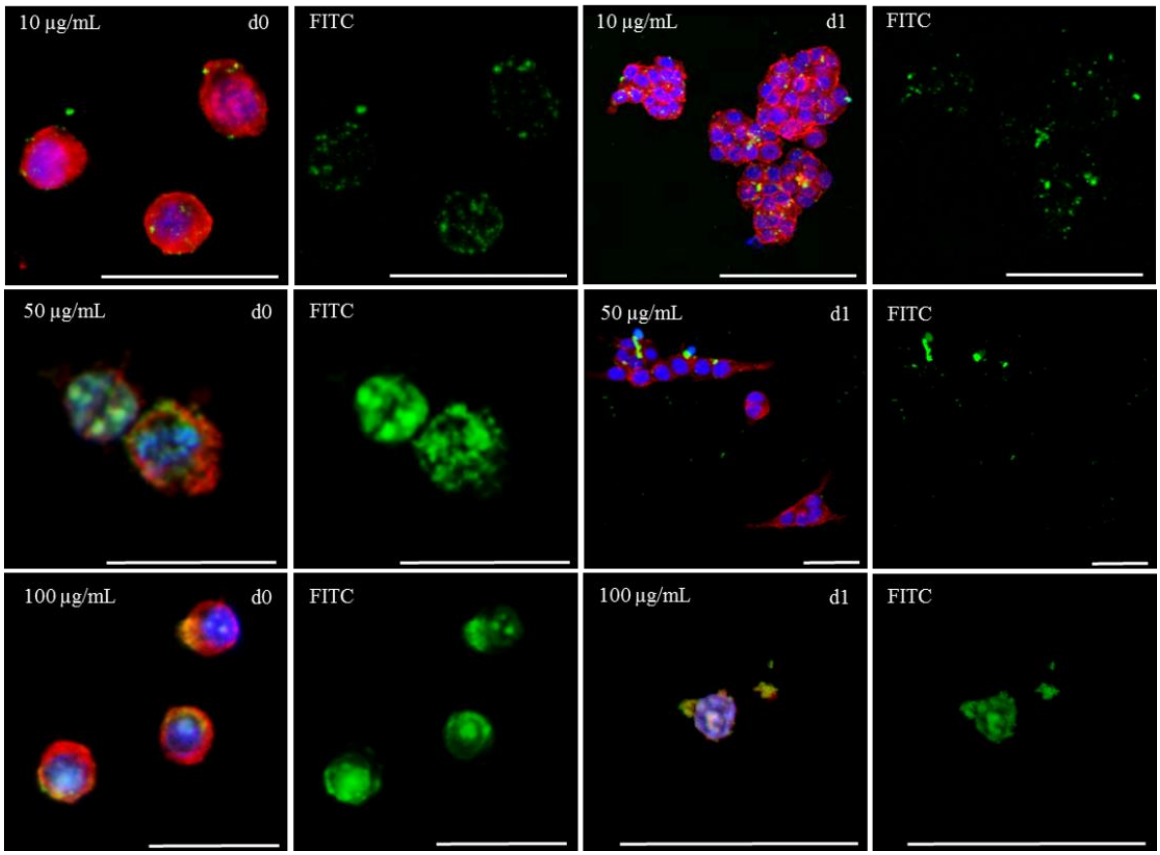

Figure 4.7 - Cell and shell morphology after PLL coating for TC-71 cells. Staining similar to that in Figure 4.6.

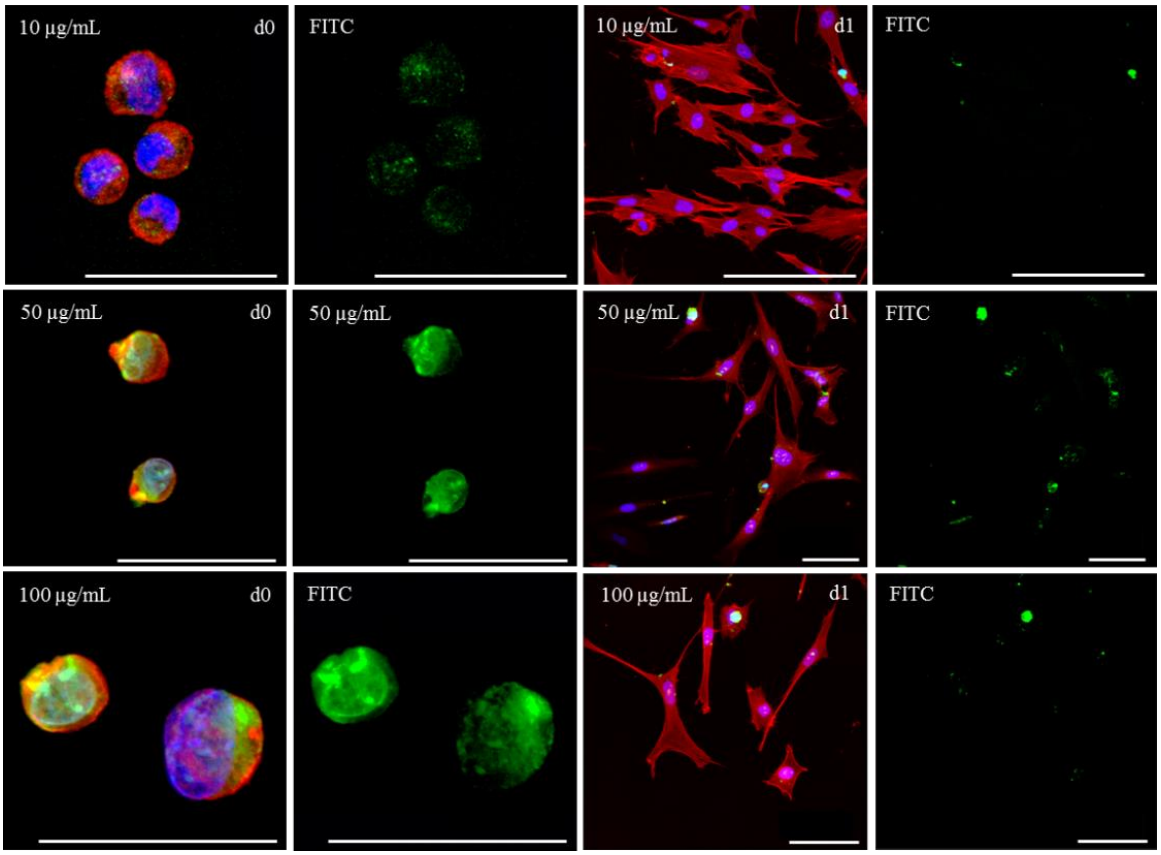

Figure 4.8 - Cell and shell morphology after PLL coating for Neo-NHDF cells. Staining similar to that in Figure 4.6.

At 50 and 100 µg/mL PLL concentrations, a reduced cell number at day 1, when compared to 10 µg/mL, was detected, which corroborates with the results obtained for the cell viability studies. Additionally, signs of increasing polymer ingestion and metabolisation by healthy cells could be observed at day one for all cell lines. The ingested PLL can clearly be seen inside the cell boundaries.

Transmission electron microscopy directly explored the effects of PLL on cell ultrastructure (Figure 4.9). For both control and 10 µg/mL coated cells a little to no harm was demonstrated, having the cells maintaintheir boundaries and all organelles and nucleus seem to be stable. Contrarily, for 100 µg/mL coated cells, ruptures on the cell membrane are observable all over. Additionally, cell organelles are difficult to identify, and the chromatin was dispersed and lost around the cell. These characteristics are normally reported on necrotic cells. On 50 µg/mL PLL coated cells a mixed population of live and dead cells was noted.

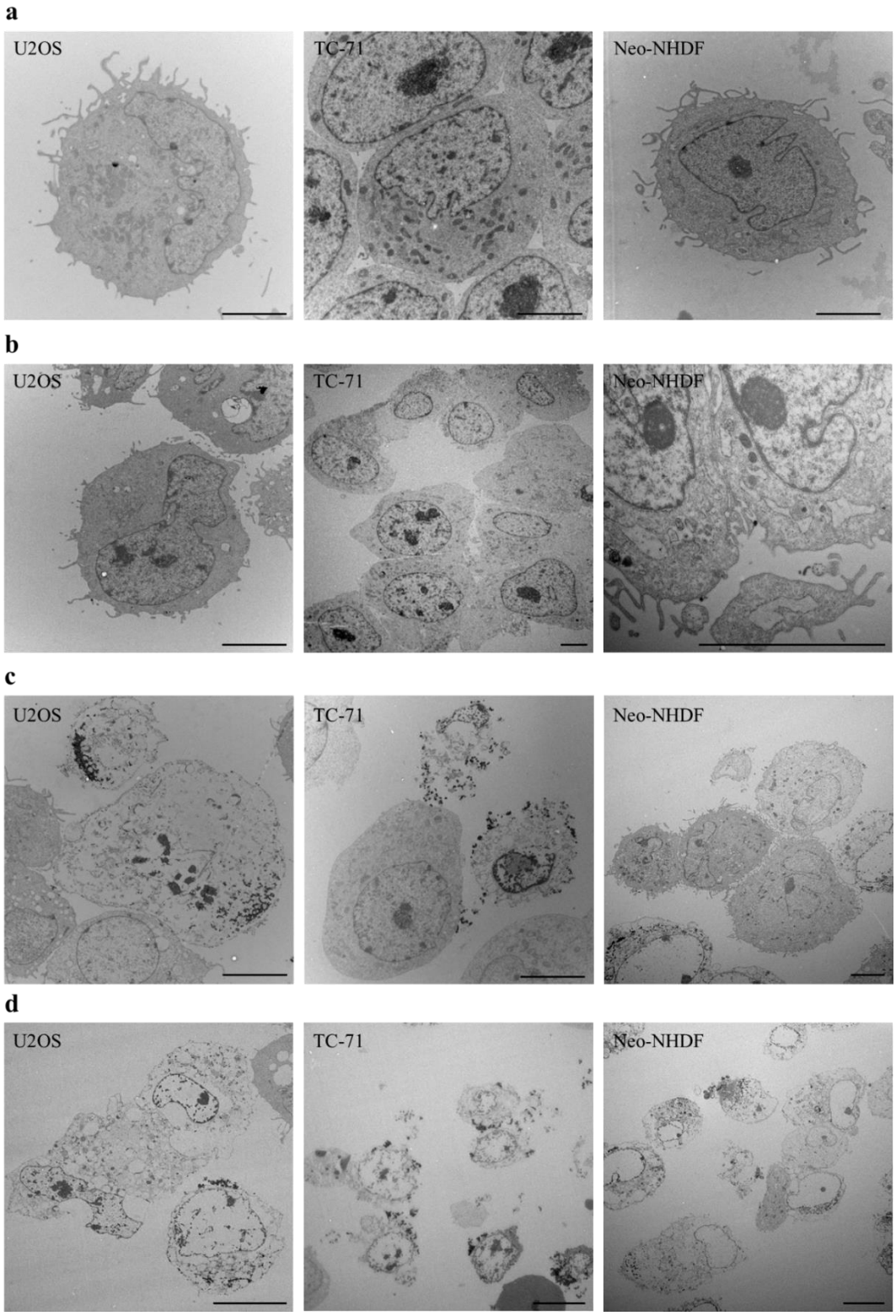

Figure 4.9 – Cell death is dependent on polymer concentration. (a) Control cells. (b) Cells present normal morphology when coated in a 10 µg/mL coating. (c) Mixed cell population when coating cells with 50 µg/mL PLL (d) High polymer concentrations (100 µg/mL) lead to cell death by necrosis. All cells fixed immediately after coating. Scale bar, 5 µm (a, b, c) and 10 µm (d).

4.5 Polymer Uptake and Metabolisation

PLL internalisation and respective metabolisation were examined through confocal microscopy, confirmed by transmission electron microscopy and quantified by flow cytometry.

Through confocal microscopy, it was observed that cells coated using the 10 μg/mL PLL solution were able to attach within 1 h, after which the polymer was rapidly internalised by all cell lineages. However, each cell type showed different PLL metabolisation rates, with the fibroblasts metabolising most of the polymer in the first 4 h post-coating, with little PLL evident at this time point (Figure 4.10). On the other hand, the U2OS and TC-71 cell lines metabolised the polymer at lower rates, with PLL still evident 4 hours after the coating procedure (Figure 4.11 and Figure 4.12, respectively).

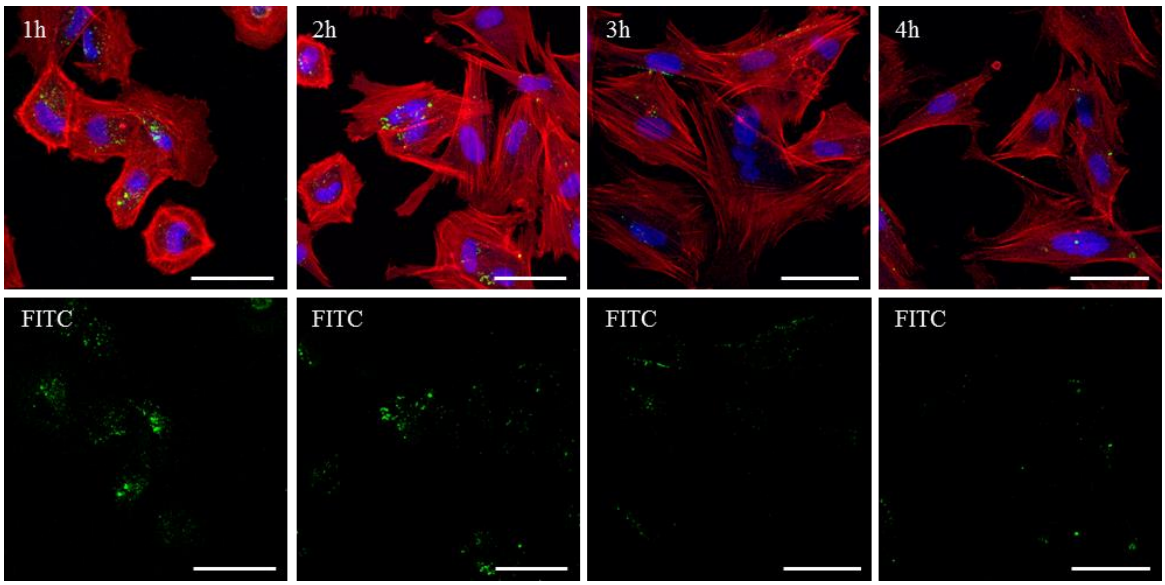

Figure 4.10 - PLL internalisation and metabolisation in the first 4 h after coating with 10 μg/mL concentration allows normal Neo-NHDF cell attachment and proliferation. Neo-NHDF cells attached within 1 h and metabolised almost all polymer within 4 h. Staining similar to that in Figure 4.6. Scale bars, 50 μm.

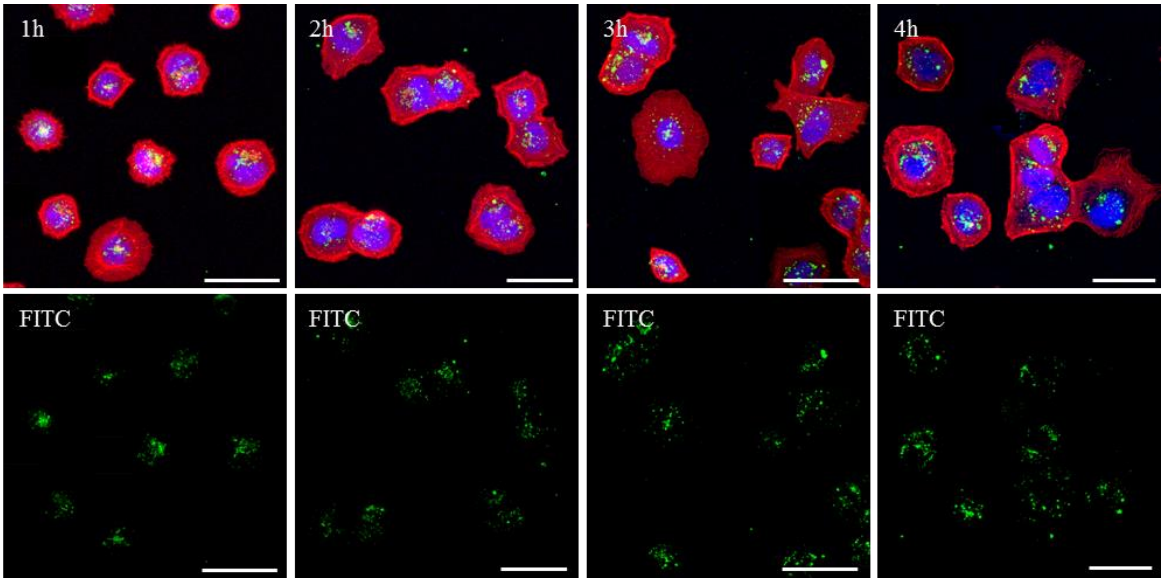

Figure 4.11 - PLL internalisation and metabolisation in the first 4 h after coating with 10 μg/mL concentration allows normal TC-71 cell attachment and proliferation. Osteosarcoma cells attached within 1 h, but slow polycation metabolisation was observed in the firsts 4 h. Staining similar to that in Figure 6. Scale bars, 50 μm.

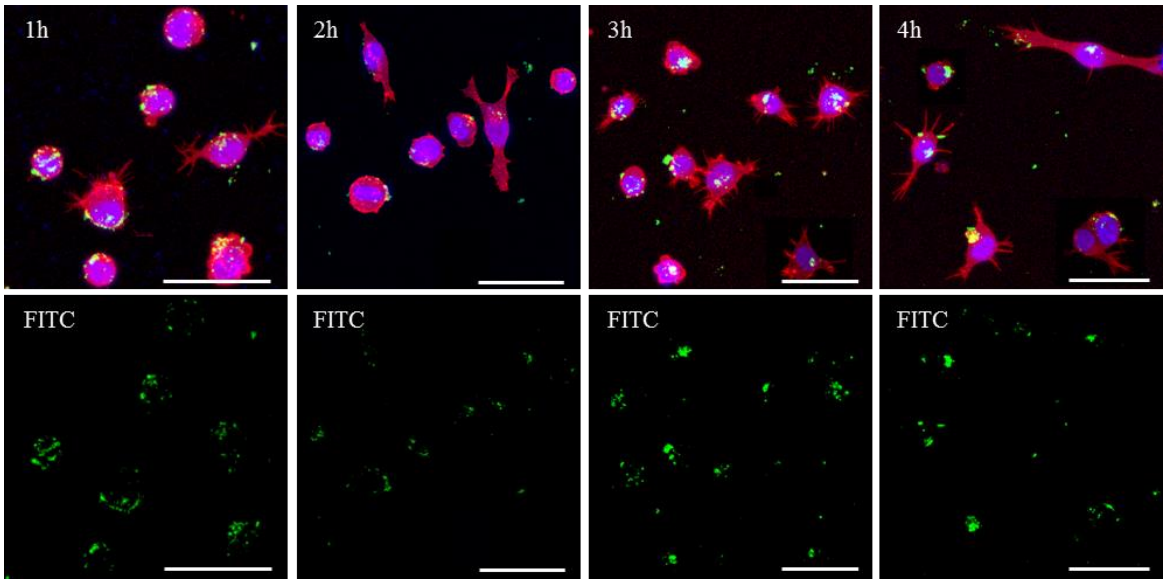

Figure 4.12 - PLL internalisation and metabolisation in the first 4 h after coating with 10 μg/mL concentration allows normal TC-71 cell attachment and proliferation. TC-71 cells started attaching soon after the coating procedure, but polymer metabolisation was again slow. Staining similar to that in Figure 6. Scale bars, 50 μm.

TEM allowed to identify a range of endocytic pathways (Figure 4.13): caveolar-type endocytosis (Figure 4.13a), micropinocytosis (Figure 4.13b), phagocytosis (Figure 4.13c) and CLIC/GEEC-type endocytosis (Figure 4.13d);

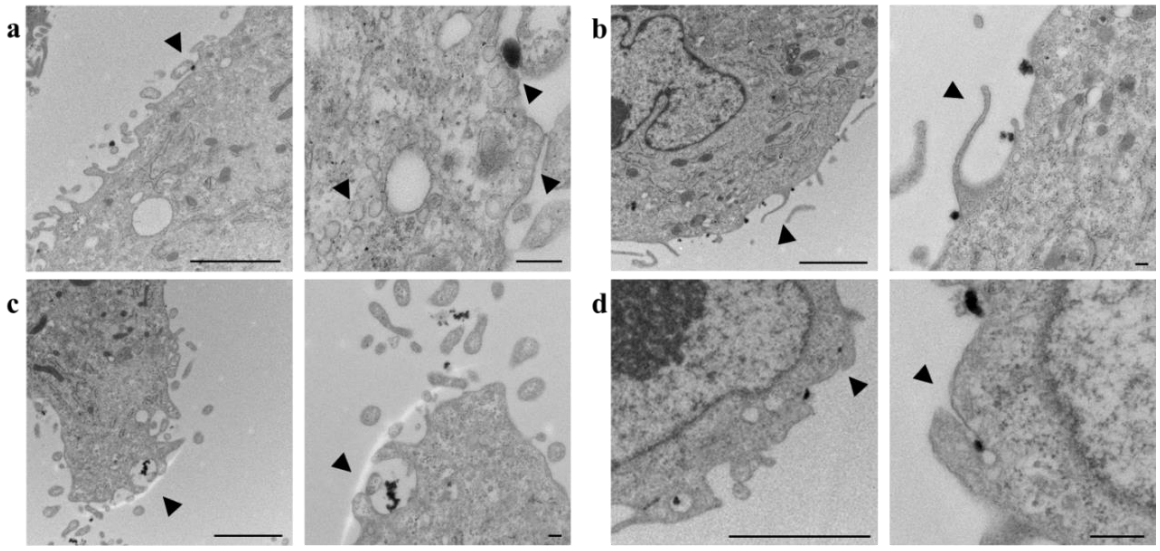

Figure 4.13 - PLL is actively internalised by coated cells using size-dependent endocytic pathways. (a–c) Three different endocytic pathways were observed for human fibroblasts once fixed immediately after coating: caveolar-type endocytosis, micropinocytosis, and phagocytosis. (d) CLIC/GEEC-type endocytosis noted on osteosarcoma cells. All micrographs represent day 0 cells coated using a 10 μg/mL PLL solution. Scale bars are 2 μm and 200 nm for the zoom out (left) and zoom in (right) columns, respectively.

To quantify the polycation metabolisation rate, the different PLL concentrations were analysed using Flow Cytometry during a period of two days (immediately after coating, 1 and 2 days after coating). For the different cells lines, when coated with the 10 μg/mL concentration (Figure 4.14), a steep rose in fluorescence intensity with PLL-FITC-coated cells was noted, when compared to the control population, decreasing progressively over the two-day period. The intensity values approached the control values after 2 days, which reflected the polymer ingestion and metabolisation. Over this longer time period, it was observed that the rates at which the TC-71 (Figure 4.14b) and fibroblasts (Figure 4.14c) cells metabolised the polymer were qualitatively higher than that for the U2OS cells (Figure 4.14a), as indicated by the relative overlaps between the control populations and the day 2 populations. Additionally, for all cells, a greater width was observed on the peaks that represent day 1.

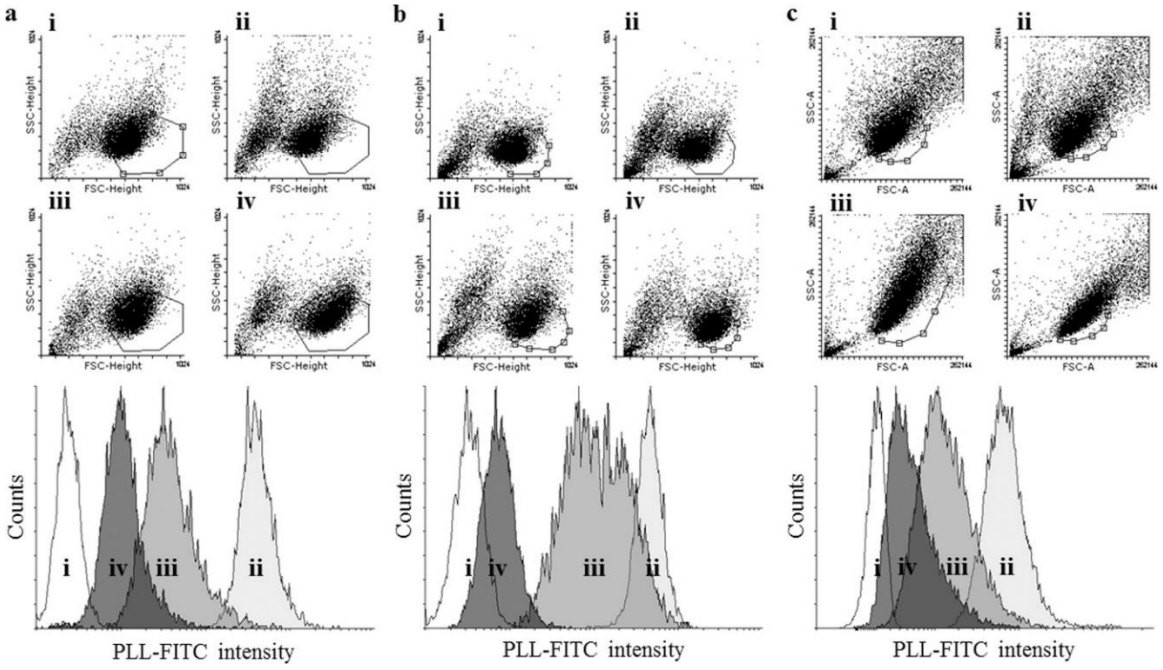

Figure 4.14 - FACS gating and histograms for live (A) U2OS, (B) TC-71, and (C) Neo-NHDF cells coated using a 10 μg/mL PLL solution. i is control (day 0), and ii, iii, and iv represent days 0, 1, and 2, respectively.

On the other hand, 50 and 100 μg/mL PLL-FITC coated cells presented a high intensity of polymer during the two days of the test (Figure 4.15 and Figure 4.16). The polymer intensity peak showed to barely move for the U2OS cells at both concentrations, staying distant from control. For TC-71 cells it was possible to observe a diminishment on the PLL-FITC intensity on 50 and 100 μg/mL, however the peaks did not reach close the control values. It was also noted that the peak representing day 1 and 2 had an increase width when compared to the one representing day 0. A reduced number of counts was detected for this cell line when coated with the 100 μg/mL polycationic concentration. Neo-NHDF cells are observed to be the fastest cells to metabolise the polymer, even at high concentrations, which is represented by the closest peaks from the control by day 2 and, additionally, presenting sharp peaks on that same day. However, the presence of two different cell populations were noted on day 0, which is expressed by the increased width of the peak and the existence of an extra peak.

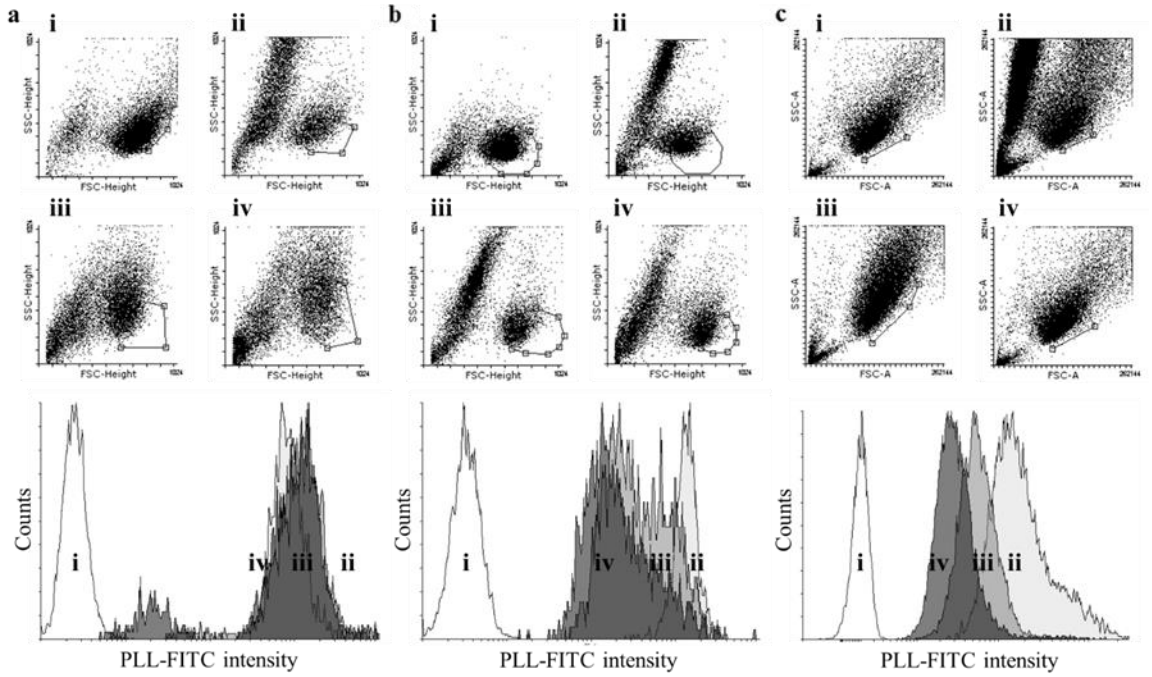

Figure 4.15 - FACS gating and histograms for live (A) U2OS, (B) TC-71, and (C) Neo-NHDF cells coated using a 50 μg/mL PLL solution. i is control (day 0), and ii, iii, and iv represent days 0, 1, and 2, respectively.

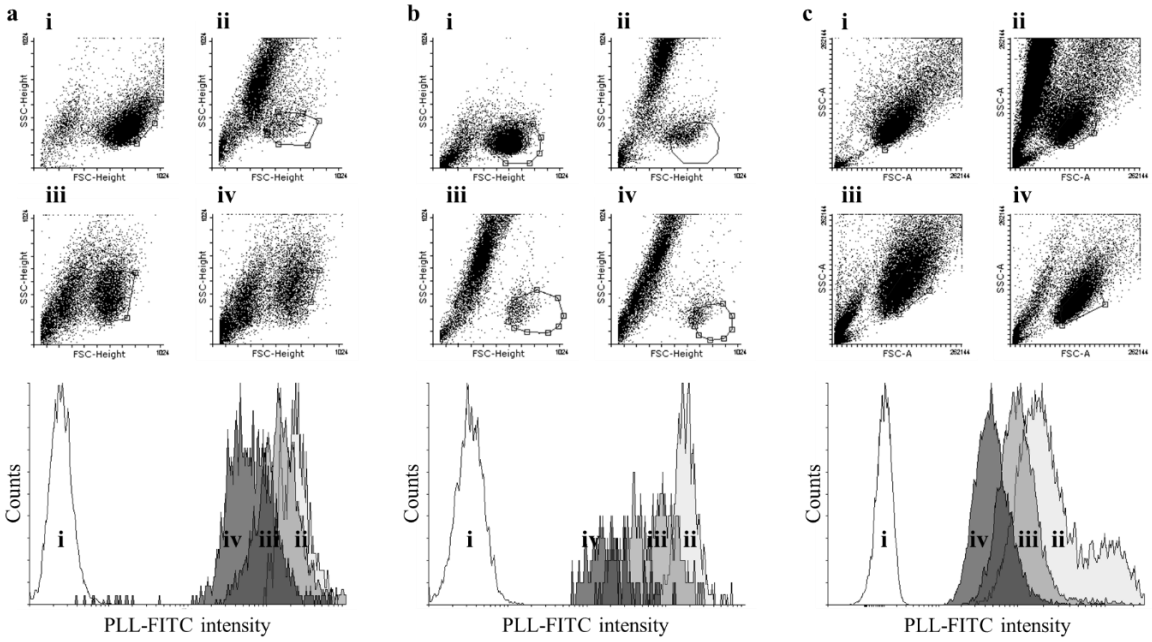

Figure 4.16 - FACS gating and histograms for live (A) U2OS, (B) TC-71, and (C) Neo-NHDF cells coated using a 100 μg/mL PLL solution. i is control (day 0), and ii, iii, and iv represent days 0, 1, and 2, respectively.

4.6 Cell agglomeration avoidance by polycationic coating

To observe the potential effect of the polycationic coating on the avoidance of cell agglomeration, coated and noncoated U2OS cells were dispensed onto glass slides using a syringe and observed under a microscope (Figure 4.17), and the areas of aggregates were quantified (Figure 4.18 and Table 4.1). Untreated cells presented increased aggregate areas at time zero, when compared to treated cells at the same time-point. After 3 h of cell incubation inside the syringe, 10 μg/mL coated cells were largely free of natural cell agglomeration, remaining dispersed with a minimum formation of small aggregates (Figure 4.17a). Cell agglomeration was observed on noncoated cells after 2h of incubation, with sizable cell clusters observed after 3 h (Figure 4.17b). By viewing Figure 4.18 and Table 4.1 it is possible to conclude that cells coated with 10 μg/mL PLL concentration did not create agglomerates as big as the uncoated cells. Additionally, coated cells formed agglomerates with more homogeneous sizes, when compared to the high size distribution observed on PLL-free cells. Finally, PLL coating determined that the agglomerate sizes of coated cells were approximately 2, 4, 5 and 10 times smaller by 0, 1, 2 and 3 hours, respectively, when compared to the uncoated cells.

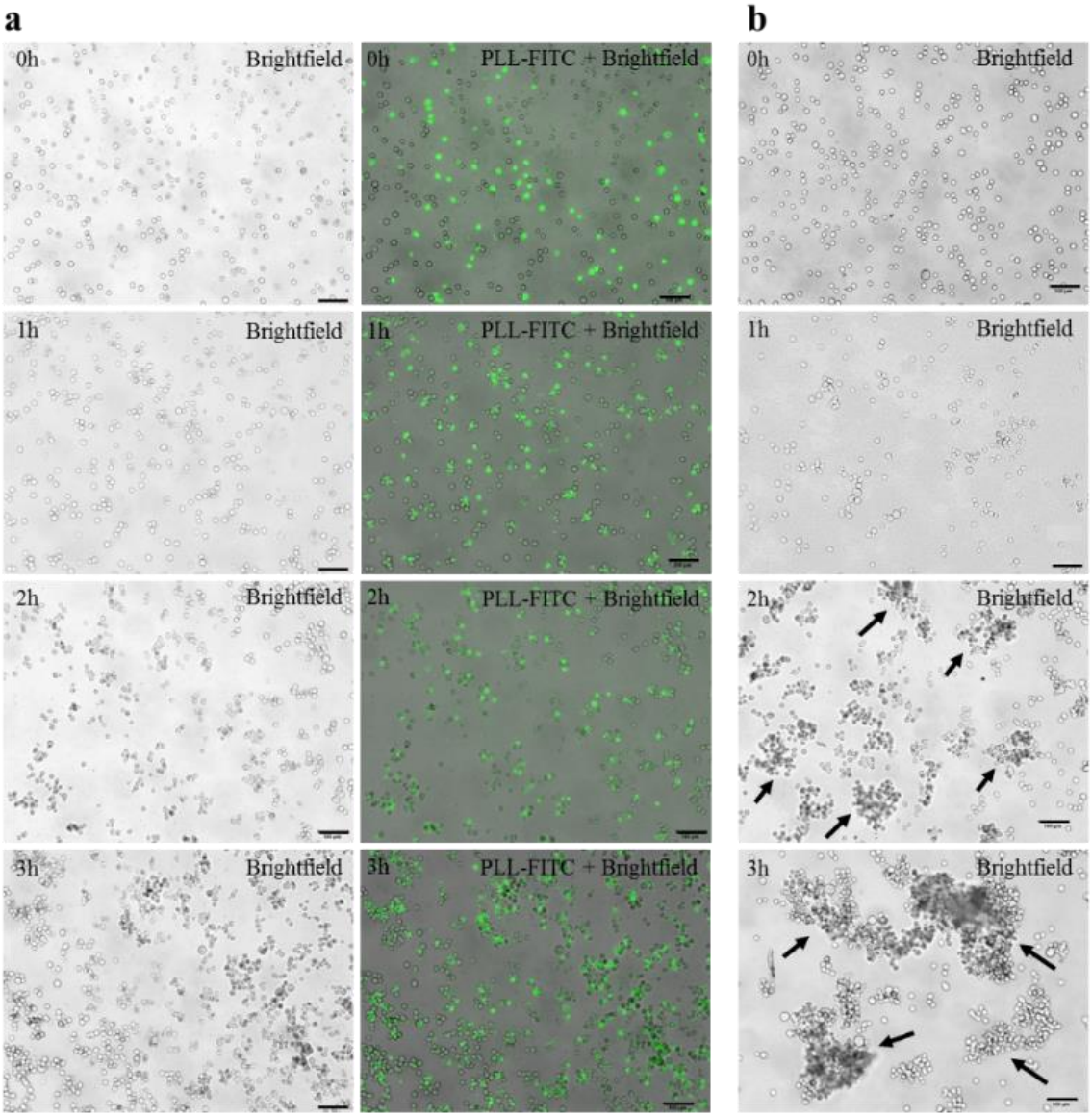

Figure 4.17 - PLL coating avoids cell aggregation and allows repeatable printing results. (a) U2OS cells coated with a 10 μg/mL coating present dispersion when deposited through a 21 G needle at different times after the coating procedure. (b) Uncoated U2OS cells present high degree of agglomeration (arrows) within the deposition times. Scale bars, 100 μm.

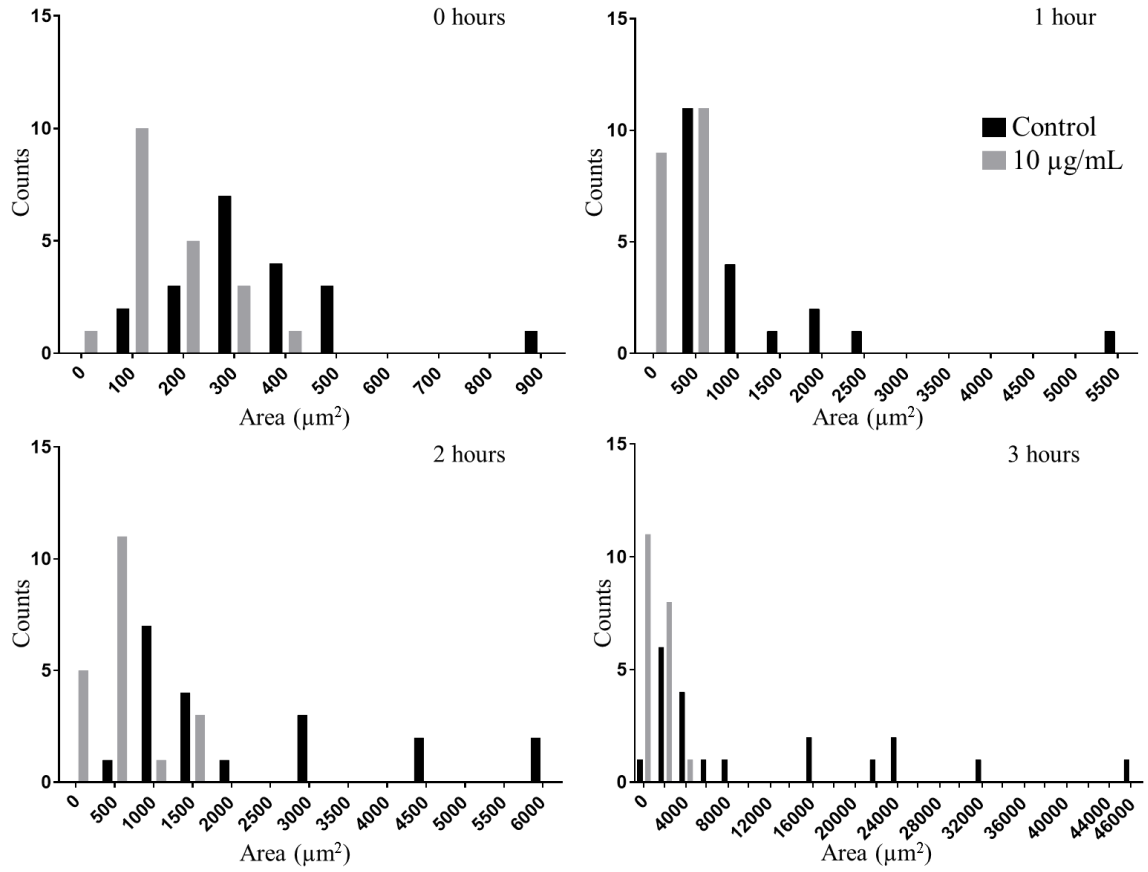

Figure 4.18 – U2OS cell agglomerate area distribution during 3-hour period.

Table 4.1 – Cell aggregates area.

Cell aggregation area (µm²)		
Time(h)	Control	10 µg/mL
0	335±169	162±106
1	1151±1164	321±153
2	2261±1677	547±448
3	11036±12552	1177±789

4.7 Inkjet cell printing reliability

Bio-inks composed by cells suspended in cell medium have shown to create agglomerates and nozzle blockage, disrupting the inkjet printing process. Figure 4.19 reports the macroscopic views of the flow inside an inkjet nozzle by using different simple bio-inks – serum free medium (Figure 4.19a) and cells suspended in serum free medium (Figure 4.19b) –, and, finally, nozzle blockage due to cell agglomeration (Figure 4.19c).

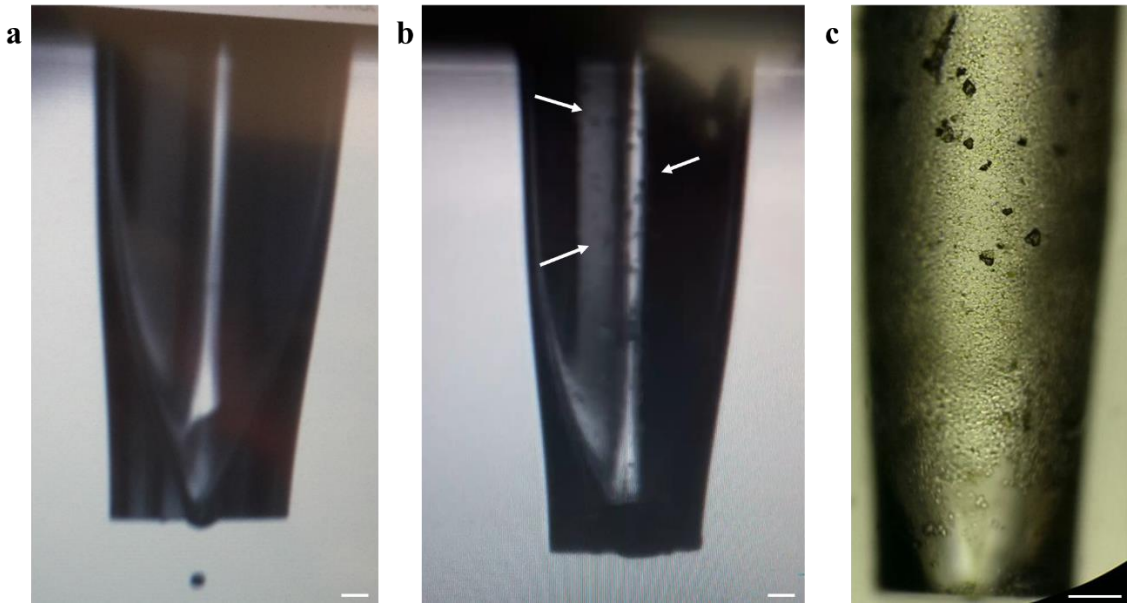

Figure 4.19 – Macroscopic view of the inkjet nozzle when using: **a** serum-free medium; **b** cells (white arrows) suspended in serum-free medium. **c** Nozzle blockage after 20 minutes of printing using a simple bio-ink (U2OS cells suspended in serum-free medium). Scale bars represent 60 µm.

Figure 4.20 shows the difference between using polycationic coated and non-coated cells on bio-inks for U2OS (Figure 4.20a), TC-71 (Figure 4.20b) and Neo-NHDF (Figure 4.20c) cells. It was demonstrated that for a 60-min period the different bio-inks with PLL coated cells were able to maintain a stable number of cells without cell agglomeration. On the other hand, bio-inks without PLL coated cells exhibited to gradually decrease the number of printed cells until nozzle blockage. This issue happened 20 and 40 minutes after starting the experiment for U2OS and Neo-NHDF, and TC-71 cells, respectively.

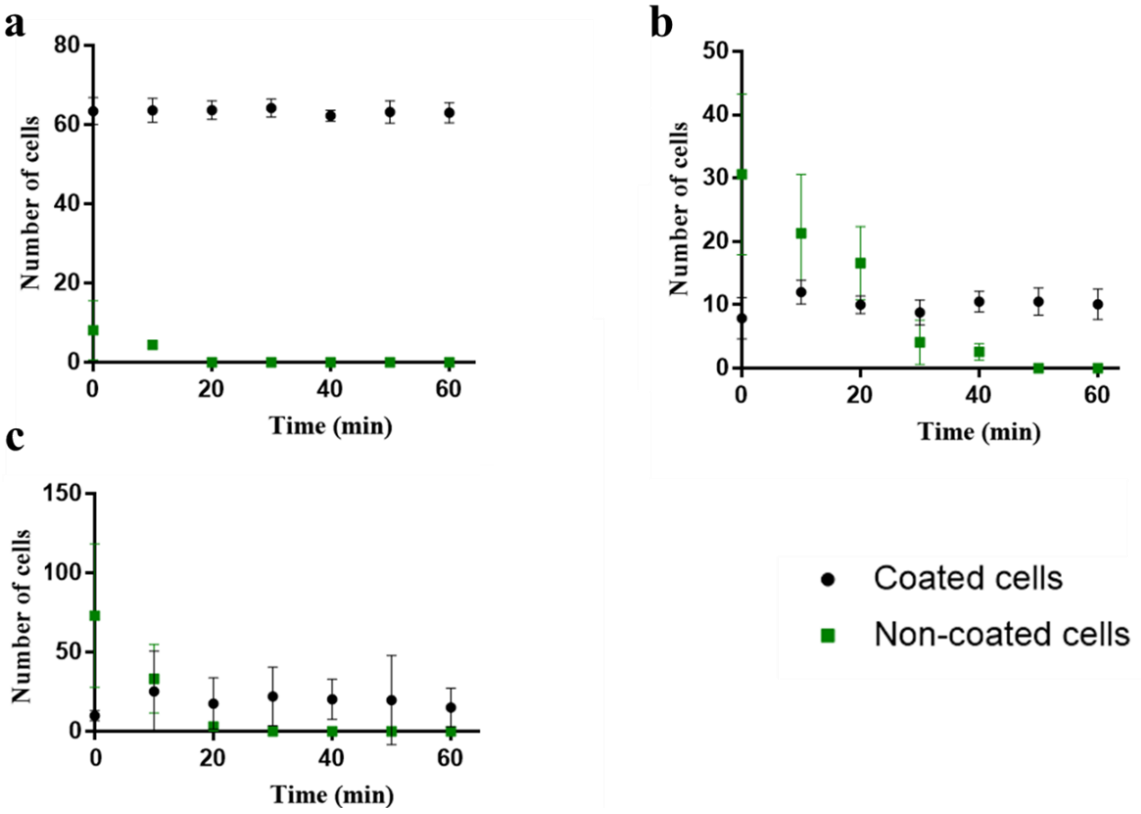

Figure 4.20 – Reliability comparison between bio-inks with coated and non-coated cells. **a** U2OS cells; **b** TC-71 cells; **c** Neo-NHDF cells.

4.8 Post-printing in vitro cell viability studies

Live/Dead assay was used to obtain qualitatively information about the after-printing cell viability (Figure 4.21). Here, it is possible to note that the majority of the cells have survived to the coating manipulation and to the printing process. Only a small number of cells for the different cell types was observed to be dead.

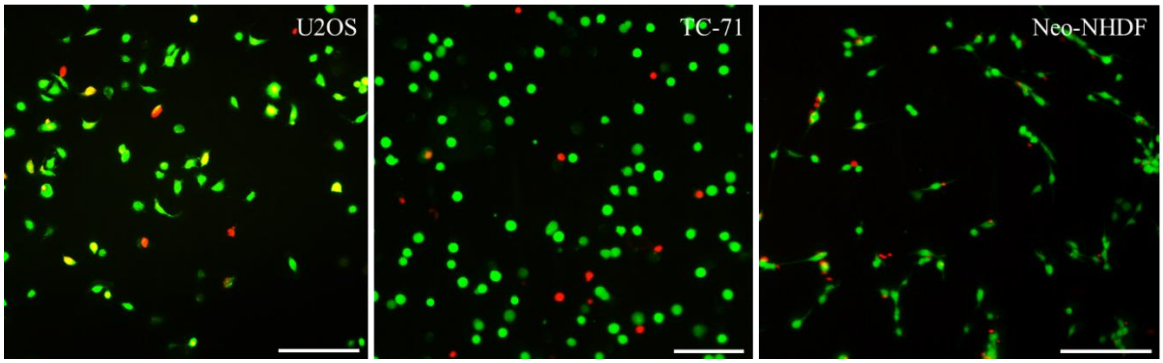

Figure 4.21 - Live/Dead assay for printed PLL coated U2OS, TC-71, Neo-NHDF. For each cell type, pictures represent cells 4 hours after printing process. Scale bars are 100 μm.

4.9 Post-printing cell and coating morphologies

Cell and coating morphologies were observed by confocal microscopy. Figure 4.22, Figure 4.23, and Figure 4.24 show the morphology of U2OS, TC-71 and Neo-NHDF, respectively, immediately after printing and 24 hours later. The morphologies obtained after printing were comparable to what was obtained and presented in chapter 4. Immediately after printing, the different cells presented round shape with PLL tightly bounded to their membrane. One day after printing, cells have attached and acquired their typical morphology: U2OS cells presented a heterogeneous population, TC-71 cells grew in clumps, and fibroblasts were flattened and elongated. Cells have retained the ability to ingest and metabolise the PLL as shown by U2OS and Neo-NHDF, which presented low amounts of PLL one day after printing. Contrarily, Ewing's sarcoma cells showed higher magnitude of polycation at the same time point.

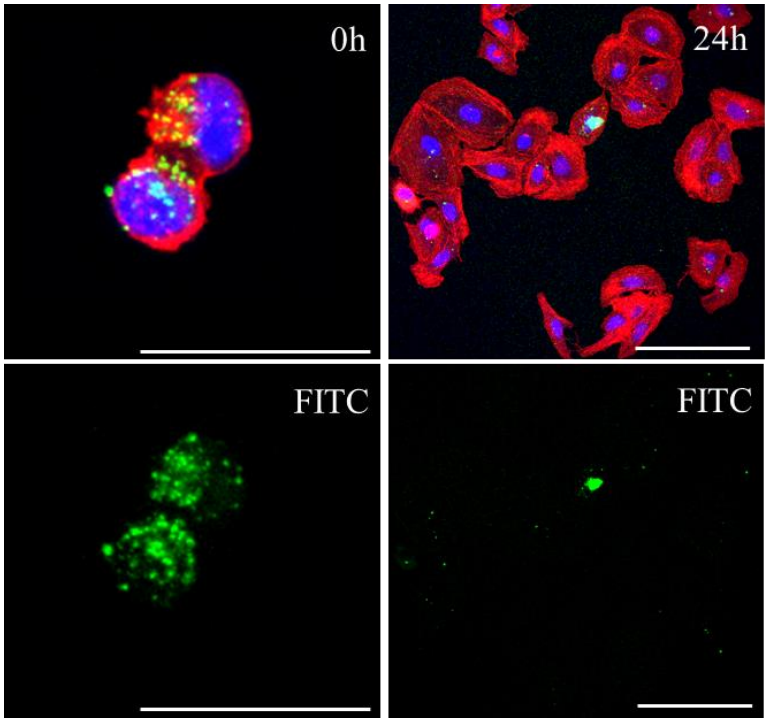

Figure 4.22 – Cell and PLL coating morphology after printing for U2OS cells. Staining similar to that in Figure 4.6. Scale bars represent 37.5 µm (left) and 150 µm (right).

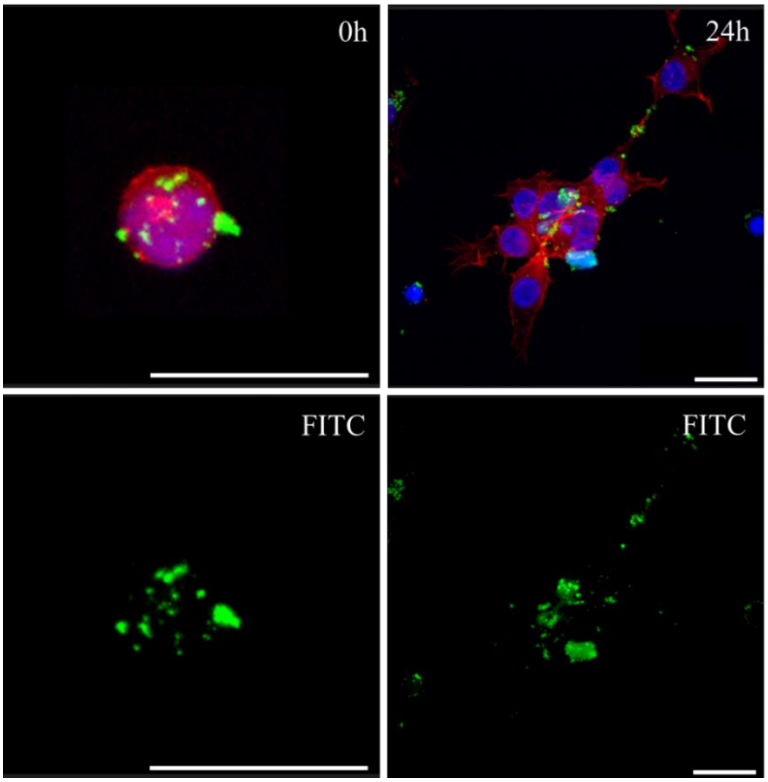

Figure 4.23 – Cell and PLL coating morphology after printing for TC-71 cells. Staining similar to that in Figure 4.6. Scale bars represent 30 µm.

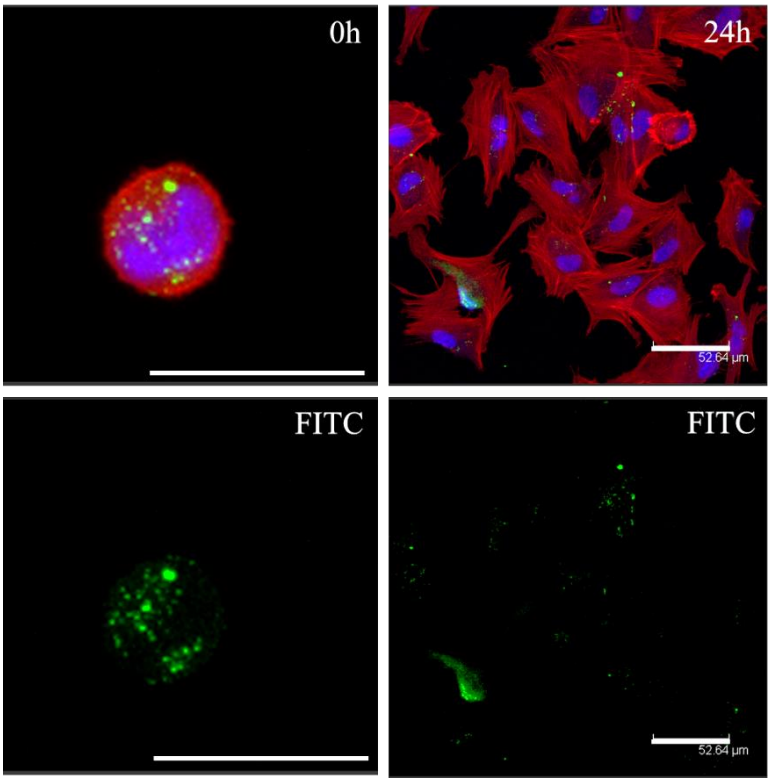

Figure 4.24 – Cell and PLL coating morphology after printing for Neo-NHDF cells. Staining similar to that in Figure 4.6. Scale bars represent 30 µm (left) and 52 µm (right).

4.10 Chapter discussion

4.10.1 *Cell viability and metabolic activity*

During this research a new, efficient and temporary single-cell PLL coating process has been developed. This procedure used a synthetic polycation that is considered cytotoxic by previous results (Menger *et al.*, 2003), however results suggest that the cytotoxic response is dose dependent, and that cell viability and metabolic activity are acceptable when using low concentrations. Metabolically, cells presented different behaviours to the PLL coating, with one cell line reporting coated cells metabolic more active than the control samples. This clearly shows that the reaction to the PLL is different from cell to cell.

For dead cells it was not possible to differentiate between late apoptosis and necrosis, perhaps as a result of caspase or other protease activity cleaving the probe in the dead cells. However, necrosis is considered as consequence of the coating process to be the most likely cause of cell death, and the cell morphologies in TEM support this view. This

is explained by the effect that PLL and other polycations cause on the cell membrane – the coupling between the negative cell membrane and the positive polymer disrupts the lipid bilayer by opening nanoholes on the cell membrane (Fischer *et al.*, 2003; Menger *et al.*, 2003; Hong *et al.*, 2006; Vaidyanathan *et al.*, 2015). This damage, when severe, destroys not only cell structures and organelles, but also its organisation, leading to cell necrosis.

When damaged, cells are susceptible to mutate and carry chromosomic aberrations that would change its characteristics (Lodish *et al.*, 2000). This way, it was observed that Neo-NHDF and TC-71 retained their normal karyotype. Osteosarcoma was not analysed due to the nature of its karyotype – completely aberrant and random, with no consistent hallmark, such as Ewing's sarcoma, which would not allow any conclusion (Morrow and Khanna, 2015).

4.10.2 *Cell morphology*

The coating protocol established in this research allows for the development of a high-efficiency and tightly fitting coating. The PLL concentration was shown to be determinant on the morphology of the coating. Therefore, depending on the polycationic solution concentration, different amounts of PLL particles will be available to anchor the cell membrane, forming from simple speckled coating to full shells. Through confocal microscopy it was also verified that cells ingest and metabolise the polycation, at the same time they attach and proliferate normally. This happened in each cell type, maintaining the characteristic phenotype during proliferation.

4.10.3 *Polymer uptake and metabolisation*

The polycation uptake and metabolisation has been confirmed by evaluating not only confocal microscopy and TEM images, but also quantified by flow cytometry. It was observed that the different cell types used during this investigation were able to attach 1 hour after coating, however their behaviour has been shown to be distinct between them. Neo-NHDF confirmed higher metabolisation capacity, when compared to the other two cells, U2OS and TC-71, as 4 hours after the coating procedure barely no PLL was observable. U2OS and TC-71 cell demonstrated to not be able to process the polycation

as fast as the Neo-NHDF. However, all the different cells were able to show endocytic pathways to uptake the PLL particles. No preference for a certain endocytic pathway was observed, which is normally determined by the particle size (Zhang *et al.*, 2009). This way, specific-pathway inhibitors must be used to clearly identify each pathway and its dependency on the size of the micro- or nanoparticles being ingested, as observed in previous studies (Vercauteren *et al.*, 2010; Dutta and Donaldson, 2012). Flow cytometry has also reported that cells internalise and metabolise PLL differently, with Neo-NHDF showing better tolerance for the polycation, even at higher concentrations.

Within this analysis it is possible to conclude that the developed PLL coating system may be used by different cells, however, depending on the application, it might need optimisation as the response to the same polycation concentrations will be distinct on the cell type. Each cell has its own characteristics that lead to certain phenotypes, proliferation rates or secreted cytokines, and, therefore, will naturally behave differently to materials and other foreign stimulus (Curtis and Wilkinson, 1999).

4.10.4 *Inhibition of agglomeration*

Agglomerates formed with non-coated cells presented an average area of approximately 10 times higher than the average area for 10 μg/mL coated cells in the last time-point studied (3 hours). This way, the coating technique demonstrated to successfully attenuate cell agglomeration by keeping the cells apart due to the electrical repulsion between the positively charged polymer.

4.10.5 *Inkjet printing reliability and post-printing cell characteristics*

Bio-inks with polycationic coated cells showed to increase inkjet printing reliability, posing as an alternative to other strategies. However, similarly to *in vitro* assays, the bio-ink behavior was distinct depending on the cell type. For U2OS and TC-71 cells, constant and repeatable results with low variability were obtained. On the other hand, bio-inks with coated Neo-NHDF presented high variability when compared to the other two. Additionally, it was noted that the number of cells per drop was different for each bio-ink, reaching approximately 1 cell per droplet for bio-inks with coated U2OS cells, when

compared to 0.2 to bio-inks with coated TC-71. Both issues are related to two characteristics – cell size and the interaction with the polymer.

Ewing's sarcoma present small round cells, being smaller than the other two. This characteristic is related to the cell mass, which make TC-71 cells potentially weight less than osteosarcoma cells and fibroblasts. Consequently, as the weight is lower, the gravity effect will be also reduced. Therefore, TC-71 cells will take more time to reach the inkjet nozzle and the number of cells per droplet will be decreased. Differently, Neo-NHDF cells show higher interaction with the PLL coating. As it was reported previously, faster internalization and metabolization of the polymer was demonstrated for these cells. Additionally, FACS showed lower FITC intensity when compared to the other two cell types. This way, the coating on these cells may be poorer, affecting the repulsion between Neo-NHDF. Both issues may grant lower and different repulsion magnitude between cells, leading to higher variability on printed cells. These results conclude that mechanical agitation and PLL concentration must be optimised for each bio-ink to obtain a reliable printing.

Viability and cell morphology were observed to remain unchanged after printing. It is concluded that the shear stress from the agitation, but also from the printing process itself, did not have impact on cell viability nor PLL internalization and metabolisation.

Chapter 5. Reactive Jet Impingement for bone microtissue bioprinting

5.1 Introduction

In this chapter, a new printhead entitled Reactive Jet Impingement, that has been created by Dr. Matthew Benning and Prof. Kenny Dalgarno (Benning and Dalgarno, 2017), is characterised and used to print a collagen-alginate-fibrin hydrogel, originally developed by Dr. Ana Marina Ferreira (Montalbano *et al.*, 2018), to allow bone microtissue development. Here, the functionality of this new printing technique using this hybrid hydrogel is analysed, showing how cell density influences several factors during microtissue formation, such as gene expression. Hydrogel properties, such as degradation or solution diffusion, cell proliferation and viability, morphology or differentiation ability are also studied during this chapter.

5.2 Reactive jet impingement concept and characterisation

To obtain cell-laden hydrogels without using an extrusion-based bioprinter, ReJI jets droplets from opposite sides that meet and mix in-air forming a hydrogel prior impact onto substrate. Simultaneous droplet jetting (Figure 5.1) is only possible after the optimisation of the electrical waveform and pressure. Specific printing patterns are possible to be obtained through a .txt script or transforming any image into a black and white bitmap file (Figure 5.2).

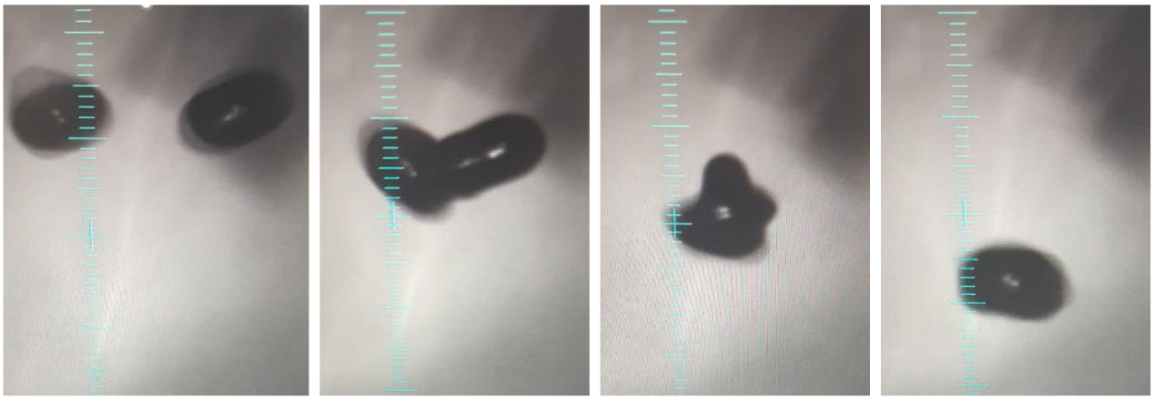

Figure 5.1 - ReJI printing technique. Stroboscopic images of gel-precursor and crosslinking droplets meeting in air.

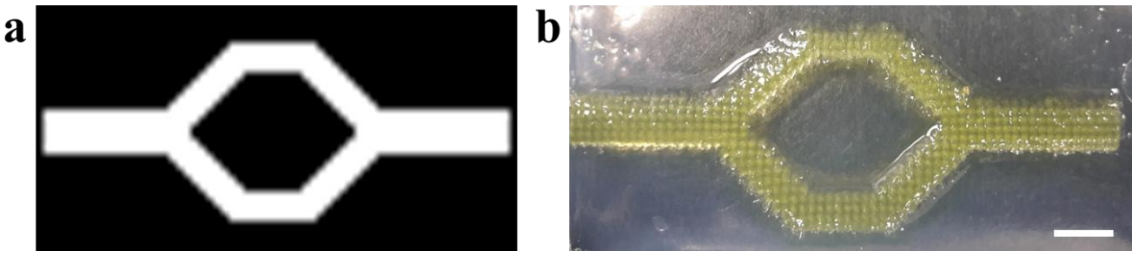

Figure 5.2 – From image to sample. **a** black and white bitmap and **b** respective printed pattern. Scale bar represents 6 mm.

To test the concept, different solutions have been jetted using the ReJI printhead: water, NaAlg and $CaCl_2$, fibrinogen, a collagen-alginate-fibrinogen mixture and thrombin combined with $CaCl_2$. Table 5.1 shows the optimal parameters used to jet each solution.

Table 5.1 – Optimal parameters for jetting different materials.

Material	[C] (mg/mL)	Frequency (Hz)	Pressure (mmHg)	Dwell Time (µs)
NaAlg	10	300	454	1000
Autoclaved NaAlg	10	400	390	800
1M $CaCl_2$	----	400	290	800
Fibrinogen	25	100	300	700
CAF	Col – 0.54 NaAlg – 4.54 Fib – 27.27	400	450	800
500 U/mL Thrombin + 6% $CaCl_2$	----	400	290	800

The printing technique was observed to be reliable, printing gel droplets of similar sizes and at equidistant locations for the different materials, as seen in Figure 5.3a-c. Printed droplets are reported to be in a sub-millimetric range with (0.701±0.021) mm for water, (0.646±0.007) mm for NaAlg hydrogel and CAF gel loaded with 40 x 10^6 cells/mL presented (0.795±0.083 mm) of diameter. Additionally, it was found that channels are able to be obtained with 1 pixel of width, which corresponded approximately to (708.2±97.2) µm, when printing CAF hydrogel (Figure 5.3d). Viscosity gains of great importance when using microvalves as after a certain threshold, droplet jetting is not

possible. Pre-gel precursors are of a higher viscosity nature, when compared to the crosslinking solutions, that present “naked eye” viscosity close to water. Therefore, optimal concentrations for NaAlg and CAF, as presented on Table 5.1, exhibited $3.6x10^{-3}$ Pa/s and 0.0249 Pa/s of viscosity, respectively.

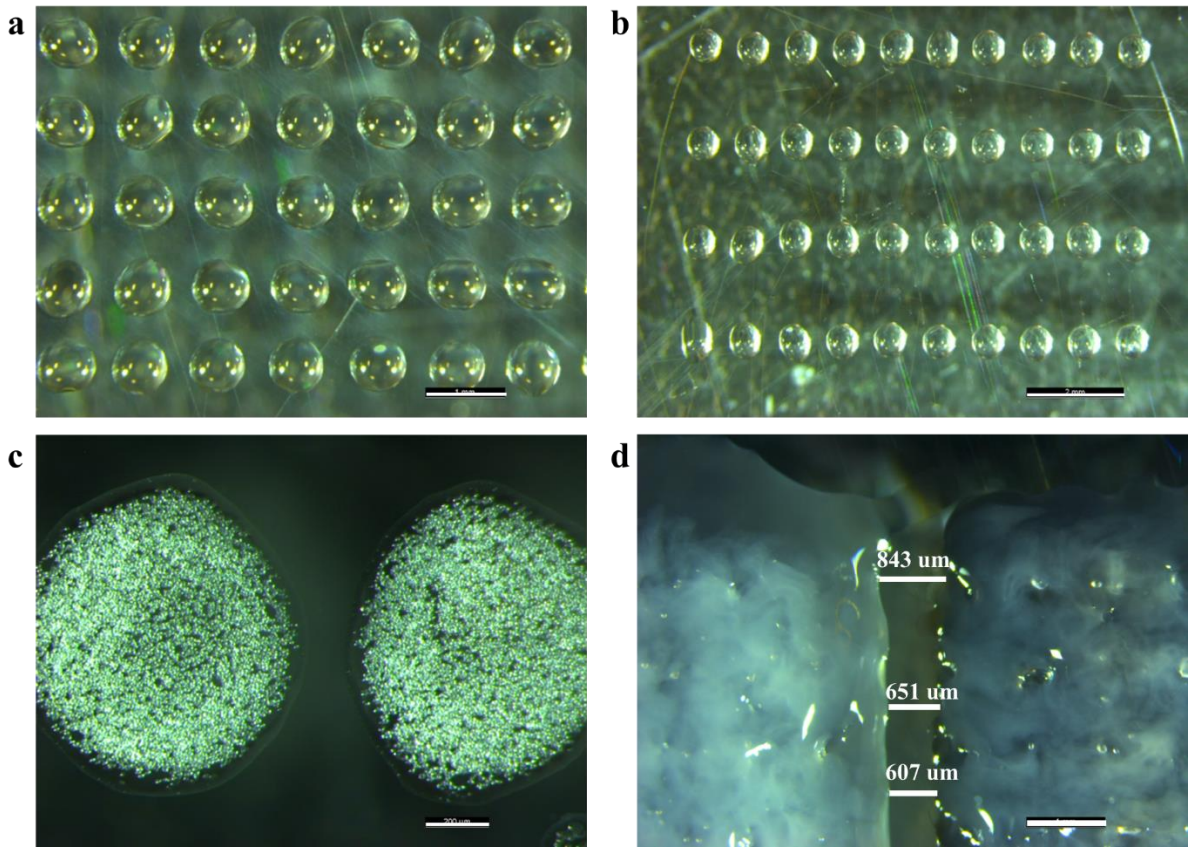

Figure 5.3 - **a-c** Water (0.701±0.021 mm), NaAlg gel (0.646±0.007 mm) and CAF gel loaded with 40 x 10^6 cells (0.795±0.083 mm) droplets spatially equidistant. **d** Channel with 1 pixel of size. Scale bars represent 1 mm, 2 mm, 200 µm, and 1 mm, respectively.

5.3 CAF hydrogels characterisation

5.3.1 *Compression test*

The mechanical properties in compression of printed CAF hydrogels were measured. A stress-strain curve for freshly printed CAF hydrogels is reported in Figure 5.4. The compressed stress was calculated from the linear region of the stress-strain curve, in the 10-20% strain interval. A similar compressive modulus was obtained for the three different samples, (1.125±0.042) kPa comparable to the modulus of similar gel formulations when prepared conventionally (0.9–1.3kPa). The conventionally formulated

CAF gels have showed similar mechanical properties to lower end of the range for soft tissues, such as pancreatic tissue (Montalbano *et al*, 2018).

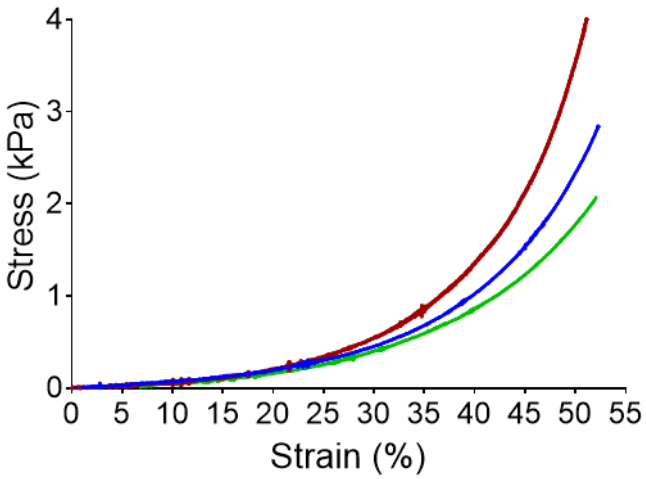

Figure 5.4 - Uniaxial compression of CAF gels. A compression modulus of (1.125±0,042) kPa was obtained for 10-20% strain interval.

5.3.2 *Degradation assay*

CAF hydrogels are composed of natural materials, including proteins, therefore, it was necessary to guarantee that no medium component would affect the printed hydrogel for long time-intervals, degrading it. This way, a degradation assay has been carried. It was observed that similar printed structures showed comparable degradation rates after different time-points, only losing around 30% of its total mass after any incubation time-point inspected (Figure 5.5).

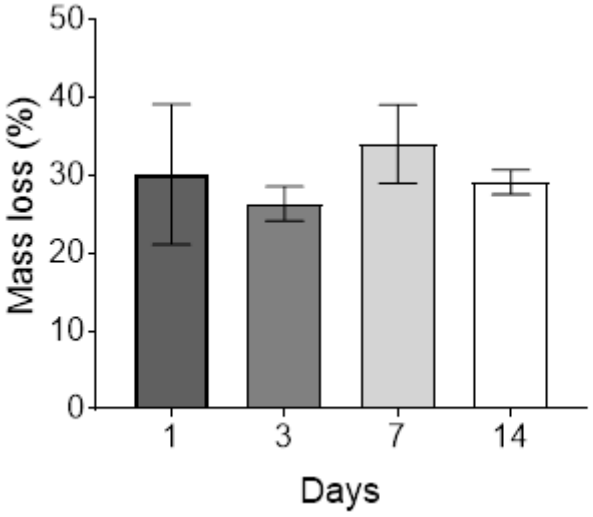

Figure 5.5 - CAF gel mass loss after incubation in medium during 1 to 14 days. Gels lost an average of 30% of its weight during the studied time-points. Not statistically significant.

5.3.3 *Diffusion assay*

As cells will be encapsulated inside the hydrogels, it is crucial that molecules are able to be delivered to the most inner site of it. Therefore, the CAF hydrogel absorbing and molecule permeation capabilities has been studied using 2-NBDG solution, a fluorescent glucose analogue (Figure 5.6). A fast increment on 2-NBDG uptake in the first 30 min was observed, reaching a close-to-maximum uptake plateau between 30 and 60 min. Between the last two time-points, 1 and 3 hours, the 2-NBDG uptake barely increase due to saturation.

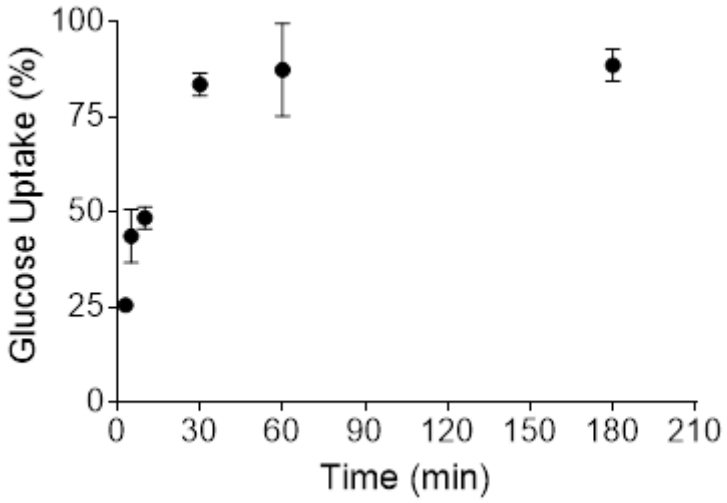

Figure 5.6 - CAF hydrogel glucose uptake. A plateau on the uptake of 2-NBDG was reached 30 to 60 minutes (corresponding to 85-90% of maximum uptake) after putting the gel in contact with this solution.

5.3.4 *CAF hydrogel morphology*

The hydrogel microstructure was observed by scanning electron microscopy (Figure 5.7). A porous network was revealed by SEM images of samples at different time-points. It was observed that incubation in cell medium at 37 °C and 5% CO_2 for 14 days did not change the hydrogel structure, presenting a similar morphology to the freshly printed samples. Outer and inner porosity can be seen with more detail in Figure 5.8. It is possible to note that the outside of the CAF hydrogel is filled with fibres, typical from fibrin, as well as small pores. Inside, the hydrogel exhibits interconnected pores similar to honeycombs.

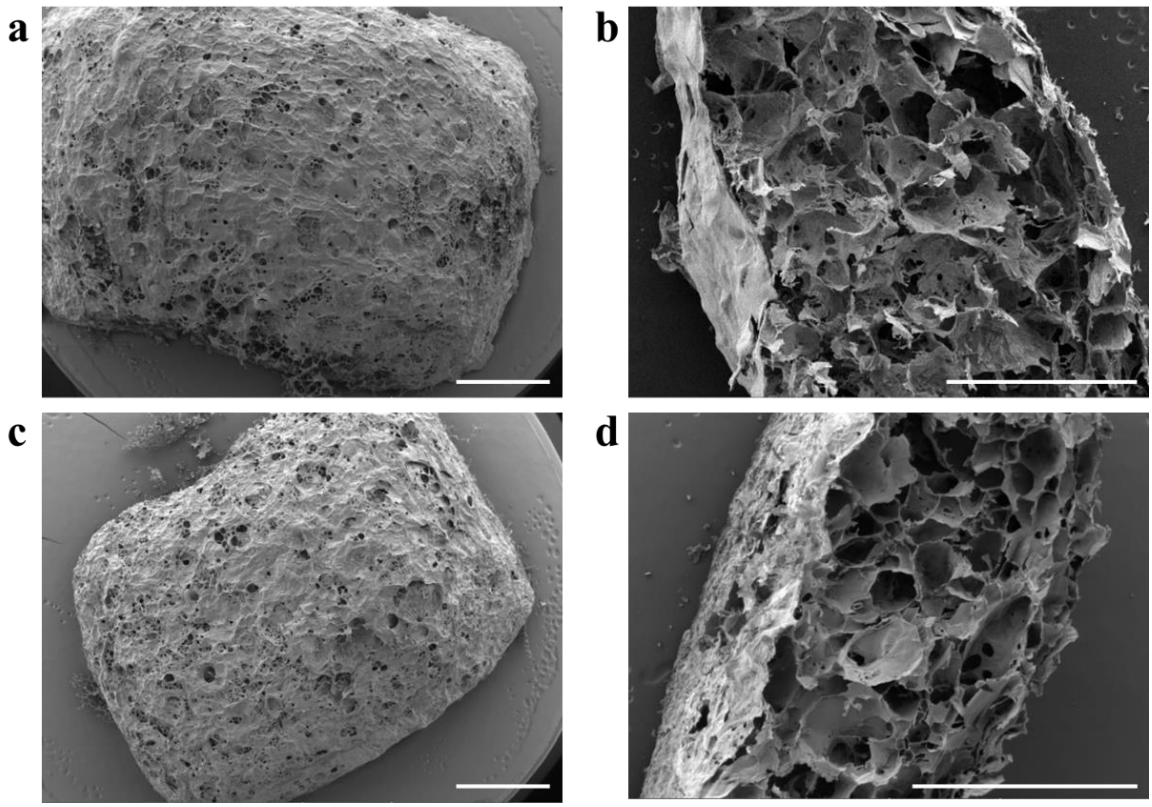

Figure 5.7 - CAF gel morphology after freeze drying. The SEM images show a highly porous fibre-like structure. a and b show a gel fixed immediately after printing and c and d reveal a gel fixed after 14 days of incubation in medium. Scale bars represent 1 mm. Each assay was conducted in triplicate.

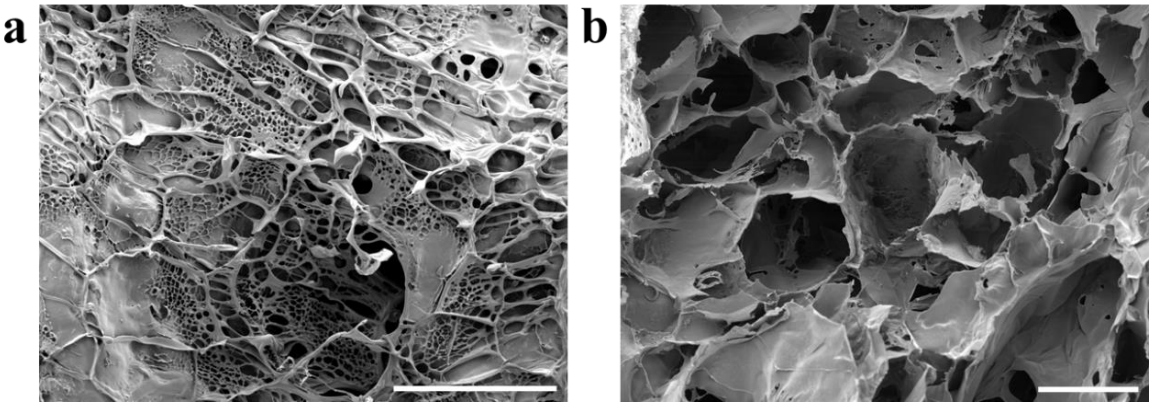

Figure 5.8 - CAF hydrogel porosity. **a** Outer porosity. **b** Inner porosity. Scale bars represent 200 µm.

5.4 Biological assays

5.4.1 *Cell proliferation and viability*

To obtain the proliferation along the days, PicoGreen was used. This assay allowed to determine the number of cells and existent DNA amount in CAF hydrogels at three different time-points (days 0, 7, and 14). To obtain these parameters, a standard curve for cell number (Figure 5.9a) and for DNA amount (Figure 5.9b) were acquired. Linearity is observable with high value of R^2.

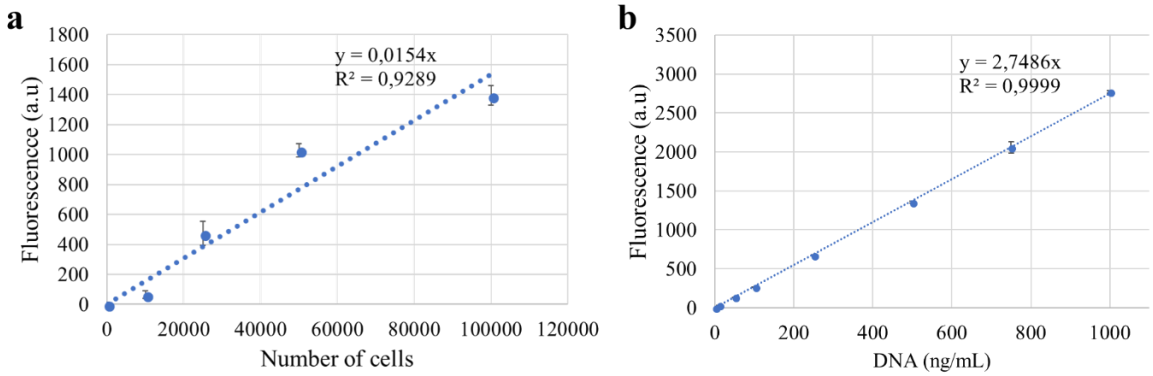

Figure 5.9 – Standard curves. **a** Cell number; **b** DNA amount.

Cell proliferation along the days is shown in Figure 5.10a. An average of $(0.611\pm0.036)x10^6$ cells was obtained for low density cell hydrogels on day 0. On the same day, high density constructs presented $(5.22\pm1.30)x10^6$ cells per sample, which represents, approximately, 9-times more cells than what was obtained for the $4x10^6$ cells/mL specimens. By day 7 a cell reduction on the high-density hydrogels and a cell increment on the $4x10^6$ cells/mL hydrogels, lead to similar cell numbers on both hydrogel types – roughly, $2.7x10^6$ cells per gel. At day 14, both hydrogel constructs had their cell proliferation increased, however the $40x10^6$ cells/mL samples presented higher proliferation rate, increasing its cell numbers to $(5.44\pm1.88)x10^6$ cells per gel. On the other hand, low cell density hydrogels presented a raise to $(3.32\pm1.04)x10^6$ cells per specimen. Using the two standard curves presented before (Figure 5.9), it was possible to calculate the DNA amount per sample, as observed in Figure 5.10b. By combining the information given by the two graphs, i.e. dividing the number cells per construct with the DNA amount for the same sample, the DNA amount per cell was determined - 5.6 pg/cell. Cell amount has also reflected on the macroscopic aspect of the hydrogels,

presenting more opaque hydrogels for the high cell density ones and more transparent specimens for the low cell density samples (Figure 5.11).

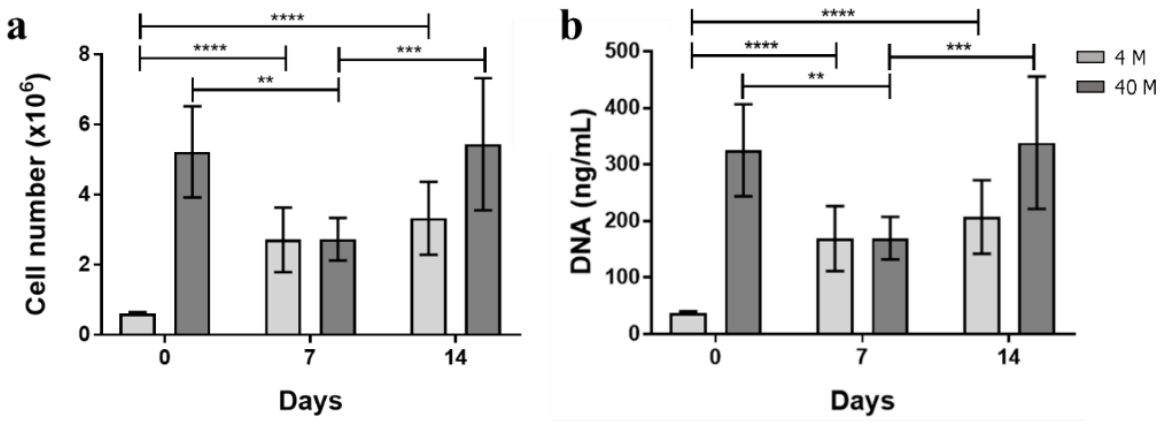

Figure 5.10 – **a** Cell number and **b** DNA amount present in CAF gels with $4x10^6$ and $40x10^6$ cells/mL after incubation during 0, 7 and 14 days in osteogenic medium. *, **, ***, and **** indicate significant difference between groups at the levels $p < 0.05$, $p < 0.01$, $p < 0.001$, and $p < 0.0001$, respectively. Error bars represent the standard deviation ($n = 3$).

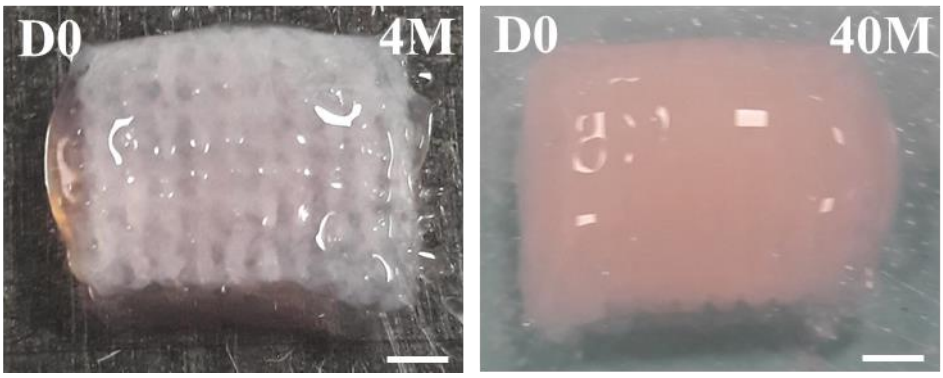

Figure 5.11 – Macroscopic look for freshly printed CAF hydrogels – low cell density (left) and high cell density (right). Scale bar represents 2 mm.

To qualitatively characterise the cells in terms of viability, Live/Dead assay was carried (Figure 5.12). A negligible number of dead cells (red) is possible to be observed in the low cell density hydrogels. Although exhibiting higher cell density, $40x10^6$ cells/mL samples presented a low dead cell number, when directly compared to the high number of live cells (green) presented.

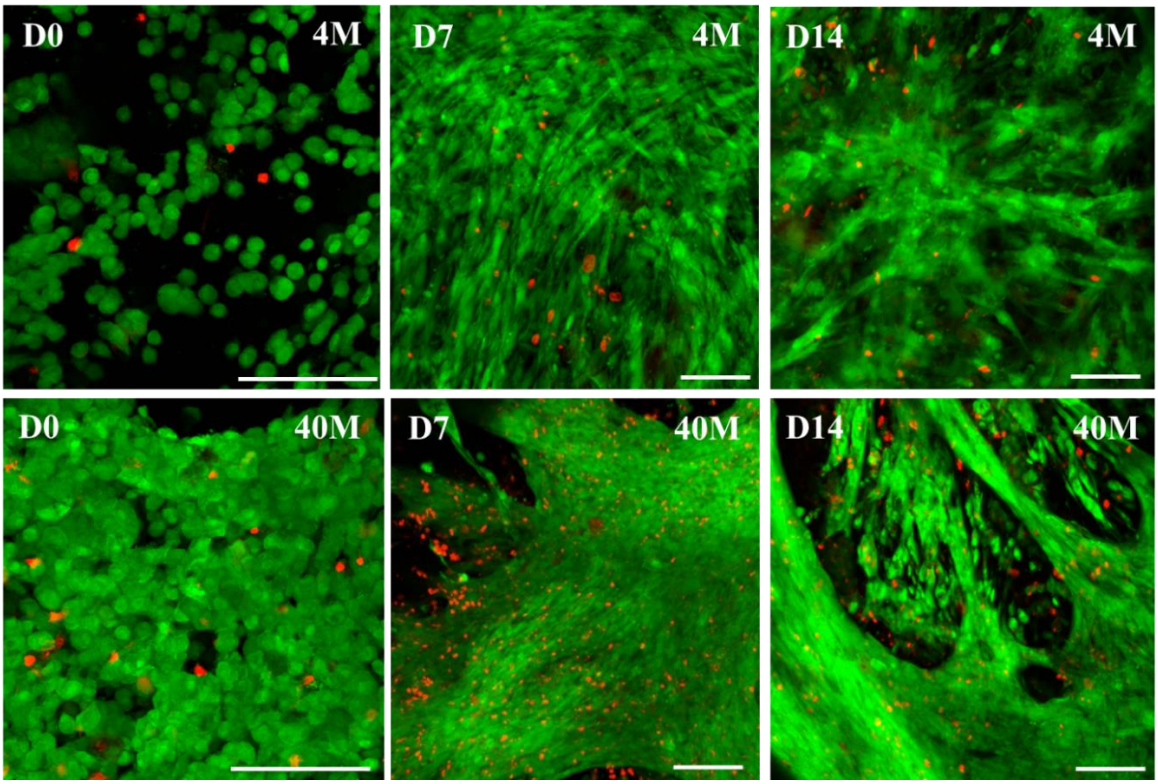

Figure 5.12 - Live/Dead assay. Cell viability of MSCs after printing, and 7 and 14 days of incubation in osteogenic medium (live cells are represented in green and dead in red). Scale bar represents 200 µm.

5.4.2 *Cell morphology*

Cell morphology and its organisation on hydrogels were studied using confocal microscopy and SEM. On day 0, random cell distribution was observed in Figure 5.13. Here, a relevant higher number of cells per unit of area is detected on the high cell density hydrogels, when compared to the $4x10^6$ cells/mL samples. The same cells are possible to be observed in Figure 5.14, but now in a 2D image. It is possible to note that day 0 present freshly printed cells for both low (Figure 5.14a) and high (Figure 5.14b) cell densities. Along the experiment, for the $4x10^6$ cells/mL structures, it is evidenced that the random cell alignment gives way to a more organised morphology – cell alignment starts to be more notorious. This is easily detected on the high-density gels, where higher orientation and contact between cells is already observable on day 7, and the degree of this organization clearly increases by day 14, as it is represented by the development of clear tissue structures due to cell migration and interaction.

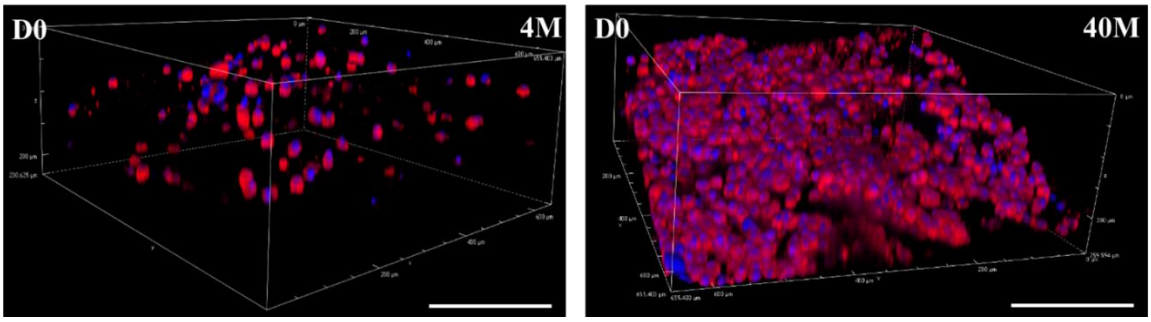

Figure 5.13 - Confocal microscopy volume stack showing cell distribution in CAF gels with different cell number. Scale bar represents 200 µm

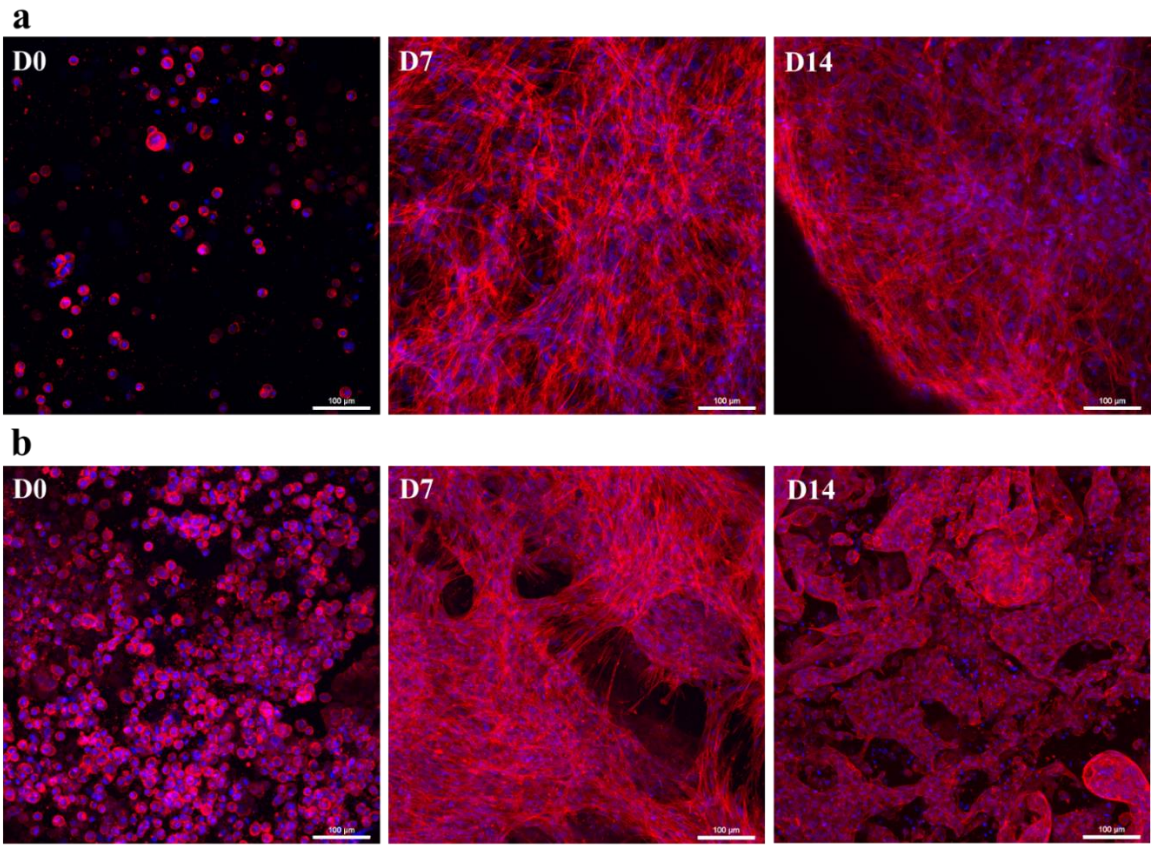

Figure 5.14 - Cell and tissue morphology after incubation during 0, 7 and 14 days in osteogenic medium by confocal microscopy. **a** shows $4x10^6$ cells/mL loaded gels with an increase on cell organization along the incubation days. **b** For $40x10^6$ cells/mL loaded gels, cell density seems to favour cell migration, organisation and highly-defined tissue formation (Red – F-Actin; Blue – Nucleus). Scale bars represent 100 µm.

SEM data revealed information consistent with what was obtained previously (Figure 5.15). For the low cell density hydrogels (Figure 5.15a), cellular organisation was noted

to increase along the days, culminating with high cell alignment by day 14. The $40x10^6$ cells/mL samples (Figure 5.15b) showed densely populated hydrogels by day 0, that allowed the formation of tissue structures with no hydrogel support by day 14.

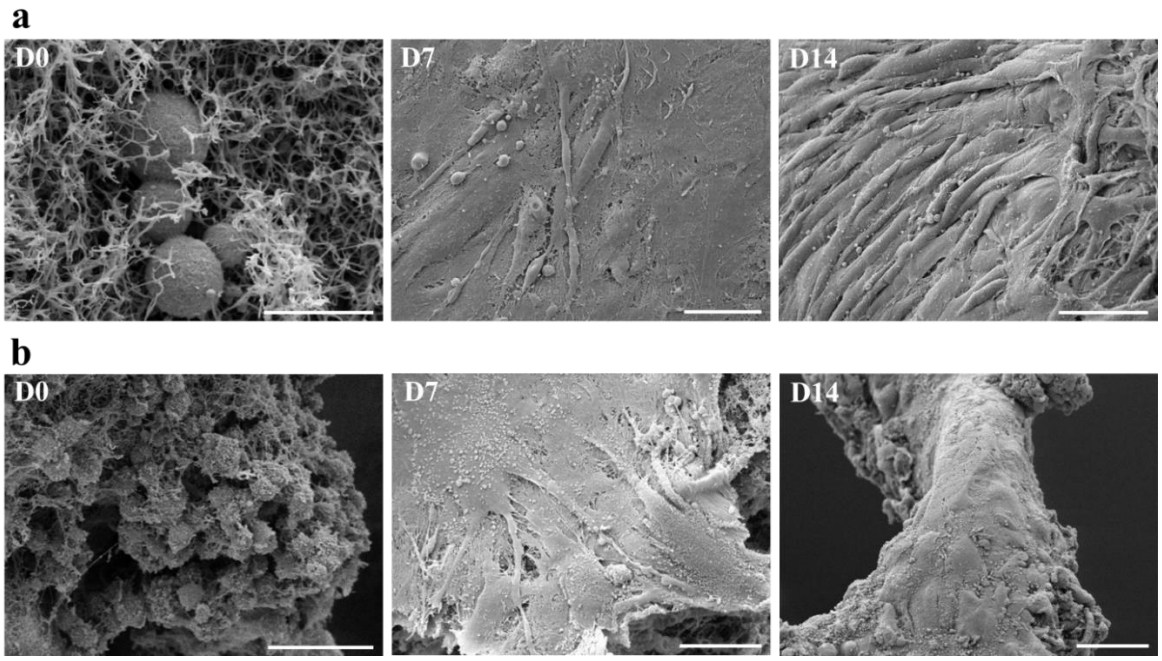

Figure 5.15 – Cell and tissue morphology by SEM. **a** Low cell density hydrogels. Scale bars represent 10, 20, and 50 µm, respectively. **b** High cell density hydrogels. Scale bars represent 50, 20, and 50 µm, respectively.

Additionally, this technique was used to explore the cell surface to understand how cell density influenced the calcium deposition. By observing Figure 5.16, it is noted that cells in low cell density hydrogels (Figure 5.16a) produce less calcium phosphates, when compared to the cells loaded in $40x10^6$ cells/mL hydrogels (5.16b). This is evidenced by day 7, where almost no calcium deposition is detected on $4x10^6$ cells/mL hydrogels. On the other hand, on the same day, cells loaded in high cell density samples already present a considerable amount of calcium deposition. On both cell densities, calcium deposition greatly increased by day 14, with particular incidence on the high cell density hydrogels that present cells trapped below high amounts of calcium phosphates.

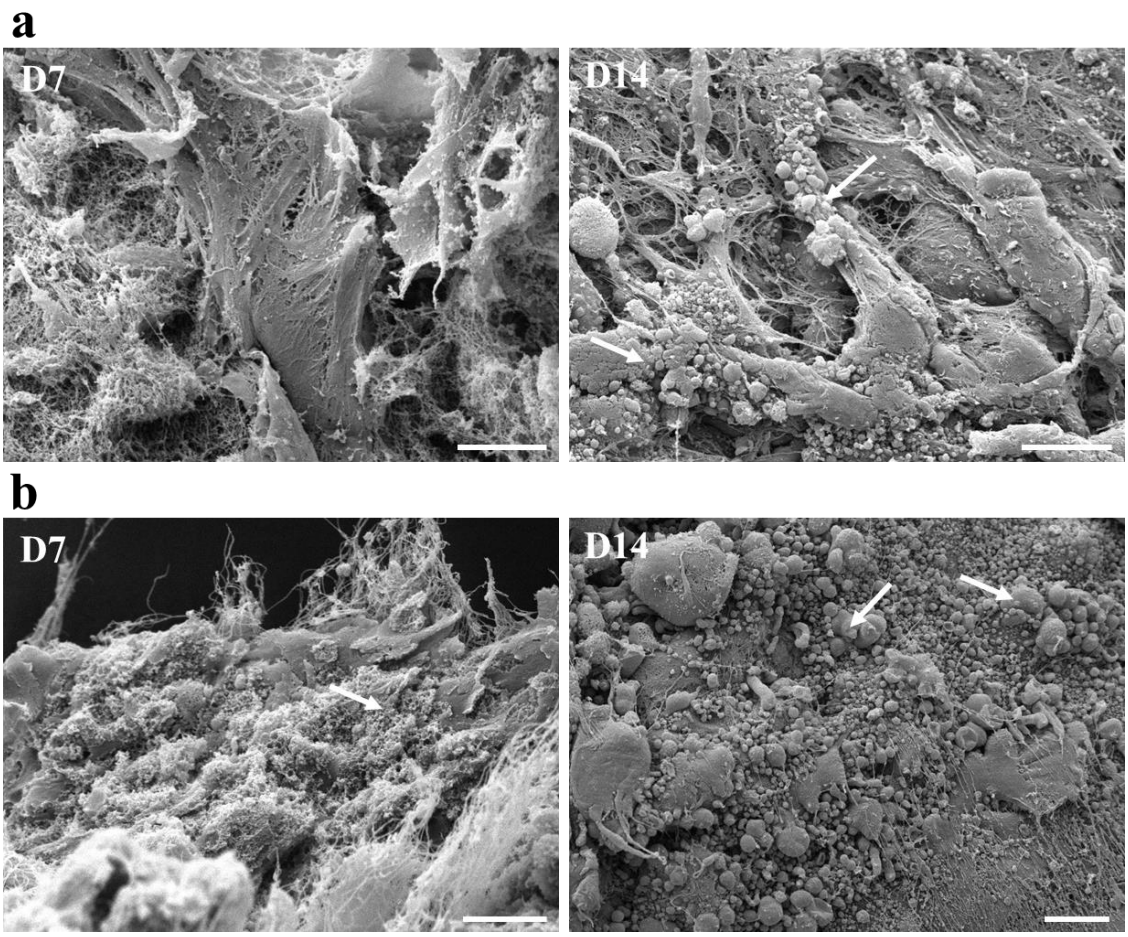

Figure 5.16 - Calcium deposition after incubation during 7 and 14 days in osteogenic medium by scanning electron microscopy. **a** and **b** show the calcium deposition (blank arrows) on low and high cell density hydrogels, respectively. A faster and increased deposition is possible to be verified on $40x10^6$ cells/mL hydrogels. Scale bars represent 10 µm.

Finally, SEM data also enlightened on MSC differentiation into osteoblasts (Figure 5.17). By day 7, low cell density hydrogels (Figure 5.17a) presented spread cells, a typical MSC morphology. However, in the same day, cuboidal cells, which are associated to osteoblasts, were already observed on $40x10^6$ cells/mL hydrogels (Figure 5.17b). By day 14, both hydrogel types presented osteoblastic cells.

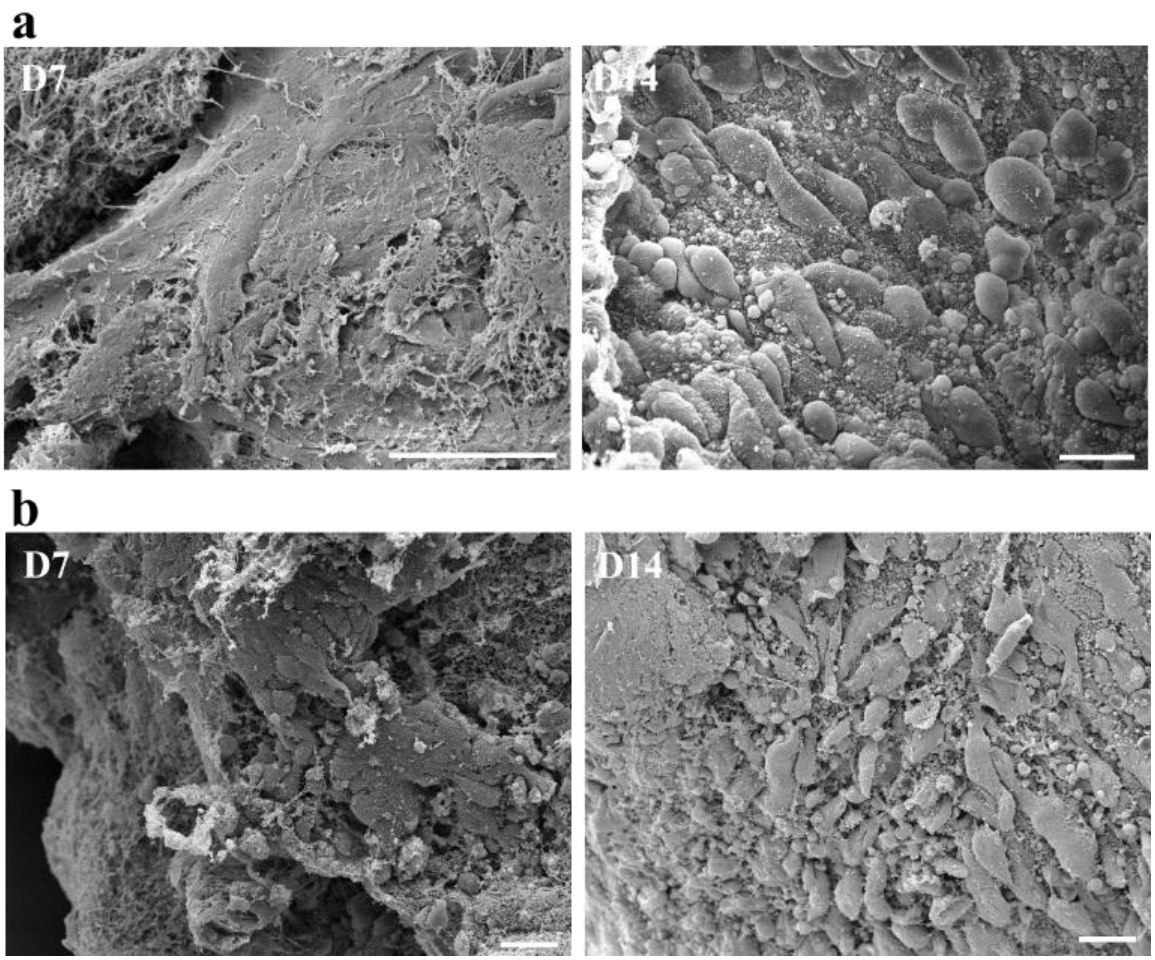

Figure 5.17 - Cell morphology changes after incubation during 7 and 14 days in osteogenic medium by scanning electron microscopy. **a** shows low cell density hydrogels and **b** exhibits high cell density hydrogels. Scale bars represent 20 µm (c and d).

5.4.3 *Cell differentiation*

Apart from the osteogenic route using hTERT MSCs, to test the hydrogel suitability on differentiation, trilineage differentiation of primary human MSCs was carried (Figure 5.18). After 30 days of incubation in basal MSC medium, MSCs presented to be widely spread and elongated following the same orientation (Figure 5.18a). Osteoblasts started forming nodular aggregations after 16 days in osteogenic differentiation (Figure 5.18b). After 16 days in chondrogenic medium, cells presented typical chondrocyte elongation and a polygonal shape (Figure 5.18c). Finally, fat deposits are observed after 16 days of incubation in adipogenic medium, which is a clear sign of adipocyte differentiation (Figure 5.18d).

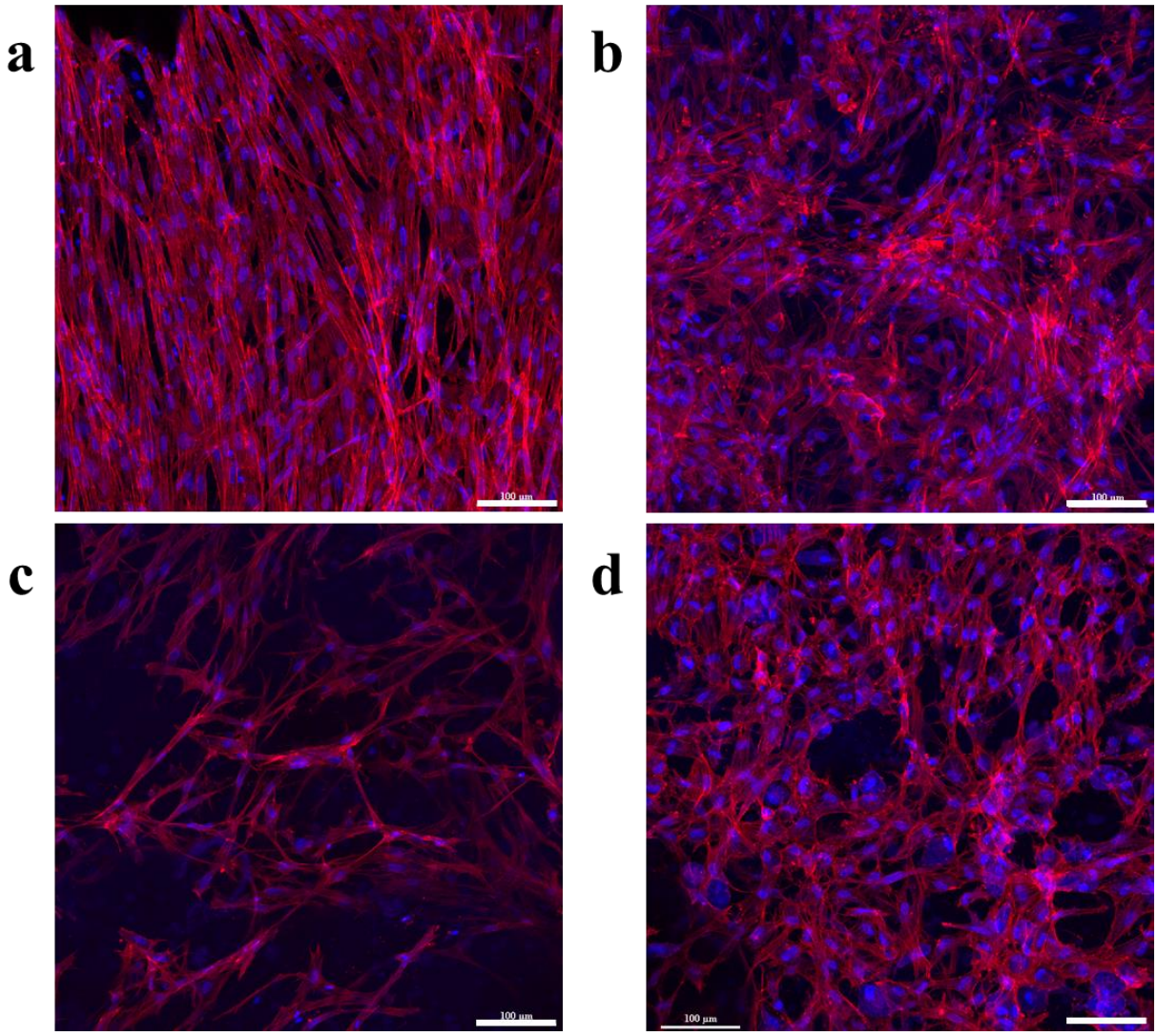

Figure 5.18 – Trilineage differentiation of primary human MSCs after 30 days in CAF hydrogels. **a** MSCs, **b** osteoblasts, **c** chondrocytes and **d** adipocytes. The nucleus is represented in blue (DAPI) and f-actin exhibited in red (phalloidin). Scale bars represent 100µm.

5.4.4 *Alkaline Phosphatase*

Alkaline Phosphatase was assessed to determine how cell density influenced its expression (Figure 5.19). ALP is an important marker on osteogenic differentiation, being crucial on the first steps of osteogenesis. The highest activity was observed by day 0, presenting no significant difference between the high and low cell density hydrogels. On the other time-points, day 7 and day 14, it was verified that the ALP value has decreased two to three-fold,

achieving similar concentrations of PnPP per cell in both samples. However, further reduction from day 7 to day 14 was observed on high cell density hydrogels.

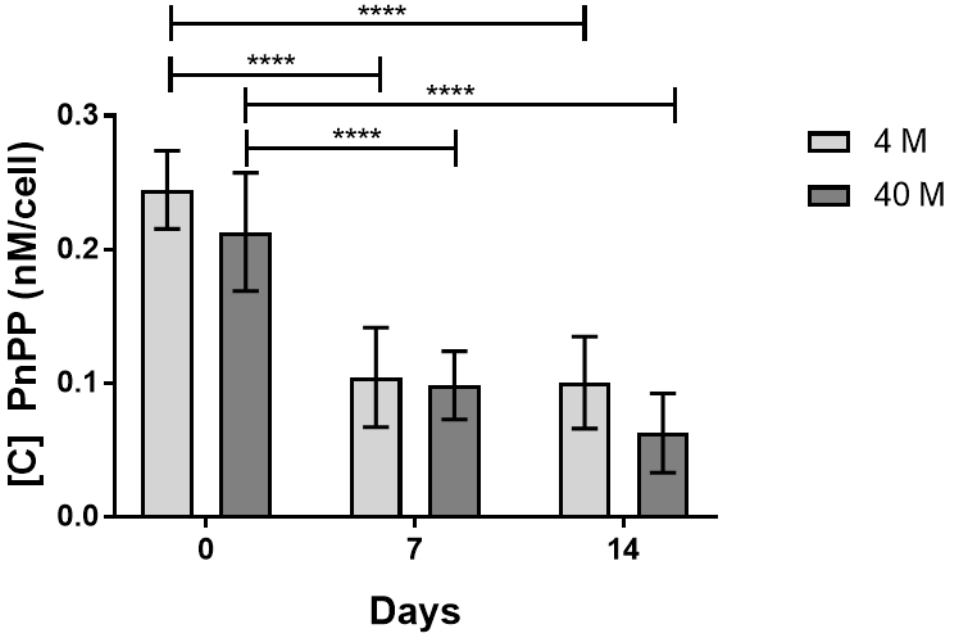

Figure 5.19 - PnPP concentration per cell obtained from ALP assay after incubation during 0, 7 and 14 days in osteogenic medium. *, **, ***, and **** indicate significant difference between groups at the levels $p < 0.05$, $p < 0.01$, $p < 0.001$, and $p < 0.0001$, respectively. Error bars represent the standard deviation (n = 3).

5.4.5 *Gene expression*

To further characterise the effect of different cell density hydrogels in cell differentiation and tissue formation, samples were analysed using PCR arrays for osteogenic specific genes and compared some of the most important genes for osteogenic differentiation.

Before PCR, the extracted RNA was quantified in table 5.2.

Table 5.2 – RNA quantification after extraction.

Day	Sample	RNA concentration (ng/µl)
0	$4x10^6$ cells/mL	35.6
	$40x10^6$ cells/mL	688.3
14	$4x10^6$ cells/mL	62.9
	$40x10^6$ cells/mL	93.8

Figure 5.20 exhibits the number of genes that were upregulated and down regulated when comparing low cell density hydrogels on day 14 with day 0 (Figure 5.20a), high cell density hydrogels on day 14 with day 0 (Figure 5.20b) and high cell density hydrogels with low density hydrogels by day 14. At day 14, lower cell density hydrogels presented encapsulated cells that overexpressed 48 genes (which 24 genes for skeletal development and 7 for bone mineral metabolism), double the number of downregulated genes (a total of 24, where 11 genes correspond to skeletal development and 2 for bone mineral metabolism), when comparing with day 0. In contrast, hydrogels containing high cell densities ($40x10^6$ cells/mL) evidenced an upregulation on 67 genes (with 36 genes for skeletal development and 11 for bone mineral metabolism), when compared to the under expression of 22 genes (which 9 genes for skeletal development and 2 for bone mineral metabolism) at day 14 to day 0 (Figure 5.20b). Comparing both cell densities on day 14, it was noted that high cell density hydrogels presented 39 overexpressed genes (with 19 genes for skeletal development and 6 for bone mineral metabolism) and 29 down-regulated genes (with 12 genes for skeletal development and 4 for bone mineral metabolism). 5 different growth factors were also overexpressed in $40x10^6$ cells/mL hydrogels by day 14.

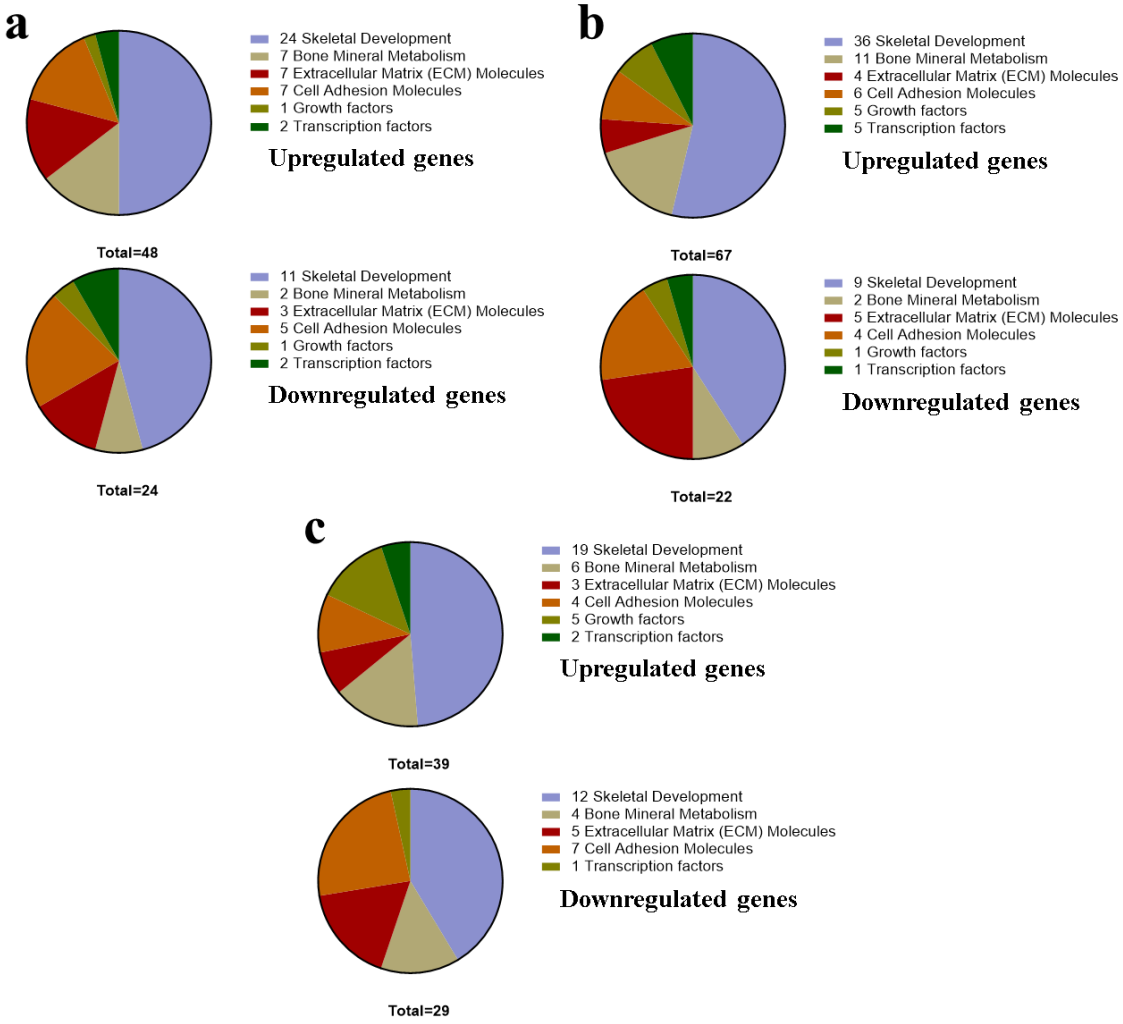

Figure 5.20 – Up and down regulated genes on different comparison between hydrogels. **a** represents the comparison between low cell density hydrogel on day 14 against day 0; **b** shows the comparison between high cell density hydrogel on day 14 against day 0; **c** exhibits the comparison between high cell density hydrogel at day 14 against low cell density hydrogel at day 14.

Table 5.3 shows the expression of the different genes for the comparison between low cell density hydrogel on day 14 against day 0, the comparison between high cell density hydrogel on day 14 against day 0, and, finally, the comparison between high cell density hydrogel at day 14 against low cell density hydrogel at day 14, respectively. On the other hand, Figure 5.21 shows the expression of the most important osteogenic genes. Specifically:

- For the comparison between low cell density hydrogel on day 14 against day 0, most genes presented mild downregulation or overexpression. However, BMP2 presented a 7.22-fold overexpression, COL14A1 exhibited a 5.74-fold upregulation, COL15A1 gene showed an underexpression of 6.77-fold, COL1A1 demonstrated a downregulation of 5.17-fold, COMP exhibited a 12.21-fold overexpression, FGF1 was downregulated by 5.02-fold, MMP9 showed an upregulation of 10.97-fold and PHEX presented a 7.69-fold overexpression. For key osteogenic genes (Figure 5.21a), RUNX2 (more than 2-fold) or SP7 (1.5-fold exchange) were overexpressed, while certain genes such as BMP-2, 3, and 7 remained the same. An underregulation was observed specifically on ALP (2.57-fold) and SPP1 (3.52-fold). BGLAP presented similar expression in day 0 and day 14.
- High cell density hydrogel at day 14 presented several highly overexpressed genes when compared to the same hydrogel at day 0, such as, CSF2 (36.60-fold), CSF3 (1382.25-fold), FLT1 (103.15-fold), MMP9 (2052.25-fold), MMP10 (1958.01) or NOG (38.82). On the other hand, some genes presented to be fairly downregulated, such as COL1A1 (12.54-fold), COL1A2 (8.13-fold), FGF1 (9.01-fold) or SMAD3 (-8.67). For key osteogenic genes showed overexpression on RUNX2 (over 10-fold), SPP1 (higher than 7-fold) and different BMPs, with a particularly high overexpression of BMP-2 and -6 with over 300 and 250-fold, respectively (Fig. 6.21b). On the other hand, ALP (3.81-fold) was underexpressed. BGLAP and SP7 were observed to be similar between day 0 and 14.
- By comparing high cell density to low cell density hydrogel at day 14, it was observed that gene expression was completely different, presenting highly overexpressed genes, such as, CSF2 (55.50-fold), CSF3 (2711.17-fold), FLT1 (73.82-fold), MMP9 (131.99-fold) and MMP10 (1401.17-fold). For key osteogenic genes, it was noted that RUNX2 (over 2.5-fold), SPP1 (nearly 15-fold) and BMPs -2 (45-fold), -3 (2-fold), -6 (nearly 60-fold) and -7 (4-fold) were upregulated on the $40x10^6$ cells/mL hydrogels (Fig. 7e). Contrarily, SP7 (1.49-fold) and ALP (1.88-fold) presented underexpression. BGLAP expression exhibited to be similar in both conditions (1.08-fold).

Table 5.3 – Gene expression for osteogenic pathway PCR array. Black, red and blue represent, respectively, the comparison between low cell density hydrogel on day 14 against day 0, the comparison between high cell density hydrogel on day 14 against day 0, and, the comparison between high and low cell density hydrogel at day 14.

ACVR1	**AHSG**	**ALPL**	**ANXA5**	**BGLAP**	**BGN**	**BMP1**	**BMP2**	**BMP3**	**BMP4**	**BMP5**	**BMP6**
1.59	1.64	-2.57	-1.86	-1.14	-1.19	1.09	7.22	2.78	-1.45	1.64	3.09
2.62	1.27	-3.81	-1.03	-1.01	-1.16	1.96	301.69	4.76	-4.23	1.27	251.61
1.35	-1.10	-1.88	1.80	1.08	1.12	1.94	45.67	2.01	-2.71	-1.10	58.21
BMP7	**BMPR1A**	**BMPR1B**	**BMPR2**	**CALCR**	**CD36**	**CDH11**	**CHRD**	**COL10A1**	**COL14A1**	**COL15A1**	**COL1A1**
1.64	2.04	1.89	1.85	1.64	3.41	1.02	1.64	2.00	5.74	-6.77	-5.17
5.68	2.08	5.00	2.73	1.27	-2.26	-1.39	1.27	2.78	-2.94	-1.74	-12.54
4.06	1.01	1.52	1.22	-1.10	-10.45	-2.05	-1.10	3.97	-19.93	6.70	-2.19
COL1A2	**COL2A1**	**COL3A1**	**COL5A1**	**COMP**	**CSF1**	**CSF2**	**CSF3**	**CTSK**	**DLX5**	**EGF**	**EGFR**
-3.20	1.64	-1.77	-2.38	12.21	4.12	1.64	-1.62	2.27	-2.63	-1.90	-1.22
-8.13	1.27	-1.97	-1.97	1.27	1.37	36.60	1382.25	1.27	-3.80	1.21	1.19
-2.40	-1.10	-1.00	1.44	-8.16	-3.80	55.50	2711.17	-2.79	-2.52	2.03	1.02
FGF1	**FGF2**	**FGFR1**	**FGFR2**	**FLT1**	**FN1**	**GDF10**	**GLI1**	**ICAM1**	**IGF1**	**IGF1R**	**IGF2**
-5.02	1.42	1.15	1.45	1.64	1.62	1.64	-2.90	-1.02	1.80	3.18	1.64
-9.01	6.33	2.53	-1.87	103.15	1.54	1.27	1.58	4.00	1.27	3.65	2.55
-1.76	4.90	1.63	1.34	73.82	-1.18	-1.10	1.17	4.11	-1.20	1.05	1.83
IHH	**ITGA1**	**ITGA2**	**ITGA3**	**ITGAM**	**ITGB1**	**MMP10**	**MMP2**	**MMP8**	**MMP9**	**NFKB1**	**NOG**
1.64	2.22	1.81	-3.43	1.64	-1.83	1.64	2.45	1.64	10.97	1.39	5.16
1.27	5.27	12.98	-1.72	1.27	1.19	1958.01	5.45	1.27	2052.25	2.92	38.82
-1.10	1.82	6.89	1.81	-1.10	1.83	1401.17	1.83	-1.10	131.99	1.87	7.50
PDGFA	**PHEX**	**RUNX2**	**SERPINH1**	**SMAD1**	**SMAD2**	**SMAD3**	**SMAD4**	**SMAD5**	**SOX9**	**SP7**	**SPP1**
-1.68	7.69	2.44	-2.36	1.05	1.54	-2.63	2.32	1.98	-3.10	1.62	-3.52
-1.98	-1.18	11.01	-2.73	1.05	2.11	-8.67	3.55	1.77	-1.17	1.08	7.18
-1.04	-8.07	3.01	1.03	-1.12	1.29	-2.51	1.55	-1.10	1.82	-1.49	14.25
TGFB1	**TGFB2**	**TGFB3**	**TGFBR1**	**TGFBR2**	**TNF**	**TNFSF11**	**TWIST1**	**VCAM1**	**VDR**	**VEGFA**	**VEGFB**
-1.57	2.25	1.02	1.67	2.05	1.64	6.66	3.93	3.07	3.72	2.27	1.04
1.01	2.89	1.74	3.70	1.54	2.67	7.33	10.19	-4.47	4.23	5.72	1.49
1.69	1.00	1.59	2.33	-1.80	1.91	2.61	2.90	-14.32	1.30	2.77	-1.13

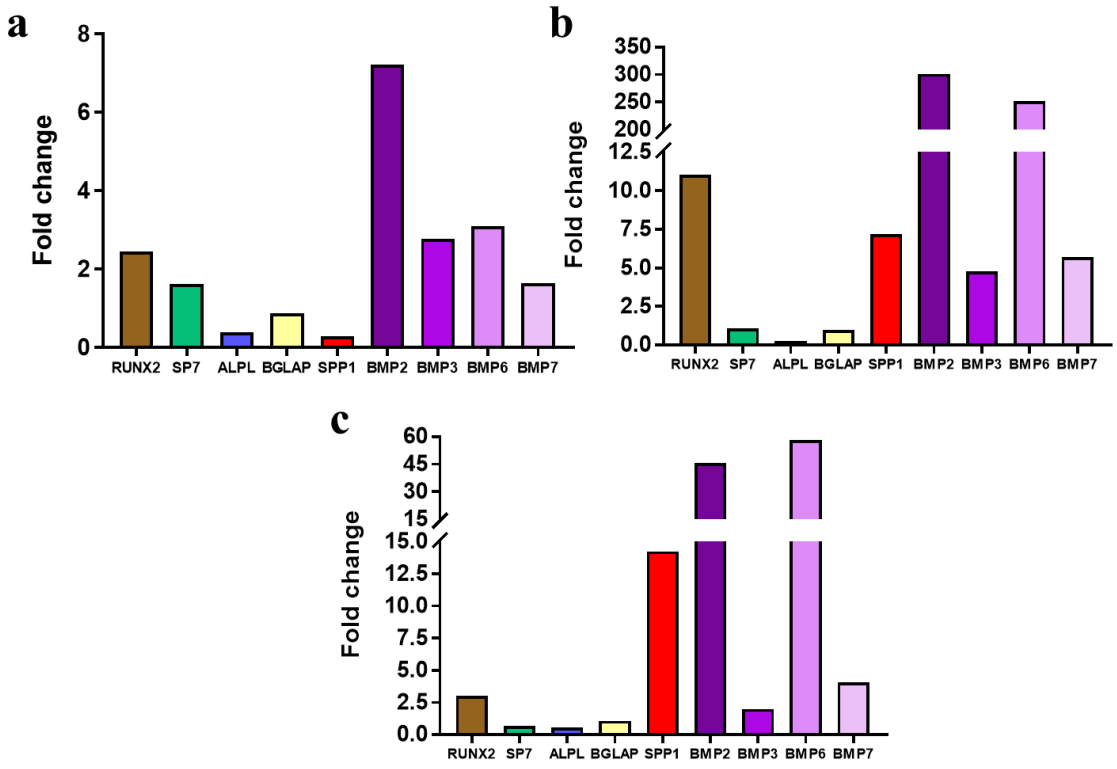

Figure 5.21 - Fold change of some of the most important osteogenic genes, comparing 4M d14 to 4M d0, 40M d14 to 40M d0, and 40M d14 to 4M d14, respectively. At day 14, $40x10^6$ cells/mL loaded gels present gene expression that reflects mature osteoblast formation, contrarily to $4x10^6$ cells/mL loaded gels that show pre-to-early osteoblast related gene expression.

5.5 Discussion of the chapter

The ReJI system is the first drop-on-demand bioprinting system that can deposit cell-laden hydrogels with a high cell density. The limitation of the ReJI process is that the system relies on rapid crosslinking to create gel droplets. However, this contrasts with other bioprinting processes, where crosslinking requires an additional process either before or after the deposition step (Gudapati *et al.*, 2016; Ozbolat and Hospodiuk, 2016). Table 5.4 compares the developed in-house technique to other common bioprinting techniques, to demonstrate that the system uniquely offers high cell density, with high cell viability, within a viscous gel, at high volume deposition rates. Additionally, ReJI does not present reliability and repeatability issues, which are commonly verified in inkjet bioprinting due

to cell agglomeration (Murphy and Atala, 2014; Bishop *et al.*, 2017). Contrarily to inkjet bioprinting, with ReJI there is no the limitation in terms of mimicking natural environments or tissue complexity due to the instant crosslinking of biomimetic hydrogels and high-cell density bio-inks. Although allowing high cell densities, when comparing to extrusion-based and laser-assisted bioprinting, it is clearly that ReJI is faster, produces high cell survival and grants high volume rate.

5.5.1 *CAF hydrogel properties*

To obtain the developed microtissues, 14 days of incubation in osteogenic medium at 37°C and 5% CO_2 was necessary. The 30% hydrogel mass loss may be connected to poorly crosslinked branches inside the CAF gel structure being washed off during the incubation period. The 3 mm thick CAF hydrogel was able to quickly absorb dissolved molecules with saturation in less than 1 hour. This guarantees stability of cells during their development. The porosity observed in the gel is essential for building up microtissues based on high cell densities, as cell migration will be necessary for tissue development (Yamada and Cukierman, 2007; Ma *et al.*, 2010; Campbell *et al.*, 2017). This porous network is preserved over a 14-day period, making this hydrogel ideal for tissue development applications.

5.5.2 *Cell viability and proliferation on bioprinted cell-laden hydrogels*

Cells survive the jetting and impingement processes. This is explained by the low viscosity of both cell carrier ink (crosslinking solution) and gel precursor (Derakhshanfar *et al.*, 2018). When leaving the microvalve nozzle, cells suffer little shear stress due to the low viscosity of each ink. Additionally, when mixing, the fast reaction instantly encapsulates the cells, giving them protection when droplet reaches the substrate, but also assuring elasticity (that fibrin enriched hydrogels are recognized to minimize stress on impact (Janmey *et al.*, 2009; Piechocka *et al.*, 2010)). One and two weeks after printing, cell viability is maintained, as fibrin and collagen are biocompatible natural materials that are widely used as scaffold materials due to their properties, including extracellular matrix promotion (Hong and Stegemann, 2008; Chan *et al.*, 2016). Precise structures were printed using two different cell density inks, producing hydrogels with an average of $6x10^5$ and $5x10^6$ cells on the low and high cell density hydrogels, respectively.

Cell detachment is considered as the main reason for cell number decrease on high cell density hydrogels on day 7. Contrarily, for the low cell density hydrogels, the underpopulation at day 0 resulted on a 5-fold cell number increase by day 7. Both hydrogels showed proliferation between days 7 and 14. High cell density hydrogels showed had a higher proliferation rate associated with cell migration and microtissue formation. The low cell density hydrogels did not increase to the same extent due to poorer cell-cell contact and, consequently, lower proliferation capability (Chan *et al.*, 2016). Microtissue development is dependent on several factors, including cell density, mechanical forces and the presence of extracellular matrix (Nelson and Chen, 2002; Griffith and Swartz, 2006; Legant *et al.*, 2009; A. S. Liu *et al.*, 2016). Here, we reinforce past studies, with special focus on the importance of high cell densities in 3D structures to obtain fast and developed microtissues by direct differentiation (Shu, 2015; Bishop *et al.*, 2017).

5.5.3 *Effect of cell density on differentiation process and microtissue formation*

Increased calcium deposition on the higher cell density hydrogels is assumed to be a result of a faster rate of MSC differentiation into osteoblasts. This was confirmed by the presence of cuboidal cells, a morphology which is associated with mature osteoblasts (Hwang *et al.*, 2008), already by day 7. ALP, an early osteogenic marker, supports this view. Increased ALP concentrations were produced at day 0, when compared to day 7 and 14, with the higher cell density hydrogels presenting the lowest concentration at day 14, as ALP levels are downregulated by the end of the osteogenesis (Liu *et al.*, 1997; Golub and Boesze-Battaglia, 2007).

Gene expression was also influenced by cell density. Typical pre-osteoblastic behaviour was observed on low cell density hydrogels due to the increased expression of RUNX2 and SP7 and reduced expression of BGLAP and SPP1 (Birmingham *et al.*, 2012). BMPs, intrinsically connected to bone formation, also increased expression.

Table 5.4 – Comparison between ReJI and other bioprinting techniques. Numbers are based on what is achievable for one deposition unit.

	ReJI bioprinting	Inkjet bioprinting	Single microvalve bioprinting	Extrusion bioprinting	Laser-assisted bioprinting	Ref.
Viscosity of Material Deposited on the Substrate	1–70 mPa/s	3–30 mPa/s	1–70 mPa/s	30 mPa/s to >$6x10^7$ mPa/s	1–300 mPa/s	(Murphy and Atala, 2014; Donderwinkel *et al.*, 2017; Ng *et al.*, 2017)
Printing Speed	6 500 droplets/s	1 – 10 000 droplets/s	6 500 droplets/s	10 µm/s – 700 mm/s.	100 – 5000 droplets/s	(Guillotin *et al.*, 2010; Murphy and Atala, 2014; Bakhshinejad and D'souza, 2015; Gudapati *et al.*, 2016; Lee and Yeong, 2016; Ovsianikov, 2016; Ozbolat and Hospodiuk, 2016; Donderwinkel *et al.*, 2017; Gao *et al.*, 2017; Ozbolat, 2017)
Volume deposition rate	80 µL/s	160 µL/s	40 µL/s	3-15 µL/s	175 - 1800 nL/s	(Guillotin *et al.*, 2010; Gudapati *et al.*, 2016; Graham *et al.*, 2017; Koch *et al.*, 2017; Zhang, 2018)
Resolution	100-300 nL droplets	pL droplets	pL to nL droplets	5 µm to mm size deposited track	<pL droplets	(Murphy and Atala, 2014; Ozbolat, 2017)
Cell viability	>90%	>85%	>90%	40-80%	>95%	(Murphy and Atala, 2014; Ozbolat, 2017)
Crosslinking Process	In process	Post-printing	Post-printing	Pre-, post-printing	Post-printing	(Murphy and Atala, 2014; Lee and Yeong, 2016)
Cell density	$9x10^7$ cells/mL	Low, <$5x10^6$ cells/mL	High, 10^7/mL	High, cell spheroids	High, 10^8 cells/mL	(Murphy and Atala, 2014; Donderwinkel *et al.*, 2017; Ozbolat, 2017)

This work has shown that cell density is crucial to the rate of functional bone microtissue formation. In cancer and in other diseases there is a clear commercial need for improved models for large scale screening, and microtissue models are considered to offer significant potential (Aubin and Triffitt, 2008; Xu, 2012). To date the scalability and reliability of microtissue models has been identified as limitations, with these issues closely related (Junaid *et al.*, 2017; Peng *et al.*, 2017). A lack of scalability means that limited replicates of any given experiment can be made, and a lack of replicates makes it difficult to understand variation in statistical terms. By reliably depositing cells and materials at rates which allow for thousands of micro-tissue precursors to be generated per hour the ReJI technology has potential to address a key problem in terms of micro-tissue model development and exploitation.

Chapter 6. General discussion

6.1 Summary

Data presented in this thesis identified two new bio-ink strategies for bioprinting. The first methodology enabled the development of a bio-ink containing cells with a temporary single cell coating. This allowed increased inkjet printing reliability when printing viable single cells. This thesis also reported on the optimisation of a pre-designed hydrogel, CAF, and a new bioprinting system, ReJI. The combination of these two tools made possible the fabrication of high cell density cell-laden hydrogels.

Chapter 4 describes the concept behind bio-inks that include single coated cells and its validation. PLL, a synthetic polycation, was applied as cell coater and different concentrations were used to understand its effect on cells. Results demonstrated that the lowest concentration tested, 10 μg/mL, exhibited higher cell viability. At higher concentrations a raise on cell death rate was noted majorly due to necrosis. The coating was observed to be temporary, with cells having the ability to uptake and metabolise the PLL within two days. Cell aggregation was shown to be reduced due to the electrostatic repulsion granted by the PLL coating. This way, nozzle blockage, which is commonly responsible for the low reliability of inkjet bioprinting, was avoided during printing for one hour. This not only increased the reliability of the process, but also allowed stable printing for periods up to 60 minutes. Additionally, single cell printing of viable cells was obtained by using this strategy.

Chapter 5 demonstrates the capabilities of an in-house developed printing strategy, ReJI. By adapting and optimising a collagen, alginate and fibrin hydrogel towards bio-ink, fast and repeatable hydrogels were fabricated. These presented porous networks and the ability to rapidly absorb solutions. Cell-laden hydrogels presented high viability and cell density was determinant on microtissue formation by influencing cell proliferation, migration and differentiation. High cell density hydrogels presented advanced osteogenic differentiation, showing osteoblastic behaviour, when compared to the pre-osteoblastic behaviour showed by low cell density hydrogels.

6.2 Novelty

As introduced in the literature review, inkjet bioprinting presents limitations regarding the reliability of the process (Murphy and Atala, 2014; Gudapati *et al.*, 2016; Bishop *et al.*, 2017). Bio-inks used within this technology must have low viscosity, generally in a liquid state, such as cell suspensions in medium. As consequence, cell sedimentation and aggregation cause blockages on the very small nozzles. Here, by using a polycationic speckled coating, electrical repulsion is able to significantly delay nozzle blockages. Additionally, the absence of nozzle blockage allows stable printing for periods up to 60 minutes and allowing to achieve single cell printing. This represents a new strategy for inkjet bioprinting. Furthermore, the temporary coating itself represents also a novelty, constituting a new coating procedure that can be applied in other bioprocessing techniques.

High cell density bio-inks are essential to produce microtissues. However, drop-on-demand bioprinting techniques are limited by bio-inks loaded with a maximum of 2-5x10^6 cells per mL, a value that does not represent the physiological cell densities of human tissues. The combination between ReJI and CAF bio-ink demonstrated to be a unique strategy to rapidly overcome this limitation. Additionally, this study reinforced the importance of cell density on microtissue development, showing that low cell density hydrogels had a much slower tissue maturation rate when compared to the high cell density hydrogels.

6.3 Inkjet bioprinting, its limitations and dependence on bio-ink development

The work presented in this study was performed using two different bioprinting techniques: inkjet bioprinting and an in-house microvalve-based bioprinting entitled ReJI. Although the technology behind these and other bioprinting strategies has been in constant development, there are still several limitations that do not allow further advances.

Inkjet bioprinting was initially adapted from commercial home/office inkjet printers (Kolesky *et al.*, 2014; Murphy and Atala, 2014). Despite having an auspicious beginning, the lack of development of the technology itself did not allow to obtain ground-breaking advances. The concept and process behind are still the same from 15 years ago, when

Boland and Wilson first reported the successful printing of viable cells (Wilson and Boland, 2003). The only evolution observed is related to the bioprinters parts, which became a little more specialised. However, the shear and thermal stress that cells suffer during printing, the nozzle blockage due to cell sedimentation and aggregation and the need for fast crosslinking to confer mechanical structure to the printed droplets are the same problems from 15 years ago. There is a need for the development of custom reservoirs that allow cells to be constantly, but gently, agitated (Gudapati *et al.*, 2016). New jetting devices to minimise nozzle blockage are also essential. Most inkjet printers have tubbing that connect the reservoir to the inkjet printhead (Figure 6.1), which poses as recurrent cell aggregation area even with a slight bend. The use of anti-adherent materials or coatings would help on solutioning this issue.

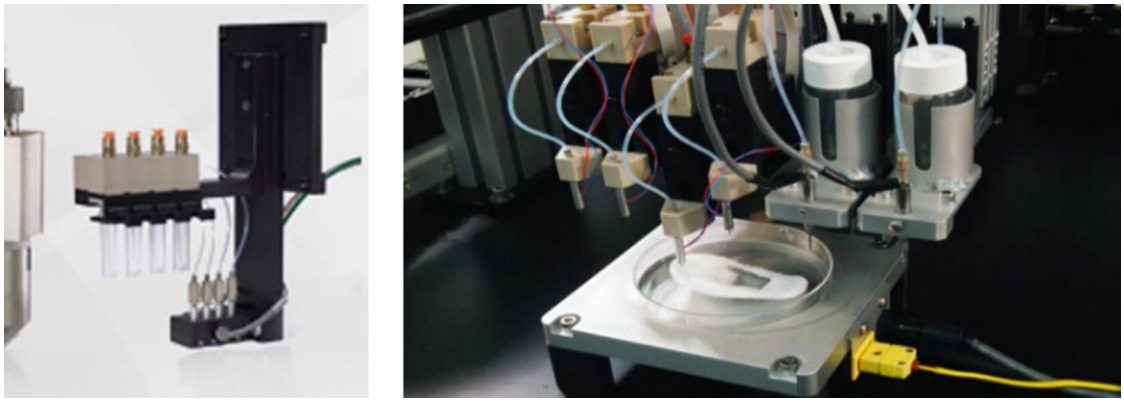

Figure 6.1 – Tubbing connection between reservoirs and inkjet nozzles.

To obtain solid structures is also a concern. Crosslinking mechanisms must be applied almost simultaneously with printing, otherwise, there is a risk of fast droplet drying due to the very small volume (Murphy and Atala, 2014; Iwanaga *et al.*, 2015). As reported before, another strategy would be to print directly into cellular medium or other cell-friendly solution, however, accuracy and resolution would be lost in the process since cells would float. With ReJI, these problems were taken in account during the system design. Nozzle blockage was avoided by combining the microvalve working principle, a constant pneumatic pressure and cells in a very low viscous solution. Additionally, the ReJI design allowed gel precursor and crosslinking solution droplets to meet in air that, once combined, immediately start the crosslinking process.

However, the inkjet bioprinting major dependence relies on bio-inks. These are the truly driving force of bioprinting, allowing or not, to release the full potential of the technology. To avoid nozzle blockage, most of the inkjet bioprinting studies use very low cell density inks, with an average of 2 x 10^6 cells/mL (Murphy and Atala, 2014). This does not represent the physiological cell density, affecting any experiment that aims to study tissue development. Hence, inkjet bioprinting is normally applied to *in vitro* experiments, such as cell-cell interaction studies or lower scale vascularisation and disease models (Cui *et al.*, 2012; Jang, 2017). Other strategy is to use very low viscous and shear thinning solutions, but these are very limited (Murphy and Atala, 2014; Gudapati *et al.*, 2016). Optimising bio-inks with so many constraints have been slowing inkjet printing outputs. This way, the use of surfactants, such as Pluronic or Ficoll-PM400, have been applied for some groups to originate neutrally buoyant cell suspensions (Chahal *et al.*, 2012; Ferris *et al.*, 2013). Although minimising cell aggregation and, consequently, resulting in reliable printing for longer periods, these additives are commonly toxic to cells (Jose *et al.*, 2016). Also, turning bio-inks into more complex systems by adding more substances is not ideal. It is important to understand the effect of surfactants or other compounds not only in terms of cell viability and functionality, but also during and after crosslinking.

The data reported in this thesis show that the use of the coated cells inhibit cell agglomeration and allow reliable cell printing for up to 60 minutes. Using minimal concentrations of a polycation, cells uptake and metabolise the polymer, resulting in few traces of PLL after 2 days. Additionally, cells start internalising the polymer immediately after cell attachment without causing any concern during this and other cell processes. However, even recurring to electrostatic repulsion, the use of this technique is still constraint to low cell densities (< 2x10^6 cells/mL), when using the optimised PLL concentration. Tests not reported in this thesis showed that only by increasing the PLL concentration up to 10-20 times more than the optimised concentration, the electrical repulsion would allow higher cell concentrations in the bio-ink – up to 30x10^6 cells/mL. Despite the effectivity of this increased PLL concentration on avoiding cell agglomeration, the impact on cell viability was highly significant, reducing cell viability to negligible values. The use of stronger but cell-friendly polycations would be important to understand if this kind of strategy could be improved.

6.4 Cell density and its relationship to microtissue development

The main aim of chapter 5 was to obtain high cell density hydrogels, via the optimisation of an in-house developed bioprinting technique, ReJI, and by adapting a collagen-alginate-fibrin hydrogel to the same bioprinting technology. The work developed showed that ReJI is the first drop-on-demand bioprinting system that can deposit cell-laden hydrogels with a high cell density. Cell density has been one of the major drawbacks of bioprinting, as it is essential on the development of tissues and, ultimately, organs (Murphy and Atala, 2014). The data generated in this chapter have clearly demonstrated that printed cell behaviour was distinct in hydrogels with a 10-fold difference in terms of cell concentration. Hydrogels printed with high cell densities showed a fast osteogenic differentiation, when compared to the low cell density ones. This resulted in an earlier and increased deposition of calcium, as well as, on the presence of cuboidal cell, typical osteoblastic phenotype. Additionally, the gene expression exhibited much higher overexpression of important osteogenic genes in the higher cell density hydrogels. This way, cells were shown to have clearly organised themselves in tissue structures.

The work reported here clearly supports prior studies that highlight the importance of cell density on tissue development. Cell density allows cells to be spatially closer to each other, which increase the cell-cell interaction between them. Cell-cell interaction has been reported to modulate basic cell processes, such as adhesion, differentiation, proliferation or migration (Ratcliffe and Niklason, 2002; G Duclos *et al.*, 2016). Groups have verified that high cell density cultures facilitated cell-cell interaction and this upregulated the proliferation rate and elastin expression of chondrocytes (Lee *et al.*, 1994). Furthermore, osteogenic activity has been reported to be affected by early cell density (Luo *et al.*, 2013). On the other hand, contact inhibition has been reported to have significant consequences on tissue formation and growth (Cheng *et al.*, 2006). In another spectrum, metastatic cancers are known for being “solitary” and able to grow with lack of cell-cell interaction (Sharif *et al.*, 2015). However, research teams observed that the vascular invasion is controlled by cell density. Finally, cell cycle dynamics have been noted to be affected by the lack of cell-cell interaction, which causes retarded tissue growth (Streichan *et al.*, 2014).

6.5 Drug discovery perspective on ReJI-produced high cell density hydrogels

Drug discovery comprises a multi-step model that starts with the identification of the probable beneficial molecule or compound, *in vitro* testing, followed by *in vivo* and human clinical trials (I-IV) (Kuhlmann, 1997; DiMasi *et al.*, 2003). *In vitro* assays are of capital importance as they must recapitulate the human environment to reliably assess the efficacy and toxicity of the new compound. For this, the industry still relies in 2D cell culture systems, which have been constantly reported to not be able to simulate the human environment (Edmondson *et al.*, 2014; Duval *et al.*, 2017). Lately, three-dimensional (3D) cell culture techniques, such as spheroids, organoids, organs-on-chip or scaffold-based cell cultures, have been developed and show the ability to emulate from natural cell-cell interactions to human organs in a much smaller scale (Di Maggio *et al.*, 2011; Huh *et al.*, 2011; Thoma *et al.*, 2014; Thakuri *et al.*, 2017; de Souza, 2018; Mosaad *et al.*, 2018). However, all the 3D cell culture systems present problems over reliability and repeatability, but also in terms of tissue complexity, which makes them not ideal for high-throughput applications (Friedrich *et al.*, 2007; Breslin and O'Driscoll, 2013; van Duinen *et al.*, 2015; Junaid *et al.*, 2017). The unique ReJI characteristics opens up new opportunities for drug development by producing fast and reliable tissue-like structures. Additionally, the lack of cell-cell interaction may inhibit the secretion of certain cytokines that are detrimental not only for tissue growth and maturation, but also necessary for the development of other cells in case of a multi-cellular constructs (Rørth, 2003; Cooper and Hausman, 2004; Lodish H *et al.*, 2007). These issues cause poor biomimicry that most of the times is not detected due to the lack of reliable 3D models to compare with.

Chapter 7. Conclusion and future work

7.1 Conclusion

The research reported in this thesis demonstrated new concepts and methodologies applicable to inkjet printing and fabrication of high density cell laden hydrogels.

7.1.1 *Single cell coating using poly-L-lysine and reliable inkjet cell printing*

The work developed in this chapter demonstrated that PLL allows for the development of an efficient and temporary single cell coating. The coating minimized cell aggregation via electrical repulsion due the positively charged polymer on the cell membrane. This effect was successfully applied to inkjet bioprinting, avoiding nozzle blockage, and the reliability and repeatability of the process was improved.

More specifically:

- The methodology developed allows high-efficiency and tightly fitting coating;
- Cell survival is dependent on PLL concentration. Increase on PLL concentration originates an increment on cell death rate;
- The optimised PLL concentration allows good cell survival and does not affect cell karyotype;
- The coating morphology is dependent on PLL concentration. Increasing PLL concentration leads to a more complete coating or even full encapsulation;
- Cells can ingest and metabolise low PLL concentrations. High concentrations cause cell death;
- Cells death is majorly caused by necrosis, which is related to the damage suffered due to PLL attachment;
- Cell behaviour with PLL coatings depends on the cell type;
- The optimised PLL coating reduced cell aggregation by 10 times, when comparing to non-coated cells;
- Cell proprieties affect inkjet cell printing reliability;
- Inkjet printing of coated cells demonstrated normal cell survival, attachment and phenotype.

7.1.2 *Reactive jet impingement technology for high cell density bioprinting*

The data present in chapter 5 indicated that ReJI system is the first drop-on-demand bioprinting system that can deposit cell-laden hydrogels with a high cell density. Cell density showed to be a crucial factor on the development of microtissues by increasing cell differentiation speed, as well as by improving cell-cell interaction. The optimised CAF hydrogel supported cell viability, proliferation, migration and differentiation.

In particular:

- ReJI offers high cell density, with high cell viability, within a viscous gel, at high volume deposition rates. This bioprinting technique allows rapid printing of precise structures;
- CAF hydrogels are suitable for long-term incubation by losing only about 30% of its mass during any incubation period studied;
- The fabricated CAF hydrogels have weak mechanical properties, however these show high uptake capability, which is essential for cell maintenance;
- CAF hydrogels show porous structures which supports cell migration. The porous network is conserved after 14-day incubation period;
- Cells survive the jetting and impingement processes showing high viability and normal cell phenotype;
- Trilineage cell differentiation of primary hMSCs is achieved with printed CAF hydrogels;
- Faster osteogenic cell differentiation is obtained with high cell density hydrogels.
- Via gene expression, typical pre-osteoblastic behaviour is observed on low cell density hydrogels. On the other hand, common osteoblast behaviour is reported on high cell density hydrogels.

7.2 Future work

7.2.1 *Single cell coating using poly-L-lysine and reliable inkjet cell printing*

- Polycationic single layered coatings and capsules are not often utilised due to the interaction between the positively charged polymer and the negatively charged membrane. Depending on the polycation structure, small or sizeable holes on the lipid membrane may be induced, which highly compromises cell survival.

Additionally, poly-l-lysine is a synthetic polymer that is often described as cytotoxic. The use of a layer-by-layer strategy would lead to an increase of cell survival, despite originating a slower methodology due to the extra steps needed. Furthermore, the use of natural polycations, such as chitosan, would increase cell survival after coating. However, a new procedure would need to be optimised for new polycations.

- The different cell lineages were observed to ingest and metabolise the PLL. By TEM it was observed that the PLL uptake was through different endocytic pathways. To clearly identify these pathways, the use of pathway inhibitors, such as genistein or chlorpromazine, that inhibit caveolae-mediated uptake and clathrin-mediated endocytosis, respectively, would be essential.
- Cell behaviour was shown to be different for the same PLL concentrations. Fibroblasts, for example, were able to ingest and metabolised the polycation much faster than the other two cell lineages. Moreover, different reliability patterns were observed during inkjet printing as a probable cause of what is reported above. This leads to the need for careful optimisation of the polycation concentration for each cell type in order to obtain similar results during inkjet printing.
- Single cell printing is of interest in cell biology as it allows the precise location of cells in equally spaced positions, improving cell-cell interaction experiments. Single cell printing of osteosarcoma cells is attractive for use in cancer development studies.

7.2.2 *Reactive jet impingement technology for high cell density bioprinting*

- CAF hydrogels have poor mechanical properties. The addition of other biomaterial(s), such as PEG, could improve the hydrogel mechanical integrity. This would be crucial if fabricating constructs for implantation.
- To show the clear difference between the produced cell-laden hydrogels, histology and the use of specific ECM markers for microscopy would be an important complement to the information already obtained.
- The ability to bioprint different cells at the same time allows the design of specific disease models using ReJI bioprinting. This represents an opportunity to demonstrate the system potential on drug screening applications.

- To efficiently develop bone tissue, other cells and growth factors may be added to the cell-laden hydrogel.
- Further repeats of gene expression experiments are important to validate the results exhibited in this work.

References

Abelardo, E. (2018) ‘Synthetic material bioinks’, Thomas, D. J., Jessop, Z. M., and Whitaker, eds., *3D Bioprinting for Reconstructive Surgery*, Woodhead Publishing, 2018, pp. 137–144.

Achilli, T.M., Meyer, J. and Morgan, J. R. (2012) ‘Advances in the formation, use and understanding of multi-cellular spheroids’, *Expert Opinion on Biological Therapy*, 12(10), pp. 1347–1360.

Ahmed, E. M. (2015) ‘Hydrogel: Preparation, characterization, and applications: A review’, *Journal of Advanced Research*, 6(2), pp. 105–121.

Ahn, S. H., Lee, H. J., Lee, J., Yoon, H., Chun, W., Kim, G. H. (2015) ‘A novel cell-printing method and its application to hepatogenic differentiation of human adipose stem cell-embedded mesh structures’, *Scientific Reports*., 5, p. 13427.

Akhtar, M. F., Hanif, M. and Ranjha, N. M. (2016) ‘Methods of synthesis of hydrogels … A review’, *Saudi Pharmaceutical Journal*, 24(5), pp. 554–559.

Akter, F. (2016) ‘Chapter 2 - Principles of Tissue Engineering’. Akter, F., ed., *Tissue Engineering Made Easy*, Academic Press, pp. 3–16.

Algire, G. H. (1943) ‘An adaptation of the transparent-chamber technique to the mouse’, *Journal of the National Cancer Institute*, 4(1), pp. 1–11.

Allazetta, S. and Lutolf, M. P. (2015) ‘Stem cell niche engineering through droplet microfluidics’, *Current Opinion in Biotechnology*, 35, pp. 86–93.

Alves, P. M., Serra, M. and Brito, C. (2012) ‘Process engineering of human pluripotent stem cells for clinical application’, *Trends in biotechnology*, 30(6), pp. 350-359.

Andersen, T. *et al.* (1980) ‘3D Cell Culture in Alginate Hydrogels’, *Microarrays*, 4, pp. 133–161.

Arora, B., Tandon, R. and Bhatia*, P. A. and R. (2017) ‘Chemical Crosslinking: Role in Protein and Peptide Science’, *Current Protein & Peptide Science*, 18(9), pp. 946–955.

Arya, A. D. *et al.* (2016) ‘Gelatin Methacrylate Hydrogels as Biomimetic Three-Dimensional Matrixes for Modeling Breast Cancer Invasion and Chemoresponse in

Vitro', *ACS Applied Materials & Interfaces*. American Chemical Society, 8(34), pp. 22005–22017.

Ashby, M. F. *et al.* (1995) 'The Mechanical Properties of Natural Materials. I. Material Property Charts', *Proceedings: Mathematical and Physical Sciences*. The Royal Society, 450(1938), pp. 123–140.

Atala, T. K. M. and M. B. and Y.-J. S. and H.-W. K. and S. J. L. and J. J. Y. and A. (2015) 'A 3D bioprinted complex structure for engineering the muscle–tendon unit', *Biofabrication*, 7(3), p. 35003.

Atala, T. X. and K. W. B. and M. Z. A. and D. D. and W. Z. and J. J. Y. and A. (2013) 'Hybrid printing of mechanically and biologically improved constructs for cartilage tissue engineering applications', *Biofabrication*, 5(1), p. 15001.

Aubin, J. and Triffitt, J. (2008) 'Mesenchymal stem cells and osteoblast differentiation', Bilezikian, J. P., Raisz, L. G., Rodan, G. A., eds., *Principles of bone biology*, Academic Press, pp. 85–107.

Axpe, E. and Oyen, M. L. (2016) 'Applications of Alginate-Based Bioinks in 3D Bioprinting', *International Journal of Molecular Sciences*, 17(12), p. 1976.

Badenes, S. M. *et al.* (2016) 'Microcarrier Culture Systems for Stem Cell Manufacturing', Cabral, C., Silva, L. S., Chase, L. G., Diogo, M. M., eds., *Stem Cell Manufacturing*, Elsevier, pp. 77–104.

Bakhshinejad, A. and D'souza, R. M. (2015) 'A brief comparison between available bio-printing methods', in *2015 IEEE Great Lakes Biomedical Conference (GLBC) proceedings*, pp. 1–3.

Ballios, B. G. *et al.* (2010) 'A hydrogel-based stem cell delivery system to treat retinal degenerative diseases', *Biomaterials*, 31(9), pp. 2555–2564.

Benning, M. and Dalgarno, K. (2017) 'Patent GB1710834.1, "Printing apparatus and method"'.

Benoit, D. S. W. *et al.* (2008) 'Small molecule functional groups for the controlled differentiation of human mesenchymal stem cells encapsulated in poly(ethylene glycol) hydrogels', *Nature materials*, 7(10), pp. 816–823.

Benton, J. A. *et al.* (2009) 'Photocrosslinking of Gelatin Macromers to Synthesize Porous Hydrogels That Promote Valvular Interstitial Cell Function', *Tissue Engineering. Part A*, 15(11), pp. 3221–3230.

Bertassoni, L. E., Cardoso J. C., Manoharan V., Cristino A. L., Bhise N. S., Araujo W. A., Zorlutuna P., Vrana N. E., Ghaemmaghami A. M., Dokmeci M. R., Khademhosseini A. (2014) 'Direct-write Bioprinting of Cell-laden Methacrylated Gelatin Hydrogels', *Biofabrication*, 6(2), p. 24105.

Bhujbal, S. V., de Haan, B., Niclou, S. P., de Vos, P. (2014) 'A novel multilayer immunoisolating encapsulation system overcoming protrusion of cells', *Scientific Reports*, 4.

Billiet, T., Gevaert, E., De Schryver, T., Cornelissen, M., Dubruel, P. (2014) 'The 3D printing of gelatin methacrylamide cell-laden tissue-engineered constructs with high cell viability', *Biomaterials*, 35(1), pp. 49–62.

Binder, K. W., Zhao, W., Aboushwareb, T., Dice, D., Atala, A., Yoo, J. J. (2010) 'In situ bioprinting of the skin for burns', *Journal of the American College of Surgeons*, 211(3), p. S76.

Birmingham, E., Niebur, G. L., McHugh, P. E., Shaw, G., Barry, F. P., McNamara, L. M. (2012) 'Osteogenic differentiation of mesenchymal stem cells is regulated by osteocyte and osteoblast cells in a simplified bone niche', *European Cells and Materials*, 23, pp. 13–27.

Bishop, E. S., Mostafa, S., Pakvasa, M., Luu, H. H., Lee, M. J., Wolf, J. M., Ameer, G. A., He, T. C., Reid, R. R. (2017) '3-D bioprinting technologies in tissue engineering and regenerative medicine: Current and future trends', *Genes & Diseases*, 4(4), pp. 185–195.

Blaeser, A., Duarte Campos, D. F., Puster, U., Richtering, W., Stevens, M. M., Fischer, H. (2015) 'Controlling Shear Stress in 3D Bioprinting is a Key Factor to Balance Printing Resolution and Stem Cell Integrity', *Advanced Healthcare Materials*, 5(3), pp. 326–333.

Bode, F., da Silva, M. A., Smith, P., Lorenz, C. D., McCullen, S., Stevens, M. M., Dreiss, C. A. (2013) 'Hybrid gelation processes in enzymatically gelled gelatin: impact on nanostructure, macroscopic properties and cellular response', *Soft Matter*, 9(29), pp. 6986–6999.

Boland, T., Xu, T., Damon, B. J., Manley, B., Kesari, P., Jalot, S., Bhaduri, S. (2007) 'Drop-on-demand printing of cells and materials for designer tissue constructs', *Materials Science and Engineering: C*, 27(3), pp. 372–376.

Borthwick, K. A. J, Coakley, W. T., McDonell, M. B., Nowotny, H., Benes, E., Groschld, M. (2005) 'Development of a novel compact sonicator for cell disruption', *Journal of Microbiological Methods*, 60(2), pp. 207–216.

Bozza, A., Coates, E. E., Incitti, T., Ferlin, K. M., Messina, A., Menna, E., Bozzi, Y., Fisher, J. P., Casarosa, S. (2014) 'Neural differentiation of pluripotent cells in 3D alginate-based cultures', *Biomaterials*, 35(16), pp. 4636–4645.

Brancato, V., Ventre, M., Imparato, G., Urciuolo, F., Meo, C., Netti, P. A. (2016) 'A straightforward method to produce decellularized dermis-based matrices for tumour cell cultures', *Journal of Tissue Engineering and Regenerative Medicine*, 12(1), pp. e71–e81.

Breslin, S. and O'Driscoll, L. (2013) 'Three-dimensional cell culture: the missing link in drug discovery', *Drug Discovery Today*, 18(5), pp. 240–249.

Brown, A. C. and Barker, T. H. (2014) 'Fibrin-based biomaterials: Modulation of macroscopic properties through rational design at the molecular level', *Acta Biomaterialia*, 10(4), pp. 1502–1514.

Burnett, K., Edsinger, E. and Albrecht, D. R. (2018) 'Rapid and gentle hydrogel encapsulation of living organisms enables long-term microscopy over multiple hours', *Communications Biology*, 1(1).

Butcher, L. A., Kang, K. H., Colangelo, N. W., Cheung, P. Y., Duan, B., Malone, E., Wu, J., Girardi, L. N., Bonassar, L. J., Lipson, H., Chu, C. C., Butcher, J. T. (2012) 'Rapid 3D printing of anatomically accurate and mechanically heterogeneous aortic valve hydrogel scaffolds', *Biofabrication*, 4(3), p. 35005.

Buwalda, S. J., Vermonden, T. and Hennink, W. E. (2017) 'Hydrogels for Therapeutic Delivery: Current Developments and Future Directions', *Biomacromolecules*. American Chemical Society, 18(2), pp. 316–330.

Caló, E. and Khutoryanskiy, V. V (2015) 'Biomedical applications of hydrogels: A review of patents and commercial products', *European Polymer Journal*, 65, pp. 252–267.

Campbell, J. J., Husmann, A., Hume, R. D., Watson, C. J., Cameron, R. E. (2017) 'Development of three-dimensional collagen scaffolds with controlled architecture for cell migration studies using breast cancer cell lines', *Biomaterials*, 114, pp. 34–43.

Campbell, P. G. and Weiss, L. E. (2007) 'Tissue engineering with the aid of inkjet printers', *Expert Opinion on Biological Therapy*, 7(8), pp. 1123–1127.

Cascalho, M., Platt, J. L. (2008) 81 - 'Challenges and potentials of xenotransplantation', Rich, R. R., Fleisher, T. A., Shearer, W. T., Schroeder, H. W., Frew, A. J., Weyand, C. M., (eds), Mosby, pp. 1215-1222.

Catros, S., Keriquel, V., Fricain, J., Guillemot, F. (2015) 'Chapter 5 - In Vivo and In Situ Biofabrication by Laser-Assisted Bioprinting', Atala, A. and Yoo, J. J., eds, Boston: Academic Press, pp. 81–87.

Catros, S., Keriquel, V., Guillemot, F., Arnault, I., Guillotin, B., Miraux, S., Amédée, J., Fricain, J. C. (2010) 'In vivo bioprinting for computer- and robotic-assisted medical intervention: preliminary study in mice', *Biofabrication*, 2(1), p. 14101.

Chahal, D., Ahmadi, A. and Cheung, K. C. (2012) 'Improving piezoelectric cell printing accuracy and reliability through neutral buoyancy of suspensions', *Biotechnology and Bioengineering*, 109(11), pp. 2932–2940.

Chan, E., Kuo, S. M., Kong, A. M., Morrison, W. A., Dusting, G. J., Mitchell, G. M., Lim, S. Y., Liu, G. S. (2016) 'Three Dimensional Collagen Scaffold Promotes Intrinsic Vascularisation for Tissue Engineering Applications', *PLOS ONE*, 11(2):e0149799.

Chang, C. C., Boland, E. D., Williams, S. K., Hoying, J. B. (2011) 'Direct-write Bioprinting Three-Dimensional Biohybrid Systems for Future Regenerative Therapies', *Journal of biomedical materials research. Part B, Applied Biomaterials*, 98(1), pp. 160–170.

Chang, R., Nam, J. and Sun, W. (2008) 'Effects of Dispensing Pressure and Nozzle Diameter on Cell Survival from Solid Freeform Fabrication–Based Direct Cell Writing', *Tissue Engineering Part A*, 14(1), pp. 41–48.

Chang, T. M. S. (1964) 'Semipermeable microcapsules', *Science*, 146(3643), pp. 524–525.

Chen, C.-Y., Ke, C. J., Yen, K. C., Hsieh, H. C., Sun, J. S., Lin, F. H. (2015) '3D Porous

Calcium-Alginate Scaffolds Cell Culture System Improved Human Osteoblast Cell Clusters for Cell Therapy', *Theranostics*, 5(6), pp. 643–655.

Chen, J. C. and Jain, S. A. (2010) 'Chapter 104 - Principles of Skin Grafts', Weinzweig, J., ed., Philadelphia: Mosby, pp. 677–683.

Cheng, G., Youssef, B. B., Markenscoff, P., Zygourakis, K. (2006) 'Cell population dynamics modulate the rates of tissue growth processes', *Biophysical Journal*, 90(3), pp. 713–724.

Cheung, S. P., Gupta, M., Loizeau, F., Cheung, K. C. (2010) 'Effects of surfactant and gentle agitation on inkjet dispensing of living cells', *Biofabrication*, 2(2), p. 25003.

Lee, J. S., Hong, J. M., Jung, J. W., Shim, J. H., Oh, J. H., Cho, D. W. (2014) '3D printing of composite tissue with complex shape applied to ear regeneration', *Biofabrication*, 6(2), p. 24103.

Choi, W. S., Ha, D., Park, S., Kim, T. (2011) 'Synthetic multicellular cell-to-cell communication in inkjet printed bacterial cell systems', *Biomaterials*, 32(10), pp. 2500–2507.

Choudhury, D., Anand, S. and Naing, M. W. (2018) 'The Arrival of Commercial Bioprinters - Towards 3D Bioprinting Revolution!', *International Journal of Bioprinting*, 4(2), pp. 1-20.

Chrisey, H. G., Yan, J., Huang, Y., Chrisey, D. B. (2014) 'Alginate gelation-induced cell death during laser-assisted cell printing', *Biofabrication*, 6(3), p. 35022.

Christensen, K., Xu, C., Chai, W., Zhang, Z., Fu, J., Huang, Y. (2014) 'Freeform inkjet printing of cellular structures with bifurcations', *Biotechnology and Bioengineering*, 112(5), pp. 1047–1055.

Chua, C. K. and Yeong, W. Y. (2014) 'Chapter 3: Bioprinting techniques', Chua, C. K. and Yeong, W. Y., eds., *Bioprinting: Principles and Applications*, World Scientific, pp. 63–116.

Combellack, E., Jessop, Z. M. and Whitaker, I. S. (2018) '20 - The commercial 3D bioprinting industry', Thomas, D. J., Jessop, Z. M., and Whitaker, I., eds., Woodhead Publishing, pp. 413–421.

Cooper, G. and Hausman, R. E. (2004) 'Chapter 16 Cell Signaling', *The Cell: A Molecular Approach*, Sinauer Associates, pp. 589-642.

Crapo, P. M., Gilbert, T. W. and Badylak, S. F. (2011) 'An overview of tissue and whole organ decellularization processes', *Biomaterials*, 32(12), pp. 3233–3243.

Di Crescenzo, A., Ettorre, V. and Fontana, A. (2014) 'Non-covalent and reversible functionalization of carbon nanotubes', *Beilstein Journal of Nanotechnology*, 5(1), pp. 1675–1690.

Cui, X., Breitenkamp, K., Finn, M. G., *et al.* (2012) 'Direct Human Cartilage Repair Using Three-Dimensional Bioprinting Technology', *Tissue Engineering. Part A*, 18(11–12), pp. 1304–1312.

Cui, X., Breitenkamp, K., Lotz, M., *et al.* (2012) 'Synergistic action of fibroblast growth factor-2 and transforming growth factor-beta1 enhances bioprinted human neocartilage formation', *Biotechnology and Bioengineering*, 109(9), pp. 2357–2368.

Cui, X., Boland, T., D'Lima, D. D., Lotzl, M. K. (2012) 'Thermal Inkjet Printing in Tissue Engineering and Regenerative Medicine', *Recent patents on drug delivery & formulation*, 6(2), pp. 149–155.

Cui, X. and Boland, T. (2009) 'Human microvasculature fabrication using thermal inkjet printing technology', *Biomaterials*, 30(31), pp. 6221–6227.

Curtis, A. and Wilkinson, C. (1999) 'New depths in cell behaviour: reactions of cells to nanotopography', *Biochem Soc Symp*, 65, pp. 15–26.

Dababneh, A. B. and Ozbolat, I. T. (2014) 'Bioprinting Technology: A Current State-of-the-Art Review', *Journal of Manufacturing Science and Engineering*. ASME, 136(6), pp. 61011–61016.

Dai, B., Wang, L., Wang, Y., Yu, G., Huang, X. (2018) 'Single-Cell Nanometric Coating Towards Whole-Cell-Based Biodevices and Biosensors', *ChemistrySelect*, 3(25), pp. 7208–7221.

Dai, X., Jiu, L., Ouyang, J., Li, X., Zhang, X., Lan, Q., Xu, T. (2017) 'Coaxial 3D bioprinting of self-assembled multicellular heterogeneous tumor fibers', *Scientific Reports*, 7(1), p. 1457.

Delgado, L. M., Bayon, Y., Pandit, A., Zeugolis, D. I. (2015) ‘To Cross-Link or Not to Cross-Link? Cross-Linking Associated Foreign Body Response of Collagen-Based Devices’, *Tissue Engineering. Part B, Reviews*, 21(3), pp. 298–313.

Derakhshanfar, S., Mbeleck, R., Xu, K., Zhang, X., Zhong, W., Zing, M. (2018) ‘3D bioprinting for biomedical devices and tissue engineering: A review of recent trends and advances’, *Bioactive Materials*, 3(2), pp. 144–156.

Derby, B. (2008) ‘Bioprinting: inkjet printing proteins and hybrid cell-containing materials and structures’, *Journal of Materials Chemistry*, 18(47), pp. 5717–5721.

Desai, T. and Shea, L. D. (2017) ‘Advances in islet encapsulation technologies’, *Nature Reviews Drug Discovery*, 16(5), pp. 338–350.

Dhariwala, B., Hunt, E. and Boland, T. (2004) ‘Rapid Prototyping of Tissue-Engineering Constructs, Using Photopolymerizable Hydrogels and Stereolithography’, *Tissue Engineering*, 10(9–10), pp. 1316–1322.

Dias, A. D., Elicson, J. M. and Murphy, W. L. (2017) ‘Microcarriers with synthetic hydrogel surfaces for stem cell expansion’, *Advanced Healthcare Materials*, 6(16), 1700072.

DiMasi, J., Hansen, R. . and Grabowski, H. (2003) ‘The price of innovation: New estimates of drug development costs’, *Journal of Health Economics*, 22(2), pp. 151–185.

Donderwinkel, I., van Hest, J. C. M. and Cameron, N. R. (2017) ‘Bio-inks for 3D bioprinting: recent advances and future prospects’, *Polymer Chemistry*, 8(31), pp. 4451–4471.

Drachuk, I., Gupta, M. K. and Tsukruk, V. V (2013) ‘Biomimetic Coatings to Control Cellular Function through Cell Surface Engineering’, *Advanced Functional Materials*, 23, pp. 4437– 4453.

Duan, B. *et al.* (2012) ‘3D Bioprinting of heterogeneous aortic valve conduits with alginate/gelatin hydrogels’, *Journal of Biomedical Materials Research Part A*, 101A(5), pp. 1255–1264.

Duarte Campos, D. F. *et al.* (2014) ‘The Stiffness and Structure of Three-Dimensional Printed Hydrogels Direct the Differentiation of Mesenchymal Stromal Cells Toward Adipogenic and Osteogenic Lineages’, *Tissue Engineering Part A*, 21(3–4), pp. 740–756.

van Duinen, V., Trietsch, S. J., Joore, J., Vulto, P., Hankemeier, T. (2015) ‘Microfluidic 3D cell culture: from tools to tissue models’, *Current Opinion in Biotechnology*, 35, pp. 118–126.

Duncan, M. D. and Wilkes, D. S. (2005) ‘Transplant-related Immunosuppression: A Review of Immunosuppression and Pulmonary Infections’, *Proceedings of the American Thoracic Society*, 2(5), pp. 449–455.

Dutta, D. and Donaldson, J. G. (2012) ‘Search for inhibitors of endocytosis: Intended specificity and unintended consequences’, *Cellular Logistics*, 2(4), pp. 203–208.

Duval, K., Grover, H., Han, L. H., Mou, Y., Pegoraro, A. F., Fredberg, J., Chen, Z. (2017) ‘Modeling Physiological Events in 2D vs. 3D Cell Culture’, *Physiology*, 32(4), pp. 266–277.

Edmondson, R., Broglie, J. J., Adcock, A. F., Yang, L. (2014) ‘Three-Dimensional Cell Culture Systems and Their Applications in Drug Discovery and Cell-Based Biosensors’, *Assay and Drug Development Technologies*, pp. 207–218.

Fakhrullin, R. F., Zamaleeva, A. I., Minullina, R. T., Konnova, S. A., Paunov, V. N. (2012) ‘Cyborg cells: Functionalisation of living cells with polymers and nanomaterials’, *Chemical Society Reviews*, 41(11), pp. 4189–4206.

Fan, R., Piou, M., Darling, E., Cormier, D., Sun, J., Wan, J. (2016) ‘Bio-printing cell-laden Matrigel–agarose constructs’, *Journal of Biomaterials Applications*, 31(5), pp. 684–692.

Fan, Y., Wu, J., Ashok, P., Hsiung, M., Tzanakakis, E. S. (2015) ‘Production of Human Pluripotent Stem Cell Therapeutics under Defined Xeno-free Conditions: Progress and Challenges’, *Stem Cell Reviews and Reports*, 11(1), pp. 96–109.

Fauzia, V., Umar, A. A., Salleh, M. M., Yahya, M. (2010) ‘Optimizing of the inkjet printing technique parameters for fabrication of bulk heterojunction organic solar cells’, in *2010 IEEE International Conference on Semiconductor Electronics (ICSE2010) Malaysia*, pp. 60–63.

Fernandes, T. G., Diogo, M. M. and Cabral, J. M. S. (2013) ‘Stem Cell Bioprocessing’, *Stem Cell Bioprocessing*, Woodhead Publishing, pp. 33–68.

Ferreira, A. M., Gentile, P., Chiono, V., Ciardelli, G. (2012) ‘Collagen for bone tissue

regeneration', *Acta Biomaterialia*, 8(9), pp. 3191–3200.

Ferris, C. J., Gilmore, K., J., Beirne, S., McCallum, D., Wallace, G. G., Panhuis, M. (2013) 'Bio-ink for on-demand printing of living cells', *Biomaterials Science*, 1(2), pp. 224–230.

Fischer, D., Li, Y., Ahlemeyer, B., Krieglstein, J., Kissel, T. (2003) 'In vitro cytotoxicity testing of polycations: Influence of polymer structure on cell viability and hemolysis', *Biomaterials*, 24(7), pp. 1121–1131.

Fletcher, D. A. and Mullins, R. D. (2010) 'Cell mechanics and the cytoskeleton', *Nature*, 463, p. 485-492.

Freudenberg, U., Liang, Y., Kiick, K. L., Werner, C. (2016) 'Glycosaminoglycan-Based Biohybrid Hydrogels: A Sweet and Smart Choice for Multifunctional Biomaterials', *Advanced Materials*, 28(40), pp. 8861–8891.

Friedrich, J., Eder, W., Castaneda, J., Doss, M., Huber, E., Ebner, R., Kunz-Schughart, L. A. (2007) 'A Reliable Tool to Determine Cell Viability in Complex 3-D Culture: The Acid Phosphatase Assay', *Journal of Biomolecular Screening*, 12(7), pp. 925–937.

Trepat, X., Sahai, E. (2018) 'Mesoscale physical principles of collective cell organization', *Nature Physics*, 14, pp. 671–682.

Gaebel, R., Ma, N., Liu, J., Guan, J., Koch, L., Klopsch, C., Gruene, M., Toelk, A., Wang, W., Mark, P., Wang, F., Chichkov, B., Li, W., Steinhoff, G. (2011) 'Patterning human stem cells and endothelial cells with laser printing for cardiac regeneration', *Biomaterials*, 32(35), pp. 9218–9230.

Gao, G., Yonezawa, T., Hubbell, K.,, Dai, G., Cui, X. (2015) Inkjet-bioprinted acrylated peptides and PEG hydrogel with human mesenchymal stem cells promote robust bone and cartilage formation with minimal printhead clogging, *Biotechnology Journal*, 10(10), pp. 1568-1577.

Gao, G., Huang, Y., Schilling, A. F., Hubbell, K., Cui, X. (2017) 'Organ Bioprinting: Are We There Yet?', *Advanced Healthcare Materials*, 7(1), p. 1701018.

Gao, Q., Zhao, H., He, Y. (2018) '2 - Practical laboratory methods for 3D bioprinting', Thomas, D. J., Jessop, Z. M. Whitaker, I. S., (eds), Woodhead Publishing, pp. 7–32.

Garg, T., Singh, O., Arora, S., Murthy, R. (2012) ‘Scaffold: A Novel Carrier for Cell and Drug Delivery’, *Critical Reviews Therapeutic Drug Carrier Systems*, 29(1), pp. 1–63.

Gasperini, L., Mano, J. F. and Reis, R. L. (2014) ‘Natural polymers for the microencapsulation of cells.’, *Journal of the Royal Society Interface*, 11(100), p. 20140817.

Geckil, H. *et al.* (2010) ‘Engineering hydrogels as extracellular matrix mimics’, *Nanomedicine*, 5(3), pp. 469–484.

Gelinsky, M. (2018) ‘6 - Biopolymer hydrogel bioinks’, Thomas, D. J., Jessop, Z. M. Whitaker, I. S., (eds), Woodhead Publishing, pp. 125–136.

Giuseppe, M. Di, Law, N., Webb, B., Macrae, R. A., Liew, L. J., Sercombe, T. B., Dilley, R. J., Doyle, B. J. (2018) ‘Mechanical behaviour of alginate-gelatin hydrogels for 3D bioprinting’, *Journal of the Mechanical Behavior of Biomedical Materials*, 79, pp. 150–157.

Golub, E. E. and Boesze-Battaglia, K. (2007) ‘The role of alkaline phosphatase in mineralization’, *Current Opinion in Orthopaedics*, 18(5), pp. 444–448.

Gómez-Guillén, M. C. *et al.* (2002) ‘Structural and physical properties of gelatin extracted from different marine species: a comparative study’, *Food Hydrocolloids*, 16(1), pp. 25–34.

Gordeev, E. G., Galushko, A. S. and Ananikov, V. P. (2018) ‘Improvement of quality of 3D printed objects by elimination of microscopic structural defects in fused deposition modeling’, *PLoS ONE*, 13(6), pp. e0198370.

Graham, A. D., Olof, S. N., Burke, M. J., Armstrong, J. P., Mikhailova, E. A., Nicholson, J. G., Box, S. J., Szele, F. G., Perriman, A. W., Bayley, H. (2017) ‘High-Resolution Patterned Cellular Constructs by Droplet-Based 3D Printing’, *Scientific Reports*, 7(1), pp. 7004.

Gray, D. W. R. (2006) ‘Commentary for Macroencapsulation Protects Against Sensitization After Allogeneic Islet Transplantation in Rats’, *Transplantation*, 82(3), pp. 310-311.

Griffith, L. G. and Swartz, M. A. (2006) ‘Capturing complex 3D tissue physiology in vitro’, *Nature Reviews Molecular Cell Biology*, 7(3), pp. 211–224.

Grix, T., Ruppelt, A., Thomas, A., Amler, A. K., Noichl, B. P., Lauster, R., Kloke, L. (2018) 'Bioprinting Perfusion-Enabled Liver Equivalents for Advanced Organ-on-a-Chip Applications', *Genes*, 9(4), pp. 1-15.

Gruene, M., Unger, C., Koch, L., Deiwick, A. and Chichkov, B. (2011) Dispensing pico to nanolitre of a natural hydrogel by laser-assisted bioprinting, *BioMedical Engineering OnLine*, 10(19), pp. 1-11.

Gruene, M., Pflaum, M., Hess, C., Diamantouros, S., Schlie, S., Deiwick, A., Koch, L., Wilhelmi, M., Jockenhoevel, S., Haverich, A., Chichkov, B. (2011) 'Laser Printing of Three-Dimensional Multicellular Arrays for Studies of Cell–Cell and Cell–Environment Interactions', *Tissue Engineering Part C: Methods*, 17(10), pp. 973–982.

Gudapati, H., Dey, M. and Ozbolat, I. (2016) 'A comprehensive review on droplet-based bioprinting: Past, present and future', *Biomaterials*, 102, pp. 20–42.

Guillotin, B., Souquet, A., Catros, S., Duocastella, M., Pippenger, B., Bellance, S., Bareille, R., Rémy, M., Bordenave, L., Amédée, J., Guillemot, F. (2010) 'Laser assisted bioprinting of engineered tissue with high cell density and microscale organization', *Biomaterials*, 31(28), pp. 7250–7256.

Gungor-Ozkerim, P. S., Inci, I., Zhang, Y. S., Khademhosseini, A., Dokmeci, M. R.(2018) 'Bioinks for 3D bioprinting: an overview', *Biomaterials Science*, 6(5), pp. 915–946.

Guo, L., Colby, R. H., Lusignan, C. P., Howe, A. M. (2003) 'Physical Gelation of Gelatin Studied with Rheo-Optics', *Macromolecules*, 36(26), pp. 10009–10020.

Gupta, R., Truong, L., Bear, D., Chafik, D., Modafferi, E., Hung, C. T. (2006) 'Shear stress alters the expression of myelin-associated glycoprotein (MAG) and myelin basic protein (MBP) in Schwann cells', *Journal of Orthopaedic Research*, 23(5), pp. 1232–1239.

Gurkan, U. A., El Assal, R., Yildiz, S. E., Sung, Y., Trachtenberg, A. J, Kuo, W. P., Demirci, U. (2014) 'Engineering Anisotropic Biomimetic Fibrocartilage Microenvironment by Bioprinting Mesenchymal Stem Cells in Nanoliter Gel Droplets', *Molecular Pharmaceutics*, 11(7), pp. 2151–2159.

Gurtner, G. C., Werner, S., Barrandon, Y., Longaker, M. T. (2008) 'Wound repair and

regeneration', *Nature*, 453, p. 314-321.

Guvendiren, M., Lu, H. D. and Burdick, J. A. (2012) 'Shear-thinning hydrogels for biomedical applications', *Soft Matter*, 8(2), pp. 260–272.

Guzmán, E., Mateos-Maroto, A., Ruano, M., Ortega, F., Rubio, R. G. (2017) 'Layer-by-Layer polyelectrolyte assemblies for encapsulation and release of active compounds', *Advances in Colloid and Interface Science*, 249, pp. 290–307.

He, P., Zhao, J., Zhang, J., Li, B., Gou, Z., Gou, M., Li, X. (2018) 'Bioprinting of skin constructs for wound healing', *Burns & Trauma*, 6(5), pp. 1-10.

Hennink, W. E. and van Nostrum, C. F. (2002) 'Novel crosslinking methods to design hydrogels', *Advanced Drug Delivery Reviews*, 54(1), pp. 13–36.

Hennis, H. L., Stewart, W. C. and Jeter, E. K. (1992) 'Infectious Disease Risks of Fibrin Glue', *Ophthalmic Surgery, Lasers and Imaging Retina*, 23(9), pp. 640–640.

Hinderer, S., Layland, S. L. and Schenke-Layland, K. (2016) 'ECM and ECM-like materials - Biomaterials for applications in regenerative medicine and cancer therapy', *Advanced Drug Delivery Reviews*, 97, pp. 260–269.

Hirashima, M. Imamura, T., Yano, K., Kawamura, R., Meta, A., Tokieda, Y., Nakashima, T.(2016) 'High-level expression and preparation of recombinant human fibrinogen as biopharmaceuticals', *Journal of Biochemistry*, 159(2), pp. 261–270.

Hoch, E., Hirth, T., Tovarab, G., Borchersa, K. (2013) 'Chemical tailoring of gelatin to adjust its chemical and physical properties for functional bioprinting', *Journal of Materials Chemistry B*, 1(41), pp. 5675–5685.

Holder, A. J., Badiei, N., Hawkins, K., Wright, C., Williams, P. R., Curtis, D. J. (2018) 'Control of collagen gel mechanical properties through manipulation of gelation conditions near the sol–gel transition', *Soft Matter*, 14(4), pp. 574–580.

Hollister, S. J. (2005) 'Porous scaffold design for tissue engineering', *Nature Materials*, 4(7), p. 518-524.

Homan, K. A., Kolesky, D. B., Skylar-Scott, M. A., Herrmann, J., Obuobi, H., Moisan, A., Lewis, J. A. (2016) 'Bioprinting of 3D Convoluted Renal Proximal Tubules on Perfusable Chips', *Scientific Reports*, 6, p. 34845.

Hong, H. and Stegemann, J. P. (2008) ‘2D and 3D collagen and fibrin biopolymers promote specific ECM and integrin gene expression by vascular smooth muscle cells’, *Journal of Biomaterials Science, Polymer Edition*, 19(10), pp. 1279–1293.

Hong, N., Yang, G. H., Lee, J., Kim, G. (2017) ‘3D bioprinting and its in vivo applications’, *Journal of Biomedical Materials Research Part B: Applied Biomaterials*, 106(1), pp. 444–459.

Hong, S., Leroueil, P. R., Janus, E. K., Peters, J. L., Kober, M. M., Islam, M. T., Orr, B. G., Baker, J. R., Banaszak, H. M. M. (2006) ‘Interaction of polycationic polymers with supported lipid bilayers and cells: Nanoscale hole formation and enhanced membrane permeability’, *Bioconjugate Chemistry*, 17(3), pp. 728–734.

Hopp, B., Smausz, T., Szab, G., Kolozsvri, L., Kafetzopoulos, D., Fotakis, C., Ngrdi, A. (2012) Femtosecond laser printing of living cells using absorbing film-assisted laser-induced forward transfer, *Optical Engineering*, 51(1), 014302.

Horváth, L., Umehara, Y., Jud, C., Blank, F., Petri-Fink, A., Rothen-Rutishauser, B. (2015) ‘Engineering an in vitro air-blood barrier by 3D bioprinting’, *Scientific Reports*, 5, pp. 7974.

Hospodiuk, M., Dey, M., Sosnoski, D., Ozbolat, I. T. (2017) ‘The bioink: A comprehensive review on bioprintable materials’, *Biotechnology Advances*, 35(2), pp. 217–239.

Howard, D., Buttery, L. D., Shakesheff, K. M., Roberts, S. J. (2008) ‘Tissue engineering: strategies, stem cells and scaffolds’, *Journal of Anatomy*, 213(1), pp. 66–72.

Hu, J., Hou, Y., Park, H., Choi, B., Hou, S., Chung, A., Lee, M. (2012) ‘Visible light crosslinkable chitosan hydrogels for tissue engineering’, *Acta Biomaterialia*, 8(5), pp. 1730–1738.

Huang, R. X., Zhang, Z., Chai, W., Chrisey, D. B., Huang, Y. (2017) ‘Study of gelatin as an effective energy absorbing layer for laser bioprinting’, *Biofabrication*, 9(2), p. 24103.

Huh, D., Hamilton, G. A. and Ingber, D. E. (2011) ‘From 3D cell culture to organs-on-chips’, *Trends in Cell Biology*, 21(12), pp. 745–754.

Hutmacher, D. W., Schantz, T., Zein, I., Ng, K. W., Teoh, S. H., Tan, K. C. (2001) ‘Mechanical properties and cell cultural response of polycaprolactone scaffolds designed

and fabricated via fused deposition modeling', *Journal of Biomedical Materials Research*, 55(2), pp. 203–216.

Hwang, N. S., Varghese, S. and Elisseeff, J. (2008) 'Controlled differentiation of stem cells', *Advanced Drug Delivery Reviews*, 60(2), pp. 199–214.

Ikada, Y. (2006) 'Challenges in tissue engineering', *Journal of the Royal Society Interface*, 3(10), pp. 589–601.

Indovina, P. L., Tettamanti, E., Micciancio-Giammarinaro, M. S., Palma, M. U. (1979) 'Thermal hysteresis and reversibility of gel–sol transition in agarose–water systemsa)', *The Journal of Chemical Physics*, 70(6), pp. 2841–2847.

Iwanaga, S., Arai, K. and Nakamura, M. (2015) 'Chapter 4 - Inkjet Bioprinting', *Essentials of 3D Biofabrication and Translation*, Atala, A., Yoo, J. J. (eds), Academic Press, pp. 61-79.

James, S. *et al.* (2015) 'Multiparameter Analysis of Human Bone Marrow Stromal Cells Identifies Distinct Immunomodulatory and Differentiation-Competent Subtypes', *Stem Cell Reports*, 4(6), pp. 1004–1015.

Jana, S. and Lerman, A. (2015) 'Bioprinting a cardiac valve', *Biotechnology Advances*, 33(8), pp. 1503–1521.

Jang, J. (2017) '3D Bioprinting and In Vitro Cardiovascular Tissue Modeling', *Bioengineering*, 4(3), p. 71.

Jang, J., Park, H. J., Kim, S. W., Kim, H., Park, J. Y., Na, S. J., Kim, H. J., Park, M. N., Choi, S. H., Park, S. H., Kim, S.W., Kwon, S. M., Kim, P. J., Cho, D. W. (2017) '3D printed complex tissue construct using stem cell-laden decellularized extracellular matrix bioinks for cardiac repair', *Biomaterials*, 112, pp. 264–274.

Janmey, P. A., Winer, J. P. and Weisel, J. W. (2009) 'Fibrin gels and their clinical and bioengineering applications', *Journal of the Royal Society Interface*, 6(30), pp. 1–10.

Ji, C. and Shi, J. (2013) 'Thermal-crosslinked porous chitosan scaffolds for soft tissue engineering applications', *Materials Science and Engineering: C*, 33(7), pp. 3780–3785.

Ji, S. and Guvendiren, M. (2017) 'Recent Advances in Bioink Design for 3D Bioprinting of Tissues and Organs', *Frontiers in Bioengineering and Biotechnology*, 5, article 23.

Johnston, A. P. R., Cortez, C., Angelatos, A. S., Caruso, F. (2006) 'Layer-by-layer engineered capsules and their applications', *Current Opinion in Colloid and Interface Science*, 11(4), pp. 203–209.

Jones, N. (2012) 'Science in three dimensions: The print revolution', *Nature*, 487(7405), pp. 22–23.

Jose, R. R., Rodriguez, M. J., Dixon, T. A., Omenetto, F., Kaplan, D. L. (2016) 'Evolution of Bioinks and Additive Manufacturing Technologies for 3D Bioprinting', *ACS Biomaterials Science & Engineering*, 2(10), pp. 1662–1678.

Junaid, A., Mashaghi, A., Hankemeier, T., Vulto, P. (2017) 'An end-user perspective on Organ-on-a-Chip: Assays and usability aspects', *Current Opinion in Biomedical Engineering*, 1, pp. 15–22.

Jung, H., Tae, G., Kim, Y. H., Johannsmann, D. (2009) 'Change of viscoelastic property and morphology of fibrin affected by antithrombin III and heparin: QCM-Z and AFM study', *Colloids and Surfaces B: Biointerfaces*, 68(1), pp. 111–119.

Kang, H.-W., Lee, S. J., Ko, I. K., Kengla, C., Yoo, J. J., Atala, A. (2016) 'A 3D bioprinting system to produce human-scale tissue constructs with structural integrity', *Nature Biotechnology*, 34(3), p. 312-319.

Kellam, B., De Bank, P. A. and Shakesheff, K. M. (2003) 'Chemical modification of mammalian cell surfaces', Chemical Society Reviews, 32, pp. 327-337.

Keriquel, V., Oliveira, H., Rémy, M., Ziane, S., Delmond, S., Rousseau, B., Rey, S., Catros, S., Amédée, J., Guillemot, F., Fricain, J. (2017) 'In situ printing of mesenchymal stromal cells, by laser-assisted bioprinting, for in vivo bone regeneration applications', *Scientific Reports*, 7(1), pp. 1778.

Kerscher, P., Turnbull, I. C., Hodge, A. J., Kim, J., Seliktar, D., Easley, C. J., Costa, K. D., Lipke, E. A. (2016) 'Direct hydrogel encapsulation of pluripotent stem cells enables ontomimetic differentiation and growth of engineered human heart tissues', *Biomaterials*, 83, pp. 383–395.

Khalil, S. and Sun, W. (2009) 'Bioprinting Endothelial Cells With Alginate for 3D Tissue Constructs', *Journal of Biomechanical Engineering*, 131(11), pp. 111002–111008.

Khan, Y., Yaszemski, M. J., Mikos, A. G., Laurencin, C.T. (2008) 'Tissue Engineering of

Bone: Material and Matrix Considerations', *The Journal of Bone and Joint Surgery*, 90, pp. 36-42.

Khetan, S., Guvendiren, M., Legant, W. R., Cohen, D. M., Chen, C. S., Burdick, J. A. (2013) 'Degradation-mediated cellular traction directs stem cell fate in covalently crosslinked three-dimensional hydrogels', *Nature Materials*, 12(5), pp. 458–465.

Kim, Y., Ko, H., Kwon, I. K., Shin, K. (2016) 'Extracellular Matrix Revisited: Roles in Tissue Engineering', *International Neurourology Journal*, 20 (Suppl 1), pp. S23-29.

Al Kindi, A. H., Asenjo, J. F., Ge, Y., Chen, G. Y., Bhathena, J., Chiu, R. C., Prakash, S., Shum-Tim, D. (2011) 'Microencapsulation to reduce mechanical loss of microspheres: Implications in myocardial cell therapy', *European Journal of Cardio-thoracic Surgery*, 39(2), pp. 241–247.

Kirk, K., Hao, E., Lahmy, R., Itkin-Ansari, P. (2014) 'Human embryonic stem cell derived islet progenitors mature inside an encapsulation device without evidence of increased biomass or cell escape', *Stem Cell Research*, 12(3), pp. 807–814.

Kizawa, H., Nagao, E., Shimamura, M., Guangyuan, Z., Torii, H. (2017) 'Scaffold-free 3D bio-printed human liver tissue stably maintains metabolic functions useful for drug discovery', *Biochemistry and Biophysics Reports*, 10, pp. 186–191.

Klotz, B. J., Gawlitta, D., Rosenberg, A. J., Malda, J., Melchels, F. (2016) 'Gelatin-Methacryloyl Hydrogels: Towards Biofabrication-Based Tissue Repair', *Trends in biotechnology*, 34(5), pp. 394–407.

Koch, L., Kuhn, S., Sorg, H., Gruene, M., Schlie, S., Gaebel, R., Polchow, B., Reimers, K., Stoelting, S., Ma, N., Vogt, P. M., Steinhoff, G., Chichkov, B. (2009) 'Laser Printing of Skin Cells and Human Stem Cells', *Tissue Engineering Part C: Methods*, 16(5), pp. 847–854.

Koch, L., Brandt, O., Deiwick, A., Chichkov, B. (2017) 'Laser-assisted bioprinting at different wavelengths and pulse durations with a metal dynamic release layer: A parametric study', *International Journal of Bioprinting*, 3(1), pp. 42–53.

Kolesky, D. B., Truby, R. L., Gladman, A. S., Busbee, T. A., Homan, K. A., Lewis, J. A. (2014) '3D Bioprinting of Vascularized, Heterogeneous Cell-Laden Tissue Constructs', *Advanced Materials*, 26(19), pp. 3124–3130.

Kołodziejczyk, J. and Ponczek, M. B. (2013) ‘The role of fibrinogen, fibrin and fibrin(ogen) degradation products (FDPs) in tumor progression’, *Contemporary Oncology*, 17(2), pp. 113–119.

Krishnan, R., Alexander, M., Robles, L., Foster, C. E., Lakey, J. R. (2014) ‘Islet and Stem Cell Encapsulation for Clinical Transplantation’, *The Review of Diabetic Studies*, 11(1), pp. 84–101.

Kuhlmann, J. (1997) ‘Drug research: from the idea to the product.’, *International journal of clinical pharmacology and therapeutics*, 35(12), pp. 541–552.

Kuss, M. A., Harms, R.,Wu, S., Wang, Y., Untrauer, J., Carlson, M. A., Duan, B. (2017) ‘Short-term hypoxic preconditioning promotes prevascularization in 3D bioprinted bone constructs with stromal vascular fraction derived cells’, *Rsc Advances*, 7(47), pp. 29312–29320.

Lai, K. K., Renneberg, R. and Mak, W. C. (2016) ‘High efficiency single-step biomaterial-based microparticle fabrication via template-directed supramolecular coordination chemistry’, *Green Chemistry*, 18(6), pp. 1715–1723.

Langer, R. and Tirrell, D. A. (2004) ‘Designing materials for biology and medicine’, *Nature*, 428(6982), pp. 487-92.

Laronda, M. M., Duncan, F. E., Hornick, J. E., Xu, M., Pahnke, J. E., Whelan, K. A., Shea, L. D., Woodruff, T. K. (2014) ‘Alginate encapsulation supports the growth and differentiation of human primordial follicles within ovarian cortical tissue’, *Journal of Assisted Reproduction and Genetics*, 31(8), pp. 1013–1028.

Lathuilière, A., Cosson, S., Lutolf, M. P., Schneider, B. L., Aebischer, P. (2014) ‘A high-capacity cell macroencapsulation system supporting the long-term survival of genetically engineered allogeneic cells’, *Biomaterials*, 35(2), pp. 779–791.

Lathuilière, A., Bohrmann, B., Kopetzki, E., Schweitzer, C., Jacobsen, H., Moniatte, M., Aebischer, P., Schneider, B. L. (2014) ‘Genetic engineering of cell lines using lentiviral vectors to achieve antibody secretion following encapsulated implantation’, *Biomaterials*, 35(2), pp. 792–802.

Lathuilière, A., Mach, N. and Schneider, B. L. (2015) ‘Encapsulated cellular implants for recombinant protein delivery and therapeutic modulation of the immune system’,

International Journal of Molecular Sciences, 16(5), pp. 10578–10600.

Lee, J. M. and Yeong, W. Y. (2016) 'Design and Printing Strategies in 3D Bioprinting of Cell-Hydrogels: A Review', *Advanced Healthcare Materials*, 5(22), pp. 2856–2865.

Lee, K. A., Pierce, R. A., Mecham, R. P., Parks, W. C. (1994) 'Increased mesenchymal cell density accompanies induction of tropoelastin expression in developing elastic tissue', *Developmental Dynamics*, 200(1), pp. 53–67.

Lee, K. Y. and Mooney, D. J. (2012) 'Alginate: properties and biomedical applications', *Progress in polymer science*, 37(1), pp. 106–126.

Lee, P. Y., Costumbrado, J., Hsu, C. Y., Kim, Y. H. (2012) 'Agarose Gel Electrophoresis for the Separation of DNA Fragments', *Journal of Visualized Experiments*, 62, p. 3923.

Lee, V., Singh, G., Trasatti, J. P., Bjornsson, C., Xu, X., Tran, T. N., Yoo, S. S., Dai, G., Karande, P. (2013) 'Design and Fabrication of Human Skin by Three-Dimensional Bioprinting', *Tissue Engineering Part C: Methods*, 20(6), pp. 473–484.

Lee, V. K. and Dai, G. (2015) 'Three-dimensional bioprinting and tissue fabrication: prospects for drug discovery and regenerative medicine', *Advanced Health Care Technologies*, 1, pp. 23–35.

Lee, W., Debasitis J. C., Lee V. K., Lee J. H., Fischer K., Edminster K., Park J. K., Yoo S. S. (2009) 'Multi-layered culture of human skin fibroblasts and keratinocytes through three-dimensional freeform fabrication', *Biomaterials*, 30(8), pp. 1587–1595.

Lee, Y.-B., Polio, S., Lee, W., Dai, G., Menon, L., Carroll, R. S., Yoo, S. S. (2010) 'Bio-printing of collagen and VEGF-releasing fibrin gel scaffolds for neural stem cell culture', *Experimental Neurology*, 223(2), pp. 645–652.

Legant, W. R., Legant, W, R, Pathak, A., Yang, M. T., Deshpande, V. S., McMeeking, R. M., and Chen C. S. (2009) 'Microfabricated tissue gauges to measure and manipulate forces from 3D microtissues', *Proceedings of the National Academy of Sciences*, 106(25), pp. 10097–10102.

Li, B., Fan, J., Li, J., Chu J., Pan, T. (2015) 'Piezoelectric-driven droplet impact printing with an interchangeable microfluidic cartridge', *Biomicrofluidics*, 9(5), p. 54101.

Li, C., Faulkner-Jones, A., Dun, A. R., Jin, J., Chen, P., Xing, Y., Yang, Z., Li, Z., Shu,

W., Liu, D., Duncan, R. R. (2015) ‘Rapid Formation of a Supramolecular Polypeptide–DNA Hydrogel for In Situ Three-Dimensional Multilayer Bioprinting’, *Angewandte Chemie International Edition*, 54(13), pp. 3957–3961.

Li, J., Chen, M., Fan, X., Zhou, H. (2016) ‘Recent advances in bioprinting techniques: approaches, applications and future prospects’, *Journal of Translational Medicine*, 14, p. 271.

Li, W., Guan, T., Zhang, X., Wang, Z., Wang, M., Zhong, W., Feng, H., Xing, M., Kong, J. (2015) ‘The Effect of Layer-by-Layer Assembly Coating on the Proliferation and Differentiation of Neural Stem Cells’, *ACS Applied Materials & Interfaces*, 7(5), pp. 3018–3029.

Li, Y., Meng, H., Liu, Y., Lee, B. P. (2015) ‘Fibrin gel as an injectable biodegradable scaffold and cell carrier for tissue engineering’, *Scientific World Journal*, 2015, 685690.

Li, Z., Huang, S., Liu, Y., Yao, B., Hu, T., Shi, H., Xie, J., Fu, X. (2018) ‘Tuning Alginate-Gelatin Bioink Properties by Varying Solvent and Their Impact on Stem Cell Behavior’, *Scientific Reports*, 8(1), p. 8020.

Liberski, A. R., Delaney, J. T. and Schubert, U. S. (2011) ‘“One Cell−One Well”: A New Approach to Inkjet Printing Single Cell Microarrays’, *ACS Combinatorial Science*, 13(2), pp. 190–195.

Lim, F. and Sun, A. M. (1980) ‘Microencapsulated islets as bioartificial endocrine pancreas’, *Science*, 210(4472), pp. 908–910.

Litvinov, R. I. and Weisel, J. W. (2016) ‘What Is the Biological and Clinical Relevance of Fibrin?’, *Seminars in thrombosis and hemostasis*, 42(4), pp. 333–343.

Liu, A. S. *et al.* (2016) ‘Matrix viscoplasticity and its shielding by active mechanics in microtissue models: Experiments and mathematical modeling’, *Scientific Reports*, 6.

Liu, F., Malaval, L. and Aubin, J. E. (1997) ‘The mature osteoblast phenotype is characterized by extensive plasticity’, *Experimental Cell Research*, 232(1), pp. 97–105.

Liu, W., Zhang, Y. S., Heinrich, M. A., De Ferrari, M., Jang, H. L., Bakht, M. S., Alvarez, M. M., Yang, J., Li, Y-C., Trujillo-de Santiago, G., Miri, A. K., Zhu, K., Khoshakhlagh, P., Prakash, G., Cheng, H., Guan, X., Zhong, Z., Ju, J., Harry, G., Xiangyu, J., Shin, S. R., Dokmeci, M. R., Khademhosseini, A. (2016) ‘Rapid Continuous

Multimaterial Extrusion Bioprinting', *Advanced Materials*, 29(3), p. 1604630.

Liu, W., Heinrich, M. A., Zhou, Y., Akpek, A., Hu, N., Liu, X., Guan, X., Zhong, Z., Jin, X., Khademhosseini, A., Zhang, Y. S. (2017) 'Extrusion Bioprinting of Shear-Thinning Gelatin Methacryloyl Bioinks', *Advanced Healthcare Materials*, 6(12), p. 1601451.

Livoti, C. M. and Morgan, J. R. (2010) 'Self-Assembly and Tissue Fusion of Toroid-Shaped Minimal Building Units', *Tissue Engineering. Part A*, 16(6), pp. 2051–2061.

Lode, J. S., Ahlfeld, T., Adolph, M., Kümmritz, S., Steingroewer, J., Krujatz, F., Bley, T., Gelinsky, M., Lode, A. (2017) 'Green bioprinting: extrusion-based fabrication of plant cell-laden biopolymer hydrogel scaffolds', *Biofabrication*, 9(4), p. 45011.

Lodish, H., Berk, A., Zipursky, S. L., Matsudaira, P., Baltimore, D., Darnell, J, eds., (2000) 'Molecular Cell Biology. 4th edition.', in *New York: W. H. Freeman*.

Luo, F., Hou, T. Y., Zhang, Z. H., Xie, Z., Wu, X. H., Xu, J. Z. (2013) 'Effects of Initial Cell Density and Hydrodynamic Culture on Osteogenic Activity of Tissue-Engineered Bone Grafts', *PLoS ONE*, 8(1).

Lutolf, M. P. and Hubbell, J. A. (2005) 'Synthetic biomaterials as instructive extracellular microenvironments for morphogenesis in tissue engineering', *Nature Biotechnology*., 23(1), pp. 47-55.

Ma, L., Zhou, C., Lin, B., Li, W. (2010) 'A porous 3D cell culture micro device for cell migration study', *Biomedical Microdevices*, 12(4), pp. 753–760.

Ma, Y., Zhang, Y., Wang, Y., Wang, Q., Tan, M., Liu, Y., Chen, L., Li, N., Yu, W., Ma, X. (2013) 'Study of the effect of membrane thickness on microcapsule strength, permeability, and cell proliferation', *Journal of Biomedical Materials Research - Part A*, 101(4), pp. 1007–1015.

Di Maggio, N., Piccinini, E., Jaworski, M., Trumpp, A., Wendt, D. J., Martin, I. (2011) 'Toward modeling the bone marrow niche using scaffold-based 3D culture systems', *Biomaterials*, 32(2), pp. 321–329.

Malda, J., Visser, J., Melchels, F. P., Jüngst, T., Hennink, W. E., Dhert, W. J., Groll, J., Hutmacher, D. W. (2013) '25th Anniversary Article: Engineering Hydrogels for Biofabrication', *Advanced Materials*, 25(36), pp. 5011–5028.

Visser, J., Peters, B., Burger, T. J., Boomstra, J., Dhert, W. J., Melchels, F. P., Malda J. (2013) 'Biofabrication of multi-material anatomically shaped tissue constructs', *Biofabrication*, 5(3), p. 35007.

Schuurman, W., Khristov, V., Pot, M. W., van Weeren, P. R., Dhert, W. J., Malda, J. (2011) 'Bioprinting of hybrid tissue constructs with tailorable mechanical properties', *Biofabrication*, 3(2), p. 21001.

Mandrycky, C., Wang, Z., Kim, K., Kim, D. (2016) '3D Bioprinting for Engineering Complex Tissues', *Biotechnology advances*, 34(4), pp. 422–434.

Manojlovic, V., Djonlagic, J., Obradovic, B., Nedovic, V., Bugarski, B. (2006) 'Immobilization of cells by electrostatic droplet generation: A model system for potential application in medicine', *International Journal of Nanomedicine*, 1(2), pp. 163–171.

Lorber, B., Hsiao, W-K., Hutchings, I. M., Martin, K. R. (2014) 'Adult rat retinal ganglion cells and glia can be printed by piezoelectric inkjet printing', *Biofabrication*, 6(1), p. 15001.

Martinez-Quintanilla, J., He, D., Wakimoto, H., Alemany, R., Shah, K. (2015) 'Encapsulated stem cells loaded with hyaluronidase-expressing oncolytic virus for brain tumor therapy', *Mol Ther*, 23(1), pp. 108–118.

Levato, R., Visser, J., Planell, J. A., Engel, E., Malda, J., Mateos-Timoneda, M. A. (2014) 'Biofabrication of tissue constructs by 3D bioprinting of cell-laden microcarriers', *Biofabrication*, 6(3), p. 35020.

Matsusaki, M., Sakaue, K., Kadowaki, K., Akashi, M. (2012) 'Three-Dimensional Human Tissue Chips Fabricated by Rapid and Automatic Inkjet Cell Printing', *Advanced Healthcare Materials*, 2(4), pp. 534–539.

Mazzitelli, S., Borgatti, M., Breveglieri, G., Gambari, R., Nastruzzi, C. (2011) 'Encapsulation of eukaryotic cells in alginate microparticles: Cell signaling by TNF-alpha through capsular structure of cystic fibrosis cells', *Journal of Cell Communication and Signaling*, 5(2), pp. 157–165.

McBeth, C., Lauer, J., Ottersbach, M., Campbell, J., Sharon, A., Sauer-Budge, A. F. (2017) '3D bioprinting of GelMA scaffolds triggers mineral deposition by primary human osteoblasts', *Biofabrication*., 9(1), pp. 15009.

Menger, F. M., Seredyuk, V. A., Kitaeva, M. V., Yaroslavov, A. A., Melik-Nubarov, N. S. (2003) 'Migration of poly-L-lysine through a lipid bilayer', *Journal of the American Chemical Society*, 125(10), pp. 2846–2847.

Michael, S., Sorg, H., Peck, C. T., Koch, L., Deiwick, A., Chichkov, B., Vogt, P. M., Reimers, K. (2013) 'Tissue Engineered Skin Substitutes Created by Laser-Assisted Bioprinting Form Skin-Like Structures in the Dorsal Skin Fold Chamber in Mice', *PLOS ONE*, 8(3), e57741.

Miller, E. D., Phillippi, J. A., Fisher, G. W., Campbell, P. G., Walker, L. M., Weiss, L. E. (2009) 'Inkjet Printing of Growth Factor Concentration Gradients and Combinatorial Arrays Immobilized on Biologically-Relevant Substrates', *Combinatorial Chemistry & High Throughput Screening*, 12(6), pp. 604–618.

Miller, J. S. (2014) 'The Billion Cell Construct: Will Three-Dimensional Printing Get Us There?', *PLOS Biology*, 12(6), e1001882.

Mironov, V., Kasyanov, V., Drake, C., Markwald, R. R. (2007) 'Organ printing: promises and challenges', *Regenerative Medicine*, 3(1), pp. 93–103.

Mironov, V., Visconti, R. P., Kasyanov, V., Forgacs, G., Drake, C. J., Markwald, R. R. (2009) 'Organ printing: Tissue spheroids as building blocks', *Biomaterials*, 30(12), pp. 2164–2174.

Mishra, M. (2015) *Handbook of Encapsulation and Controlled Release*, CRC Press.

Montalbano, G., Toumpaniari, S., Popov, A., Duan, P., Chen, J., Dalgarno, K., Scott III, W. E., Ferreira, A. M.*et al.* (2018) 'Synthesis of bioinspired collagen/alginate/fibrin based hydrogels for soft tissue engineering', *Materials Science and Engineering C*, 91, pp. 236–246.

Morouço, P., Lattanzi, W., Alves, N. (2017) 'Four-Dimensional Bioprinting As a New Era for Tissue Engineering and Regenerative Medicine', *Frontiers in Bioengineering and Biotechnology*, 5(61), pp. 1-3.

Morrow, J. J. and Khanna, C. (2015) 'Osteosarcoma Genetics and Epigenetics: Emerging Biology and Candidate Therapies.', *Critical reviews in oncogenesis*, 20(3–4), pp. 173–97.

Mosaad, E. O., Chambers, K. F., Futrega, K., Clements, J. A., Doran, M. R. (2018) 'The Microwell-mesh: A high-throughput 3D prostate cancer spheroid and drug-testing

platform', *Scientific Reports*, 8(1), 253.

Murphy, C. M., Haugh, M. G.,O'Brien, F. J. (2010) 'The effect of mean pore size on cell attachment, proliferation and migration in collagen–glycosaminoglycan scaffolds for bone tissue engineering', *Biomaterials*, 31(3), pp. 461–466.

Murphy, S. V and Atala, A. (2014) '3D bioprinting of tissues and organs', *Nature Biotechnology*, 32, pp. 773-785.

Murua, A., Portero, A., Orive, G., Hernández, R. M., de Castro, M., Pedraz, J. L. (2008) 'Cell microencapsulation technology: Towards clinical application', *Journal of Controlled Release*, 132(2), pp. 76–83.

Nafea, E. H., Poole-Warren, L. A. and Martens, P. J. (2011) 'Immunoisolating semi-permeable membranes for cell encapsulation: Focus on hydrogels', *Journal of Controlled Release*, 154(2), pp. 110–122.

Nair, K., Gandhi, M., Khalil, S., Yan, K. C., Marcolongo, M., Barbee, K., Sun,W. (2009) 'Characterization of cell viability during bioprinting processes', *Biotechnology Journal*, 4(8), pp. 1168–1177.

Nakamura, M., Kobayashi, A., Takagi, F., Watanabe, A., Hiruma, Y., Ohuchi, K., Iwasaki, Y., Horie, M., Morita, I., Takatani, S. (2005) 'Biocompatible Inkjet Printing Technique for Designed Seeding of Individual Living Cells', *Tissue Engineering*, 11(11–12), pp. 1658–1666.

Nelson, C. M., Chen, C. S. (2002) 'Cell-cell signaling by direct contact increases cell proliferation via a PI3K-dependent signal', *FEBS Letters*, 514(2–3), pp. 238–242.

Némethová, V., Lacík, I., Rázga, F. (2017) 'Vibration technology for cell encapsulation: Viscosity as the Achilles heel', *Chemical Papers*, 71(9), pp. 1563–1567.

Nerem, R. M., Schutte, S. C. (2014) 'Chapter 2 - The Challenge of Imitating Nature', Lanza, R., Langer, R., and Vacanti, J., eds, Academic Press, pp. 9–24.

Ng, W. L., Lee, J. M., Yeong, W. Y., Naing M. W. (2017) 'Microvalve-based bioprinting – process, bio-inks and applications', *Biomaterials Science*, 5(4), pp. 632–647.

Ng, W. L., Yeong, W. Y.,Naing, M. W. (2016) 'Polyelectrolyte gelatin-chitosan hydrogel optimized for 3D bioprinting in skin tissue engineering', *International Journal of*

Bioprinting, 2(0).

Ng, W. L., Yeong, W. Y., Win Naing, M. (2016) 'Microvalve bioprinting of cellular droplets with high resolution and consistency', *2nd International Conference on Progress in Additive Manufacturing (Pro-AM 2016)*, Singapore.

Nichol, J. W., Koshy, S. T., Bae, H., Hwang, C. M., Yamanlar, S., Khademhosseini, A. (2010) 'Cell-laden microengineered gelatin methacrylate hydrogels', *Biomaterials*, 31(21), pp. 5536–5544.

Nicodemus, G. D. and Bryant, S. J. (2008) 'Cell Encapsulation in Biodegradable Hydrogels for Tissue Engineering Applications', *Tissue Engineering Part B: Reviews*, 14(2), pp. 149–165.

Ning, L. and Chen, X. (2017) 'A brief review of extrusion-based tissue scaffold bio-printing', *Biotechnology Journal*., 12(8), p. 1600671.

Nakamura, M., Iwanaga, S., Henmi, C., Arai, K., Nishiyama, Y. (2010) 'Biomatrices and biomaterials for future developments of bioprinting and biofabrication', *Biofabrication*, 2(1), 14110.

Norotte, C., Marga, F. S., Niklason, L. E., Forgacs, G. (2009) 'Scaffold-free vascular tissue engineering using bioprinting', *Biomaterials*, 30(30), pp. 5910–5917.

O'Brien, F. J. (2011) 'Biomaterials & scaffolds for tissue engineering', *Materials Today*, 14(3), pp. 88–95.

Odde, D. J. and Renn, M. J. (1999) 'Laser-guided direct writing for applications in biotechnology', *Trends in Biotechnology*, 17(10), pp. 385–389.

Okubo, N., Quershi, A. J., Derebail, S., Dalgarno, K., Goh, K L. (2016) 'Cost effective open source microvalve bioprinting of therapeutic cells', *Front. Bioeng. Biotechnol. Conference Abstract: 6th Malaysian Tissue Engineering and Regenerative Medicine Scientific Meeting (6th MTERMS) 2016 and 2nd Malaysian Stem Cell Meeting*.

Olabisi, R. M. (2015) 'Cell microencapsulation with synthetic polymers', *Journal of Biomedical Materials Research - Part A*, 103(2), pp. 846–859.

Oliveira, M. B., Kossover, O., Mano, J. F., Seliktar, D. (2015) 'Injectable PEGylated fibrinogen cell-laden microparticles made with a continuous solvent- and oil-free

preparation method', *Acta Biomaterialia*, 13, pp. 78–87.

Olsen, D., Yang, C., Bodo, M., Chang, R., Leigh, S., Baez, J., Carmichael, D., Perälä, M., Hämäläinen, E. R., Jarvinen, M., Polarek, J. (2003) 'Recombinant collagen and gelatin for drug delivery', *Advanced Drug Delivery Reviews*, 55(12), pp. 1547–1567.

Onoe, H., Okitsu, T., Itou, A., Kato-Negishi, M., Gojo, R., Kiriya, D., Sato, K., Miura, S., Iwanaga, S., Kuribayashi-Shigetomi, K., Matsunaga, Y. T., Shimoyama, Y., Takeuchi, S. (2013) 'Metre-long cell-laden microfibres exhibit tissue morphologies and functions', *Nature Materials*, 12(6), pp. 584–590.

Orive, G., Hernández, R. M., Hernández, R. M, Gascón, A. R., Calafiore, R., Chang, T. M., De Vos, P., Hortelano, G., Hunkeler, D., Lacík, I., Shapiro, A. M., Pedraz, J. L. *et al.* (2003) 'Cell encapsulation: Promise and progress', *Nature Medicine*, 9(1), pp. 104–107.

Orive, G., Gascón, A. R., Gascón, A. R, Hernández, R. M., Igartua, M., Pedraz, J. L. (2003) 'Cell microencapsulation technology for biomedical purposes: Novel insights and challenges', *Trends in Pharmacological Sciences*, 24(5), pp. 207–210.

Orive, G., Hernández, R. M., Gascón, A. R., Calafiore, R., Chang, T. M., de Vos, P., Hortelano, G., Hunkeler, D., Lacík, I., Pedraz, J. L. (2004) 'History, challenges and perspectives of cell microencapsulation', *Trends in Biotechnology*, 22(2), pp. 87–92.

Orive, G., Santos, E., Poncelet, D., Hernández, R. M., Pedraz, J. L., Wahlberg, L. U., De Vos, P., Emerich, D. (2015) 'Cell encapsulation: technical and clinical advances', *Trends in Pharmacological Sciences*, 36(8), pp. 537–546.

Orlando, G., Gianello, P., Salvatori, M., Stratta, R. J., Soker, S., Ricordi, C., Domínguez-Bendala, J. (2014) 'Cell replacement strategies aimed at reconstitution of the β-cell compartment in type 1 diabetes', *Diabetes*, 63(5), pp. 1433–1444.

Osorio, F. A., Bilbao, E., Bustos, R., Alvarez, F. (2007) 'Effects of Concentration, Bloom Degree, and pH on Gelatin Melting and Gelling Temperatures Using Small Amplitude Oscillatory Rheology', *International Journal of Food Properties*, 10(4), pp. 841–851.

Hölzl, K., Lin, S., Tytgat, L., Van Vlierberghe, S., Gu, L., Ovsianikov, A. (2016) 'Bioink properties before, during and after 3D bioprinting', *Biofabrication*, 8(3), p. 32002.

Ozbolat, I. and Gudapati, H. (2016) 'A review on design for bioprinting', *Bioprinting*, 3–4, pp. 1–14.

Ozbolat, I. T. (2015) ‘Scaffold-Based or Scaffold-Free Bioprinting: Competing or Complementing Approaches?’, *Journal of Nanotechnology in Engineering and Medicine*, 6(2), pp. 24701–24706.

Ozbolat, I. T. (2017) ‘5 - Droplet-Based Bioprinting’, *3D Bioprinting*, Academic Press, pp. 125–163.

Ozbolat, I. T. and Hospodiuk, M. (2016) ‘Current advances and future perspectives in extrusion-based bioprinting’, *Biomaterials*, 76, pp. 321–343.

Park, J. A., Yoon, S., Kwon, J., Now, H., Kim, Y. K., Kim, W-J., Yoo, J-Y., Jung, S. (2017) ‘Freeform micropatterning of living cells into cell culture medium using direct inkjet printing’, *Scientific Reports*, 7(1), 14610.

Park, J. H., Kim, K., Lee, J., Choi, J. Y., Hong, D., Yang, S. H., Caruso, F., Lee, Y., Choi, I. S. (2014) ‘A cytoprotective and degradable metal-polyphenol nanoshell for single-cell encapsulation’, *Angewandte Chemie - International Edition*, 53(46), pp. 12420–12425.

Pati, F., Jang, J., Ha, D-H., Kim, S. W., Rhie, J-W., Shim, J-H., Kim, D-H., Cho, D-W. (2014) ‘Printing three-dimensional tissue analogues with decellularized extracellular matrix bioink’, *Nature Communications*, 5, 3935.

Pati, F., Ha, D-H., Jang, J., Han, H. H., Rhie, J-W., Cho, D-W. (2015) ‘Biomimetic 3D tissue printing for soft tissue regeneration’, *Biomaterials*, 62, pp. 164–175.

Pati, F., Gantelius, J. and Svahn, H. A. (2016) ‘3D Bioprinting of Tissue/Organ Models’, *Angewandte Chemie International Edition*, 55(15), pp. 4650–4665.

Patra, S. and Young, V. (2016) ‘A Review of 3D Printing Techniques and the Future in Biofabrication of Bioprinted Tissue’, *Cell Biochemistry and Biophysics*, 74(2), pp. 93–98.

Paulo, B. B., Ramos, F. de M. and Prata, A. S. (2017) ‘An investigation of operational parameters of jet cutting method on the size of Ca-alginate beads’, *Journal of Food Process Engineering*, 40(6).

Paxton, N., Smolan, W., Böck, T., Melchels, F., Groll, J., Jungst, T. (2017) ‘Proposal to assess printability of bioinks for extrusion-based bioprinting and evaluation of rheological properties governing bioprintability’, *Biofabrication*, 9(4), p. 44107.

Peng, W., Datta, P., Ayan, B., Ozbolat, V., Sosnoski, D., Ozbolat, I. T. (2017) ‘3D

bioprinting for drug discovery and development in pharmaceutics', *Acta Biomaterialia*, 57, pp. 26–46.

Perán, M., García, M. A., López-Ruiz, E., Bustamante, M., Jiménez, G., Madeddu, R., Marchal, J. A. (2012) 'Functionalized nanostructures with application in regenerative medicine', *International Journal of Molecular Sciences*, 13(3), pp. 3847–3886.

Pereira, R. F., Bartolo, P. J. (2015) '3D Photo-Fabrication for Tissue Engineering and Drug Delivery', *Engineering*, 1(1), pp. 90-112.

Pereira, R. F., Sousa, A., Barrias, C. C., Bartolo, P. J., Granja, P. L. (2018) 'A single-component hydrogel bioink for bioprinting of bioengineered 3D constructs for dermal tissue engineering', *Material Horizons*, 5, pp. 1100-1111.

Pfister, A., Landers, R., Laib, A., Hübner, U., Schmelzeisen, R., Mülhaupt, R. (2003) 'Biofunctional rapid prototyping for tissue-engineering applications: 3D bioplotting versus 3D printing', *Journal of Polymer Science Part A: Polymer Chemistry*., 42(3), pp. 624–638.

Piechocka, I. K., Bacabac, R. G., Potters, M., Mackintosh, F. C., Koenderink, G.H. (2010) 'Structural hierarchy governs fibrin gel mechanics', *Biophysical journal*, 98(10), pp. 2281–2289.

Place, E. S., George, J. H., Williams, C. K., Stevens, M. M. (2009) 'Synthetic polymer scaffolds for tissue engineering', *Chemical Society Reviews*, 38(4), pp. 1139–1151.

Place, E. S., Evans, N. D. and Stevens, M. M. (2009) 'Complexity in biomaterials for tissue engineering', *Nature Materials*, 8(6), p. 457-470.

Prescher, J. A. and Bertozzi, C. R. (2005) 'Chemistry in Living Systems', *Nature Chemical Biology*, 1(1), pp. 13–21.

Rabanel, J. M., Banquy, X., Zouaoui, H., Mokhtar, M., Hildgen, P. (2009) 'Progress technology in microencapsulation methods for Cell therapy', *Biotechnology Progress*, 25(4), pp. 946–963.

Rabuka, D., Forstner, M. B., Groves, J. T., Bertozzi, C. R. (2008) 'Noncovalent cell surface engineering: Incorporation of bioactive synthetic glycopolymers into cellular membranes', *Journal of the American Chemical Society*, 130(18), pp. 5947–5953.

Rakszewska, A., Tel, J., Chokkalingam, V., Huck, W. T. (2014) ‘One drop at a time: Toward droplet microfluidics as a versatile tool for single-cell analysis’, *NPG Asia Materials*, 6(10), e133.

Ratcliffe, A. and Niklason, L. E. (2002) ‘Bioreactors and bioprocessing for tissue engineering’, *Annals of the New York Academy of Sciences*, 961, pp. 210–215.

Rathore, S., Desai, P. M., Liew, C. V., Chan, L. W., Heng, P. W. (2013) ‘Microencapsulation of microbial cells’, *Journal of Food Engineering*, 116(2), pp. 369–381.

Reig, G., Pulgar, E. and Concha, M. L. (2014) ‘Cell migration: from tissue culture to embryos’, *Development*, 141(10), pp. 1999-2013.

Rengier, F., Mehndiratta, A., von Tengg-Kobligk, H., Zechmann, C. M., Unterhinninghofen, R., Kauczor, H. U., Giesel, F. L. (2010) ‘3D printing based on imaging data: review of medical applications’, *International Journal of Computer Assisted Radiology and Surgery*, 5(4), pp. 335–341.

Ribeiro, R. D. C., Pal, D., Jamieson, D., Rankin, K. S., Benning, M., Dalgarno, K. W., Ferreira, A. M. (2017) ‘Temporary Single-Cell Coating for Bioprocessing with a Cationic Polymer’, *ACS Applied Materials and Interfaces*, 9(15).

Rørth, P. (2003) ‘Communication by Touch’, *Cell*, 112(5), pp. 595–598.

Rose, J. B., Pacelli, S., Haj, A. J. E., Dua, H. S., Hopkinson, A., White, L. J., Rose, F. R. A. J. (2014) ‘Gelatin-Based Materials in Ocular Tissue Engineering’, *Materials*. MDPI, 7(4), pp. 3106–3135.

Roth, E. A., Xu, T., Das, M., Gregory, C., Hickman, J. J., Boland, T. (2004) ‘Inkjet printing for high-throughput cell patterning’, *Biomaterials*, 25(17), pp. 3707–3715.

Ryan, E. A., Lakey, J. R., Paty, B. W., Imes, S., Korbutt, G. S., Kneteman, N. M., Bigam, D., Rajotte, R. V., Shapiro, A. M. (2002) ‘Successful islet transplantation: Continued insulin reserve provides long-term glycemic control’, *Diabetes*, 51(7), pp. 2148–2157.

Reid, J. A., Mollica, P. A., Johnson, G. D., Ogle, R. C., Bruno, R. D., Sachs, P. C. (2016) ‘Accessible bioprinting: adaptation of a low-cost 3D-printer for precise cell placement and stem cell differentiation’, *Biofabrication*, 8(2), p. 25017.

Saha, K., Pollock, J. F., Schaffer, D. V., Healy, K. E. (2007) ‘Designing synthetic materials to control stem cell phenotype’, *Current opinion in chemical biology*, 11(4), pp. 381–387.

Sánchez, P., Hernández, R. M., Pedraz, J. L., Orive, G. (2013) ‘Encapsulation of cells in alginate gels’, *Methods in Molecular Biology*, 1051, pp. 313–325.

Saunders, R. E. and Derby, B. (2014) ‘Inkjet printing biomaterials for tissue engineering: bioprinting’, *International Materials Reviews*, 59(8), pp. 430–448.

Saunders, R. E., Gough, J. E. and Derby, B. (2008) ‘Delivery of human fibroblast cells by piezoelectric drop-on-demand inkjet printing’, *Biomaterials*, 29(2), pp. 193–203.

Scharp, D. W. and Marchetti, P. (2014) ‘Encapsulated islets for diabetes therapy: History, current progress, and critical issues requiring solution’, *Advanced Drug Delivery Reviews*, 67–68, pp. 35–73.

Schop, D., Janssen, F. W., Borgart, E., de Bruijn, J. D., van Dijkhuizen-Radersma, R. (2008) ‘Expansion of mesenchymal stem cells using a microcarrier-based cultivation system: growth and metabolism’, *Journal of Tissue Engineering and Regenerative Medicine*, 2(2-3), pp. 126–135.

Schuurman, W., Levett, P. A., Pot, M. W., van Weeren, P. R., Dhert, W. J., Hutmacher, D. W., Melchels, F. P., Klein, T. J., Malda, J. (2013) ‘Gelatin-Methacrylamide Hydrogels as Potential Biomaterials for Fabrication of Tissue-Engineered Cartilage Constructs’, *Macromolecular Bioscience*, 13(5), pp. 551–561.

Schwenter, F., Zarei, S., Luy, P., Padrun, V., Bouche, N., Lee, J. S., Mulligan, R. C., Morel, P., Mach, N. (2011) ‘Cell encapsulation technology as a novel strategy for human anti-tumor immunotherapy’, *Cancer Gene Therapy*, 18(8), pp. 553-562.

Selimović, Š., Oh, J., Bae, H., Dokmeci, M., Khademhosseini, A. (2012) ‘Microscale strategies for generating cell-encapsulating hydrogels’, *Polymers*, 4(3), pp. 1554–1579.

Senuma, Y., Lowe, C., Zweifel, Y., Hilborn, J. G., Marison, I. (2000) ‘Alginate hydrogel microspheres and microcapsules prepared by spinning disk atomization’, *Biotechnology and Bioengineering*, 67(5), pp. 616–622.

Seol, Y.-J., Kang, H. W., Lee, S. J., Atala, A., Yoo, J. J. (2014) ‘Bioprinting technology and its applications’, *European Journal of Cardio-Thoracic Surgery*, 46(3), pp. 342–348.

Serra, M., Correia, C., Malpique, R., Brito, C., Jensen, J., Bjorquist, P., Carrondo, M. J., Alves, P. M. (2011) 'Microencapsulation technology: A powerful tool for integrating expansion and cryopreservation of human embryonic stem cells', *PLoS ONE*, 6(8), e23212.

Sharif, G. M., Sharif, G. M., Schmidt, M. O., Yi, C., Hu, Z., Haddad, B. R., Glasgow, E., Riegel, A. T., Wellstein, A. (2015) 'Cell growth density modulates cancer cell vascular invasion via Hippo pathway activity and CXCR2 signaling', *Oncogene*, 34(48), pp. 5879–5889.

Shirahama, H., Shirahama, H., Lee, B. H., Tan, L. P., Cho, N. J. (2016) 'Precise Tuning of Facile One-Pot Gelatin Methacryloyl (GelMA) Synthesis', *Scientific Reports*, 6, 31036.

Shoulders, M. D. and Raines, R. T. (2009) 'Collagen Structure and Stability', *Annual Review of Biochemistry*, 78(1), pp. 929–958.

Faulkner-Jones, A., Fyfe, C., Cornelissen, D. J., Gardner, J., King, J., Courtney, A., Shu, W. (2015) 'Bioprinting of human pluripotent stem cells and their directed differentiation into hepatocyte-like cells for the generation of mini-livers in 3D', *Biofabrication*, 7(4), 44102.

Faulkner-Jones, A., Greenhough, S., King, J. A., Gardner, J., Courtney, A., Shu, W. (2013) 'Development of a valve-based cell printer for the formation of human embryonic stem cell spheroid aggregates', *Biofabrication*, 5(1), 15013.

Singh, M., Haverinen, H. M., Dhagat, P., Jabbour, G. E. (2009) 'Inkjet Printing—Process and Its Applications', *Advanced Materials*, 22(6), pp. 673–685.

Skardal, A., Mack, D., Kapetanovic, E., Atala, A., Jackson, J. D., Yoo, J., Soker, S. (2012) 'Bioprinted Amniotic Fluid-Derived Stem Cells Accelerate Healing of Large Skin Wounds', *Stem cells translational medicine*, 1(11), pp. 792–802.

Skardal, A., Devarasetty, M., Kang, H. W., Mead, I., Bishop, C., Shupe, T., Lee, S. J., Jackson, J., Yoo, J., Soker, S., Atala, A. (2015) 'A hydrogel bioink toolkit for mimicking native tissue biochemical and mechanical properties in bioprinted tissue constructs', *Acta Biomaterialia*, 25, pp. 24–34.

Skardal, A. and Atala, A. (2015) 'Biomaterials for Integration with 3-D Bioprinting',

Annals of Biomedical Engineering, 43(3), pp. 730–746.

Skardal, A., Zhang, J. and Prestwich, G. D. (2010) 'Bioprinting vessel-like constructs using hyaluronan hydrogels crosslinked with tetrahedral polyethylene glycol tetracrylates', *Biomaterials*, 31(24), pp. 6173–6181.

Skrzypek, K., Nibbelink, M. G., van Lente, J., Buitinga, M., Engelse, M. A., de Koning, E. J. P., Karperien, M., van Apeldoorn, A., Stamatialis, D. (2017) 'Pancreatic islet macroencapsulation using microwell porous membranes', *Scientific Reports*, 7(1), 9186.

Slaughter, B. V., Khurshid, S. S., Fisher, O. Z., Khademhosseini, A., Peppas, N. A. (2009) 'Hydrogels in Regenerative Medicine', *Advanced Materials*, 21, pp. 3307–3329.

Tse, C., Whiteley, R., Yu, T., Stringer, J., MacNeil, S., Haycock, J. W., Smith, P. J. (2016) 'Inkjet printing Schwann cells and neuronal analogue NG108-15 cells', *Biofabrication*, 8(1), 15017.

Smith, G. F. (1980) 'Fibrinogen–fibrin conversion. The mechanism of fibrin-polymer formation in solution', *Biochemical Journal*, 185(1), pp. 1–11.

Song, S. and Roy, S. (2016) 'Progress and challenges in macroencapsulation approaches for type 1 diabetes (T1D) treatment: Cells, biomaterials, and devices', *Biotechnology and Bioengineering*, 113(7), pp. 1381–1402.

Sorkio, A., Koch, L., Koivusalo, L., Deiwick, A., Miettinen, S., Chichkov, B., Skottmana, H. (2018) 'Human stem cell based corneal tissue mimicking structures using laser-assisted 3D bioprinting and functional bioinks', *Biomaterials*, 171, pp. 57–71.

de Souza, N. (2018) 'Organoids', *Nature Methods*, 15, p. 23.

Stanton, M. M., Samitier, J. and Sánchez, S. (2015) 'Bioprinting of 3D hydrogels', *Lab on a Chip*, 15(15), pp. 3111–3115.

Steele, J. A. M., Hallé, J. P., Poncelet, D., Neufeld, R. J. (2014) 'Therapeutic cell encapsulation techniques and applications in diabetes', *Advanced Drug Delivery Reviews*, 67–68, pp. 74–83.

Stellwagen, N. C. (2009) 'Electrophoresis of DNA in agarose gels, polyacrylamide gels and in free solution', *Electrophoresis*, 30 (Suppl 1), pp. S188–S195.

Stratesteffen, H., Köpf, M., Kreimendahl, F., Blaeser, A., Jockenhoevel, S., Fischer, H.

(2017) ‘GelMA-collagen blends enable drop-on-demand 3D printablility and promote angiogenesis’, *Biofabrication*, 9(4), 045002.

Streichan, S. J., Hoerner, C. R., Schneidt, T., Holzer, D., Hufnagel, L. (2014) ‘Spatial constraints control cell proliferation in tissues.’, *Proceedings of the National Academy of Sciences of the United States of America*, 111(15), pp. 5586–91.

Su, J., Hu, B. H., Lowe, W. L., Kaufman, D. B., Messersmith, P. B. (2010) ‘Anti-Inflammatory Peptide Functionalized Hydrogels for Insulin-Secreting Cell Encapsulation’, *Biomaterials*, 31(2), pp. 308–314.

Sun, J., Ng, J. H., Fuh, Y. H., Wong, Y. S., Loh, H. T., Xu, Q. (2009) ‘Comparison of micro-dispensing performance between micro-valve and piezoelectric printhead’, *Microsystem Technologies*, 15(9), pp. 1437–1448.

Suntornnond, R., Tan, E. Y. S., An, J., Chua, C. K. (2017) ‘A highly printable and biocompatible hydrogel composite for direct printing of soft and perfusable vasculature-like structures’, *Scientific Reports*, 7(1), 16902.

Suntornnond, R., An, J. and Chua, C. K. (2016) ‘Bioprinting of Thermoresponsive Hydrogels for Next Generation Tissue Engineering: A Review’, *Macromolecular Materials and Engineering*, 302(1), 1600266.

Tan, Y. J., Tan, X., Yeong, W. Y., Tor, S. B. (2016) ‘Hybrid microscaffold-based 3D bioprinting of multi-cellular constructs with high compressive strength: A new biofabrication strategy’, *Scientific Reports*, 6, 39140.

Tarassoli, S. P., Jessop, Z. M., Kyle, S., Whitaker, I. (2018) ‘8 - Candidate bioinks for 3D bioprinting soft tissue’, *3D Bioprinting for Reconstructive Surgery - Techniques and Applications*, Jessop, Z. M., Kyle, S., Whitaker, eds, Woodhead Publishing, pp. 145–172.

Tasoglu, S. and Demirci, U. (2013) ‘Bioprinting for stem cell research’, *Trends in Biotechnology*, 31(1), pp. 10–19.

Teunou, E. and Poncelet, D. (2005) ‘Rotary disc atomisation for microencapsulation applications-prediction of the particle trajectories’, *Journal of Food Engineering*, 71(4), pp. 345–353.

Thakuri, P. S., Liu, C., Luker, G. D., Tavana, H. (2017) ‘Biomaterials-Based Approaches to Tumor Spheroid and Organoid Modeling’, *Advanced Healthcare Materials*, 7(6),

1700980.

Thayer, P. S., Orrhult, L. S. and Martínez, H. (2018) ‘Bioprinting of Cartilage and Skin Tissue Analogs Utilizing a Novel Passive Mixing Unit Technique for Bioink Precellularization’, *Journal of Visualized Experiments*, 131, 56372.

Thibault, R. J., Hotchkiss, P. J., Gray, M., Rotello, V. M. (2003) ‘Thermally reversible formation of microspheres through non-covalent polymer cross-linking’, *Journal of the American Chemical Society*, 125(37), pp. 11249–11252.

Thoma, C. R., Zimmermann, M., Agarkova, I., Kelm, J. M., Krek, W. (2014) ‘3D cell culture systems modeling tumor growth determinants in cancer target discovery’, *Advanced Drug Delivery Reviews*, 69–70, pp. 29–41.

Thomas, A., Müller, S. S. and Frey, H. (2014) ‘Beyond Poly(ethylene glycol): Linear Polyglycerol as a Multifunctional Polyether for Biomedical and Pharmaceutical Applications’, *Biomacromolecules*, 15(6), pp. 1935–1954.

Thomas, M. and Willerth, S. M. (2017) ‘3-D Bioprinting of Neural Tissue for Applications in Cell Therapy and Drug Screening’, *Frontiers in Bioengineering and Biotechnology*, 5, 69.

Tibbitt, M. W. and Anseth, K. S. (2009) ‘Hydrogels as Extracellular Matrix Mimics for 3D Cell Culture’, *Biotechnology and bioengineering*, 103(4), pp. 655–663.

Tomeit, A. A., Villa, C. and Ricordi, C. (2015) ‘Development of an encapsulated stem cell-based therapy for diabetes’, *Expert Opinion on Biological Therapy*, 15(9), pp. 1321–1336.

Tønnesen, H. H. and Karlsen, J. (2002) ‘Alginate in Drug Delivery Systems’, *Drug Development and Industrial Pharmacy*, 28(6), pp. 621–630.

Toprakhisar, B., Nadernezhad, A., Bakirci, E., Khani, N., Skvortsov, G. A., Koc, B. (2018) ‘Development of Bioink from Decellularized Tendon Extracellular Matrix for 3D Bioprinting’, *Macromolecular Bioscience*, 10(18), 1800024.

Trimaille, T., Pertici, V. and Gigmes, D. (2016) ‘Recent advances in synthetic polymer based hydrogels for spinal cord repair’, *Comptes Rendus Chimie*, 19(1), pp. 157–166.

Ullah, F., Othman, M. B., Javed, F., Ahmad, Z., Akil, H. M. (2015) ‘Classification,

processing and application of hydrogels: A review', *Materials Science and Engineering: C*, 57, pp. 414–433.

Uludag, H., De Vos, P. and Tresco, P. A. (2000) 'Technology of mammalian cell encapsulation', *Advanced Drug Delivery Reviews*, 42(1–2), pp. 29–64.

Vacanti, J. P. and Langer, R. (1999) 'Tissue engineering: the design and fabrication of living replacement devices for surgical reconstruction and transplantation', *The Lancet*, 354, pp. S32–S34.

Vacanti, J. P. and Vacanti, C. A. (2014) 'Chapter 1 - The History and Scope of Tissue Engineering', Lanza, R., Langer, R., and Vacanti, J., eds., *Principles of Tissue Engineering*, Academic Press, pp. 3–8.

Vaidyanathan, S., Anderson, K. B., Merzel, R. L., Jacobovitz, B., Kaushik, M. P., Kelly, C. N., van Dongen, M. A., Dougherty, C. A., Orr, B. G., Holl, M. M. B. (2015) 'Quantitative Measurement of Cationic Polymer Vector and Polymer-pDNA Polyplex Intercalation into the Cell Plasma Membrane', *ACS Nano*, 9(6), pp. 6097–6109.

Vaithilingam, V. and Tuch, B. E. (2011) 'Islet transplantation and encapsulation: An update on recent developments', *Review of Diabetic Studies*, 8(1), pp. 51–67.

Veiseh, O. *et al.* (2015) 'Size- and shape-dependent foreign body immune response to materials implanted in rodents and non-human primates', *Nature Materials*, 14(6), pp. 643–651.

Vercauteren, D., Vandenbroucke, R. E., Jones, A. T., Rejman, J., Demeester, J., De Smedt, S. C., Sanders, N. N., Braeckmans, K. (2010) 'The use of inhibitors to study endocytic pathways of gene carriers: Optimization and pitfalls', *Molecular Therapy*, 18(3), pp. 561–569.

Van Vlierberghe, S., Dubruel, P. and Schacht, E. (2011) 'Biopolymer-based hydrogels as scaffolds for tissue engineering applications: A review', *Biomacromolecules*, 12(5), pp. 1387–1408.

Vormoor, B., Knizia, H. K., Batey, M. A., Almeida, G. S., Wilson, I., Dildey, P., Sharma, A., Blair, H., Hide, G., Heidenreich, O., Vormoor, J., Maxwell, R. J., Bacon, C. M. (2014) 'Development of a preclinical orthotopic xenograft model of ewing sarcoma and other human malignant bone disease using advanced in vivo imaging', *PLoS ONE*, 9(1),

e85128.

De Vos, P., Spasojevic, M., de Haan, B. J., Faas, M. M. (2012) ‘The association between in vivo physicochemical changes and inflammatory responses against alginate based microcapsules’, *Biomaterials*, 33(22), pp. 5552–5559.

De Vos, P., Spasojevic, M. and Faas, M. M. (2010) ‘Treatment of diabetes with encapsulated islets’, *Advances in Experimental Medicine and Biology*, 670, pp. 38–53.

Wang, H., Zhou, L., Liao, J., Tan, Y., Ouyang, K., Ning, C., Ni, G., Tan, G. (2014) ‘Cell-laden photocrosslinked GelMA–DexMA copolymer hydrogels with tunable mechanical properties for tissue engineering’, *Journal of Materials Science: Materials in Medicine*, 25(9), pp. 2173–2183.

Wang, J.-Z., Ding, Z-Q., Zhang, F., Ye, W-B. (2017) ‘Recent development in cell encapsulations and their therapeutic applications’, *Materials Science and Engineering C*, 77, pp. 1247–1260.

Wang, K., Liu, D., Vunjak-Novakovic, G. (2015) ‘The paracrine effects of adipose-derived stem cells on neovascularization and biocompatibility of a macroencapsulation device’, *Acta Biomaterialia*, 15, pp. 65–76.

Wang, K., Hou, W. D., Wang, X., Han, C., Vuletic, I., Su, N., Zhang, W. X., Ren, Q. S., Chen, L., Luo, Y. (2016) ‘Overcoming foreign-body reaction through nanotopography: Biocompatibility and immunoisolation properties of a nanofibrous membrane’, *Biomaterials*, 102, pp. 249–258.

Wang, X., Yan, Y., Pan, Y., Xiong, Z., Liu, H., Cheng, J., Liu, F., Lin, F., Wu, R., Zhang, R., Lu, Q. (2006) ‘Generation of Three-Dimensional Hepatocyte/Gelatin Structures with Rapid Prototyping System’, *Tissue Engineering*, 12(1), pp. 83–90.

Wang, X., Ao, Q., Tian, X., Fan, J., Tong, H., Hou, W., Bai, S. (2017) ‘Gelatin-based hydrogels for organ 3D bioprinting’, *Polymers*, 9(9), 401.

Wang, Z., Abdulla, R., Parker, B., Samanipour, R., Ghosh, S., Kim, K. (2015) ‘A simple and high-resolution stereolithography-based 3D bioprinting system using visible light crosslinkable bioinks’, *Biofabrication*, 7(4), 045009.

Webb, B. and Doyle, B. J. (2017) ‘Parameter optimization for 3D bioprinting of hydrogels’, *Bioprinting*, 8, pp. 8–12.

Weisel, J. W. (2005) ‘Fibrinogen and Fibrin’, *Advances in Protein Chemistry*, , 70, pp. 247–299.

Westman, J. O., Ylitervo, P., Franzén, C. J., Taherzadeh, M. J. (2012) ‘Effects of encapsulation of microorganisms on product formation during microbial fermentations’, *Applied Microbiology and Biotechnology*, 96(6), pp. 1441–1454.

Wichterle, O. and Lim, D. (1960) ‘Hydrophilic Gel for Biological Use’, *Nature*, 185, pp. 117–118.

Wilson, J. L., Najia, M. A., Saeed, R., McDevitt, T. C. (2014) ‘Alginate encapsulation parameters influence the differentiation of microencapsulated embryonic stem cell aggregates’, *Biotechnology and Bioengineering*, 111(3), pp. 618–631.

Wilson, J. L. and Mcdevitt, T. C. (2013) ‘Stem cell microencapsulation for phenotypic control, bioprocessing, and transplantation’, *Biotechnology and Bioengineering*, 110(3), pp. 667–682.

Wilson, J. T., Krishnamurthy, V. R., Cui, W., Qu, Z., Chaikof, E. L. (2009) ‘Noncovalent cell surface engineering with cationic graft copolymers’, *Journal of the American Chemical Society*, 131(51), pp. 18228–18229.

Wilson, W. C. and Boland, T. (2003) ‘Cell and organ printing 1: Protein and cell printers’, *The Anatomical Record Part A: Discoveries in Molecular, Cellular, and Evolutionary Biology*, 272A(2), pp. 491–496.

Wipff, P. J., Majd, H., Acharya, C., Buscemi, L., Meister, J. J., Hinz, B. (2009) ‘The covalent attachment of adhesion molecules to silicone membranes for cell stretching applications’, *Biomaterials*, 30(9), pp. 1781–1789.

Wolfe, R. P. and Ahsan, T. (2013) ‘Shear stress during early embryonic stem differentiation promotes hematopoietic and enothelial phenotypes’, *Biotechnology and bioengineering*, 110(4), pp. 1231–1242.

Wong Po Foo, C. T., Lee, J. S., Mulyasasmita, W., Parisi-Amon, A., Heilshorn, S. C. (2009) ‘Two-component protein-engineered physical hydrogels for cell encapsulation’, *Proceedings of the National Academy of Sciences*, 106(52), pp. 22067–22072.

Mekhileri, N. V., Lim, K. S., Brown, G. C. J., Mutreja, I., Schon, B. S., Hooper, G. J., Woodfield, T. B. F. (2018) ‘Automated 3D bioassembly of micro-tissues for

biofabrication of hybrid tissue engineered constructs', *Biofabrication*, 10(2), 24103.

Wu, Z., Su, X., Xu, Y., Kong, B., Sun, W., Mi, S. (2016) 'Bioprinting three-dimensional cell-laden tissue constructs with controllable degradation', *Scientific Reports*, 6, 24474.

Xiao, W., He, J., Nichol, J. W., Wang, L., Hutson, C. B., Wang, B., Du, Y., Fan, H., Khademhosseini, A. (2011) 'Synthesis and characterization of photocrosslinkable gelatin and silk fibroin interpenetrating polymer network hydrogels', *Acta Biomaterialia*, 7(6), pp. 2384–2393.

Xie, A. W., Binder, B. Y. K., Khalil, A. S., Schmitt, S. K., Johnson, H. J., Zacharias, N. A., Murphy, W. L. (2017) 'Controlled Self-assembly of Stem Cell Aggregates Instructs Pluripotency and Lineage Bias', *Scientific Reports*, 7, 14070.

Xu, C., Chai, W., Huang, Y., Markwald, R. R. (2012) 'Scaffold-free inkjet printing of three-dimensional zigzag cellular tubes', *Biotechnology and Bioengineering*, 109(12), pp. 3152–3160.

Rodríguez-Dévora, J. I., Zhang, B., Reyna, D., Shi, Z. D., Xu, T. (2012) 'High throughput miniature drug-screening platform using bioprinting technology', *Biofabrication*, 4(3), 35001.

Xu, M., Wang, X., Yan, Y., Yao, R., Ge, Y. (2010) 'An cell-assembly derived physiological 3D model of the metabolic syndrome, based on adipose-derived stromal cells and a gelatin/alginate/fibrinogen matrix', *Biomaterials*, 31(14), pp. 3868–3877.

Xu, T., Gregory, C. A., Molnar, P., Cui, X., Jalota, S., Bhaduri, S. B., Boland, T. (2006) 'Viability and electrophysiology of neural cell structures generated by the inkjet printing method', *Biomaterials*, 27(19), pp. 3580–3588.

Xu, T., Zhao, W., Zhu, J. M., Albanna, M. Z., Yoo, J. J., Atala, A. (2013) 'Complex heterogeneous tissue constructs containing multiple cell types prepared by inkjet printing technology', *Biomaterials*, 34(1), pp. 130–139.

Xue, B., Kozlovskaya, V., Liu, F., Chen, J., Williams, J. F., Campos-Gomez, J., Saeed, M., Kharlampieva, E. (2015) 'Intracellular Degradable Hydrogel Cubes and Spheres for Anti-Cancer Drug Delivery', *ACS Applied Materials and Interfaces*, 7(24), pp. 13633–13644.

Yamada, K. M. and Cukierman, E. (2007) 'Modeling Tissue Morphogenesis and Cancer

in 3D', *Cell*, 130(4), pp. 601–610.

Yanez, M., Rincon, J., Dones, A., De Maria, C., Gonzales, R., Boland, T. (2015) 'In Vivo Assessment of Printed Microvasculature in a Bilayer Skin Graft to Treat Full-Thickness Wounds', *Tissue Engineering. Part A*, 21(1–2), pp. 224–233.

Yang, G., Xiao, Z., Ren, X., Long, H., Qian, H., Ma, K., Guo, Y. (2016) 'Enzymatically crosslinked gelatin hydrogel promotes the proliferation of adipose tissue-derived stromal cells', *PeerJ*, 4, p. e2497.

Yang, G., Xiao, Z., Long, H., Ma, K., Zhang, J., Ren, X., Zhang, J. (2018) 'Assessment of the characteristics and biocompatibility of gelatin sponge scaffolds prepared by various crosslinking methods', *Scientific Reports*, 8, 1616.

Yang, Q., Lian, Q. and Xu, F. (2017) 'Perspective: Fabrication of integrated organ-on-a-chip via bioprinting', *Biomicrofluidics*, 11(3), 31301.

Yang, X., Lu, Z., Wu, H., Li, W., Zheng, L., Zhao, J. (2018) 'Collagen-alginate as bioink for three-dimensional (3D) cell printing based cartilage tissue engineering', *Materials Science and Engineering: C*, 83, pp. 195–201.

Yin, J. Yan, M., Wang, Y., Fu, J., Suo, H. (2018) '3D Bioprinting of Low-Concentration Cell-Laden Gelatin Methacrylate (GelMA) Bioinks with a Two-Step Cross-linking Strategy', *ACS Applied Materials & Interfaces*, 10(8), pp. 6849–6857.

Yoon, H., Lee, J., Yim, H., Kim, G., Chun, W. (2016) 'Development of cell-laden 3D scaffolds for efficient engineered skin substitutes by collagen gelation', *RSC Advances*, 6(26), pp. 21439–21447.

Yourek, G., McCormick, S. M., Mao, J. J., Reilly, G. C. (2010) 'Shear stress induces osteogenic differentiation of human mesenchymal stem cells', *Regenerative medicine*, 5(5), pp. 713–724.

Yuan, X., Wei, Y., Villasante, A., Ng, J. J. D., Arkonac, D. E., Chao, P. G., Vunjak-Novakovic, G. (2017) 'Stem cell delivery in tissue-specific hydrogel enabled meniscal repair in an orthotopic rat model', *Biomaterials*, 132, pp. 59–71.

Yue, K., Trujillo-de Santiago, G., Alvarez, M. M., Tamayol, A., Annabia, N., Khademhosseini, A. (2015) 'Synthesis, properties, and biomedical applications of gelatin methacryloyl (GelMA) hydrogels', *Biomaterials*, 73, pp. 254–271.

Yurie, H., Ikeguchi, R., Aoyama, T., Kaizawa, Y., Tajino, J., Ito, A., Ohta, S., Oda, H., Takeuchi, H., Akieda, S., Tsuji, M., Nakayama, K., Matsuda, S. (2017) 'The efficacy of a scaffold-free Bio 3D conduit developed from human fibroblasts on peripheral nerve regeneration in a rat sciatic nerve model', *PLOS ONE*, 12(2), e0171448.

Zanoletti, A., Vassura, I., Venturini, E., Monai, M., Montini, T., Federici, S., Zacco, A., Treccani, L., Bontempi, E. (2018) 'A New Porous Hybrid Material Derived From Silica Fume and Alginate for Sustainable Pollutants Reduction', *Frontiers in Chemistry*, 6, 60.

Zarrinpar, A., Lee, D. K., Silva, A., Datta, N., Kee, T., Eriksen, C., Weigle, K., Agopian, V., Kaldas, F., Farmer, D., Wang, S. E., Busuttil, R., Ho, C. M., Ho, D. (2016) 'Individualizing liver transplant immunosuppression using a phenotypic personalized medicine platform', *Science Translational Medicine*, 8(333), 333ra49.

Zein, I., Hutmacher, D. W., Tan, K. C., Teoh, S. H. (2002) 'Fused deposition modeling of novel scaffold architectures for tissue engineering applications', *Biomaterials*, 23(4), pp. 1169–1185.

Zhang, B., Luo, Y., Ma, L., Gao, L., Li, Y., Xue, Q., Yang, H., Cui, Z. (2018) '3D bioprinting: an emerging technology full of opportunities and challenges', *Bio-Design and Manufacturing*, 1(1), pp. 2–13.

Zhang, Q., Nguyen, P. D., Shi, S., Burrell, J. C., Cullen, D. K., Le, A. D. (2018) '3D bio-printed scaffold-free nerve constructs with human gingiva-derived mesenchymal stem cells promote rat facial nerve regeneration', *Scientific Reports*, 8(1), 6634.

Zhang, S., Li, J., Lykotrafitis, G., Bao, G., Suresh, S. (2009) 'Size-dependent endocytosis of nanoparticles', *Advanced Materials*, 21(4), pp. 419–424.

Liu, W., Zhong, Z., Hu, N., Zhou, Y., Maggio, L., Miri, A. K., Fragasso, A., Jin, X., Khademhosseini, A., Zhang, Y. S. (2018) 'Coaxial extrusion bioprinting of 3D microfibrous constructs with cell-favorable gelatin methacryloyl microenvironments', *Biofabrication*, 10(2), p. 24102.

Zhang, Y. and Ma, M. (2016) 'Microscale Cell Encapsulation Materials and Fabrication Techniques for Type 1 Diabetes', *Microscale Technologies for Cell Engineering*, Singh, A. and Gaharwar, A. K., eds, Springer International Publishing, pp. 231–248.

Zhang, Y. S., Duchamp, M., Oklu, R., Ellisen, L. W., Langer, R., Khademhosseini, A.

(2016) ‘Bioprinting the Cancer Microenvironment’, *ACS Biomaterials Science & Engineering*, 2(10), pp. 1710–1721.

Zhao, X., Lang, Q., Yildirimer, L., Lin, Z. Y., Cui, W., Annabi, N., Ng, K. W., Dokmeci, M. R., Ghaemmaghami, A. M., Khademhosseini, A. (2016) ‘Photocrosslinkable Gelatin Hydrogel for Epidermal Tissue Engineering’, *Advanced Healthcare Materials*, 5(1), pp. 108–118.

Zheng, Z., Wu, J., Liu, M., Wang, H., Li, C., Rodriguez, M. J., Li, G., Wang, X., Kaplan, D. L. (2018) ‘3D Bioprinting of Self-Standing Silk-Based Bioink’, *Advanced Healthcare Materials*, 7(6), 1701026.

Zhu, J. and Marchant, R. E. (2011) ‘Design properties of hydrogel tissue-engineering scaffolds.’, *Expert review of medical devices*, 8(5), pp. 607–26.

Appendix – Conferences, journal papers and awards arising from this work

Invited Talks

2018 1st Meeting of the Portuguese Association for the Biofabrication, Porto (University of Porto, Portugal): Drop-on-demand bioprinting – from single cell to microtissue bioprinting. **R Ribeiro**;

2016 Biology and bioengineering tools in the treatment of H2020 age-related diseases, (University of Cambridge, UK): *Bioprinting technologies in Tissue Engineering*. **R Ribeiro**.

Oral communications at international and national conferences

2017 Biofabrication 2017, Beijing (Tsinghua University, China): *Inkjet printing of single cells*. **R Ribeiro**, D Pal, D Jamieson, KS Rankin, M Benning, K Dalgarno, AM Ferreira;

2016 Biofabrication 2016, Winston-Salem (Wake Forest University, USA): *Polycationic single cell encapsulation for inkjet printing bio-inks*. **R Ribeiro**, AM Ferreira, M Benning, D Pal, D Jamieson, KS Rankin, K Dalgarno;

2016 TCES 2016, London (University College of London, UK): *Single cell encapsulation-based bio-inks for inkjet bioprinting*. **R Ribeiro**, AM Ferreira, M Benning, D Pal, D Jamieson, KS Rankin, K Dalgarno;

2015 Biofabrication 2015, Utrecht (Utrecht University, The Netherlands): *Cell encapsulation for bio-ink formulation*. **R Ribeiro**, AM Ferreira, M Benning, D Pal, D Jamieson, KS Rankin, K Dalgarno.

Poster communications at national meetings and conferences

2018 MeDe Innovation Fifth Annual Conference (University of Sheffield, UK): *Reactive Jet Impingement for Hydrogel Bioprinting*. **R Ribeiro**, M Benning, D Pal, AM Ferreira, K Dalgarno;

2017 Arthritis Research UK/MeDe Research Day (Newcastle University, UK): *Single cell coating for bio-inks*. **R Ribeiro**, D Pal, D Jamieson, KS Rankin, M Benning,K Dalgarno, AM Ferreira;

2016 EPSRC visit (Newcastle University, UK): *Single cell encapsulation for bio-ink formulation*. **R Ribeiro**, AM Ferreira, M Benning, D Pal, D Jamieson, KS Rankin, K Dalgarno;

2016 MeDe Innovation Third Annual Conference (Newcastle University, UK): *Osteosarcoma cell encapsulation for bio-ink formulation*. **R Ribeiro**, AM Ferreira, M Benning, D Pal, D Jamieson, KS Rankin, K Dalgarno;

2015 TCES 2015 (University of Southampton): *Osteosarcoma cell encapsulation for biomedical applications*. **R Ribeiro**, AM Ferreira, M Benning, D Pal, D Jamieson, KS Rankin, K Dalgarno;

Awards

2017 **Travel Award for the 2017 Biofabrication Conference** attributed by the International Society for Biofabrication (ISBF);

2017 **Travel Bursary** awarded by the Tissue and Cell Engineering Society (TCES);

2017 **Honourable Mention Award** attributed by the Association of British Turkish Academics (ABTA);

2016 **PARSUK Xperience grant** attributed by the Portuguese Association of Researchers and Students in the United Kingdom (PARSUK);

2015 **Travel Bursary** awarded by the Tissue and Cell Engineering Society (TCES);

Media appearances

2018 Interview to the Portuguese magazine "Ponto de Vista".

Http://pontosdevista.pt/2018/06/14/tecnologia-favor-da-medicina

(in Portuguese).

2017 **Ribeiro RDC**. Single Cell Speckled Coating for Reliable Inkjet Bioprinting. **3DMedNet** (online invited editorial).

https://www.3dmednet.com/users/14012-3dmednet/posts/19276-single-cell-speckled-coating-for-reliable-inkjet-bioprinting

Publications

2018 **Ribeiro RDC**, Pal D, Ferreira AM, Gentile P, Benning M, Dalgarno KW. Reactive jet impingement technology for high cell density bioprinting, 11(1), 015014. IF=6.838;

2018 Etxabide A, **Ribeiro RDC**, Guerrero P, Ferreira AM, Stafford GP, Dalgarno K, de la Caba K, Gentile P. Lactose-crosslinked fish gelatin-based porous scaffolds embedded with tetrahydrocurcumin for cartilage regeneration. **Int J Biol Macromol**, 117, 199-208. IF= 3.909;

2017 **Ribeiro RDC**, Pal D, Jamieson, D, Rankin KS, Benning M, Dalgarno KW, Ferreira AM. Temporary single-cell coating for bioprocessing with a cationic polymer. **ACS Appl. Mater. Interfaces**, 9(15), 12967-12974. IF= 8.097;

2017 Gamie Z, Kapriniotis K, Papanikolaou D, Haagensen E, **Ribeiro RDC**, Dalgarno K, Krippner-Heidenreich A, Gerrand C, Tsiridis E, Rankin KS. TNF-related apoptosis-inducing ligand (TRAIL) for bone sarcoma treatment: Pre-clinical and clinical data. **Cancer Lett**, 409, 66-80. IF= 6.491;